Optical and Structural Characterisation of III-V Semiconductor Quantum Wire and Quantum Dot Structures.

Matthew John Steer

Department of Physics

&

Department of Electronic and Electrical Engineering

Thesis submitted to the University of Sheffield for the
Degree of Doctor of Philosophy, October 1997.

Optical and Structural Characterisation of III-V Semiconductor Quantum Wire and Quantum Dot Structures

Matthew John Steer

University of Sheffield

Abstract

This thesis describes an extensive study of the optical and structural properties of GaAs/AlGaAs V-groove quantum wire and InAs/GaAs self-organised quantum dot structures. For the optical characterisation, the spectroscopic techniques of photoluminescence (PL), photoluminescence excitation (PLE), cathodoluminescence (CL) and electroluminescence (EL) have been used. In addition important information concerning the structural properties of the quantum wires and quantum dots has been obtained by high resolution transmission electron microscopy (TEM) measurements.

Initial characterisation and optimisation of the quantum wire structures was conducted using CL and TEM imaging. Further optical characterisation of optimised structures was performed using a micro-focusing PL set-up which produced a laser spot size of ~2μm, allowing individual wires to be studied. Excitation under both high and low power density conditions revealed important information concerning the quality of the growth and the nature of the one-dimensional confinement within the structure. Structures were grown with the quantum wires placed in the intrinsic region of a *p-i-n* junction. EL spectroscopy measurements allowed the observation of subband filling effects and an enhanced luminescence intensity for the quantum wire for low forward bias currents. This latter behaviour has important implications for device applications. An investigation of these *p-i-n* samples in magnetic fields up to 14T, revealed further evidence for 1D confinement in the quantum wires and 2D confinement of carriers in a vertical quantum well. This vertical quantum well, a feature that arises automatically during the growth, appears to channel carriers into the quantum wire, providing a possible mechanism for the enhanced wire electroluminescence intensity observed. In addition, evidence is presented for a possible excitonic-free carrier transition which is observed for high carrier densities in the wires.

TEM structural analysis of self-organised InAs/GaAs quantum dots has shown that the dots can show a high degree of surface ordering, aligning themselves on the step edges of the underlying substrate. Excitation under high laser power densities using the micro-PL set-up has shown subband separations of around 75meV, which is very promising for room temperature opto-electronic device applications. In addition, very narrow linewidth emission has been observed from individual quantum dots on a small sub-micron etched mesa which contains ~100 dots. The electronic structure of the quantum dots has been probed using resonant PL and PLE. These techniques have revealed important information regarding carrier relaxation mechanisms that exist in the quantum dots. In PLE features are observed at approximately 60 and 90meV from the detection energy and which move rigidly in energy when the detection energy is varied. This behaviour is attributed to carrier relaxation by the emission of multiple LO-phonons, a process that appears to bypass any 'phonon bottleneck'. Similar features are also observed in resonantly excited PL spectra. Two distinct carrier relaxation mechanisms are demonstrated by this technique: a non-resonant mechanism from the upper excited state and a resonant mechanism involving the emission of multiple LO phonons, from the first excited state.

Publications

'*Electronic Energy Levels and Energy Relaxation Mechanisms in Self-Organised InAs/GaAs Quantum Dots.*' M.J. Steer, D.J. Mowbray, W.R. Tribe, M.S. Skolnick, M.D. Sturge, M. Hopkinson, A.G. Cullis, C.R. Whitehouse. Phys. Rev. B, **54**, (24), 17738, (1996).

'*Electronic Energy Levels and Energy Relaxation Mechanisms in Self-Organised InAs/GaAs Quantum Dots.*' M.J. Steer, D.J. Mowbray, M.S. Skolnick, W.R. Tribe, M.D. Sturge, M. Hopkinson, A.G. Cullis, C.R. Whitehouse. 23rd Int. Conf. on the Physics of Semiconductors Berlin, 1996 (edited by M.Scheffler and R. Zimmermann), World Scientific, Singapore, **2**, 1389, (1996).

'*Emission Mechanisms and Band Filling Effects in GaAs-AlGaAs V-groove Quantum Wires.*' W.R. Tribe, M.J. Steer, D.J. Mowbray, M.S. Skolnick, A.N. Forshaw, J.S. Roberts, G. Hill, M.A. Pate, C.R. Whitehouse, G.M. Williams. Appl. Phys. Lett. **70**, (8), 993, (1997).

'*Magneto-optical spectroscopy of InAs/GaAs self-organised quantum dots.*' L.R. Wilson, D.J. Mowbray, M.S. Skolnick, L. Harris, M. Morifuji, M.J. Steer and M. Hopkinson. Accepted for publication, J. Physica E (1998).

'*Optical spectroscopy of GaAs/AlGaAs V-groove quantum wires.*' M.J. Steer, D.J. Mowbray, M.S. Skolnick, W.R. Tribe, A.N. Forshaw, D.M. Whittaker, J.S. Roberts, A.G. Cullis, G. Hill, M.A. Pate, C.R. Whitehouse, Accepted for publication, J. Physica E (1998).

Acknowledgements

There are a large number of people who have made significant contributions to the work contained in this thesis. I would like to thank them all for their help during the course of my studies.

Firstly, I would like to express my sincere thanks to Dr. David Mowbray, who has given me a tremendous amount of support, advice and help during the preparation of this thesis, and for his clear explanation of various aspects of experimental procedure and very useful discussions regarding the results obtained.

Thank you to Professor Colin Whitehouse for his supervision and input of ideas and to Professor Maurice Skolnick for allowing me to conduct the majority of my research in the Physics Dept and for very useful discussions of results and experiments, also Professor G.A. Gehring for allowing the use of the Physics Dept. facilities.

A lot of this work has been conducted through a sponsorship with the Defence Research Agency at Malvern, who have provided financial assistance and an extensive use of their facilities. My thanks go to Professor Tony Cullis and Gerald Williams who have enabled us to gain a much greater understanding of the structural properties of the samples under investigation through analysis by TEM and CL and some very useful discussions. Thank you also to Peter Smith for the TEM sample preparation.

The preparation of quantum wires and quantum dots has involved several people, I would like to thank Dr. Geoff Hill and Malcolm Pate for the pre-growth patterning of the V-grooves and the subsequent SEM images they obtained from a number of samples, which aided the initial optimisation considerably. I would also thank them for the time spent etching small mesas (that I could find!) in quantum dot samples for the single dot studies, and for other post growth processing. Thanks are also due to Dr. John Roberts for the MOVPE growth of the quantum wires studied in this thesis and for his useful input during optimisation and to Dr. Mark Hopkinson for the MBE growth of the quantum dot samples and for allowing me to observe their growth.

I would like to thank Dr Bill Tribe for designing the μPL equipment and spending a considerable amount of time teaching me how to set it up and use it. Without μPL a lot of the interesting results contained in this thesis could not have been obtained. Thanks, also to Dr. Richard Hogg, Dr. Derek Peggs and Dr. John David for the help they gave me in the lab when I started my studies, and to the other lecturers and RAs in the group, Dr. John Cockburn, Dr. Nik Cain, Dr. Yi Bi Lee, Dr. Vasiliy Astratov, Dr. Kimberly Schumacher and Dr. Masato Morifuji. Thanks are also due to Dr. Aaron Forshaw and Dr. David Whittaker for the extensive amount of theoretical modelling of quantum wires they conducted, which led to a much greater understanding of the experimental results obtained. I am also very grateful to John Kelly and Paul Russell from the workshop for the building and repair of various pieces of equipment and to Chris Vickers for the provision of liquid helium.

I would also like to thank all the post-graduate students I have worked with, for their good humour, help and advice during the past years. Especially Martin Birkett, Luke Wilson and Lee Harris for their many useful discussions and advice regarding Fantasy Football and Cricket team selection and substitution, along with the odd physics related discussion. Also to Arbinder Pabla, Jon Finley, Olek Kowalski, Afaz Afshar, Adam Armitage, Diane Baxter Jeremy Duck, Peter Keigthley, Mark Stevenson, Ian Culshaw and Max Migliorato.

Finally I would like to thank my parents for their continued support and general nagging, and my sister Helen and her husband Colin for their entertaining stories on my fairly infrequent visits home.

Contents

CHAPTER 1

CHAPTER 2

Growth of Quantum Wires and Quantum Dots

CHAPTER 3

Experimental Techniques

CHAPTER 4

Structural Characterisation of GaAs-AlGaAs V-groove Quantum Wires

CHAPTER 5

Optical Studies of V-groove GaAs-AlGaAs Quantum Wires

CHAPTER 6

Structural and Optical Characterisation of InAs-GaAs Self-Organised Quantum Dots

CHAPTER 7

Optical Studies of Self-Organised Quantum Dots

Chapter 1

Introduction

1.1 General Introduction

Over the past 40 years the electronics industry has worked towards producing electronic devices which have ever smaller physical dimensions and are more reliable. There have been significant advances in these areas from the early days of the valve to the sub-micron scale silicon devices employed in today's integrated circuits. The aim of this progress has been to make circuits smaller, faster and more efficient in their power consumption. The size of the components in a circuit has a direct bearing on the speed and the power consumed. High power consumption, with the associated problems of heat dissipation and device reliability, is a serious problem, for example, in battery operated equipment, aircraft applications etc., and, in addition, can also prove costly if a device needs to be cooled to enable it to work.

Current electronic technology is dominated by silicon based devices. However, III-V, particularly GaAs, semiconductor technology is breaking through in the field of high speed microwave communications[1] and is already very important for opto-electronic applications.[2] The interaction between electrons and the surrounding crystal lattice in GaAs is weaker than in silicon. Electrons therefore have a smaller effective mass in GaAs, which leads to a higher mobility[1] (a direct indication of the speed electrons attain and the distance they travel before a scattering event occurs). For devices exhibiting high switching speeds, materials with very high mobility electrons are required and GaAs is a common choice. In addition, unlike Si and Ge, GaAs and related materials (e.g. GaInAs, GaInP etc.) have a direct bandgap making them suitable for electro-optical device applications, including light emitting diodes (LEDs) and lasers.

Of particular importance in semiconductor research is the trend towards smaller and smaller devices, leading to devices which are at the absolute limit in size; devices operating on an atomic scale. Future demands on electronic circuits will eventually require this level of size reduction. At these small dimensions, when the length scale of components is of the order of the de-Broglie wavelength for electrons (50nm in GaAs),[3] quantum mechanics begins to have a dramatic effect on the electronic and optical properties of the device.[4]

1.2 Properties of III-V Semiconductors

Opto-electronic circuits are envisioned in which photons are used instead of electrons to carry information in the circuit. In these opto-electronic systems the inter-chip communication time will be at its ultimate limit, restricted only by the spatial separation of the components on the chip. For these and more general opto-electronic applications a material that will efficiently convert an electrical signal into an optical signal, and vice-versa, is required. GaAs, which has a direct bandgap, has this property. It can efficiently absorb and emit photons at or above the bandgap energy as electrons are promoted to the conduction band or relax to the valence band. This makes GaAs and related III-V semiconductors very attractive systems for use in opto-electronic devices.

By contrast the lowest energy bandgap in silicon is indirect, i.e. the bottom of the conduction band and the top of the valence band are not aligned in **k**-space. For optical transitions, particularly photon emission, relaxation of electrons from the bottom of the conduction band to the top of the valence band (where there are hole states) must involve a scattering event, with generally either emission or absorption of a phonon (a quantum of lattice vibration) as shown in Figure 1.1. This additional interaction allows crystal momentum to be conserved as carriers recombine across the bandgap from different points in **k**-space. It is required because of the very small momentum of the emitted photon. However, this two step process (photon and phonon emission) is very slow (~30ns)[5] compared to the single step process (photon emission) which occurs in direct gap semiconductors (~1ns).[5] Hence competing non-radiative processes are more important in indirect bandgap semiconductors and so a typical indirect bandgap semiconductor generates light much less efficiently (by a factor of ~10^3) than direct bandgap semiconductors.[6] For this reason opto-electronic devices generally utilise only direct bandgap semiconductors.

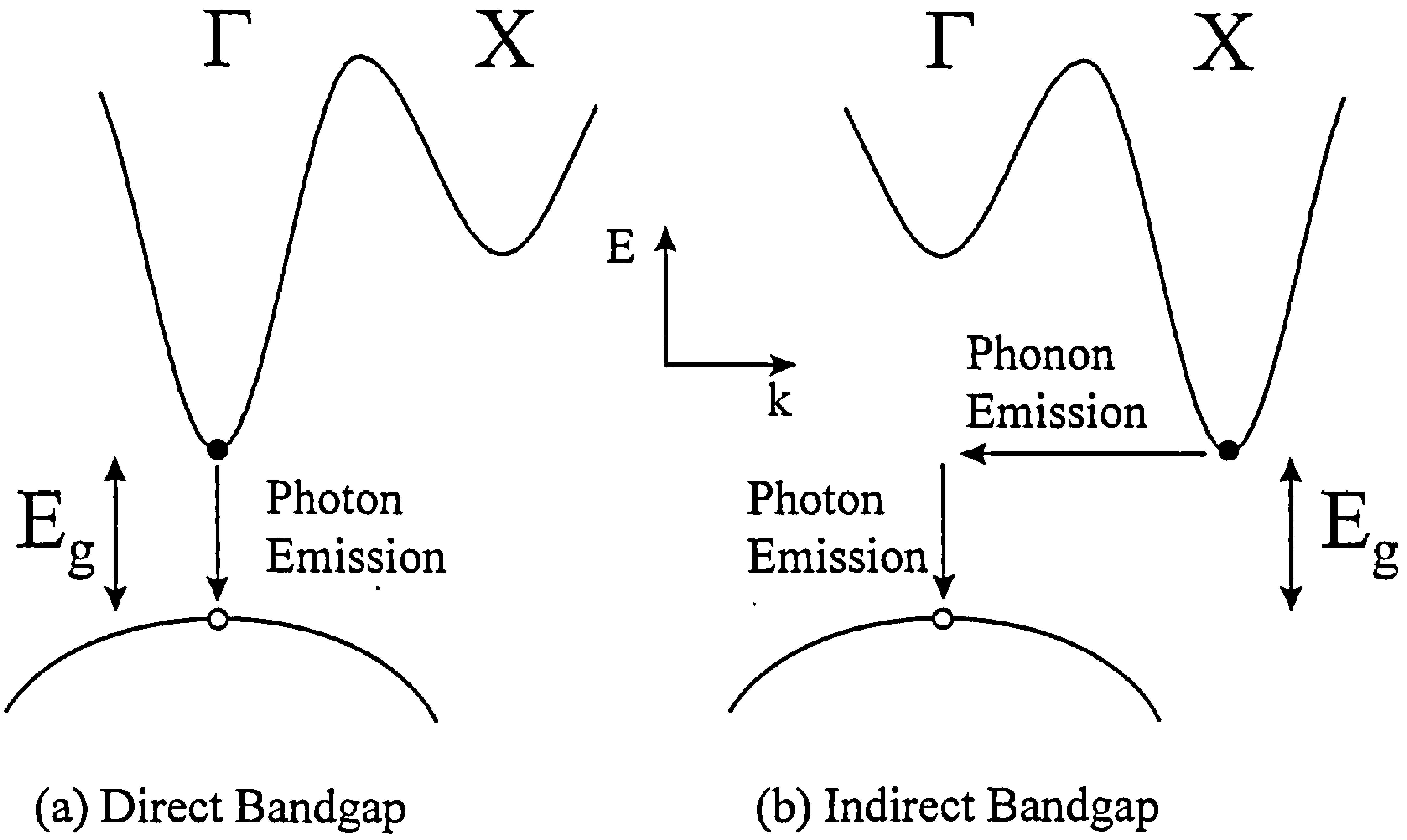

(a) Direct Bandgap (b) Indirect Bandgap

Figure 1.1 Optical recombination processes in (a) Direct bandgap and (b) Indirect bandgap semiconductors. For a direct semiconductor a vertical transition can occur very efficiently, resulting in the emission of a photon. In an indirect semiconductor the optical transition requires the assistance of a scattering mechanism to conserve momentum.

1.2.1 Band Structure of III-V Semiconductors

The band structure of a crystalline material is a representation of the allowed energy levels available for electrons and holes as a function of their momentum or wavevector (k). It is usually depicted for various high symmetry directions. A band structure calculation[7] of GaAs is shown in Figure 1.2. The band structures of all the samples discussed in this thesis are similar to that of GaAs, in that they are all composed of direct bandgap materials. As shown schematically in Figure 1.1 above, in a direct bandgap semiconductor the lowest minima in the conduction band and the highest maxima in the valence band lie at the zone centre (the Γ-point) at k=0. All the optical transitions observed for the samples under investigation in this thesis occur across this direct bandgap. Carriers that are excited into states higher up in the conduction and valence band can relax to their respective band extrema by fast LO and LA phonon emission, followed by recombination via a direct optical transition.

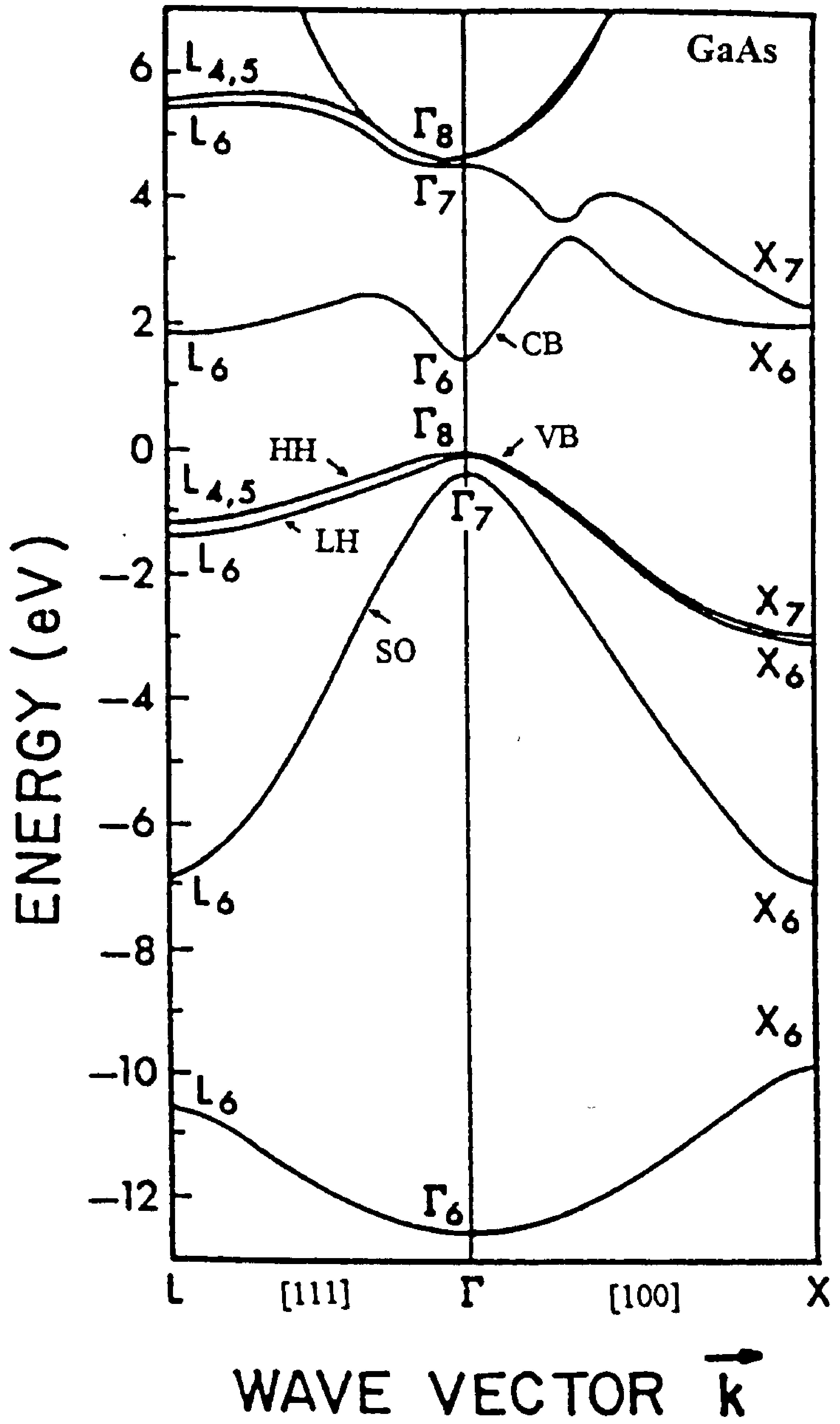

Figure 1.2 Band Structure of bulk GaAs obtained using pseudopotential calculations.[7]

Significant modifications of the band structure of semiconductors has been achieved by restricting the motion of carriers to a two dimensional plane, by confinement within a quantum well. Quantum wells are now common place in III-V semiconductor research and are used in some commercial electro-optical devices (e.g. quantum well lasers). These structures have mainly been fabricated or 'grown' using the epitaxial techniques of Molecular Beam Epitaxy (MBE) and Metal-Organic Vapour Phase Epitaxy

(MOVPE). These techniques are described in Chapter 2. Quantum wells are formed by depositing a very thin layer (<200Å) of a narrow bandgap (1.42eV for GaAs) semiconductor in between a semiconductor with a wider bandgap (>1.42eV, i.e. AlGaAs with varying Al compositions). The narrow bandgap material is said to form the well whilst the wider gap material forms the barriers. A schematic band diagram of a quantum well is shown in Figure 1.3a. The discontinuity in the conduction band edge results in electrons within the quantum well experiencing potential energy barriers for one of their degrees of freedom (the growth direction), confining them so that their motion is restricted to a plane in just two dimensions. This confinement results in a quantisation of the allowed energy levels for motion in the growth direction and produces a modification of the 3D band structure which leads to the appearance of 2D subbands. In a similar manner, holes in the valence band are also confined.

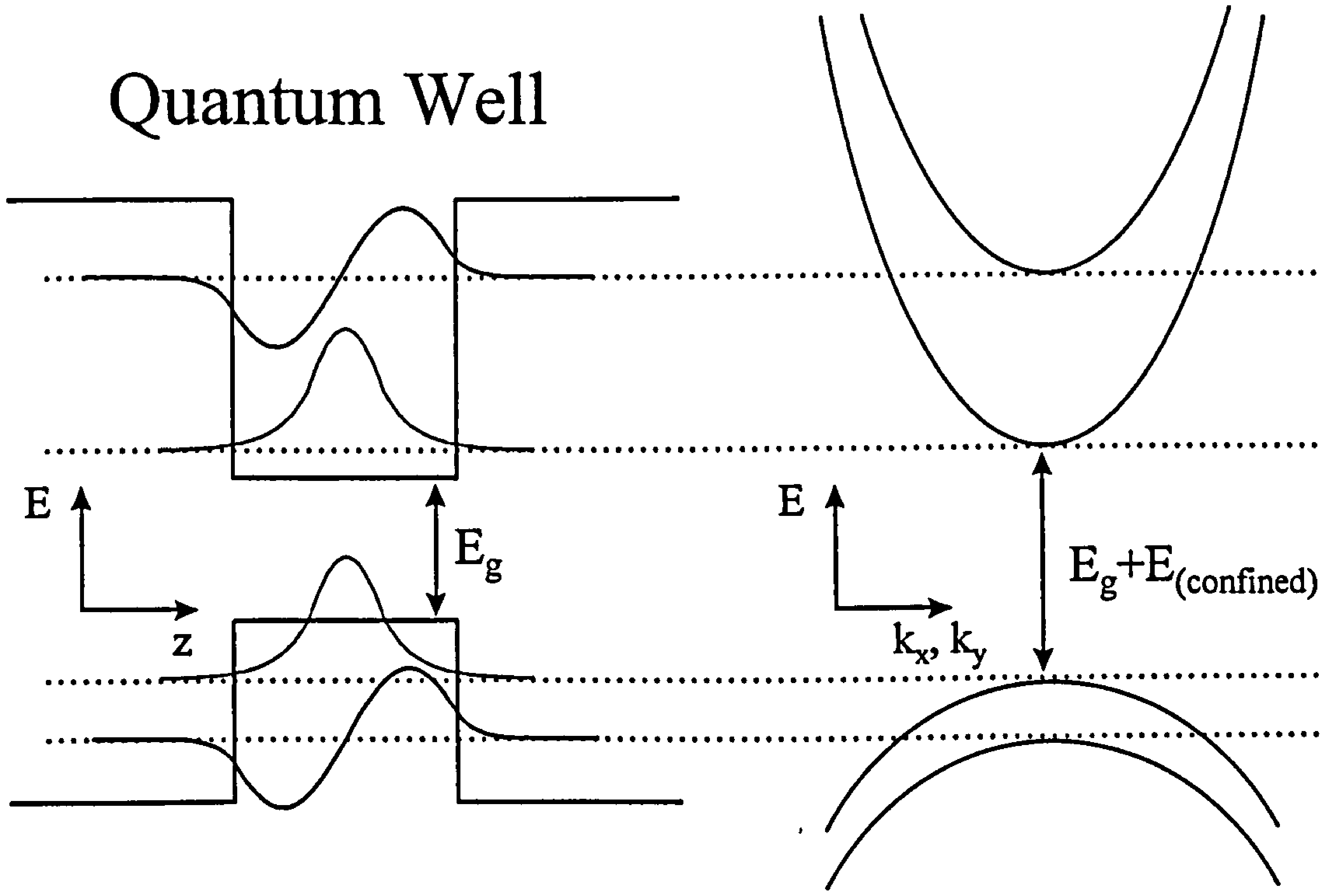

(a) Band Diagram

(b) Subband Structure

Figure 1.3 (a) A schematic band diagram for a quantum well where electrons and holes have their motion restricted in one dimension. (b) Subband structure that appears in a quantum well as a result of carrier confinement.

A simple numerical solution of Schrödinger's equation for a quantum well allows the confined levels to be calculated, the problem can be simplified by assuming infinite barriers. This so-called particle in a box calculation is outlined in many standard quantum mechanics text books[8] and leads to an infinite series of energy levels of the form:

$$E_n = \frac{\hbar^2}{2m^*}\left(\frac{n\pi}{W}\right)^2 \qquad (1.1)$$

where W is the width of the well, m^* is the effective mass of the particle and n is an integer quantum number referring to the n^{th} energy level. The associated wavefunctions have a sine or cosine form with no penetration into the barriers. This infinite depth approximation holds reasonably well for the lower energy states that are deep in the well, giving a total energy for electrons as follows (the growth direction is assumed to lie along the z-axis):

$$E = E_n + \frac{\hbar^2}{2m^*}(k_x^2 + k_y^2) \qquad (1.2)$$

Carriers are still free to move in the plane of the well and this in-plane dispersion for conduction band states can be approximated as parabolic for low values of **k** near the zone centre. This modified 2D band structure for quantum wells is shown schematically in Figure 1.3b. For higher energy excited states or for small barrier heights, where the penetration of the wave-function into the barrier is significant, an infinite depth well is no longer a good approximation. The Schrödinger equation for a finite depth well (as outlined in any standard quantum mechanics text book)[8] must be solved with suitable modifications to the boundary conditions which are necessary because of the different carrier effective masses in the well and barrier. Unlike the case of an infinite depth well the equation for a finite depth well can not be solved exactly but solutions can be found numerically. For a finite depth well the form of the wave-functions is sinusoidal in the well but with an exponential decay in the barriers.

The in-plane dispersion of allowed energy levels for the hole states within each valence subband is complicated by the multiple degeneracy that occurs at the zone centre (the light and heavy hole states). This degeneracy is lifted at **k**=0 in a quantum well due to the different quantum confinement of the states due to their carriers having different effective masses. The hole dispersion should be calculated using the more complex pseudopotential[7] or **k.p**[9] theories which take into account the interactions between the various bands and correctly describe the mixing and anti-crossing which occurs between the valence subbands.

Optical emission is observed when electrons and holes recombine across the bandgap following excitation of the semiconductor (i.e. when electron-hole pairs are created) by photons in photoluminescence (PL), electrons in cathodoluminescence (CL) or electrical injection of electrons and holes in electroluminescence (EL). In a quantum well the energy of the emitted photon is the sum of the bulk bandgap energy and the electron and hole confinement energies. As the latter two depend upon the width of the quantum well, the emission energy of the system can be tailored to a particular value by a suitable choice of the well width. This has a number of applications including the fabrication of different colour LEDs and the matching of laser wavelengths to the minimum attenuation band of optical fibres. In addition studying and exploiting the various electrical and optical properties of 2D systems new and novel devices such as Quantum Well LASERs,[10] Resonant Tunnelling Diodes,[2] which exhibit negative differential resistance effects and Self Electro-optic Effect Devices (SEEDs),[11] which exhibit the capacity for optical switching, have been demonstrated.

1.3 Properties of Low Dimensional Semiconductors

There has been a considerable amount of research into III-V semiconductor quantum wells during the last twenty years. From a fundamental physics point of view the interest lies in the study and behaviour of 2D systems. This has led to remarkable discoveries such as the Quantum Hall Effect, which has resulted in the establishment of a resistance standard based purely on fundamental constants.[12] For device applications there is tremendous scope for engineering devices that respond to, or emit, photons at specific energies (i.e. energies suitable for optical communications through the multi-mode optical fibres available today), as the effective bandgap, and hence emission energy of photons, can be tailored by varying the width of the quantum wells and/or the composition of both the barrier and quantum well material. In addition, many other properties of quantum wells (e.g. the modified density of electronic states, see below) are advantageous for device applications.

The natural progression in this research has been to reduce the dimensionality of these nano-structures even further so that carriers are confined such that their motion is restricted to one, and ultimately zero, dimensions in Quantum Wires and Quantum Dots respectively. The samples studied in this thesis are based on these types of structure. As in the case of quantum wells there is potentially much interesting physics to be discovered by studying these structures, particularly zero dimensional quantum dots where the carriers are confined in all three dimensions forming essentially an atomic-like system with energy levels that are fully quantised and discrete.

This reduced dimensionality has been theoretically predicted[13,14] to lead to increased carrier mobilities in quantum wires because scattering can only occur into available states that lie in the same or opposite direction as the current. In a 2D system the carrier mobility is similarly enhanced, but to a lesser extent, as carriers can only scatter to states that lie in the same plane on the Fermi surface. In contrast, in a 3D system electrons can scatter into a continuous range of states around the Fermi surface so increasing the chance of scattering and hence reducing the mobility. The modified density of states in 1D and 0D systems also has important advantages for the operation of semiconductor lasers, as discussed below.

1.3.1 The Density of Electronic States in Low Dimensional Semiconductors

The electronic Density of States (DOS) is an important concept in semiconductors as it can be used to explain a number of features observed in their optical spectra. In addition it is an important factor in the performance of electronic and electro-optic devices.

The density of states is defined as the number of available electronic states per unit volume per unit energy at an energy E. Assuming a parabolic E vs. **k** dispersion relationship, $E = \frac{\hbar^2 k^2}{2m^*}$, the density of states can be easily calculated for structures having various dimensionalities. These DOS functions are briefly derived in the following section.

1.3.1.1 The DOS in Three Dimensions (Bulk Material)

For bulk materials in three dimensions the available states in k-space lie on a sphere, such that the volume occupied by states between **k** and **k**+d**k** is given by $4\pi k^2 dk$, with each point in **k**-space occupying a volume $\left(\frac{2\pi}{L}\right)^3$ where L is the length of the sample. The number of **k** states within this range in **k**-space is therefore: $\left(\frac{k^2}{2\pi^2}\right) V dk$ where $V=L^3$. Taking into account the two possible spin orientations for each point in **k**-space the number of electron states per unit volume in k-space is $g(k)dk=k^2/\pi^2 dk$. The corresponding value for the energy range E→E+dE is given by: g(E)dE=g(k)dk

Substitution of **k** in terms of E from the parabolic dispersion relationship above gives the density of states in 3-dimensions:

$$g(E) = \frac{1}{2\pi^2}\left(\frac{2m^*}{\hbar^2}\right)^{3/2} E^{1/2} \tag{1.3}$$

The density of states for a three dimensional material is shown in Figure 1.4.

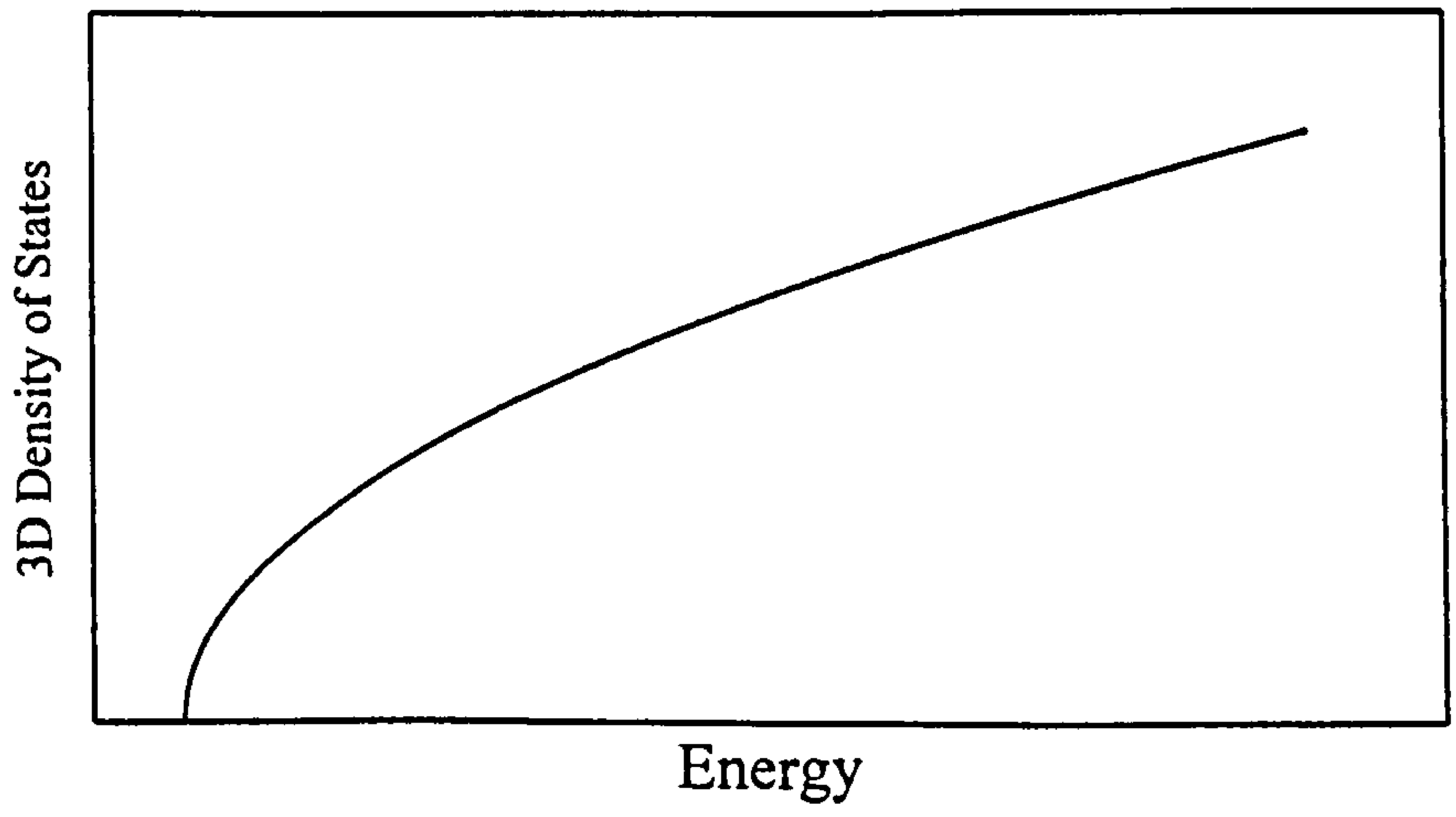

Figure 1.4 Density of states in a three dimensional bulk material.

1.3.1.2 The DOS in Two Dimensions (Quantum Well)

Similar arguments lead to the density of states for two dimensional systems. In this case the available k-states lie on a circular disc, so states between k and k+dk occupy an area $2\pi k dk$, with each state occupying an area $\left(\frac{2\pi}{L}\right)^2$. The number of states in this area is hence $\left(\frac{k}{2\pi}\right) A dk$, where $A=L^2$. The density of states for two dimensions is therefore given by:

$$g(E) = \frac{m^*}{\pi\hbar^2} \qquad (1.4)$$

For two-dimensions the density of states is independent of energy, depending only on the number of subbands present at the specified energy.

The density of states for a two dimensional quantum well is shown in Figure 1.5. It has a step-like appearance with a non-zero density of states at the band edge and additional steps occurring at the subband energies. This is in contrast to the 3D case where the density of states at the band edge is zero but increases with increasing energy above the band edge.

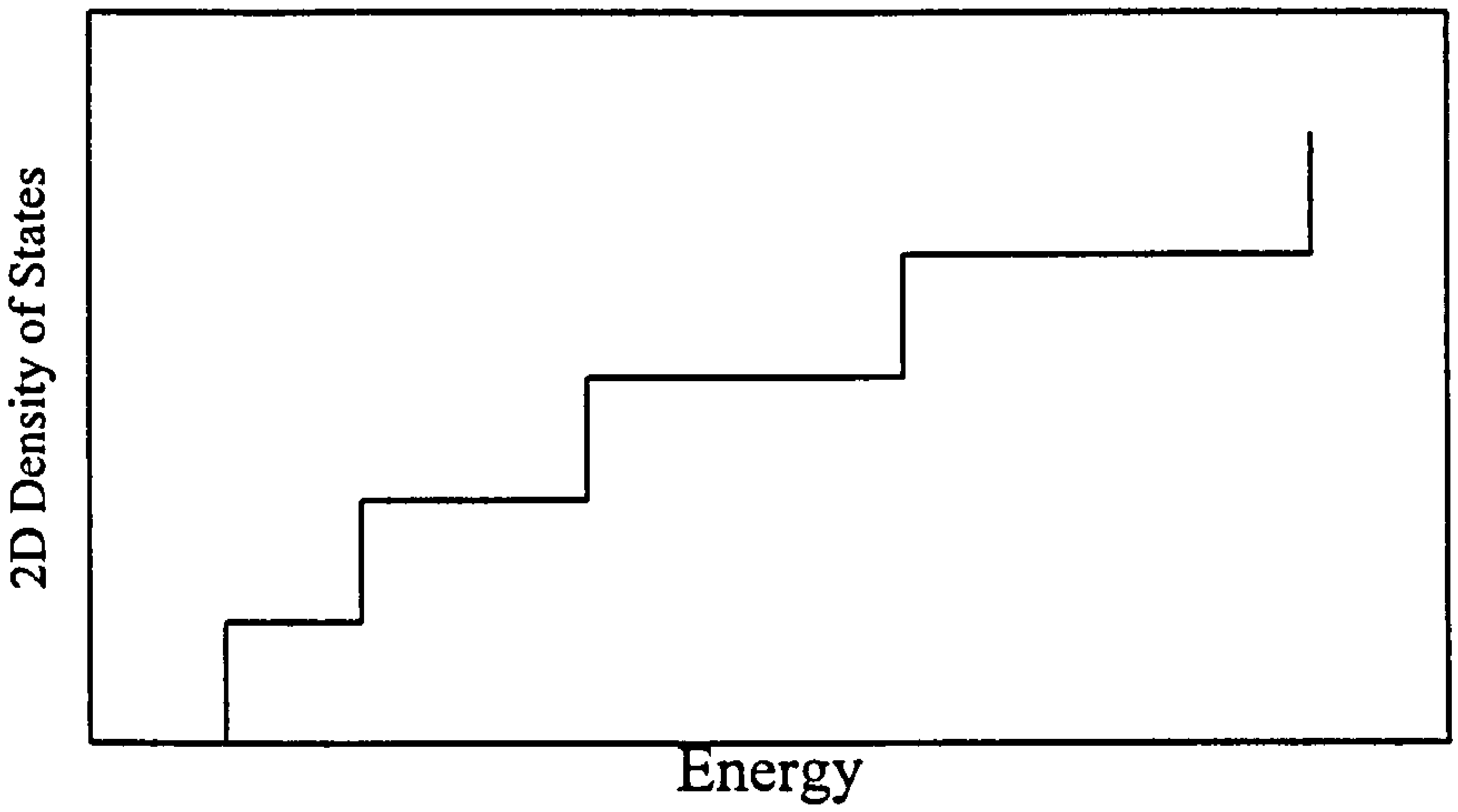

Figure 1.5 Density of states in two dimensional quantum well.

1.3.1.3 The DOS in One Dimension (Quantum Wire)

In one dimension the allowed states essentially lie on a straight line in k-space. The length taken up by states between k and k+dk is simply 2dk, taking into account the two opposite directions in k-space. Each state hence occupies a length $\left(\frac{2\pi}{L}\right)$ and the number of states in a length dk is $\left(\frac{dk}{2\pi}\right)L$. The one-dimensional density of states is therefore:

$$g(E) = \frac{(2m^{*})^{1/2}}{\pi\hbar^{2}} E^{-1/2} \qquad (1.5)$$

Unlike the 2D case, where the density of states is independent of energy, the 1D density of states shows an $E^{-1/2}$ dependence which has a maximum at the subband edge.

The density of states for a one dimensional quantum wire is shown in Figure 1.6. The density of states tends to infinity at the subband edges but falls off rapidly with increasing energy. This leads to a narrow distribution of allowed energy levels at the subband edges.

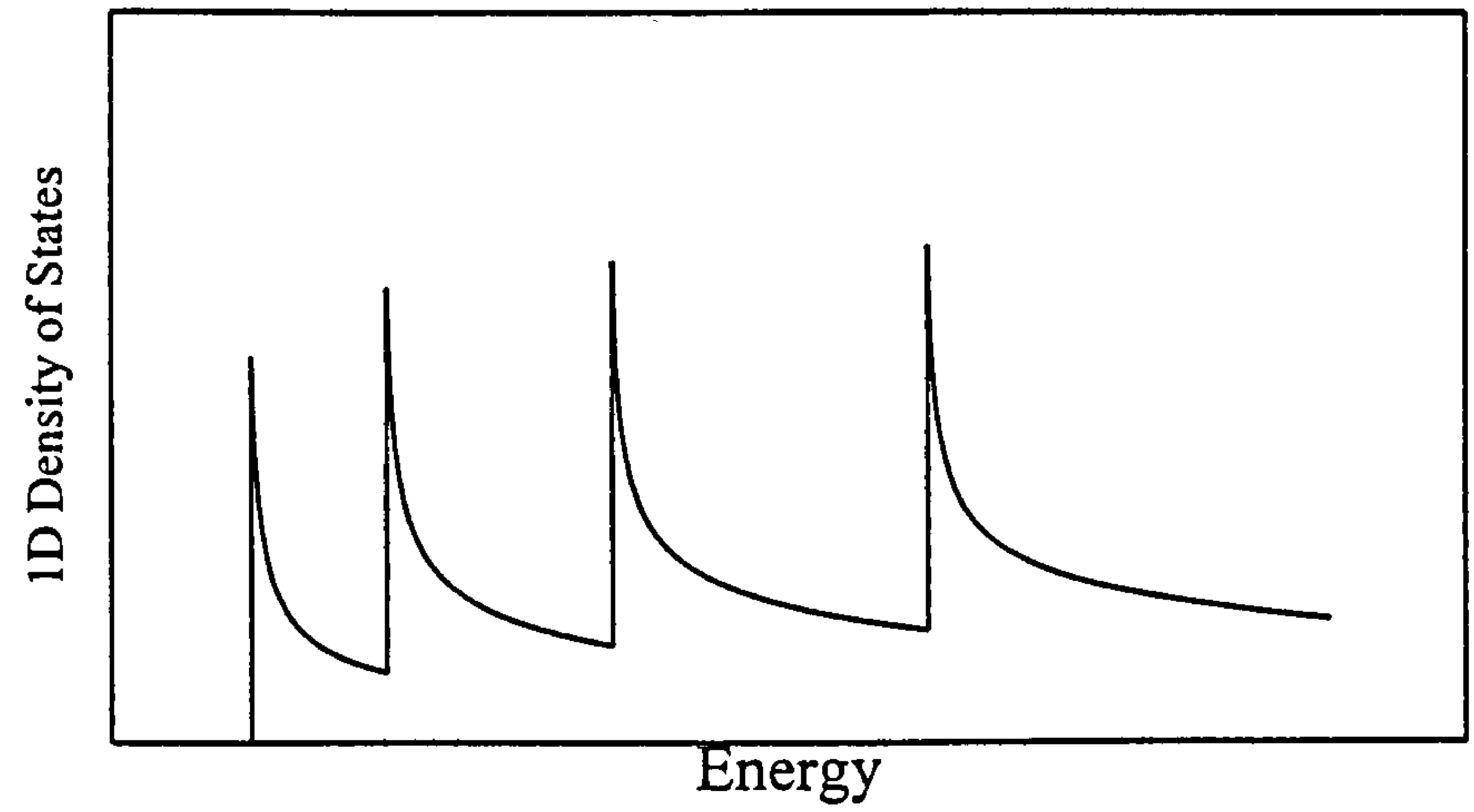

Figure 1.6 Density of states in a one dimensional quantum wire.

1.3.1.4 The Zero Dimensional DOS (Quantum Dot)

In a quantum dot the form of the density of states is essentially δ-function-like at the allowed energy levels. This is a direct result of confinement in all three dimensions which causes a complete quantisation of the energy levels. There are simply no available states except at the discrete levels which are defined by the confinement potential. The number of states available at these energies depends upon the nature of the confinement potential. For a system with cylindrical symmetry, angular momentum is a good quantum number and the lowest energy state is s-like (angular momentum of zero). In this case the state can hold a maximum of two electrons of opposite spins.[15]

The density of states for a zero dimensional quantum dot is shown in Figure 1.7, with δ-function spikes occurring at the allowed energy levels.

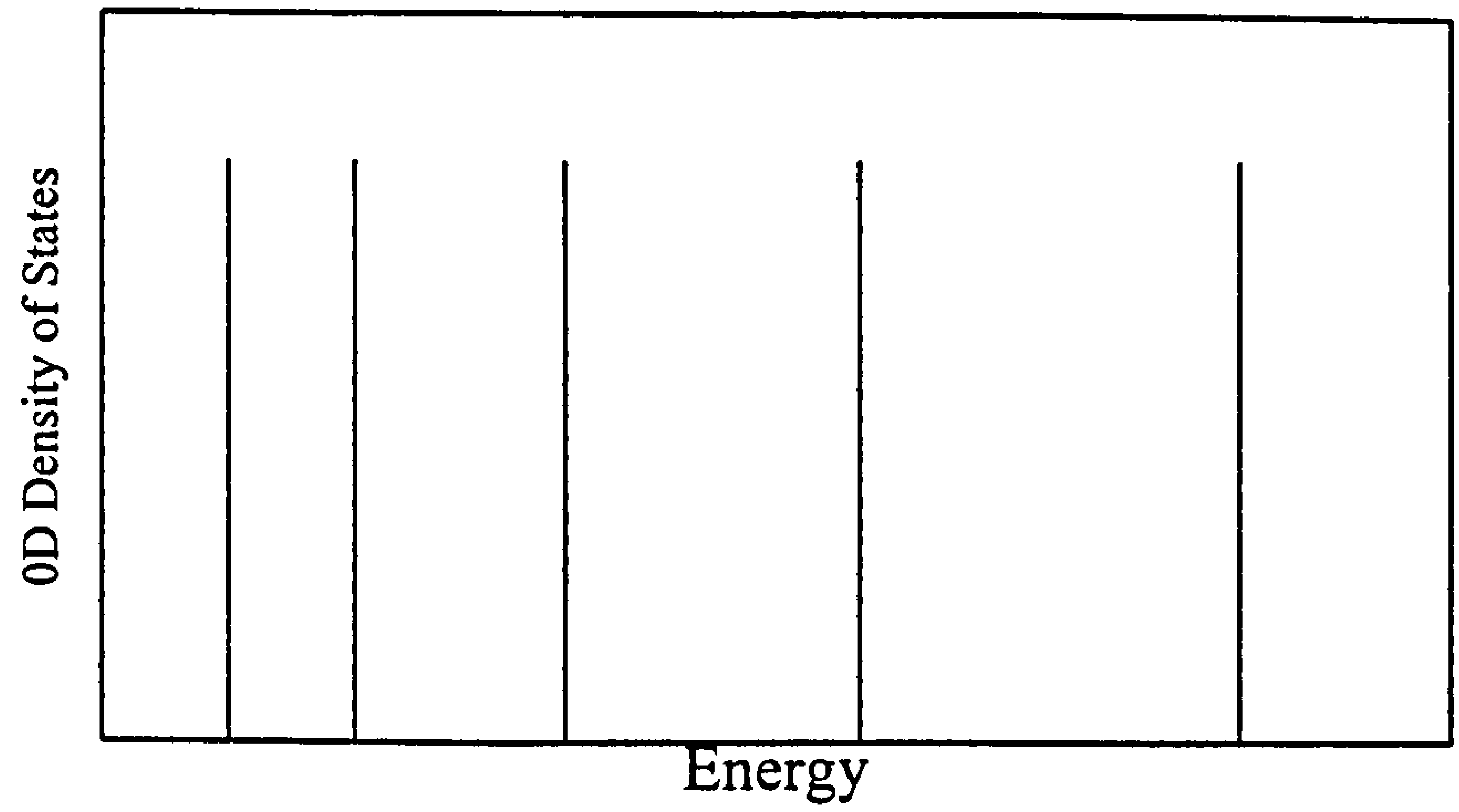

Figure 1.7 The zero dimensional density of states for a quantum dot.

1.3.2 Predicted Improvements in Laser Performance for Devices Utilising Reduced Dimensionality Active Regions

The sharpening and enhancement of the electronic Density of States, which occurs at the band edge as the dimensionality decreases, along with enhanced non-linearities in the optical properties (see below) has important implications for device applications. The exploitation of the modified density of states is predicted[13] to lead to very high efficiency lasers that exhibit improved performance compared to conventional bulk lasers. For example, very low threshold currents, greater temperature stability of the threshold current[13] and narrower spectral linewidths[16] have all been predicted for quantum well, quantum wire, and quantum dot based lasers.

The lasing threshold current was immediately reduced by a factor of about 100 when the dimensionality of the active region was reduced from that of a conventional 3D diode laser to a 2D quantum well laser.[3] This reduction is partly due to the reduction in the size of the active region of the device, but also results from the higher density of states at the band edge. In the 3D case, the injected carriers are spread out over a wide range of energies. Because of the low density of states at the band edge, the band needs to be filled to a point where the density of states is sufficient to obtain a population inversion that will overcome the losses of the laser. A large number of states are hence occupied which do not contribute to the lasing process, resulting in a high threshold current. For 2D quantum wells, the density of states is non-zero at the band edge, making a population inversion much easier to achieve and a much lower threshold current is obtained. Reducing the dimensionality again to 1D in quantum wires is expected to show a further reduction in the threshold current. The density of states is enhanced at the subband edge, producing a narrow distribution of carrier energies with the result that the spectral linewidth is narrower and the overall gain is increased. For a quantum dot, which represents the ultimate reduction in dimensionality, the δ-function density of states allows a population inversion to be obtained for very low currents and with the emission having an extremely narrow spectral linewidth.

The reduced dimensionality of the active region has further consequences for laser device performance. As the dimensionality is reduced the differential gain, which represents the gain increase resulting from the injection of an additional electron-hole pair, increases because of the reduced effective spread of the available electronic states.[17] This increased differential gain results in increased modulation bandwidths with obvious applications for communication systems.[18]

The temperature sensitivity of the threshold current is also expected to fall as the dimensionality is reduced. This is because, as the temperature is raised, the high energy tail of the Fermi distribution of carriers enters an energy range that contains a reduced number of states. Consequently only a small number of carriers are thermally excited to these levels maintaining the population inversion at the energy where the lasing is occurring.[13,19,20]

Figure 1.8 shows the calculated temperature dependencies of the threshold currents for lasers having 3D, 2D, 1D and 0D active regions.[13] For the ultimate limit of a 0D system, in the absence of thermal excitation of carriers to excited states which is negligible if the energy level spacing >>kT, the threshold current is independent of temperature.

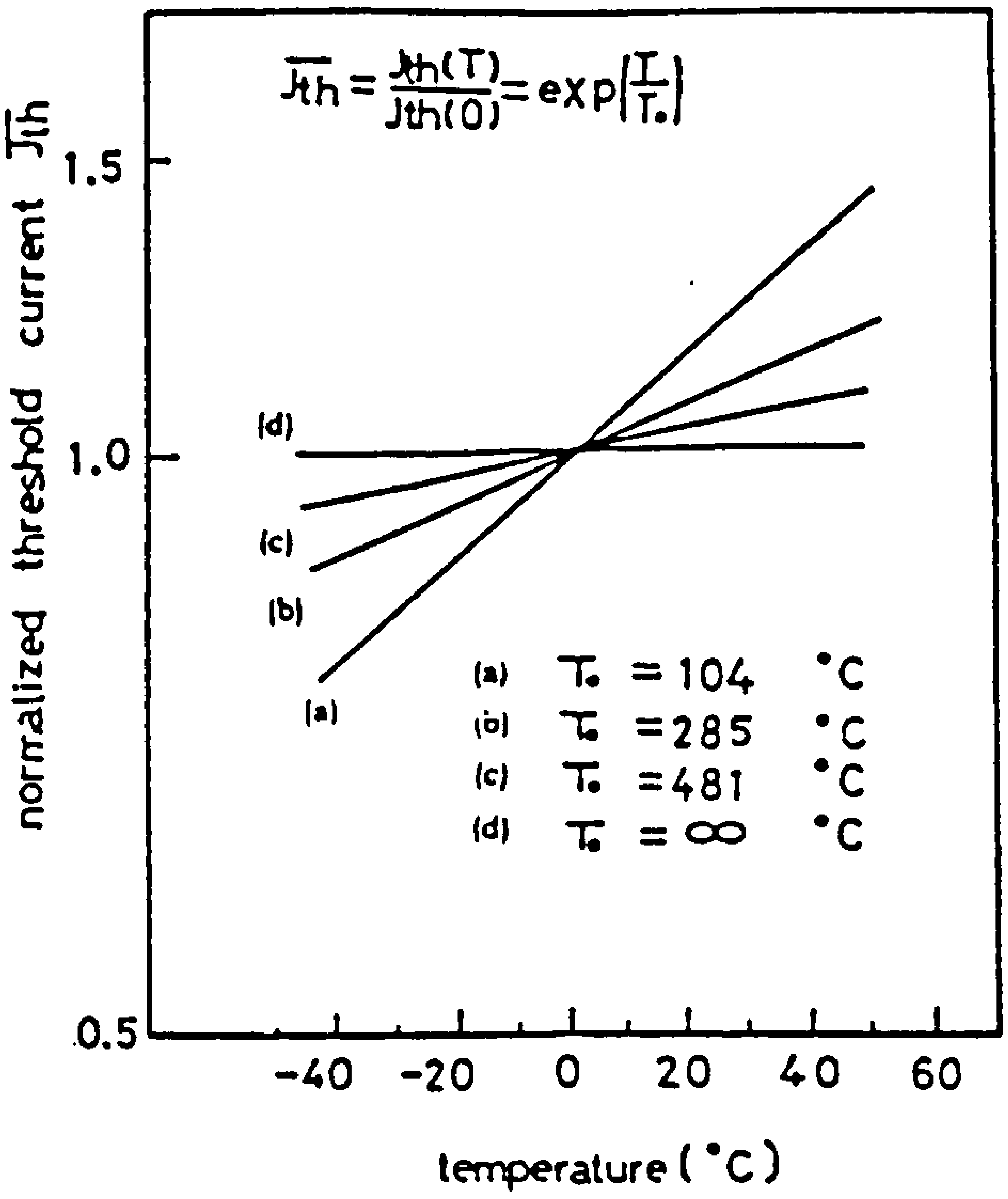

Figure 1.8 Temperature dependence of the threshold current for lasers having different active region dimensionalities. (a) 3D, (b) 2D, (c) 1D and (d) 0D. Reproduced from Arakawa.[13]

These predicted advantageous properties of quantum wire and quantum dot based lasers make them attractive devices for use in opto-electronic interconnects, exhibiting low power consumption and high modulation speeds, and laser arrays for all optical computers. In addition, quantum wires and dots have considerable potential for use as optical modulators. Both lasers and modulators are required for optical computing applications. Although commercial devices are not yet available, it is interesting to note that the operation of quantum wire and quantum dot based lasers have been reported which exhibit very promising operating characteristics (see Chapter 2).

1.3.3 Excitonic Effects in Semiconductors

Excitonic effects are important in the optical properties of semiconductors. Excitons can be formed when an electron-hole pair is created in a semiconductor. There is an attractive Coulomb force between the electron and hole, which results in a bound, hydrogenic-like system. This serves to reduce the total energy gap of the system by a characteristic exciton binding energy, E_{bind}, as shown in Figure 1.9a. The excitonic levels lie just below the band edge and result in an enhancement of the absorption coefficient at these energies, as shown in Figure 1.9b.

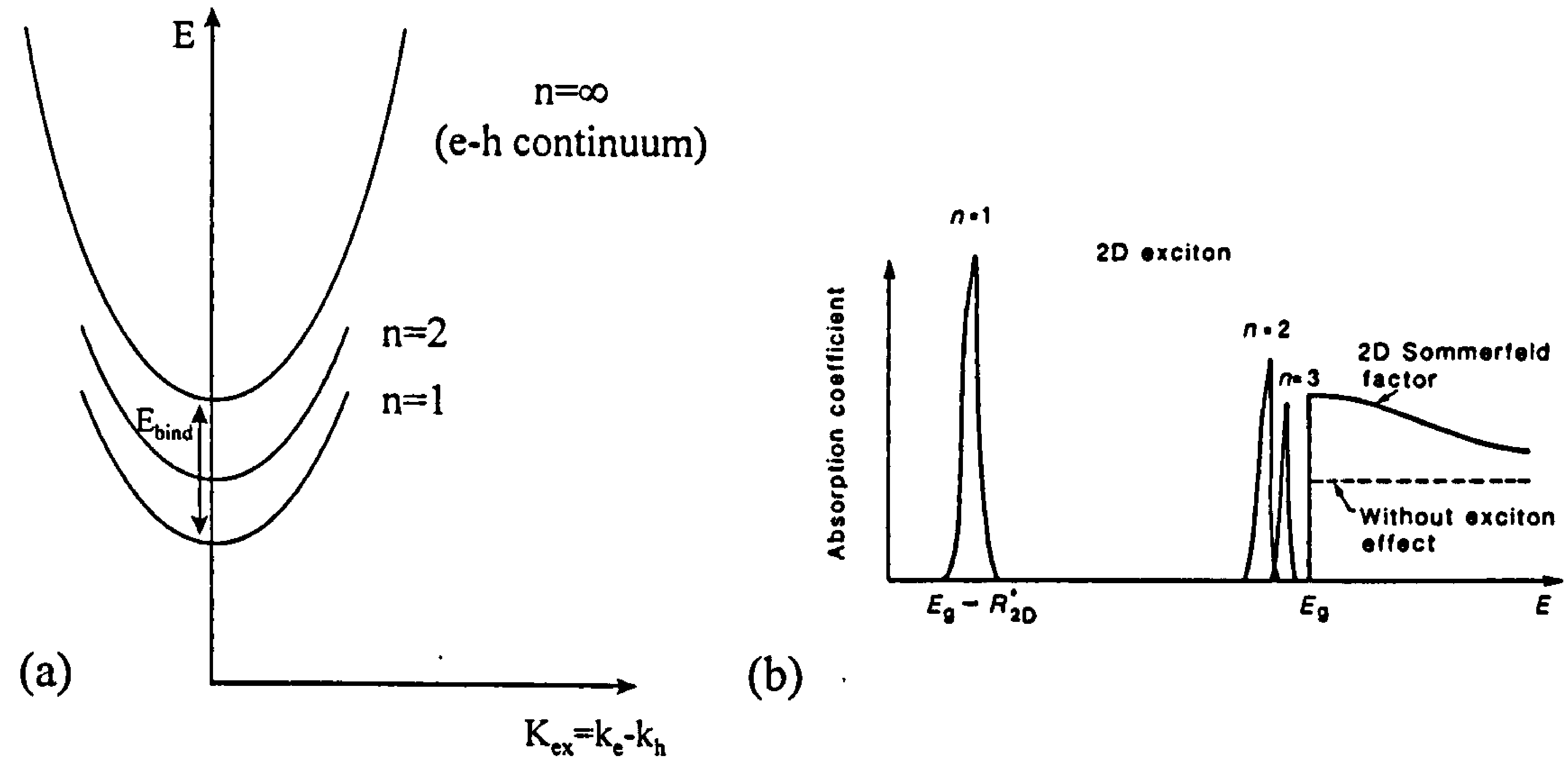

Figure 1.9 (a) The ground and first excited states of an exciton shown in relation to the free carrier continuum states. (b) The absorption spectra for a 2D system, showing the modification to the density of states expected when excitonic effects are included.[2]

In a bulk semiconductor the exciton binding energy typically has a value of ~ 4meV.[21] A reduction in the dimensionality to 2D is predicted to enhance this by a factor of 4 due to the increased overlap of the electron and hole wavefunctions.[2] In practice penetration of the wavefunctions into the barriers, due to the finite barrier height, means that this overlap is reduced and typically observed quantum well exciton binding energies are therefore smaller (~10meV)[2] than that predicted for a true 2D system. In a quantum wire or a quantum dot, the exciton binding energy is expected to show a further increase as a result of the reduced dimensionality. For example, in InAs self-organised quantum dots the exciton binding energy has been predicted to increase from 1meV in the bulk to 20meV in the dot.[22]

The main advantage of a larger exciton binding energy is that excitons still exist at high temperatures, in contrast to bulk semiconductors where excitonic ionisation by phonons at room temperature generally occurs.[2] Hence devices that exploit the properties of excitons, such as optical switches and optical modulators, can be operated at room temperatures. Excitons are useful because they provide a high contrast absorption ratio at the band edge, which is advantageous for modulators based on the quantum confined Stark effect (QCSE).[2] The carrier confinement is also beneficial as it prevents the field ionisation of the exciton which occurs in a bulk semiconductor. In addition, the exciton can be quenched by the introduction of free carriers or additional excitons into the structure by absorption. This quenching occurs because the Coulomb interaction between the electron and hole is effectively screened by the new carriers. The absorption at the exciton energy will hence decrease as the power of the laser beam probing the absorption increases, increasing the number of electron hole pairs created and quenching the excitons. Non-linear absorption therefore occurs and this is the basis for many non-linear optical and device applications.[2]

1.3.4 Carrier Relaxation in Semiconductors

In general luminescence observed from direct bandgap semiconductors occurs when carriers recombine across the bandgap from states that are close to **k**=0, i.e. at the zone centre. The photons observed therefore have an energy, $E_{photon}=E_g-E_{bind}$, where E_g is the bandgap of the semiconductor and E_{bind} is the binding energy of the exciton. Energy terms due to the quantum confinement of carriers can be added to this expression for low dimensional semiconductor structures. However, direct vertical transitions (Δ**k**=0) can occur from states away from the zone centre when a photon having an energy $E_{photon}>E_g$ is absorbed. In this case electrons and holes are created in high energy states in the conduction and valence bands and to recombine radiatively these carriers generally relax, losing both momentum and energy, to the edges of their respective bands. Alternatively, in electro-optical devices carriers are injected electrically into the barrier material where they diffuse and are captured, for example, by a quantum well. At the point of capture the carriers have excess energy and momentum and must relax to the lowest state in the quantum well before they can participate in the optical process.

The mechanism by which carriers relax usually involves the emission of a phonon (lattice vibration) which allows some of the momentum and energy of the carrier to be lost. An LO phonon in GaAs can transfer 36meV of energy with a range of momentum transfer, although $\Delta k=0$ is the most efficient (the probability varies as $1/\Delta k^2$).[23] Because of the polar nature of GaAs, carrier interactions with LO phonons is very strong and hence the emission time for a single LO phonon emission is very fast (170fs).[5] Acoustic phonons (LA and TA) have smaller energies than the LO phonon and their interaction with carriers is weaker so relaxation by acoustic phonon emission occurs on a timescale at least an order of magnitude slower than for LO phonons.[23] Acoustic phonon mediated relaxation therefore becomes important when the carriers are close to bottom of the band (when $\Delta E<\hbar\omega_{LO,}$ where $\hbar\omega_{LO}$ is the LO phonon energy). Figure 1.10a shows schematically carrier relaxation by LO phonon emission. In a quantum well carriers can be injected or absorbed into excited subbands. In this case inter-subband relaxation must occur if the carrier is to reach the bottom of the ground state subband and recombine. A phonon can be emitted in this process, resulting in the transfer of the carrier from the excited subband to a lower energy excited or ground state subband. In a quantum wire the subband structure is similar to a quantum well so the relaxation mechanisms are the same. However, as is described in the following section, the situation in a quantum dot is very different.

1.3.4.1 The Phonon Bottleneck in Quantum Dots

Efficient carrier relaxation by LO phonon emission is a process that may not be possible in a quantum dot. Because the energy levels are discrete and do not consist of subbands of states, carrier relaxation by single LO phonon emission will only be possible if the energy level spacings are equal to the phonon energy, a highly unlikely occurrence. In structures of higher dimensionality, a continuum of states essentially exists and carriers are able to relax by emitting a cascade of single LO phonons (see previous section). This restriction imposed on efficient carrier relaxation by LO phonon emission in quantum dots is known as the 'phonon bottleneck'[24] and the diagram in Figure 1.10 shows a schematic representation of the phonon bottleneck in quantum dots. It has been suggested that the performance of devices utilising quantum dots may be impaired as a result of this effect because fast carrier relaxation to the ground state, a prime requirement for laser devices, may be inhibited. Other carrier relaxation mechanisms may therefore become important in quantum dots, for example emission of multiple phonons[25] and Auger mediated relaxation.[26] These mechanisms are discussed in detail in Chapter 7.

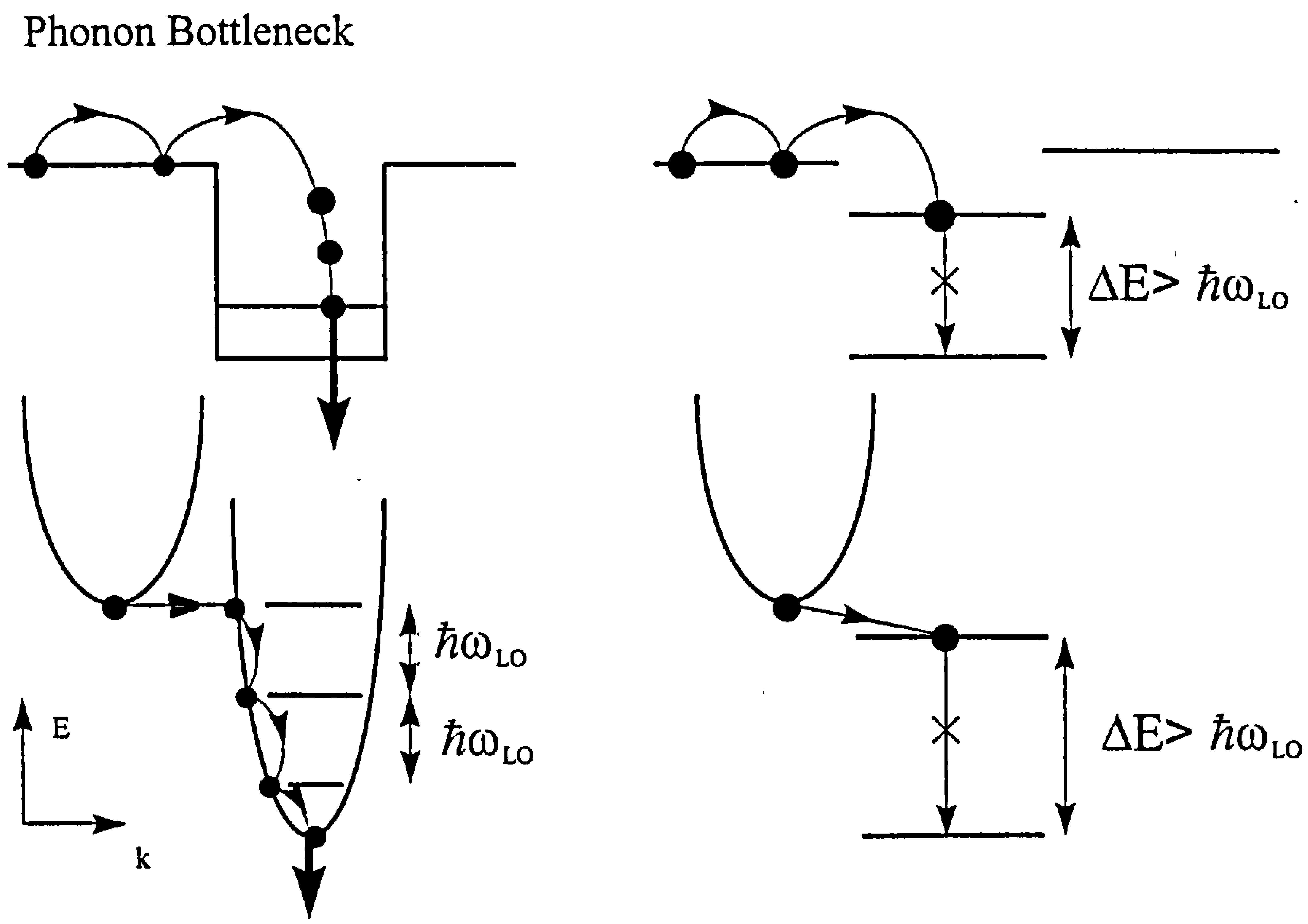

(a) Quantum Well (b) Quantum Dot

Figure 1.10 The Phonon Bottleneck in Quantum dots. (a) In a quantum well carrier relaxation can occur via the emission of LO phonons due to the continuum of states within each subband. (b) In a quantum dot this efficient relaxation mechanism is inhibited if the energy level spacing does not equal the LO phonon energy.

1.4 Outline of Thesis

The rest of the work contained in this thesis describes the optical and structural characterisation performed on III-V semiconductor quantum wires and quantum dots fabricated by the EPSRC Central Facility for III-V Semiconductors, Sheffield.

Chapter 2 contains a brief description of some of the techniques that have been employed by other groups to fabricate quantum wires and quantum dots. This is followed by a more detailed description of the growth mechanisms that lie behind the growth of GaAs/AlGaAs V-groove quantum wires and InAs/GaAs self-organised growth of GaAs/AlGaAs V-groove quantum wires and InAs/GaAs self-organised quantum dots that are the subject of the investigations in the present thesis.

In Chapter 3 the various experimental techniques of photoluminescence, photoluminescence excitation, electroluminescence and cathodoluminescence are described. These are the techniques used to investigate the optical properties of quantum wires and quantum dots. Also, a description of the micro-focusing, photoluminescence set-up, used extensively in the present thesis is presented.

Chapters 4 and 5 contain the experimental results obtained from the optical and structural investigations performed on GaAs/AlGaAs V-groove quantum wires. Chapter 4 deals mainly with the structural characterisation of quantum wires and the optimisation procedure used to obtain quantum wires with good optical properties, suitable for the detailed optical investigations described in Chapter 5.

Chapters 6 and 7 contain the experimental results obtained from the optical and structural investigations performed on InAs/GaAs self-organised quantum dots. Chapter 6 contains details of the growth investigations performed to obtain quantum dots and also describes the structural analysis by Transmission Electron Microscopy. An optical study by photoluminescence is also described. Chapter 7 contains details of optical investigations by selectively excited photoluminescence and photoluminescence excitation spectroscopy. These techniques provide information on the carrier relaxation mechanisms that occur in self-organised quantum dots.

1.5 References

[1] M.H. Brodsky, Sci. Amer., **Feb**, 56, (1990).

[2] M.J. Kelly in 'Low Dimensional Semiconductors Materials, Physics, Technology, Devices', Clarendon Press, Oxford, (1995).

[3] R. Nötzel, Semi. Cond. Sci. Tech., **11**, 1365, (1996).

[4] C. Weisbuch and B. Vinter in '*Quantum Semiconductor Structures*', Academic Press, New York, (1991).

[6] S.M. Sze, in '*Physics of Semiconductor Devices*', 2nd Edition, Wiley, (1981).

[7] J.R. Chelikowsky, M.L. Cohen, Phys. Rev. B **14**, 556, (1976).

[8] A.I.M. Rae, Quantum Mechanics 2nd Ed. Adam Hilger, (1990).

[9] J. Luttinger, and W. Kohn, Phys. Rev. **97**, 869, (1955).

[10] N. Holonyak. Jr., R. M. Kolbas, R.D. Dupuis and P.D. Dapkus, IEEE J. Quan. Elec. **QE-16**, 170, (1980).

[11] D.A.B. Miller, D.S. Chemla, T.C. Damen, A.C. Gossard, W. Weigmann, T.H. Wood and C.A. Burrus, Appl. Phys. Lett. **45**, (1), 13, (1984).

[12] K. Von Klitzing, G. Dorda, M. Pepper, Phys. Rev. Letts. **45**, 494, (1980).

[13] Y.Arakawa and H. Sakaki, Appl. Phys. Lett. **40**, (11), p 939 (1982).

[14] K.Shum, J. Appl. Phys., **69**, (9), 6484, (1991).

[15] A. Wois and P. Hawrylak, Phys. Rev. B **51**, 10880, (1995).

[16] Y. Arakawa, K. Vahala, A. Yariv and K. Lau, Appl. Phys. Lett. **48**, (6), 384, (1986).

[17] Y. Arakawa, K. Vahala, A. Yariv, and K. Lau, Appl. Phys. Lett. **47**, (11), 1142, (1985).

[18] L.A. Coldren and S.W. Corzine in 'Diode Lasers and Photonic Integrated Circuits' Wiley, (1995).

[19] E. Kapon, Proc. of the IEEE, **80**, (3), 398, (1992).

[20] E. Kapon, Optoelectronics, **8**, (4), 429, (1993).

[21] J. Singh, '*Physics of Semiconductors and their Heterostructures*'. McGraw Hill International (1993).

[22] M. Grundmann, O. Stier, D. Bimberg, Phys. Rev. B **52**, (16), 11969, (1995).

[23] J.J. Finley, PhD Thesis, University of Sheffield (1997).

[24] H. Bensity, C.M. Sotomayor-Torrès and C. Weisbuch, Phys. Rev. B **44**, (19), 10945, (1991).

[25] R. Heitz, M. Grundmann, N.N. Ledentsov, L. Eckey, M. Veit, D. Bimberg, V.M Ustinov, A. Yu. Egorov, A.E. Zhukov, P.S. Kop'eV, and Zh. I. Alferov, Appl. Phys. Lett. **68**, (3), 361, (1996).

[26] U. Bockelmann and T. Egeler, Phys. Rev. B **46**, (23), 15574, (1992).

Chapter 2

Growth of Quantum Wires and Quantum Dots

2.1 Introduction

As has been briefly discussed in the previous chapter, quantum wires and quantum dots exhibit a number of properties which are advantageous for electro-optical device applications. However, unlike quantum wells, their successful fabrication is not straightforward. Numerous attempts have been made to manufacture quantum wires and quantum dots, with varying degrees of success.[1,2,3] In this chapter some of the methods that have been employed by various research groups will be briefly described. This is followed by a more detailed description of the methods we have used to make the quantum wires and quantum dots which are the subject of investigation in this thesis.

Whilst discussing these various techniques it is useful to keep in mind the properties that quantum wires and dots should exhibit if they are to be used for device applications. Five main requirements can be identified: high optical quality, confinement of both electrons and holes, large energy level spacings ($\gg kT$), high size and shape uniformity and large densities.

2.2 Description of Current Wire and Dot Fabrication Techniques

2.2.1 Lateral Confinement with a Magnetic Field

Early investigations into the properties of 1D systems were performed by confining electrons in two dimensions by using a strong magnetic field (~20T).[4] This causes the electrons to move in cyclotron orbits, quantised into Landau levels with spacings of $\hbar\omega_c$ (where $\omega_c = eB/m^*$, the cyclotron frequency), leading to a one dimensional density of states which is similar to that of a quantum wire. Experiments performed on AlGaAs double-heterostructure lasers showed enhancements in the modulation bandwidth[5] and a reduction of the spectral linewidth,[6] in agreement with predictions made for quantum wire behaviour.[4] Confining electrons in the same way, but using quantum wells instead of bulk material, simulates the properties of a quantum dot. It should be noted that these experiments only simulate quantum wires and quantum dots. In reality the subband separations in actual dot or wire structures are not equally spaced like $\hbar\omega_c$, but by values that depend on the dimensions of the structures and the confining potential. Although these magnetic field experiments served to test the theoretical predictions of reduced dimensionality in semiconductors, they do not provide a practical means of utilising wire or dot behaviour in electro-optical devices.[7]

2.2.2 Etching and Regrowth

Quantum wires and quantum dots have been fabricated by patterning lithographically nano-meter scale features onto an existing planar quantum well structure. The small scale patterns required can be defined by electron beam lithography, and etched either chemically (see Section 2.3.1) or by Reactive Ion Beam techniques.[8] In some cases the resulting nano-structures are overgrown during a second growth step. The main problem with this technique arise from the surface damage that occurs as a result of the destructive etching process. This damage can extend deep into the structure, providing non-radiative recombination sites that significantly reduce the optical efficiency of the quantum wires or quantum dots formed and this can prevent the size being reduced to a point where quantum effects are significant.[9] InGaAs/InP quantum wires have been fabricated using etching techniques with feature sizes down to 10nm. However size fluctuations are thought to prevent true 1D behaviour.[10] Given these potential problems it appears that direct etching techniques are not a practical proposition for device fabrication.

2.2.3 Etched Stressor Wires and Dots

The major disadvantage of directly etched wires and dots is the high resultant surface damage which, in the worse case, can destroy the optical efficiency of the structure. This problem can be reduced if the etched region can be kept separate from the optically active region. In stressor wires and dots a quantum well is grown close to the surface of the sample, which is then coated with a thin layer of a non-semiconductor material, typically carbon[11] or tungsten.[12] The carbon layer is stressed due to it having a different lattice constant compared to the underlying semiconductor. The surface is next patterned using standard lithographical techniques and etched to a depth which passes through the carbon but does not penetrate the semiconductor as far as the quantum well. The resultant isolated islands (for dots) or stripes (for wires) of carbon, which are known as stressors, are now able to relax laterally and consequently produce a strain field in the semiconductor immediately below them. If this strain field is of the correct sign then the resultant strain modulation of the quantum well band gap produces a lowering of the conduction band and a rise in the valence band edges, resulting in carrier localisation at this point. It is this localised strain reduction of the quantum well band gap which produces the dot or wire. Because of the highly non-uniform strain field the effective size of the dot or wire is smaller than that of the etched stressor. Although post-growth etching has been performed, it is spatially separate from the wires or dots and hence the effect of any surface damage is limited. The main disadvantage of this technique is that the strain modulation of the quantum well band gap is relatively weak, resulting in weak carrier confinement potentials and hence small energy level spacings in the wires or dots. Hence, although this technique allows the study of physics in 1D and 0D systems it is probably not suitable for device applications.

2.2.4 Electrostatically Defined Dots and Wires

In this technique a metallic Schottky contact is deposited on the surface of a structure which generally contains a single quantum well. By applying a suitable voltage to the gate, an electric field is produced which extends into the semiconductor. This field modulates the band structure of the quantum well and, for suitable shaped metallic contacts, either a quantum wire or dot may be formed. An advantage of this technique is that, due to the lateral spread of the electric field, the resultant dots or wires can be significantly smaller than the physical gate structure on the sample surface. An example is the so-called 'split-gate' where a wire is formed below the gap between two gates, the size of the wire, which can be controlled by the size of the electric field, being significantly smaller than the physical gap between the gates.[13] The disadvantages of this technique is that, because of the relatively large size and small confinement potential of the dots and wires, they have very closely spaced energy levels. In addition, the electric field modulates the valence and conduction band edges in the same sense so that only electrons or holes are confined. This latter property makes these structures unsuitable for electro-optical device applications.

2.2.5 Growth on Non Planar Substrates

2.2.5.1 Fractional Layer Superlattices

Quantum wires have been formed by growing alternate 1/2 mono-layers of AlAs and GaAs on vicinal surfaces. The (001) substrates are typically 2° off axis, this results in steps of 1ML height and terrace lengths of ~8nm. If quantum wires are to be formed on these substrates then very careful control of the growth conditions is essential. The growth mechanism relies on being in the regime where growth occurs on the step edges and proceeds across the surface without the formation of isolated islands on the step terraces as shown in Figure 2.1a. In Figure 2.1b 1/2ML of GaAs is grown followed by 1/2ML of AlAs (Figure 2.1c) and this pattern is repeated until a quantum wire of the required height is formed (Figure 2.1d). The wire is then capped with AlGaAs. Growth of these Fractional Layer Superlattices has been achieved by both MBE[14] and MOVPE.[15] In order that high quality wires are produced, the surface needs to be prepared so that the steps have equal length. This can be achieved, to some extent, by growing an initial buffer layer which can be monitored by RHEED in MBE; growth commencing when the steps are of uniform size and distribution. A polarisation anisotropy has been observed in the PL and absorption spectra of these structures, for polarisation $\perp$ and $\parallel$ to the wires, and this has been taken as evidence of the lateral confinement of the carriers.[16]

The final quality of these fractional layer superlattices is obviously very high if the growth can be controlled to the required tolerance. In particular there is no post growth processing damage of the structure and impurity incorporation is minimised. However, the growth sequence is very complicated and also very slow, suggesting that this technique is not suitable for mass device production, even if the necessary growth control can be achieved.

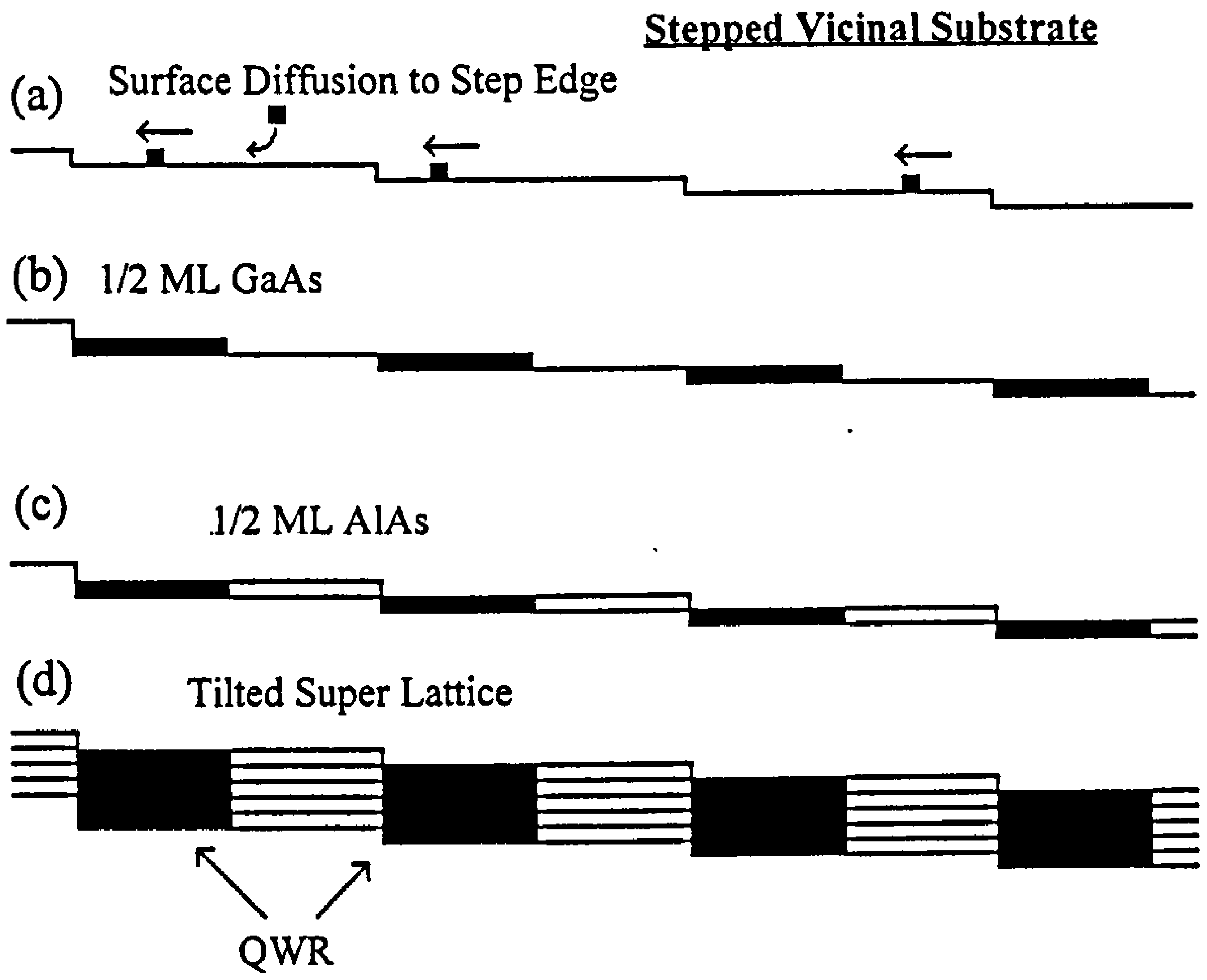

Figure 2.1 Schematic diagram showing the growth of fractional layer superlattice quantum wires on Vicinal Substrates.

2.2.5.2 Patterned Vicinal Surfaces

This technique involves the lithography and etching of off-axis, ~6° (001), GaAs substrates to produce periodic corrugations along the $[0\bar{1}1]$ direction. The subsequent overgrowth with AlGaAs by MOVPE results in the formation of stable (001) facets having a regular step density with the periodicity of the original grooves. This technique hence provides a controllable method for forming quantum wires of a specified density. Growth of GaAs results in enhanced growth at the step edges, Figure 2.2, thus forming a quantum wire in these regions with connecting quantum wells on the (001) facets.[17]

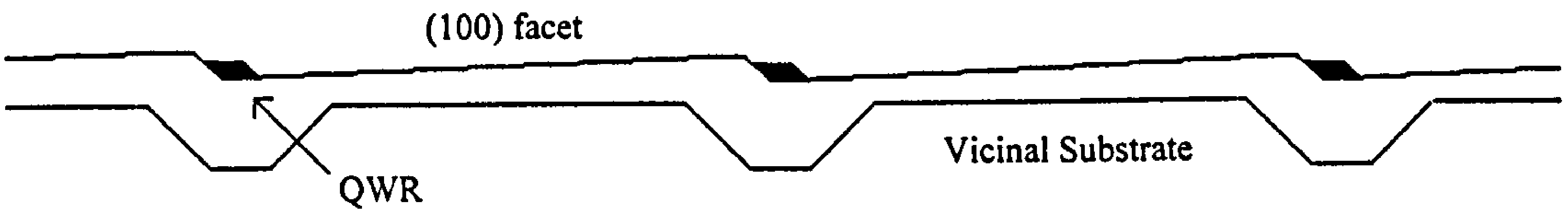

Figure 2.2 Quantum wires grown on a patterned Vicinal Substrate.

2.2.5.3 Ridge Grown Quantum Wires

Patterned (001) GaAs substrates, with reverse mesa etched stripes running along the [110] direction, have been used to form very sharp, narrow ridges ~10nm, following the growth of GaAs.[18,19]

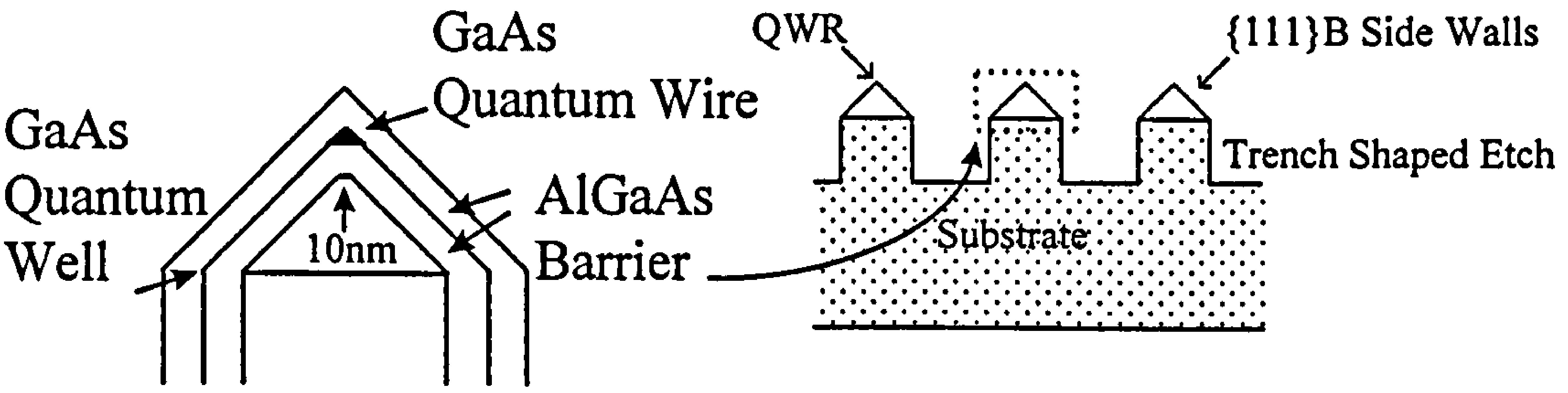

Figure 2.3 Ridge grown quantum wires.

The (111)B side walls of the ridge grow at a much lower rate than the (001) top, thus narrowing the ridge. The sharpness of the ridge top is a function of the growth mechanism and is therefore independent of the uniformity of the substrate pattern, a key advantage of this process. A 10nm AlGaAs cladding layer is grown on top of the resultant structure shown in Figure 2.3. This follows the existing pattern, maintaining the profile of the ridge. GaAs is next deposited and grows preferentially on the apex of the ridge to form the quantum wire. Quantum wells also form on the side walls and the base of the trenches. The optical spectra of these structures appear very good with a spectrally isolated wire emission. Hence this technique appears to be very promising for the fabrication of small (18×9nm), high quality quantum wires.

2.3 The V-Groove Method for Growing Quantum Wires

The V-groove method for growing quantum wires is the technique used to create the quantum wires studied in this thesis. This technique has many advantages compared to the other quantum wire fabrication methods. Similar to growth on vicinal substrates[15] it provides a method whereby quantum wires can be formed in a one-step, in-situ growth run, without the need for post-growth processing. This removes the possibility of inducing damage into the wire, which can potentially destroy its optical properties.

The V-groove technique was first used by Kapon *et al.*[20] and has lead to the fabrication of quantum wire lasers with very low threshold currents of 0.6mA.[21] Briefly, the technique involves growing an AlGaAs buffer layer on an etched V-Groove substrate. This tends to sharpen the V as the Al species has a small diffusion length on the (111)A facets of the side walls. The AlGaAs growth is followed by growth of a quantum well of GaAs. Differences in the diffusion lengths of Ga on (111)A and (001) facets cause Ga to diffuse to the base of the grooves and form a crescent shaped quantum well. The lateral tapering of this well provides confinement for carriers in a second dimension, leading to the formation of a quantum wire.

The preparation of quantum wires by the V-Groove technique is a two stage process. The first stage involves patterning the substrates by photo-lithography and, by using an anisotropic wet chemical etch, the formation of a saw-tooth shaped surface profile results. The second stage involves the epitaxial growth of a quantum well on the patterned substrate using the growth technique Metal-Organic Vapour Phase Epitaxy, (MOVPE).

2.3.1 Etching the Substrates: The Formation of the V-Grooves

The substrates used in our experiments were (001) n^+ GaAs, with exact (001) giving the best results (see chapter 4). Whole wafers were used for most of the samples described in this thesis as it was found in the course of our investigations that the most uniform growth occurred on fully patterned wafers. To pattern the substrate photo-resist, a chemical that reacts when exposed to ultra-violet light, is dropped onto the surface of the substrate which is then spun at high speed to form a thin uniform layer of resist, any excess photo-resist is spun off.

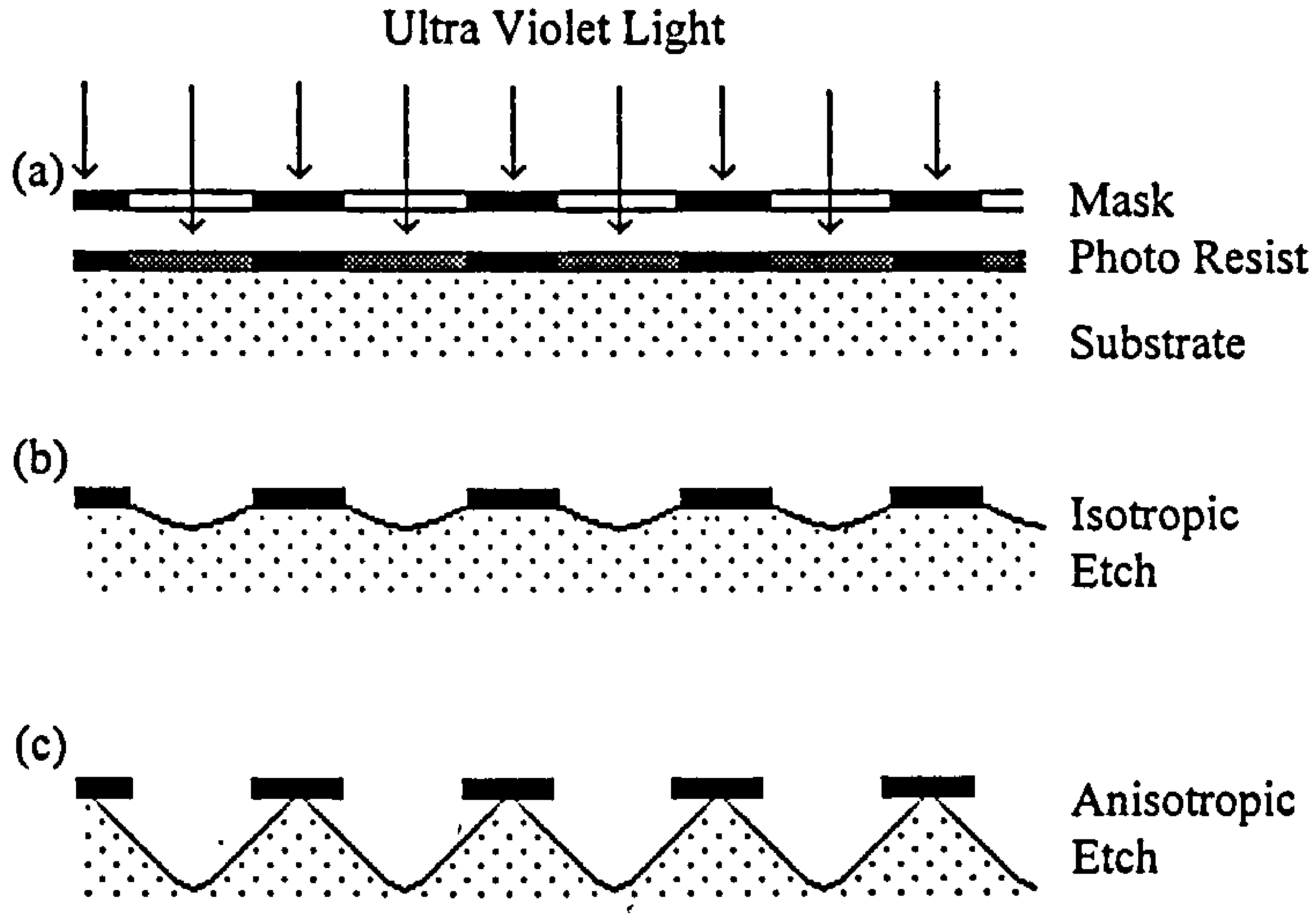

Figure 2.4 Three stages of the Etching Process. (a) Patterning of the mask, (b) Isotropic etch, (c) Anisotropic etch forming the V-Grooves.

The substrates are then mounted below a mask which has been patterned with lines spaced at the required groove pitch. Our initial experiments used masks with line spacings of 4 or 8 μm. The lines on the mask are aligned so that they lie parallel to the $[01\bar{1}]$ crystallographic direction of the wafer. Ultra-Violet light is then shone through the mask onto the substrate, exposing only thin lines of resist, Figure 2.4a. The UV light changes the structure of the resist in these exposed areas. The substrate is then rinsed for ~60s. in a developing solution, this is an alkaline solution which cleans off the exposed areas of resist. A short, 3s. dip in HCl de-oxidises the surface. The wafers are then etched through the photo-resist pattern for 10s. in a solution of HBr : CH_3COOH : $K_2Cr_2O_7$ in the proportion (1:1:1). This is an isotropic etch which attacks all crystal planes at similar rates, leaving shallow U-shaped valleys between the areas of resist, Figure 2.4b. The wafers are next rinsed twice in de-ionised water and then etched in a (1:8:40) solution of H_2SO_4 : H_2O_2 (30%) : H_2O. This etch is a selective etch which tends to preferentially etch (001) planes faster than (111) planes. The use of a selective etch means that at the resist windows etching will occur down into the substrate, any lateral etching which would tend to undercut the resist, is much slower. Because of the different (001) and (111) etch rates, a V-shaped groove, formed by the intersection of two (111)A planes, is produced, Figure 2.4c. The etching time depends on the mask used, the 8μm pitch samples were etched for 4.5 mins. and the 4μm for 2.5 mins. The substrates are again rinsed twice in de-ionised water and the photoresist is removed with acetone. Finally the substrates are rinsed in isopropyl alcohol and de-ionised water and are blown dry with inert nitrogen. At this point they are ready to be loaded into the MOVPE reactor.

2.3.2 Growth on V-Groove Substrates by MOVPE

MOVPE is one of the primary epitaxial growth techniques used to fabricate III-V semiconductors. For the growth of GaAs/AlGaAs semiconductors the Group III chemical precursors are Tri-Methyl Gallium (TMGa) and Tri-Methyl Aluminium (TMAl). The Group-V element, arsenic, is derived from the gas arsine, (AsH_3). The growth process depends on the reaction between the metal-organic compounds and arsine, with the growth of GaAs/AlGaAs semiconductors utilising the following reactions.[22]

$$Ga(CH_3)_3 + AsH_3 \rightarrow GaAs + 3CH_4$$

$$Al(CH_3)_3 + AsH_3 \rightarrow AlAs + 3CH_4$$

The reactor used to grow the quantum wire structures studied in this thesis is a horizontal flow type, operating at a pressure of 920 torr. A schematic diagram of the reactor is shown in Figure 2.5. The substrate is loaded into the reactor and baked under a high arsine over-pressure. This deoxidises the surface to make it ready for growth, the arsine over-pressure preventing decomposition of the substrate. Heating is induced with an r.f. coil, the temperatures used are typically in the range from 600°C - 750°C. The Group-III chemical precursors are in a liquid form. H_2 is passed through their containers which cause them to vaporise and mix with the H_2 carrier gas. The gas flow rate is controlled by automated valves which allow the passage of the required volume of gas. The gases are transported to the reactor cell which consists of a quartz tube inside of which is the heated substrate. As the gases pass over the substrate they react and the desired semiconductor grows epitaxially. The gas reaction process can be summarised into four stages.

1. Gas flow over the substrate is assumed to be ideal laminar flow. Hence, at the substrate boundary it is assumed that there is no gas flow (stagnant layer) so the reactants are transported to the surface of the substrate by diffusion.

2. The temperature of the substrate causes the reactants to decompose on the surface where the reactions take place.

3. Surface diffusion of the decomposed elements occurs until favourable bonding sites are found on the substrate and the elements are incorporated into the growing layer.

4. Finally, the by-products of the reaction, the methane and hydrogen carrier gas are removed from the reactor.

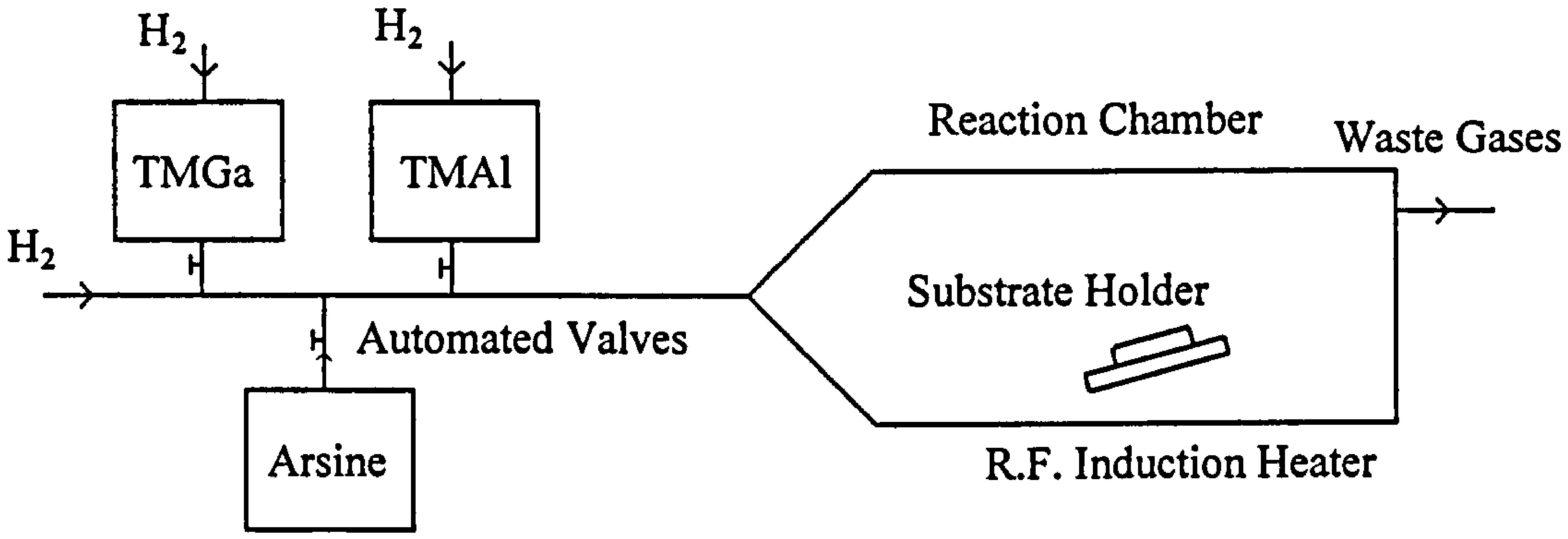

Figure 2.5 Schematic diagram of an MOVPE reactor.

By varying the relative proportions of the TMGa and TMAl precursors AlGaAs of different compositions can be grown. Generally materials are grown with a high arsine over-pressure as this ensures that arsenic quickly incorporates itself into the layer providing As bonds for the Ga^+ or Al^+ to attach themselves to. This prevents the desorption of the grown layer by the loss of the Group-III elements which could occur due to the high temperature of the substrate.

Growth of quantum wires on a V-groove substrate does not require any particularly special conditions for growth, although higher growth temperatures lead to a greater selectivity in the growth of GaAs and AlGaAs on different surfaces which is a crucial factor for the formation of the quantum wires.[23] Higher temperature growth does, however, lead to carbon incorporation into the layers with an associated reduction in the quality of the material.[24]

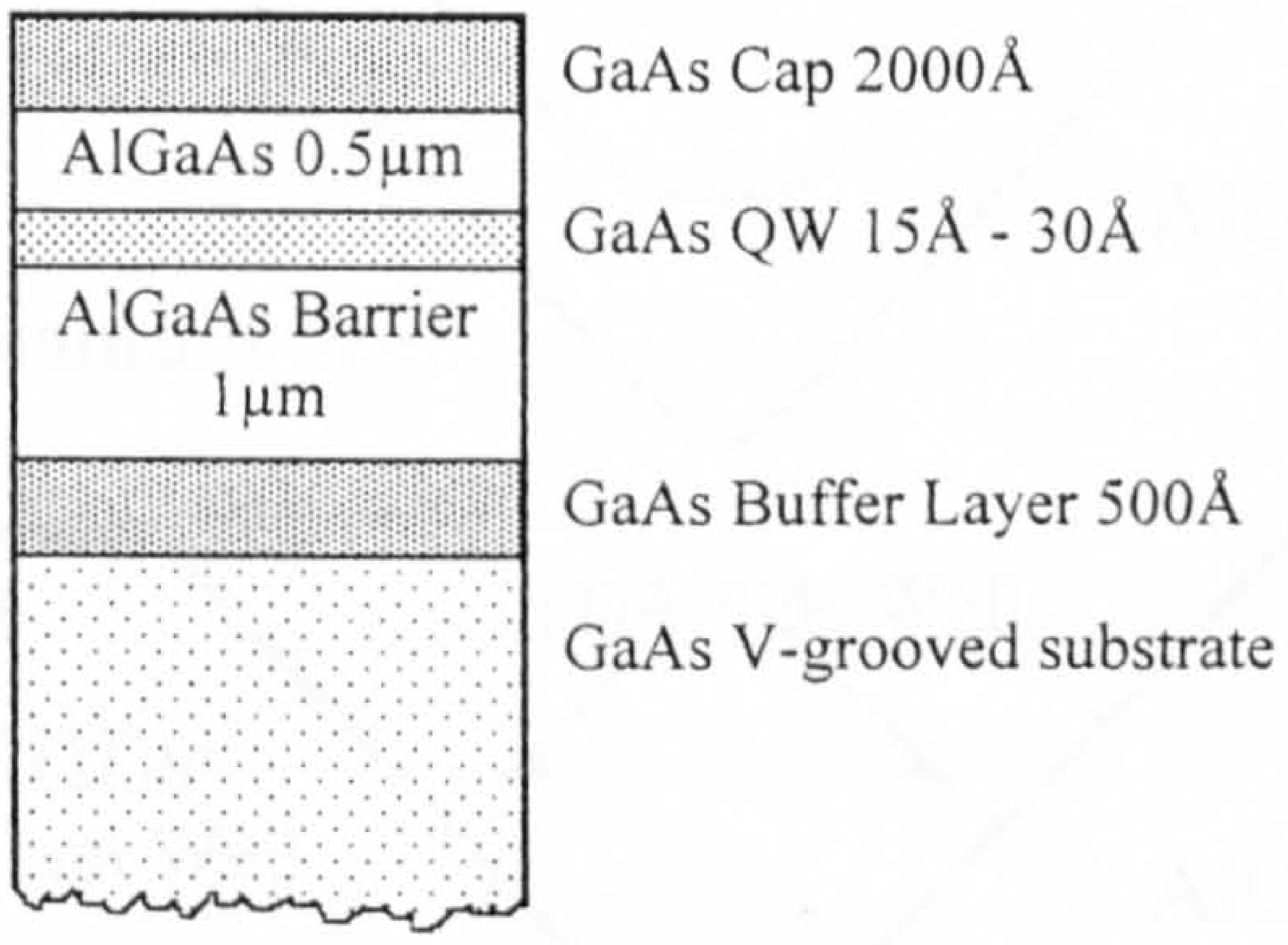

Figure 2.6 Typical growth structure of a quantum wire grown on a V-groove patterned substrate.

A schematic diagram of a typical V-groove structure is shown in Figure 2.6. A GaAs buffer layer is grown, followed by an AlGaAs cladding layer and the thin GaAs quantum well which forms the quantum wire. The wire is overgrown by a second AlGaAs barrier and a GaAs cap to prevent oxidation of the aluminium containing layers.

2.3.3 Theory of the V-Groove Method for Producing Quantum Wires

The mechanism behind the growth of quantum wires on patterned substrates relies on differences in the growth rates on different crystallographic surfaces.[23] During the growth on patterned substrates the incoming atoms in the gas phase are presented with a series of (001) and (111)A planes. The atoms diffuse across these surfaces until they reach a site that is energetically favourable for them to bond to. Atoms involved in the growth have surface diffusion lengths which depend on the orientation of the crystal plane they are growing on. This is because the arrangement of atoms on a given plane is different, so the density of bonding sites and hence the availability for bonding on the surface is different. For V-groove patterned substrates, the side walls have a (111)A orientation whilst the tops and base of the grooves expose (001) facets. A curved (001)-like surface is formed at the base of the groove as a result of the fact that the two

(111)A side walls formed by the original etching do not intersect sharply, but form a smooth, circular base, as shown in Figure 2.7.

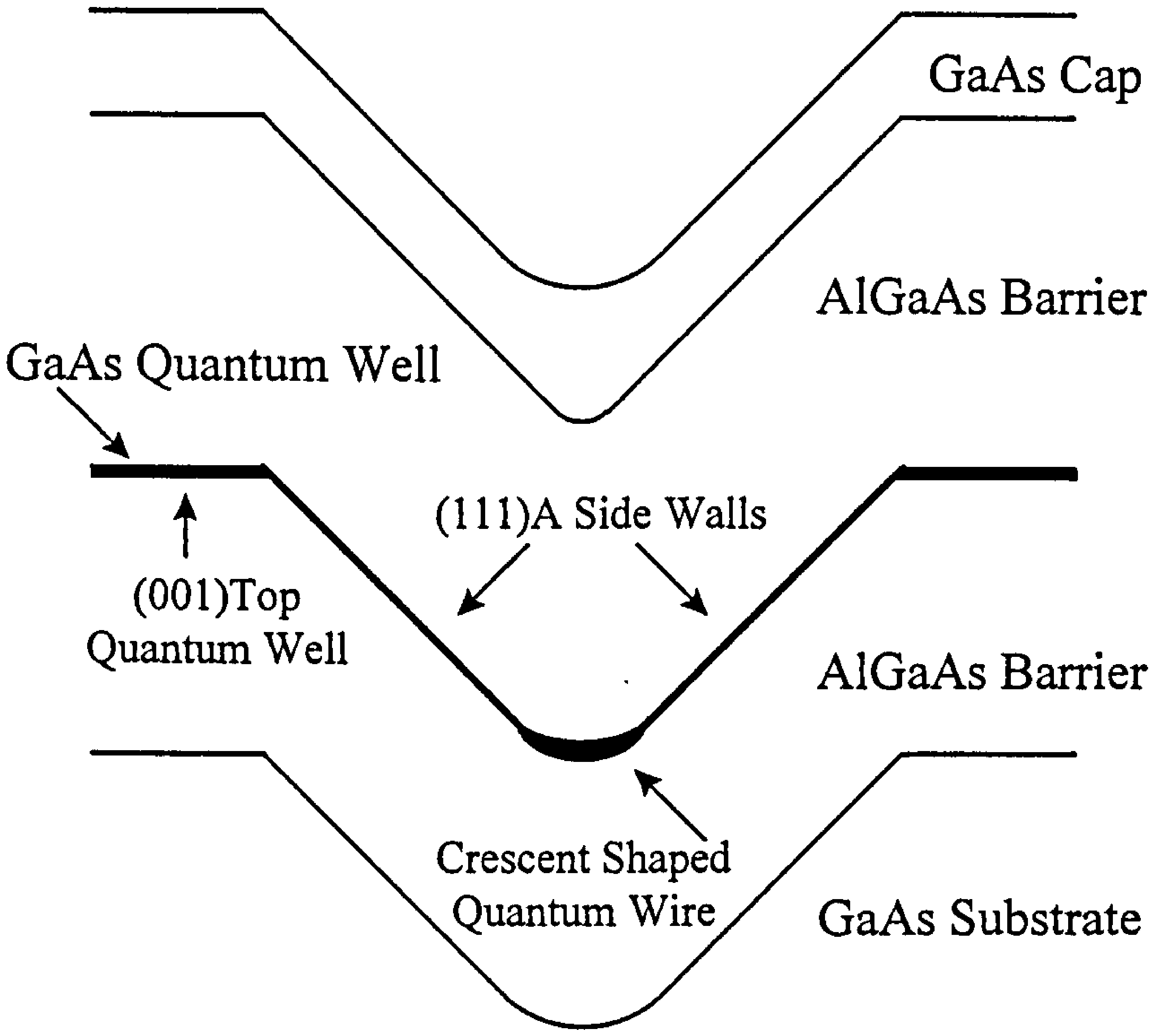

Figure 2.7 Diagram showing the resultant shape of the quantum well grown on a V-Groove substrate. Note the enhanced GaAs growth at the bottom of the groove which tends to planarise the base, resulting in a crescent shaped quantum wire. There is less GaAs growth on the side walls.

The growth rate of GaAs is faster on (001) planes than (111)A, this means that the thicknesses of layers grown on these two surfaces are unequal. This results in thicker deposits forming on the (001) planes. Conversely growth of AlGaAs on (111)A is faster than that on (001) and this has the effect of sharpening the base of the groove by reducing the radius of curvature at the base. The actual degree of sharpening depends on the aluminium composition of the grown layer.[25]

These growth properties are exploited to obtain a GaAs quantum well at the bottom of the groove, which has a lateral thickness variation. This results in carrier confinement in this lateral dimension. Growth of the first AlGaAs cladding layer sharpens up the groove leaving a template for the GaAs quantum well to form a quantum wire. The growth of the GaAs tends to planarise the grooves; migration of the gallium species to the bottom of the groove forces the (001) facet to widen and creep up the side walls, resulting in a crescent shaped quantum wire which tapers into the (111)A side wall quantum wells. The radius of curvature at the bottom of the groove is increased as a result of the GaAs growth. The AlGaAs cladding layer grown after the wire resharpens the groove profile, providing the possibility for the growth of a second GaAs quantum wire if required. It is therefore possible to grow a vertical stack of quantum wires in the groove, one of the major advantages of this technique.

The V-groove technique for quantum wire formation is not limited to MOVPE, growth by MBE[26] has also been demonstrated. In an interesting development, the formation of very sharp V-Grooves has been achieved when AlAs barriers have been grown by MBE,[27] which has an important bearing on the final lateral width of the quantum wire. Growth of quantum wires on V-Groove substrates has not been restricted to the GaAs/AlGaAs system; strained InGaAs/GaAs[28] and lattice matched InP/InGaAsP[29] quantum wires have also been fabricated. The later material system is very attractive as lasers can be fabricated with a lasing emission in the 1.3-1.55μm range, suitable for long distance optical communications.

2.3.4 Trench Buried Quantum Wires on V-Groove Substrates

Growth of AlAs on V-Groove substrates, having a pitch of 100nm and using suitable MOVPE growth conditions, results in the V shape transforming into a U shape with (110) side wall facets. This causes a narrowing of the trench down to ~20nm and depth ~30nm. Subsequent GaAs growth fills the trench, resulting in a quantum wire of these dimensions, which are small enough to provide strong carrier confinement. This technique, which is related to the more conventional V-groove technique studied in this thesis, is attractive because the size of the quantum wire can, to a certain degree, be tailored to the size required and the wire density can also be controlled. Recent results show there to be a PL anisotropy and blue shift of these wires, both of which are expected for a 1D system.[30,31]

2.4 Growth of Self Organised InAs/GaAs Quantum Dots

The quantum dots investigated in this thesis have been grown by Molecular Beam Epitaxy (MBE), employing a self-organised growth mechanism which relies on the large lattice mismatch between the two semiconductors used. This is a one stage process that involves no post- or pre-growth processing. However the results appear to be very sensitive to the growth conditions used (see chapter 6) and a wide range of conditions have been reported by various groups growing nominally identical structures.

2.4.1 MBE Growth

In an MBE reactor the substrate is held on a heated, rotating holder inside a chamber which is under ultra high vacuum, $\sim 10^{-10}$ Torr. Attached to the chamber are a series of Knudsen cells which contain the basic elements that are used in the growth. The cells are heated to a point where the elements evaporate, and a series of baffles result in the production of an atomic beam. Shutters, which are capable of switching in ~0.1s, are used to switch these beams on and off. The atomic beams impinge on the surface of the substrate where the epitaxial growth occurs. Growth rates are typically of the order of 1 monolayer per second, ($\equiv 3\text{Å}s^{-1}$) so the level of control over the growth provided by the shutter switching has essentially monolayer accuracy.[32]

2.4.2 Stranski-Krastanov Growth Mechanism

Normal MBE growth of unstrained layers proceeds with layer-by-layer growth in a two dimensional growth mode. Atoms which land on the growth surface diffuse laterally until an atomic site which is energetically favourable is found. At any point in time the growth surface will consist of a series of mono-layer steps and terraces. Atoms that find their way to a step edge will be easily incorporated as the energy needed to break all the bonds which exist at this point is generally high compared to the available thermal energy. A lower number of bonds are present on the terraces between the step edges making the incorporation of atoms here less likely. This growth selectivity at the step edges has the effect of keeping the growth surface flat to within a single monolayer.

When a material is grown that is lattice mismatched to the underlying layer(s) strain is introduced into the growing layer. Strain energy is stored in the layer and this can affect the growth process. As the system will always attempt to be in the lowest possible energy state the strain energy may be relieved by the formation of mis-fit dislocations if sufficient energy exists to form these dislocations. As the strain energy increases with increasing layer thickness, a critical thickness, which is a function of the material, the size of the strain and the substrate orientation, exists above which strain relaxation occurs by mis-fit dislocation formation.[33] These dislocations are essentially a disruption of the lattice periodicity and in semiconductor materials they are not desirable as they provide non-radiative recombination centres for free carriers, greatly reducing the luminescence efficiency of any device.

An alternative mechanism for strain relief in layers that are under compression is provided by the Stranski-Krastanov growth process.[34] This occurs when the growth mode changes from a 2D layer-by-layer mode to a 3D growth mode where coherent islands of material are formed on the surface. Plastic deformation of the islands reduces the strain energy although at the expense of an increased surface energy.[35] These islands can be dislocation free and may have a size of the order of the de Broglie wavelength for electrons and holes, giving rise to the possibility of strong carrier confinement in all three spatial dimensions.[36] This is the basis for the Stranski-Krastanov self-organised growth of quantum dots.

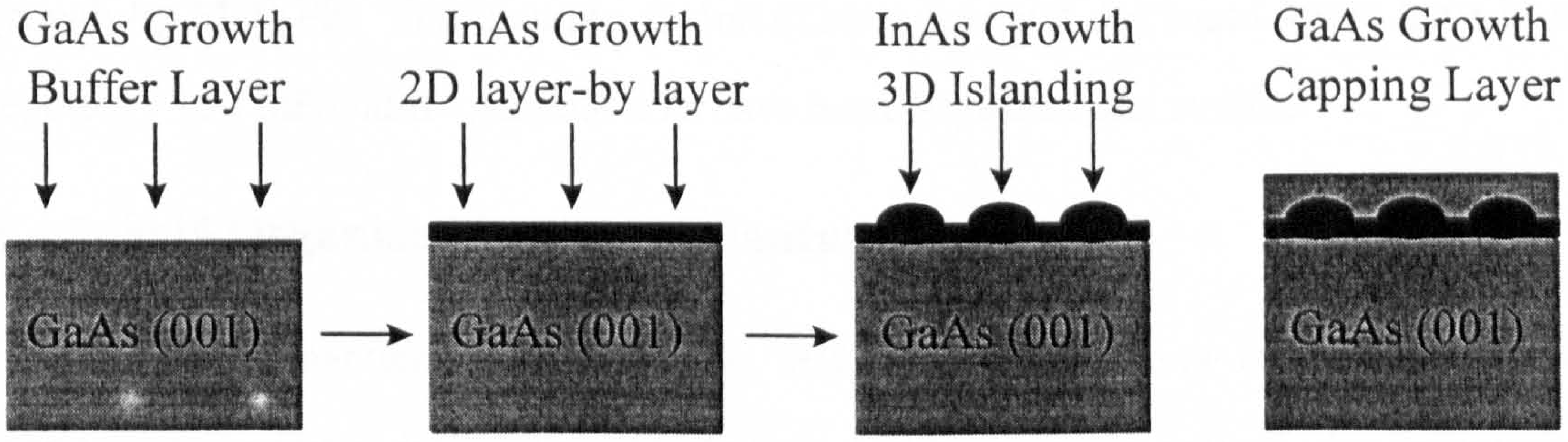

Figure 2.8 Schematic diagram of quantum dot formation utilising the Stranski-Krastanov growth mechanism. At first InAs grows in a 2D layer-by-layer mode, beyond a critical thickness 3D islanding occurs forming the dots.

Figure 2.8 shows a schematic diagram of the Stranski-Krastanov growth mechanism. The growth of the strained InAs material is initially 2D layer-by-layer and this forms a 2D quantum well wetting layer which underlies the quantum dots. Evidence for the existence of this 2D layer will be presented in Chapters 6 and 7. When the strain has built up to levels such that it is energetically unfavourable to continue 2D growth a transition to 3D growth occurs and the material on the surface begins to coalesce and form islands (quantum dots). The growth mode reverts back to 2D during the growth of the nominally unstrained GaAs cap which results in a rapid covering of the islands and normal 2D growth continues.

Self-organised quantum dots have been fabricated in several material systems, the main requirement being sufficiently large strain of the correct sign. The most commonly studied system is InAs/GaAs where there is a 7% lattice mis-match, resulting in islands which have a typical base size of ~10-25nm and heights of ~2-10nm,[37,38,39] the exact size and shape being dependent on the growth conditions used. Other material systems with less strain have resulted in larger dots, examples include GaInAs/GaAs,[40] InP/GaInP[41] and Si/Ge.[42] The quantum dots investigated in this thesis are InAs/GaAs where the InAs forms the dots and GaAs the confining material.

Although the majority of self-organised dots are grown by MBE, probably because of the low growth rates required and also because in MBE the 2D→3D transition can be monitored by RHEED (see chapter 6), there have been a few limited reports of their growth by MOVPE. For example, GaInAs/GaAs dots and dot based lasers have been reported[43] and InP/GaInP quantum dots have been fabricated and studied.[44]

2.4.3 Self-Organised Stressor Quantum Dots

Strain-induced quantum dots formed by self-organised stressors is a technique for fabricating quantum dots which employs a combination of two of the techniques described above.[45] Using this technique strain induced dots (see section 2.2.3) have been produced using the strain field which results from the growth of strained InP/GaAs self-organised islands close to an existing InGaAs/GaAs quantum well. The strain modulation of the quantum well creates a two-dimensional parabolic potential well which confines carriers in the other two dimensions. A quantum dot is hence formed. Excited state separations of ~20meV have been observed from these samples.[46]

2.5 Summary

To study the physics of quantum wires and quantum dots and to incorporate them into opto-electronic devices, they need to be formed with clean, damage free interfaces. This ensures that the non-radiative recombination of carriers is kept to a minimum, maintaining good optical efficiency. Techniques that involve etching a pregrown quantum well are inherently problematic as the resultant surface damage provides a high density of non-radiative recombination centres. Further contamination of the samples, particularly oxygen incorporation during growth is also a potential problem that needs to be minimised to ensure good quality growth. The accuracy required in the etching time and etch concentrations also needs to be very tightly controlled when aiming for reproducible results. These problems appear to make these methods impractical for the fabrication of high optical quality wires and dots.

In situ processes, which rely on pre-patterning a substrate to encourage preferential growth on certain planes, are very attractive. Full control of the resultant wire density, down to the limit of the lithography used, is possible. In addition, these techniques result in excellent interface quality. Devices can be grown which are removed from the original pattern and so any irregularities in the original etch are eliminated. As a consequence etch related damage in the active region is low and contamination is negligible, resulting in very high optical quality structures. The growth of quantum wires by the V-Groove method appears to be the most effective technique, with promising laser structures having been produced using this process.[25] The resultant wires have a high optical quality, are reasonably uniform and subband spacings ~30-45meV have been reported.[47]

For the growth of quantum dots, the self-organised islanding approach is accepted as being the most promising so far.[35] Apart from possibly size and shape uniformity this technique satisfies the requirements listed at the start of this chapter. A large amount of work is being performed world-wide on quantum dots prepared using this method and promising laser devices have already been reported.[35]

In conclusion, self organised techniques represent possibly the simplest and most optimum method for producing low dimensional quantum wire and quantum dot structures. For quantum wires, increases in the size of the 1D subband spacings are desirable and for quantum dots improvements need to be made to reduce the size and shape inhomogeneities that exist. However, laser devices exhibiting very promising characteristics have already been reported which utilise both self-organised quantum wires[25] and quantum dots,[35] demonstrating the promising nature of these techniques.

The rest of work in this thesis describes the structural and optical investigations that have been carried out on GaAs/AlGaAs V-groove quantum wires (chapters 4 and 5) and InAs/GaAs self-organised quantum dots (chapters 6 and 7).

2.6 References

[1] J.L.Merz and P.M.Petroff, Mat. Sci. and Eng., **B9**, 275 (1991).

[2] K. Kash, Jour. of Luminescence, **46**, 69, (1990).

[3] T. Fukui, S. Ando, H. Saito, Ex. Abs. of the 22nd Conf. on Solid State Devices and Mats., p753, (1990).

[4] Y.Arakawa and H. Sakaki, Appl. Phys. Lett. **40**, (11), p 939 (1982).

[5] Y. Arakawa, K. Vahala, A. Yariv, and K. Lau, Appl. Phys. Lett. **47**, (11), 1142, (1985).

[6] Y. Arakawa, K. Vahala, A. Yariv and K. Lau, Appl. Phys. Lett. **48**, (6), 384, (1986).

[7] Y. Arakawa, S. Tsukamoto, Y. Nagamune and M. Nishioka, Optoelectronics, **8**, (4), 499, (1993).

[8] J.S. Weiner, J.M. Calleja, A. Pinezuk, A. Schmeller, B.S. Dennis, A.R. Goñi, L.N. Pfeiffer and K.W. West, Appl. Phys. Lett. **63**, (2), 237, (1993).

[9] R. Hogg, PhD Thesis, University of Sheffield (1995).

[10] M. Notomi and T. Tamamura, Optoelectronics, **8**, (4), 563, (1993).

[11] K. Kash, D.D. Mahoney, B.P. Vandergaag, A.S. Gozdz, J.P. Harrison and L.T. Florez, J. Vac. Sci. Tech. B, **10**, (4), 2030, (1992).

[12] J.A. Yater, A.S. Plaut, K. Kash, P.S.D. Lin, L.T. Florez, J.P. Harrison, S.R. Das and L. Lebrun, J. Vac. Sci. Tech. B, **13**, (6), 2284, (1995).

[13] T.J. Thornton, M. Pepper, H. Ahmed, D. Andrews and G.J. Davies, Phys. Rev. Letts. **56**, 1198, (1986).

[14] J.M.Gaines, P.M. Peteroff, H. Kroemer, R.J. Simes, R.S. Geels and J.H. English, J.Vac. Sci. Tech. **B6**, 1381, (1988).

[15] T.Fukui, Optoelectronics, **8**, (4), 557, (1993).

[16] M. Kasu, H. Ando, H. Saito and T. Fukui, Appl. Phys. Lett. **59**, (3), 301, (1991).

[17] E.Colas, E.M. Clausen Jr., E. Kapon, D.M. Hwang and S. Simhony, Appl. Phys. Letts., **57**, (23), 2472, (1990).

[18] S. Koshiba, H. Noge, H. Akiyama, T. Inoshita, Y. Nakamura, A. Shimizu, Y. Nagamune, M. Tsuchiya, H. Kano and H. Sakaki, Appl. Phys. Letts., **64**, (3), 363 (1994).

[19] H. Akiyama, S. Koshiba, T. Someya, K. Wada, H. Noge, Y. Nakamura, T. Inoshita, A. Shimizu and H. Sakaki, Phys. Rev. Letts., **72**, (6), 924 (1994).

[20] R. Bhat, E. Kapon, D.M. Hwang, M.A. Koza and C.P. Yun, J. Crys. Growth, **93**, 850, (1988).

[21] E. Kapon, S. Simpony, R. Bhat and D.M Hwang, Appl. Phys. Lett. **55**, (26), 2715, (1989).

[22] P. Daniel Dapkus, Ann. Rev. Mat. Sci., **12**, 243, (1982).

[23] S.D. Herse, E. Barbier and R. Blondeau, J. Crys. Growth, **77**, 310, (1986).

[24] M.J. Ludowise, J. Appl. Phys. **58**, (8), R31, (1985).

[25] E. Kapon, Optoelectronics, **8**, (4), 429, (1993).

[26] F.S.Turco, S. Simpony, K. Kash, D.M. Hwang, T.S. Ravi, E. Kapon and M.C. Tamargo J. Crys. Growth, **104**, 766, (1990).

[27] X.Q.Shen M. Tanaka and T. Nishinaga, J. Cry. Growth, **127**, 932, (1993).

[28] M. Walther, E. Kapon, C. Caneau, D.M. Hwang and L.M. Schiavone, Appl. Phys. Lett. **62**, (18), 2170, (1993).

[29] R. Bhat, E. Kapon, D.M. Hwang, N.G. Stoffel and M.A. Koza, Appl. Phys. Lett. **56**, (9), 863, (1990).

[30] T. Sogawa, S. Ando, H. Kanbe, Appl. Phys. Lett., **64**, (4), 472, (1994).

[31] T. Sogawa, S. Ando, H. Kanbe, Appl. Phys. Lett., **64**, (24), 3299, (1994).

[32] B.A. Joyce and C.T. Foxton, Philips Tech. Rev. **43**, (5/6), 143, (1987).

[33] J. Singh, *'Physics of Semiconductors and their Heterostructures'*. McGraw Hill International (1993).

[34] I.N. Stranski, L. Krastanov, Akad. Wiss. Lit. Mainz Math.-Natur Kl. **11b**, (146), 797, (1939).

[35] D. Bimberg, N.N. Ledentsov, M. Grundmann, N. Kirstaedter, O.G. Schmidt, M.H. Mao, V.M. Ustinov, A. Yu. Egorov, A.E. Zhukov, P.S.Kop'eV, Zh. I. Alferov, S. Ruvinmov, U. Gösele and J. Heydenreich, Phys. Stat. Sol. (b), **194**, 159, (1996).

[36] R. Nötzel, Semi. Cond. Sci. Tech., **11**, 1365, (1996).

[37] J.M. Moison, F. Houuzay, F. Barthe, L. Leprince, E. André and O. Vatel, Appl. Phys. Lett. **64**, (2), 196, (1994).

[38] D. Leonard, K. Pond, and P.M. Petroff, Phys. Rev. B **50**, (16), 11687, (1994).

[39] S. Ruvinmov, P. Werner, K. Scheerschmidt, U. Gösele, J. Heydenreich, U. Richter, N.N. Ledentsov, M. Grundmann, D. Bimberg, V.M. Ustinov, A. Yu. Egorov, P.S.Kop'ev, Zh. I. Alferov, Phys. Rev. B 51, (20), 14766, (1995).

[40] D. Leonard, M. Krishnamurthy, S. Fafard, J.L. Merz and P.M. Petroff, J. Vac. Sci. Tech., **B12**, (2), 1063, (1994).

[41] M. Vollmer, E.J. Mayem, W.W. Rühle, A. Kurtenbach and K. Eberl, Phys. Rev. B **54**, (24), 17292, (1996).

[42] F.K. LeGoues, J. Tersoff, M.C. Reuter, M. Hammar and R. Tromp, Appl. Phys. Lett. **67**, (16), 2317, (1995).

[43] F. Heinrichsdorff, M-H. Mao, N. Kirkstaedter, A. Krost, D. Bimberg, A.O. Kosogov and P. Werner. Appl. Phys. Lett. **71**, (1), 22, (1997).

[44] P. Castrillo, D. Hessman, M-E. Pistol, S. Anand, N. Carlsson, W. Seifert and L. Samuelson Appl. Phys. Lett. **67**, (13), 1905, (1995).

[45] M. Sopanen, H. Lipsanen and J. Ahopelto, Appl. Phys. Lett. **66**, (18), 2364, (1995).

[46] H. Lipsanen, M. Sopanen and J. Ahopelto, Phys. Rev. B **51**, (19), 13868, (1995).

[47] E. Kapon, G. Biasiol, D.M. Hwang and E. Colas, Microelectronics Journal, **26**, 881, (1995).

Chapter 3

Experimental Techniques

3.1 Introduction

This chapter contains an outline of the experimental techniques used to investigate the optical properties of the III-V semiconductor quantum wires and quantum dots studied in this thesis.

The techniques of Photoluminescence (PL) and Photoluminescence Excitation (PLE) are described, along with a description of the micro photoluminescence (μPL) equipment used for the study of individual dots and wires. In addition for the study of quantum wires the techniques of Cathodoluminescence (CL) and Electroluminescence (EL) were also used. A description of both of these experimental techniques is given.

3.2 Photoluminescence (PL)

3.2.1 Description of the Photoluminescence Technique

Photoluminescence (PL) is an experimental technique that provides information about the size and quality of semiconductor structures containing quantum wells, wires or dots.[1] In a PL experiment the sample is excited with a light source (generally a laser which provides an intense monochromatic source) which emits photons of an energy greater than the bandgap of the material under investigation. This incident light is absorbed by the material, creating electron-hole pairs in the semiconductor. These photoexcited carriers relax to the band edges, as described in Chapter 1 and shown schematically in Figure 3.1. Once the electrons and holes have relaxed to their band edges excitons may form. Recombination of the carriers now occurs via either radiative or non-radiative processes. In a PL experiment it is the radiative recombination events that are recorded, with the emitted photons analysed by a suitable spectrometer and detector. The energy of the emitted photons provides information regarding the bandgap of the material and, in a quantum system, the additional energy which results from confinement of the carriers. The energy of the emitted photons can, however, be modified by potential fluctuations of the band edges[2] or the influence of impurities,[3] both leading to a photon energy which is less than true bandgap of the material. In addition, any inhomogeneity of the structure will result in a spatial variation of the band edges which will be reflected in a spread in the energies of the emitted photons. Hence both the energy and linewidth of the PL can be used to give a direct indication of the quality of the sample. In most of the experiments described in this thesis PL was used to assess both the degree of carrier confinement in the various structures under investigation and also their structural quality.

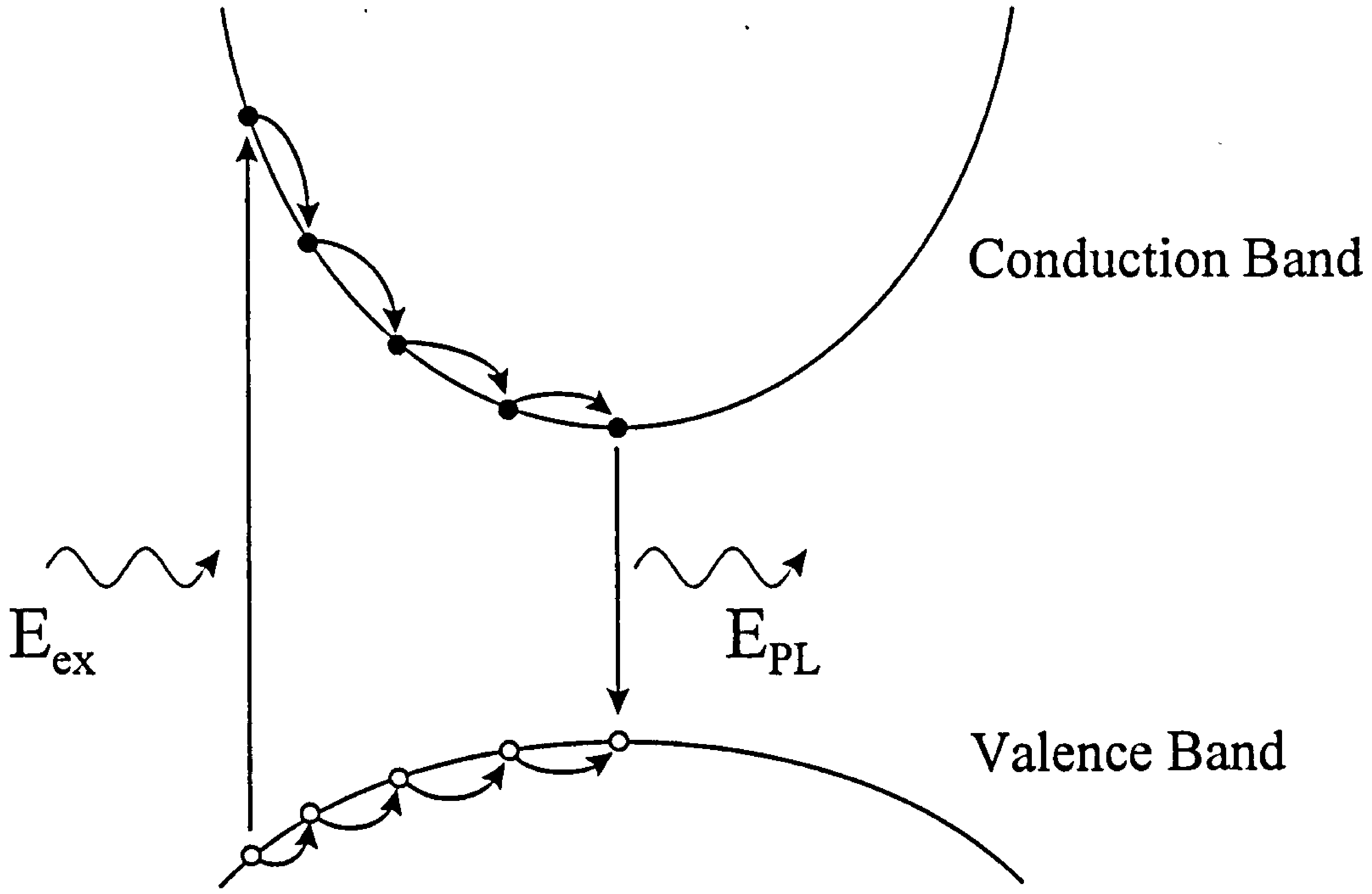

Figure 3.1 Schematic diagram of the PL process in a semiconductor. A photon E_{ex} is absorbed, creating an electron-hole pair which undergo rapid energy relaxation to their respective band extrema. The carriers may then recombine radiatively with the emission of a photon E_{PL}.

3.2.2 Experimental Details of PL Measurements

The basic photoluminescence experimental arrangement is shown in Figure 3.2. The laser excitation was provided by various sources, HeNe λ_{ex}=6328Å, HeCd λ_{ex}=4420Å, Argon ion λ_{ex}=4880Å and a diode laser λ_{ex}=7850Å. For some of the experiments described in Chapter 7, selective excitation was performed using a lamp and monochromator combination or a tuneable, Ar^+ pumped, Ti-Sapphire laser. These arrangements are described in more detail in Chapter 7.

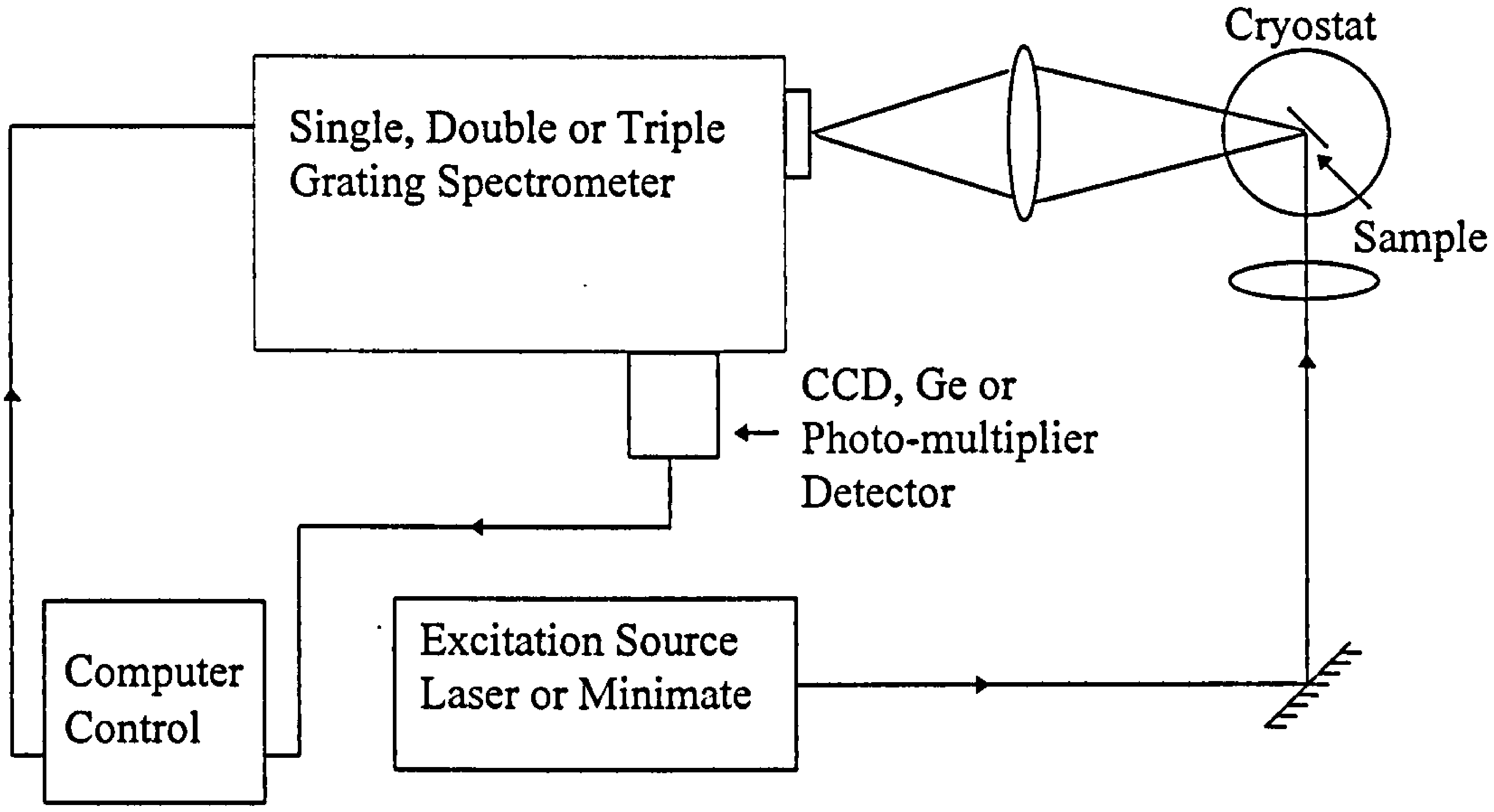

Figure 3.2 Schematic diagram showing the apparatus used to perform the PL measurements.

To allow spectral analysis, the emitted photoluminescence was dispersed using a grating spectrometer, for which one of three systems were used. The first spectrometer was a 0.75m single grating device with a 600l/mm, 1μm blazed grating. This provided a resolution of 20Å/mm slit-width. The second system was a double grating 0.85m spectrometer with 1200l/mm, 700nm blazed gratings giving a resolution 4.5Å/mm slit-width. Although the resolution of the second spectrometer is considerably better than the first, this is at the price of a significantly lower throughput of light. However the double grating spectrometer also exhibits excellent stray light rejection qualities which makes it particularly suitable for the photoluminescence excitation measurements described below. Finally, for most of the experiments performed on quantum wires, a two-stage triple grating spectrometer was used. The first stage consists of a 0.22m double spectrometer which acts as a bandpass filter allowing transmission of an undispersed portion of the incident light. This relatively narrow range of wavelengths is then dispersed by the second 0.65m spectrograph stage, equipped with either a 300 or 1200l/mm grating. Detection of the light in this system was by a multi-channel, nitrogen cooled Charge Coupled Device (CCD) chip which allowed the rapid acquisition of data and hence a high degree of light sensitivity for wavelengths ≤9000Å. Detection for the other two spectrometers was with a nitrogen cooled Germanium *p-i-n* photodiode, sensitive to near infra-red radiation ~8000-17,000Å. For all experiments the spectrometer and data acquisition were computer controlled.

3.3 Micro-Photoluminescence (μPL)

For the majority of photoluminescence experiments performed on quantum wires a micro-photoluminescence set-up was used. A schematic diagram of the micro-photoluminescence set-up used is shown in Figure 3.3. This consists of a very high quality microscope objective (NA=0.65) with a long working distance of ~6mm. This long working distance allows a sample contained within the cryostat to be imaged by the externally mounted objective. The incident laser excitation is reflected through the microscope objective by a pelicle beamsplitter and focused onto the sample which is held in a liquid helium cooled cold finger cryostat. A special Oxford Instruments Microscope Cryostat is used which allows the sample to be placed very close (≈5mm) to the window. In addition, the cryostat has only a single, very thin window to minimise distortion of the focused laser beam. The microscope objective can focus the laser light down to spot size of ~1-2μm, the exact size being dependent on the wavelength of the light being used. The emitted photoluminescence is collected by the same microscope objective and, by a series of mirrors and lenses, is focused onto the slits of the spectrometer for analysis. A rotating table with eyepieces of various magnifications allows a visual image of the sample to be obtained, hence enabling the accurate positioning of the laser spot onto the region of interest on the sample. Before a spectrum is recorded a mirror (also mounted on the rotating table) is moved into position which directs the light onto the slits of the spectrometer. At this stage the sample can no longer be viewed by eye. The cryostat is mounted on motorised x-y stages which allow horizontal translational movement. The position of the laser spot relative to the sample is therefore altered by moving the whole cryostat. The microscope is not moved by this operation, hence all the optics remain in position.

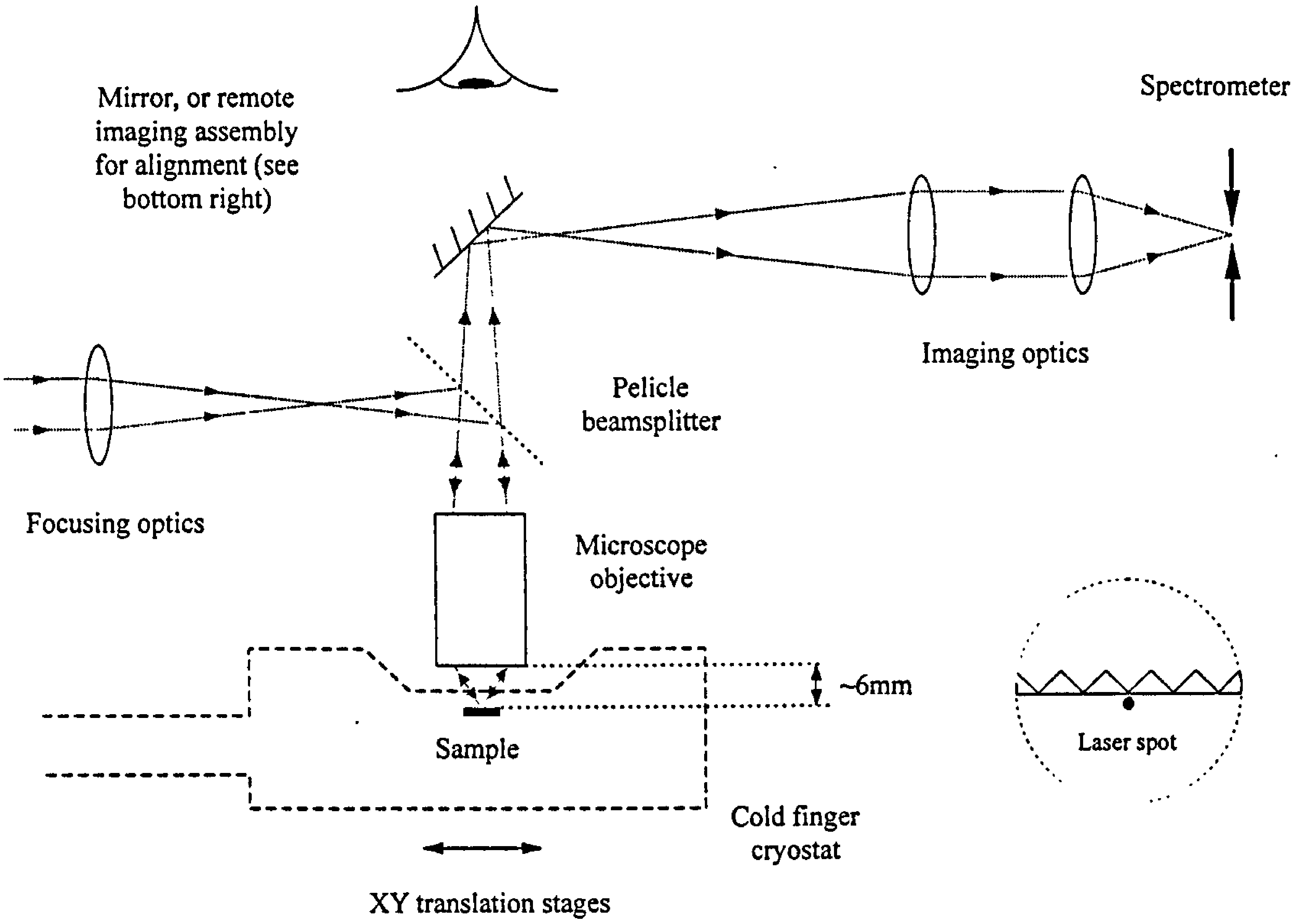

Figure 3.3 Schematic diagram of the micro-photoluminescence set-up.

The micro-photoluminescence equipment was used primarily for the optical study of individual quantum wires. The spacing (2 of 4μm) between the grooves containing the wires was such that the laser spot could be focused unambiguously onto the base of one groove and hence one wire. Also, due to the small laser spot size, very high laser power densities were obtainable using this system and this was used to measure high laser power density spectra of quantum dot structures.

3.4 Photoluminescence Excitation (PLE)

3.4.1 Description of the Photoluminescence Excitation Technique

The technique of photoluminescence excitation (PLE) involves the detection of luminescence at an energy on or around the peak (often the low energy side) of the luminescence observed in a photoluminescence experiment. In PLE however the excitation energy is scanned over a range of energies, which are higher than the detection energy, whilst the intensity of the luminescence at the detection energy is recorded as a function of excitation energy. For excitation energies larger than the bandgap of the structure being measured, the absorbed light creates electron-hole pairs.

These electron-hole pairs then relax, generally to the ground state of the system, and subsequently recombine to give a contribution to the PL being detected. The strength of the PLE signal is hence proportional to the absorption of the incident light and a PLE spectrum will be related to the true absorption spectrum of the sample. In a quantum well, for example, the energy associated with an excited state transition can be observed because an increase in the absorption is expected due to an increase in available electronic states.[4] Hence PLE can be used to give an indication of the density of states of the material. It is important to note, however, that a PLE spectrum will only be identical to the absorption spectrum if the probability for carrier relaxation to the detection energy is independent of the energy with which they are initially created. This requirement is usually approximately satisfied in bulk semiconductors[5] and quantum wires[6] and wells[4] but appears not to be true for the quantum dots studied in this thesis (Chapter 7).

3.4.2 Experimental Details of PLE Measurements

The experimental set-ups used for the PLE experiments are very similar to those used for the PL experiments shown in Figure 3.2, the main difference being that the excitation source is now tuneable. In the PLE experiments described in this thesis two excitation sources and detection configurations were used: a high resolution set-up and a lower resolution system. The lower resolution system consisted of a lamp and monochromator arrangement using a 150W tungsten halogen lamp dispersed by a 0.22m monochromator. In this case detection was with the single grating spectrometer and a Ge detector. A broad range of wavelengths (4600Å-13000Å) could be obtained using this arrangement, although the band width of the excitation is relatively broad and the power incident upon the sample is low. The high resolution set-up used a tuneable Ar^+ pumped Ti-Sapphire laser as the excitation source with detection provided by the double spectrometer and Ge detector. This arrangement had its limitations in that the range of energies provided by the laser was limited by the mirror set used. For the experiments described the mirror set used gave photon energies in the range 1110-1350meV (11200Å-9200Å). In addition, the output power of the laser was strongly dependent on energy, requiring the PLE signal to be ratioed against a split-off portion of the excitation beam to normalise the spectra. However the laser system provided a considerably narrower excitation linewidth and higher power than the lamp and monochromator combination.

3.5 Cathodoluminescence (CL)

Cathodoluminescence (CL) is the technique that has provided the most important insights into the nature of the luminescence observed from the quantum wire samples studied in this thesis.[7,8] CL is qualitatively similar to PL in that it can give information about quantum structures by exciting the material to create electron-hole pairs which recombine across the bandgap emitting luminescence. However, the excitation source for cathodoluminescence is a beam of electrons, instead of photons allowing the possibility for greater spatial resolution. The apparatus used for the CL measurements, shown in Figure 3.4, is a modified scanning electron microscope (SEM), which provides the electron beam. The sample is held in a cryostat which can be cooled to liquid helium temperatures (4K). An optical waveguide arrangement is attached to the SEM so that any luminescence emitted by the sample under excitation can be efficiently coupled into a spectrometer where it is dispersed and detected by a photomultiplier tube. The main advantage of the CL technique is that the excitation area ($\sim 0.03\mu m^2$)[9] is very small compared to that of a PL measurement ($\sim 1\mu m^2$). The spatial resolution of CL however, is ultimately limited by the diffusion lengths of the excited carriers in the sample. Hence even if a small excitation spot size is used the excited carriers will still diffuse for distances of typically ~0.5μm before recombining and emitting luminescence.[10] The spatial resolution is therefore considerably less than the original excitation area although it is still better than is achievable with PL. For normal PL measurements the laser spot is focused to ~100μm and for μPL experiments (described above) it is ~1-2μm, depending on the wavelength of the light. The latter value is still larger than the typical diffusion length of carriers, hence smaller areas can be probed with CL. Greater spatial resolution (<0.05μm)[12] has been achieved in CL experiments by using lower beam currents and acceleration voltages[11] which reduces the effective diffusion length of the excited carriers. This has been useful for the investigation of self organised quantum dots[12] where a small number of dots have been excited and luminescence from individual dots has been observed. The SEM used for the measurements described in this thesis could also be used in its normal mode with the sample under investigation imaged using the emitted secondary electrons. This allowed the accurate positioning of the excitation source as the same electron beam is then subsequently used to excite the same region of interest on the sample.

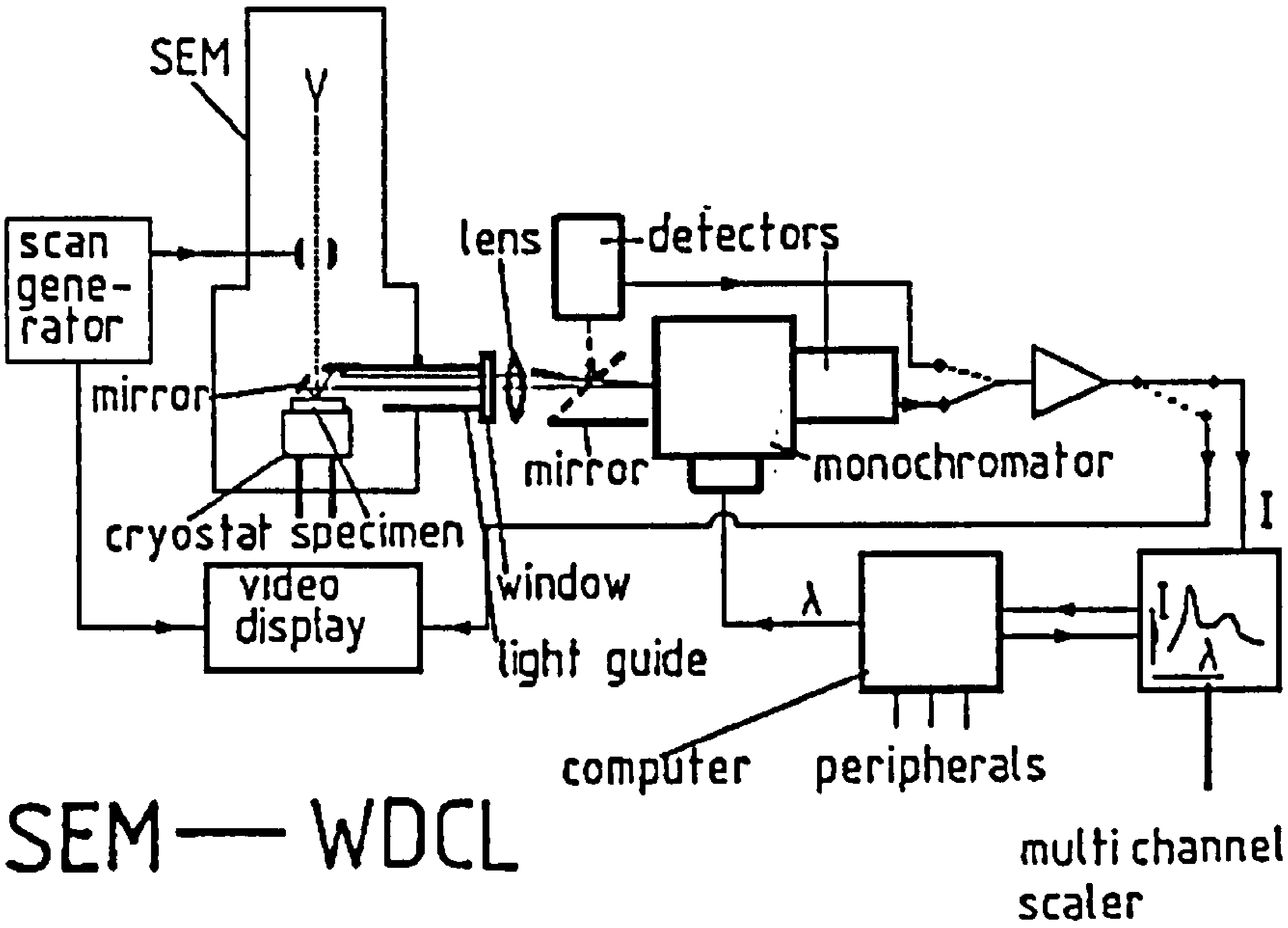

Figure 3.4 Schematic diagram of the Low Temperature Wavelength-Dispersive Cathodoluminescence apparatus used in the experiments.

The CL apparatus used could obtain a full luminescence spectrum by recording the intensity of the light passing through the spectrometer as a function of wavelength, when the electron beam was scanned rapidly across a small area of the sample. However the true power of CL is obtained when the spectrometer is used as a monochromator, fixed at a specified wavelength. The electron beam in this case is slowly scanned over the spatial region of interest on the sample, whilst the output from the detector (which only records light of the pre-determined wavelength) is fed to the amplifier that generates the SEM pictures. Instead of recording the secondary electron intensity, the detector intensity is recorded on the Polaroid film. The image obtained is hence a visual representation of the spatial origin of the luminescence at the specified wavelength, allowing information on the origin of the luminescence to be obtained.

In the present work, CL was extensively used to identify the origin of the large number of features that are present in the luminescence spectra of quantum wires. In addition it proved an invaluable tool for the optimisation of the quantum wire growth. These results will be discussed in detail in the following chapter.

3.6 Electroluminescence (EL)

Electroluminescence (EL) is an experimental technique that is very similar to photoluminescence. The difference is related to the mechanism by which electron-hole pairs are created in the semiconductor. In PL the sample is optically excited, whilst in EL experiments it is excited electrically. For this to be possible the sample structure has to be modified so that the active region is situated within the intrinsic region of a *p-i-n* structure. A typical quantum wire device structure suitable for EL measurements is shown in Chapter 5. Electrical contacts are made to the device by fabricating a contact directly to the substrate and a gold contact to the epitaxial surface. For the experiments described in this thesis a circular mesa 80μm in diameter was etched into the sample and fabricated with a gold annular top contact. When a forward bias is applied across the device electrons and holes are injected from the *n* and *p* regions respectively into the *intrinsic* region where they are captured by the quantum wells and subsequently radiatively recombine. The emitted light (EL) is detected in a similar manner to that used in the PL experiments (see Figure 3.2). For the quantum wire devices studied in this thesis the emission, which occurred in the range 6000-8400Å, was detected using the single grating spectrometer and a thermoelectrically cooled GaAs photomultiplier tube.

3.7 Cryostats and Magnets

All the measurements described in this thesis were performed at sub-room temperatures, usually liquid helium temperatures. For basic PL, EL, CL, and PLE measurements the samples were placed in an Oxford Instruments continuous flow cryostat which allowed cooling to 4.2K. By using an electrical heater the sample temperature could be varied between 4.2 and 300K, allowing the temperature dependence of the optical processes to be studied. For the μPL measurements a special cryostat was used, as described above. Because of the single window and cold finger arrangement used for this cryostat the base temperature is expected to be some what above 4.2K (possibly 20-30K).

Magnetic field measurements were performed in an Oxford Instruments 14T (16T for pumped He) vertical bore magnet. The sample was placed in super-fluid liquid He (1.8K) and the EL from the sample was transmitted to the triple grating spectrometer by either an optical fibre or a series of lenses and mirrors. This arrangement is described in more detail in Chapter 5.

3.8 References

[1] H.B. Beeb and E.W. Williams in '*Semiconductors and Semimetals*', edited by R.K Willardson and A.C. Beer, Vol. **8**, p.181, (Academic, New York, 1972).

[2] R.J. Nelson in '*Excitons*' edited by E.I. Rashba and M.D. Sturge, p319, North-Holland, (1982).

[3] P.J. Dean in '*Collected Excitations in Solids*' edited by B. Di Bartolo, p247, Plenum, (1983).

[4] K.J. Moore, G. Duggan, G. Th Jaarsma, P.F. Fewster, K Woodbridge, R.J. Nicholas, Phys. Rev. B **43**, (15), 12393, (1991).

[5] J.E. Fouquet, M.S. Minsky and S.J. Rosner, Appl. Phys. Lett. **63**, (23), 3212, (1993).

[6] H. Akiyama, T. Someya and H. Sakaki, Phys. Rev. B **53**, (24), R16160, (1996).

[7] D.B.Holt and F.M.Saba, 'The CL mode of the SEM: A Powerful Microcharacterisation Technique', Scanning Electron Microscopy, p.1023, (1985).

[8] C.A.Warwick, Scanning Microscopy, **1**, (1), 51, (1987).

[9] G.M. Williams, private communication.

[10] D.E. Aspnes and A.A. Studna Phys. Rev. B., **(27)**, 985, (1983).

[11] D. Bimberg and J. Christen, Inst. Phys. Conf. Ser. **134**, (11), 629, (1993).

[12] M. Grundmann, J. Christen, N.N. Ledentsov, J. Böhrer, D. Bimberg, S. Ruvinmov, P. Werner, U. Richter, U. Gösele, J. Heydenreich, V.M. Ustinov, A. Yu. Egorov, A.E. Zhukov, P.S. Kop'ev and Zh. I. Alferov, Phys. Rev. Letts. **74**, (20), 4043, (1995).

Chapter 4

Structural Characterisation of GaAs-AlGaAs V-groove Quantum Wires

4.1 Introduction

The results presented in this chapter describe a series of structural studies of GaAs-AlGaAs V-groove quantum wire samples. Initial measurements were performed with a scanning electron microscope (SEM), providing a quick assessment of the growth uniformity by imaging the cleaved edge of the sample. This was performed by G. Hill at the EPSRC Central Facility for III-V Semiconductors, University of Sheffield. Although useful, this technique gave no information about the size and shape of the quantum wire; this structural information was obtained using a high resolution transmission electron microscope (TEM) to take images from a thinned cross-section of the sample. The procedure followed to obtain the optimum quantum wire structure, suitable for the extensive optical studies which are described in the following chapter, is discussed. Cathodoluminescence (CL) measurements were used to determine the origin of the numerous features observed in the optical spectra and to assess the effect of changes in the growth conditions made in the course of the optimisation procedure. Finally, a full CL and TEM study of the optimised structure is presented. CL and TEM analysis was carried out using the facilities at the Defence Research Agency, Malvern as part of a CASE award sponsorship in collaboration with G.M. Williams and A.G. Cullis.

4.2 Scanning Electron Microscopy Measurements

In the initial stages of the project, routine analysis of the V-groove quantum wire samples using a Scanning Electron Microscope (SEM) provided important information about growth uniformity. The shape of the sidewalls of the V-groove, after growth, gave a good indication of whether or not quantum wires had formed. The growth of V-groove quantum wires relies on the preferential growth of the AlGaAs barriers on the

(111)A sidewall facets, with respect to the other exposed surfaces. This produces a sharpening of the original etched V, leaving a template for the GaAs which grows preferentially at the bottom of the V to form the quantum wire. This sharpening has to produce a consistent, reproducible curvature, as any variation of the shape present when the GaAs is deposited would lead to unpredictable growth of the quantum wire. The prospects for growing a stack of identical wires would also be severely affected if the groove did not re-sharpen reliably after the growth of successive quantum wires and AlGaAs barriers. Ideally, in V-groove structures, the growth of AlGaAs should be self-organised in nature, quickly reaching a self-limiting, equilibrium curvature at the base of the groove, after which there is no further change in shape. If these requirements are satisfied then the conditions should exist for the necessary reproducibility of the growth of the GaAs quantum wires.

4.2.1 Growth on off-axis Substrates

III-V semiconductor crystal growth by Metal Organic Vapour Phase Epitaxy (MOVPE) is normally performed on GaAs substrates that are mis-oriented slightly off-axis (~3°) from the (001) direction.[1] This provides a series of mono-layer step edges on the surface which act as nucleation sites for atoms arriving on the surface, leading to controllable growth. Initial V-groove quantum wire samples were grown on these off-axis substrates. However, in the course of structural investigations using SEM, it was discovered that more symmetrical growth occurred when exactly on-axis substrates were used. The etchant used to produce the V-grooves attacks an (001) plane in preference to a (111)A sidewall. Hence, after etching, (111)A sidewalls are produced regardless of the original substrate orientation, as long as it is close to (001). The net effect of this process when used with off-axis substrates is that it is possible to end up with side walls of different lengths because the V-grooves do not point in a direction perpendicular to the substrate surface. The growth of the quantum wire relies on the transport of Ga adatoms from the sidewalls to the base of the groove. Hence if the two sidewalls on either side of the grooves are of different lengths it is possible that this could lead to an asymmetric quantum wire shape. An asymmetrical wire shape is not, in principle, disadvantageous for device applications. However, if the side wall quantum wells are of different thicknesses, further complications of the optical spectra will result. Hence, for the growth optimisation process described in this chapter, where the simplest possible PL spectrum is advantageous, symmetrical structures are desirable. Although it might be thought that a mis-orientation angle of only ~3° would introduce insignificant distortions to the cross-sectional shape of the structure, the results presented below suggest that this may not be the case.

For the present growth experiments nominal 50Å quantum wires were grown on V-groove patterned GaAs substrates having a groove separation of 8μm. 500Å of GaAs was deposited initially as a buffer layer to provide a smooth growth surface, followed by 1μm of AlGaAs, a single 50Å GaAs quantum wire, 0.5μm of AlGaAs and a 500Å GaAs cap. All these thicknesses refer to values which would occur for growth on (001) planar surfaces. Because of the complicated growth processes which occur on the non-planar V-groove surfaces the actual layer thicknesses are expected to be significantly modified and, in addition, will be spatially variant.

The growth of a series of quantum wire samples was performed simultaneously on (001) substrates having a mis-orientation of 10°→{111}A, 3°→{110} and 0° (exactly on-axis) to investigate the effects on growth of the substrate orientation. The 3° mis-oriented substrates are those generally used for the growth of high quality GaAs-AlGaAs structures.[1] SEM images of these samples after growth are shown in Figure 4.1. These images clearly show the line of the original etch, above which the shape of the post-growth groove is visible. The 10° off-axis sample, Figure 4.1a, exhibits a large difference in the lengths of the side walls. In addition, the growth rate on the shorter face is greater than that on the longer face, resulting in an asymmetry in the thickness of the sidewalls. On the planar region between the grooves the growth has tended to reconstruct the (001) surface, resulting in the grooves appearing even more asymmetric. Growth on the side walls of the 3° off-axis sample, Figure 4.1b, exhibits some discontinuity near the base of the groove. The mis-orientation direction is →{110} so the lengths of the two side walls should be the same. At the base of the groove the growth has continued to follow the underlying (111)A surface while further up the sidewall a different facet has formed. This results in a kink where the two facets meet and this also appears to result in the tops of the grooves widening, thereby producing a larger (001) top quantum well. It is not clear whether this behaviour will affect the shape and structural quality of the quantum wire at the base of the groove although the groove does not appear to be particularly sharp. This behaviour does not occur in the on-axis sample, Figure 4.1c, where a narrowing of the top (001) facet is observed. The growth front for this sample also appears to be much more uniform, with highly symmetrical side wall growth which is parallel to the original etched surfaces.

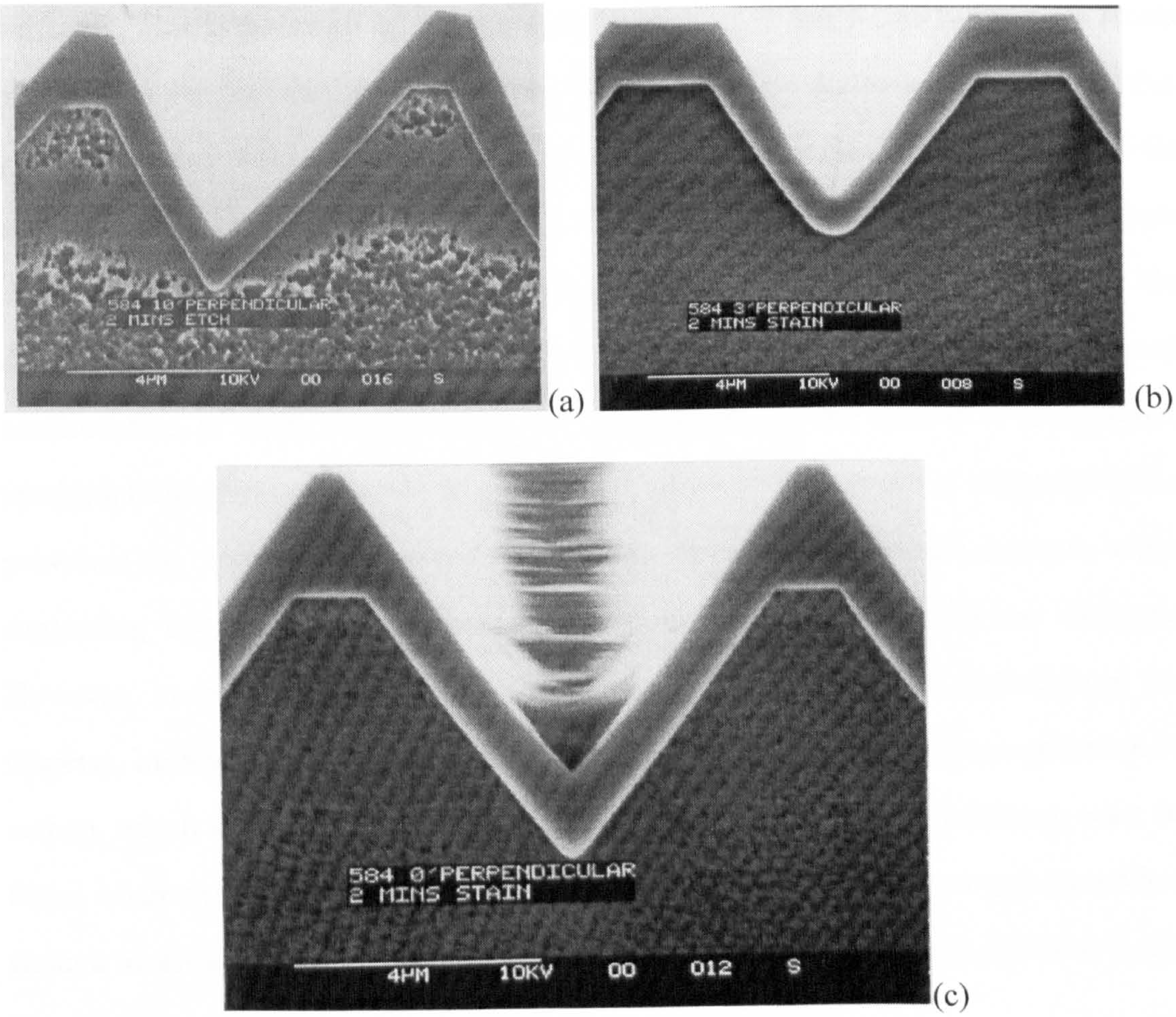

Figure 4.1 Cross-sectional SEM images showing the very different growth uniformities resulting from growth on three different substrate orientations (a)10°, (b)3° and (c) on-axis.

These studies indicate clearly that exact (001) substrates provide the optimum orientation for the growth of GaAs-AlGaAs quantum wires and we note that this orientation is used by the group of Kapon to grow similar quantum wire structures.[2] Such substrates produce a minimal variation in the thickness of the quantum wells contained in the structure, a factor that leads to a simplified luminescence spectra. Following these initial studies exact (001) substrates were used to provide the quantum wire samples suitable for the optical investigations described later.

4.2.2 Growth Temperature Study

The mechanism behind the growth of quantum wires on V-groove substrates depends on the different growth rates of GaAs and AlGaAs on the different crystallographic surfaces. This is governed by the diffusion lengths of Al and Ga on the various facets exposed on the surface. Studies of this phenomenon by Herse *et al.*[3] indicate that growth at higher temperatures leads to a greater difference in the diffusion lengths of Ga and Al on the (111)A and (001) facets. This implies that the groove will become sharper when the AlGaAs barrier is grown at high temperatures. In addition, as the Ga diffusion length is greater on the (111)A surface than on (001), an enhanced accumulation of GaAs will occur on the latter surface at the bottom of the groove, resulting in the formation of the quantum wire. Sharper V-grooves and enhanced GaAs growth at the bottom of the groove will result in sharper, better defined quantum wires, suggesting that high growth temperatures should result in the optimum structure. However, as the temperature is increased the amount of carbon, cracked from the reagents, incorporated into the layer also increases.[1] The uncontrolled incorporation of carbon, which is a p-type dopant,[4] is generally undesirable. Hence, a balance must be found where the growth temperature is sufficiently high to promote wire growth but low enough to avoid excessive carbon incorporation. Reported growth temperatures in the literature are in the range ~675-750°C.[5,6]

In the present investigation V-groove samples having the same structure as used in the previous section and 3° off-axis substrate orientation were grown at various temperatures. Figure 4.2 shows SEM images of samples grown at these different temperatures. The lowest growth temperature of 600°C resulted in growth on the side walls which was severely tapered. This suggests that there is a variation in the growth rate on the side wall which increases from a low rate at the base of the groove to a high rate towards the top. The net effect of this is that the top (001) facet tends to widen laterally giving a much broader top facet between the grooves, almost to the extent that adjacent tops touch, effectively filling in the groove. As the temperature is raised to 620°C and 670°C the variation in the growth rate along the side walls decreases. Growth at the highest temperature of 720°C shows a minimal tapering of the side wall facet. All these samples were grown on 8μm pitch gratings, growth on a narrower 4μm pitch grating resulted in good growth uniformity at 680°C, although growth on 2μm samples, (shown later in the TEM micrograph of Figure 4.13), showed a significant in-filling of the grooves as opposed to a tapering of the side walls. Most of this in-filling occurred during the growth of a 2000Å thick GaAs capping layer, so this effect does not present a problem for producing a stacked array of identical quantum wires where an accurate reproduction of the groove profile is required after each wire is grown. This effect, however, needs to be minimised before the AlGaAs barriers and wires are grown, so the thickness of the GaAs buffer layer should ideally be kept to a minimum.

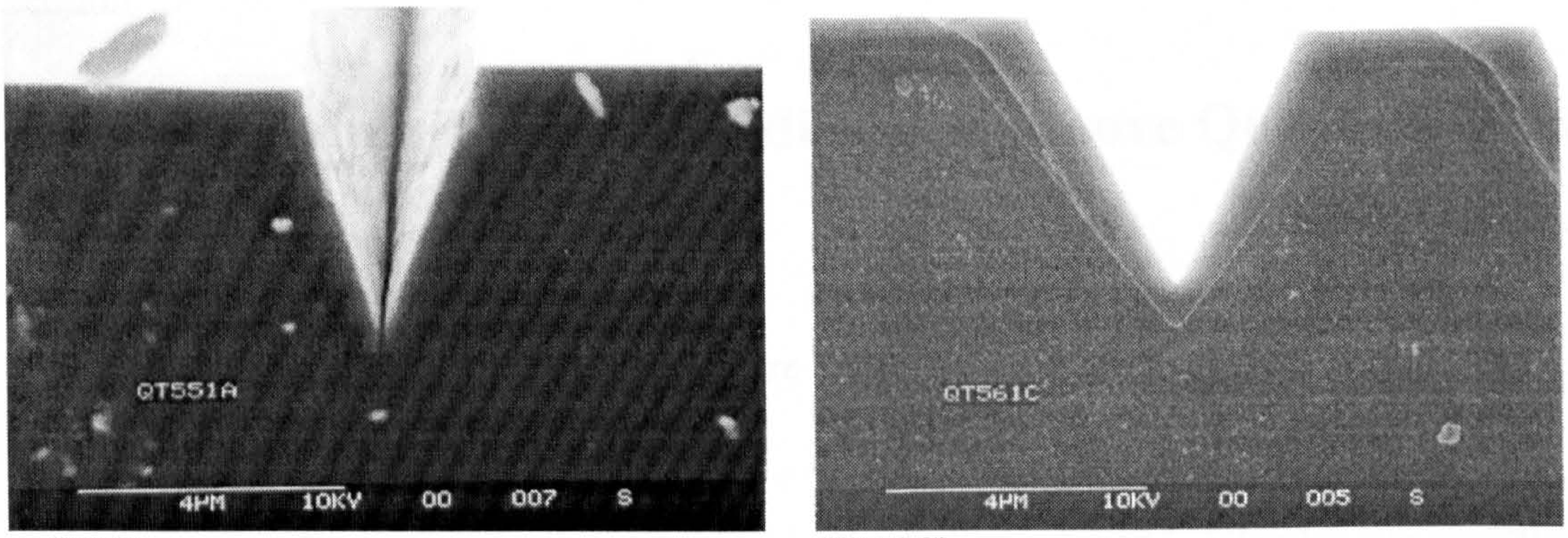

(600°C) (620°C)

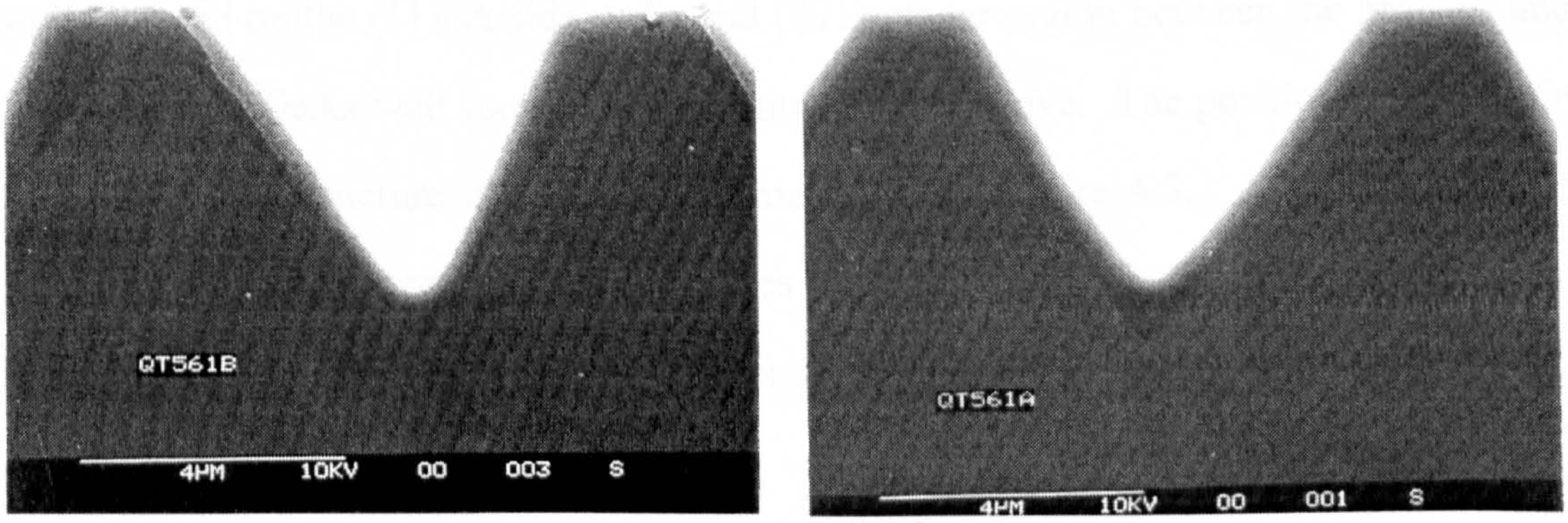

(670°C) (720°C)

Figure 4.2 Cross-sectional SEM images of samples grown at different growth temperatures, 600-720°C.

4.2.3 Optimisation of the Structure

After an extensive investigation of the important growth parameters needed to produce quantum wires of good structural and optical quality, a set of growth conditions was found that resulted in spectrally isolated quantum wire emission with good luminescence efficiency. All further investigations were based around this structure. The effects of altering the growth temperature and substrate orientation were visibly assessed by SEM imaging. This showed that it is preferable to grow on on-axis substrates at high temperature. Reducing the groove pitch to 4μm from the original 8μm had the beneficial effect that the wire area doubled in relation to that of the quantum wells, resulting in an enhanced wire luminescence intensity. The uniformity of the growth also improved considerably when the smaller groove pitch was used. This allowed the growth temperature to be reduced to 680°C whilst still obtaining good quality structures. Further optimisation of the structure was achieved by using the results of CL imaging, the results of these investigations are described in the following section.

4.3 Cathodoluminescence Studies of V-groove Quantum Wire Samples

The emission spectra of the quantum wire structures are highly complicated, with a large number of emission lines observed. In addition to the quantum wire emission, emission arises from carriers recombining in the bulk GaAs and AlGaAs, the quantum wells formed on the (111)A side walls and (001) planar region between the grooves and the vertical AlGaAs well formed in the centre of the groove. The positions of the main features in the structure are shown schematically in Figure 4.3. All these different spatially, separate recombination processes result in energetically different emission. However the precise origin of the various recombination features observed in the PL spectra is initially not obvious.

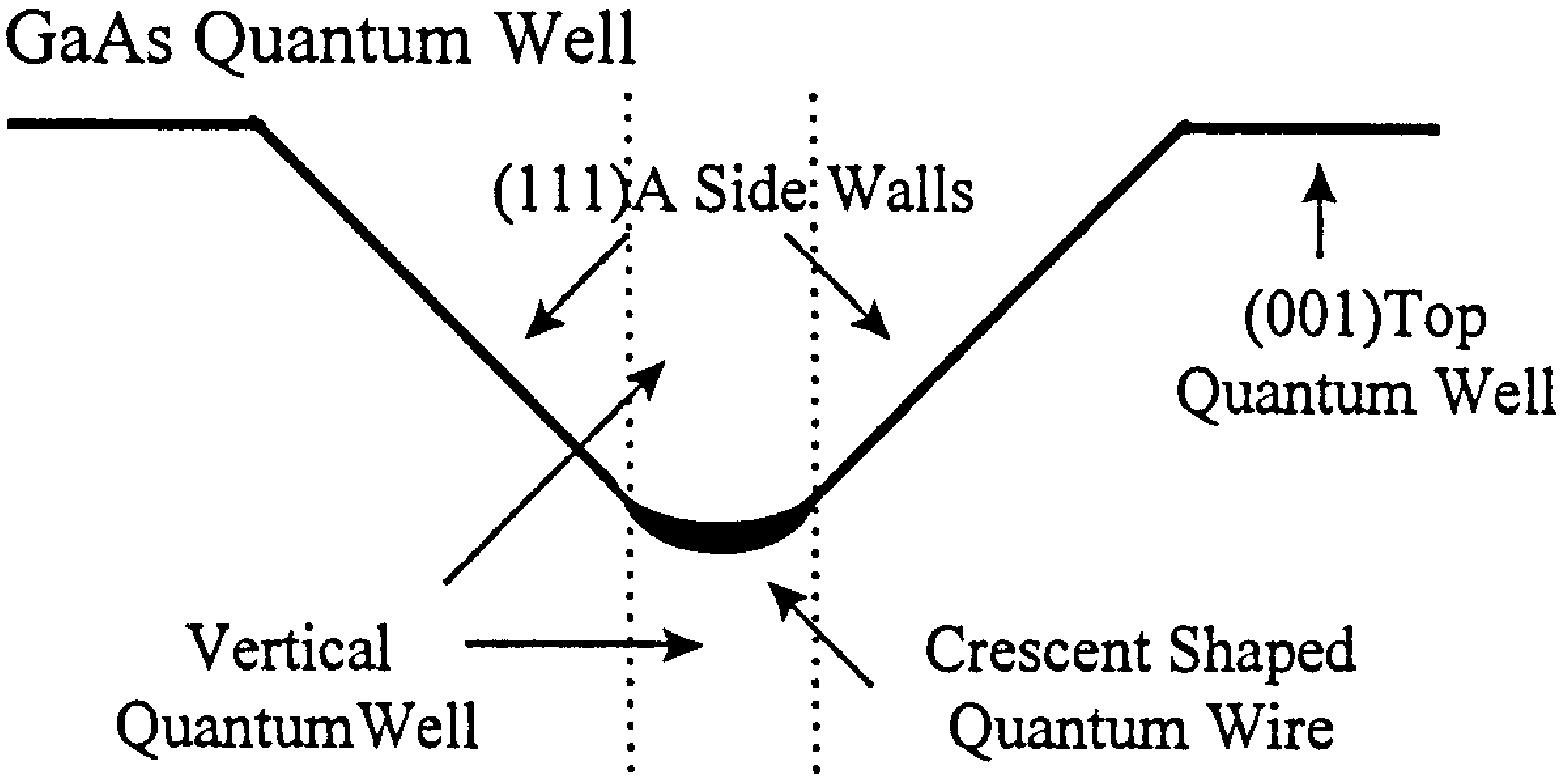

Figure 4.3 Schematic diagram of the various facets and active regions in the quantum wire structure.

Cathodoluminescence (CL), in which the sample is excited with a high energy electron beam, provides high spatial resolution (the e-beam spot size is ≈0.2μm although carrier diffusion results in a significantly poorer resolution of ~0.5μm for the beam currents used in these experiments).[7] This resolution coupled with the ability to spatially scan the beam position on the sample allows the identification of features which arise from spatially and energetically distinct carrier recombination. This technique has therefore been applied to the quantum wires where it has allowed the origin of the numerous emission features to be determined.[8,9]

4.3.1 CL Study of an Early 30Å Quantum Wire Sample (QT688)

A typical spectrally resolved CL spectrum for sample QT688 with 30Å thickness of GaAs is shown in Figure 4.4. 30Å is the nominal thickness of the deposited GaAs. This will be the thickness for the growth on a (001) planar surface, the enhanced growth at the bottom of the V-grooves will result in a considerably larger thickness as demonstrated by the transmission electron microscopy (TEM) results presented below. As expected, the CL spectrum contains a number of features, the origins of which require identification by spatially and spectrally resolved CL measurements. To obtain the spectrum of Figure 4.4 the electron beam was scanned over a small area (typically ~80×100μm) of the sample in plan view. This is shown schematically in Figure 4.5a. A number of grooves were excited by the beam to ensure that the excitation of all the different features in the structure occurred in proportion to the area they occupied. The resultant luminescence was spectrally resolved using a monochromator and photomultiplier detector.

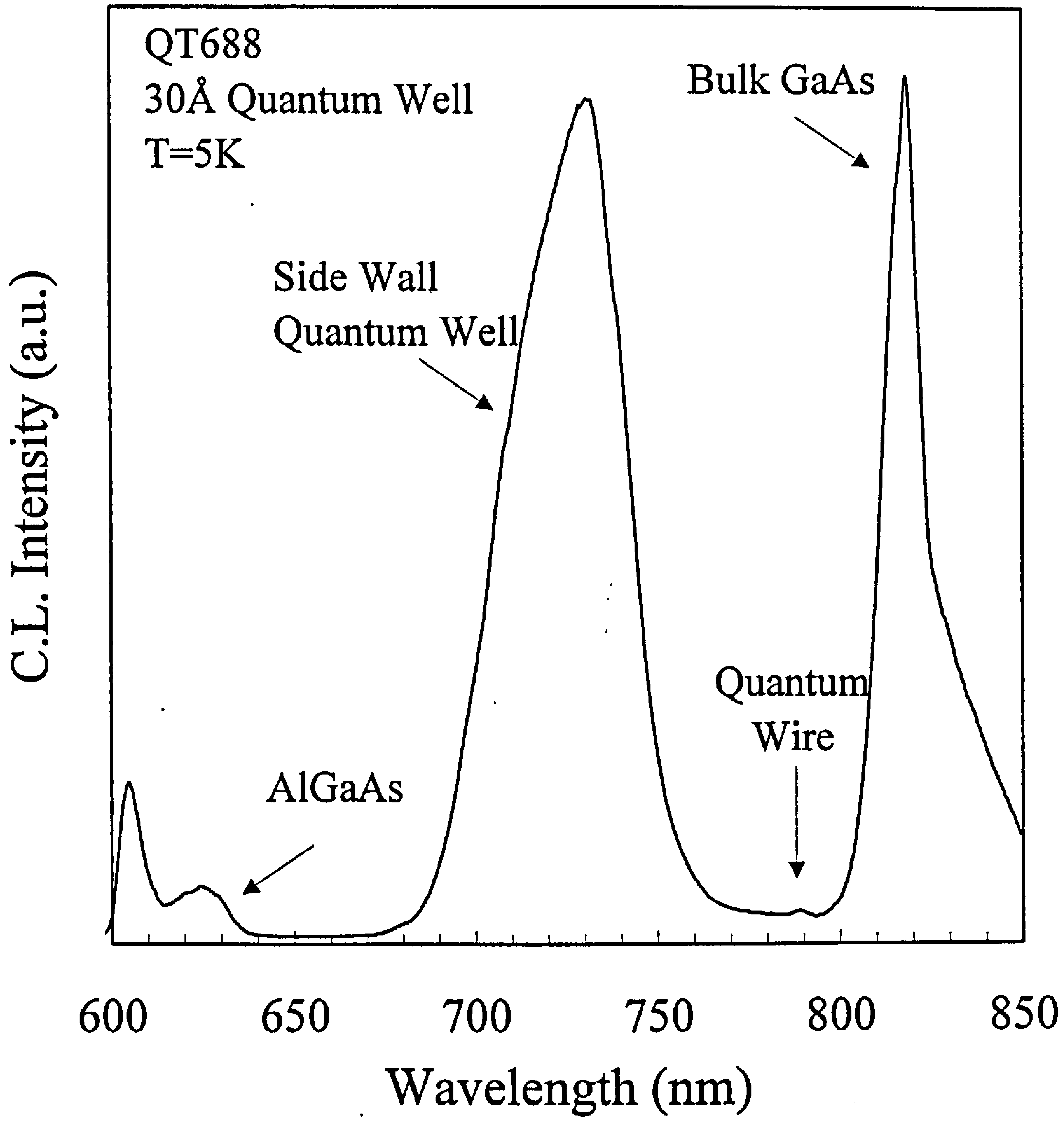

Figure 4.4 CL spectrum of sample QT688 showing strong luminescence from the side wall quantum wells and a weak feature attributed to luminescence from the quantum wires.

The main features observed in the spectrum of Figure 4.4 are the bulk GaAs emission at 820nm, a broad peak at 730nm, narrower peaks at around 600nm and a small peak at 788nm. To identify the origin of these features the sample was mounted on its side so that excitation on a cleaved edge could be performed, this edge view orientation is shown schematically in Figure 4.5b. For these measurements the magnification of the CL system was increased to reduce the number of grooves imaged, hence allowing a positive identification of the spatial origin of the emitted luminescence. A secondary electron image, using the SEM's monitor, enabled the accurate positioning of the sample so that the grooves were clearly visible in the field of view. This edge view arrangement therefore enabled the cleaved cross-section of the structure to be observed and allowed the origin of the various emission features to be unambiguously correlated with the positions of the quantum wells and the quantum wire.

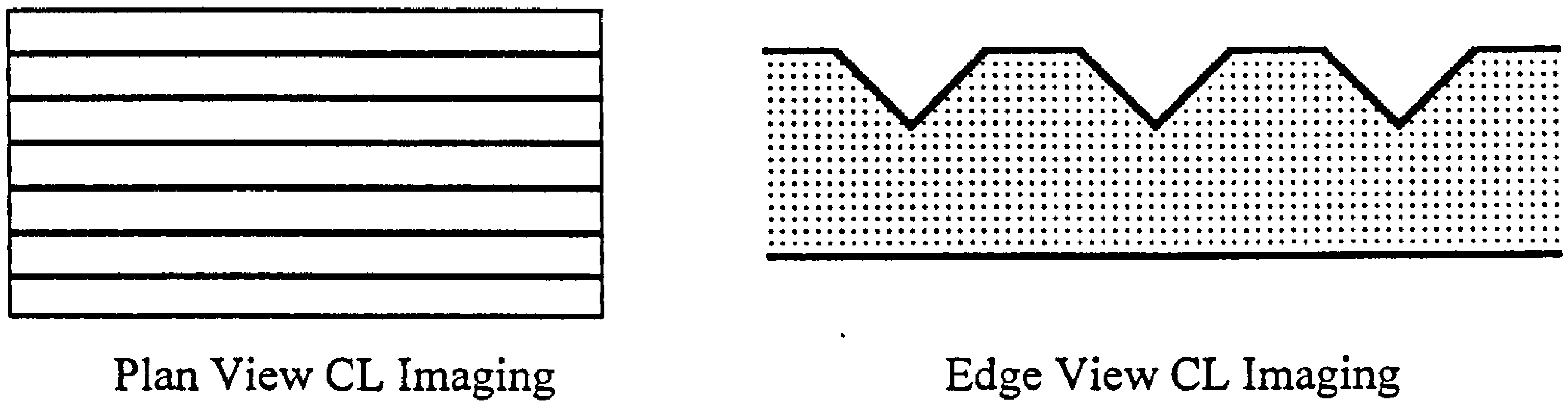

Figure 4.5 The two orientations used when viewing the samples for CL measurements. In plan view the grooves are imaged from above whilst the cross-sectional, edge view, images down the length of the grooves, from a cleaved edge.

Figure 4.6 shows monochromatic CL images of the sample (QT688) with the wavelength of the monochromator set to the values indicated. With the wavelength set to 730nm (the main peak in the spectrum) luminescence is observed from the sample, following the profile of the etched V-groove surface. This behaviour is consistent with this emission arising from the quantum wells formed between the grooves: on the planar (001) surface (top quantum well), and on the (111)A side walls of the grooves (the side quantum well). It is expected that the luminescence from the top quantum well will occur at a lower energy than that from the side quantum well due to the higher growth rate of GaAs on the (001) surface which results in a thicker quantum well being deposited.[8] However, in the measurements of the present sample this difference can not be clearly resolved. The CL spectrum of Figure 4.4 does show a shoulder on the long wavelength side (lower energy) of the main quantum well peak at 730nm which is probably due to emission from the top quantum well.

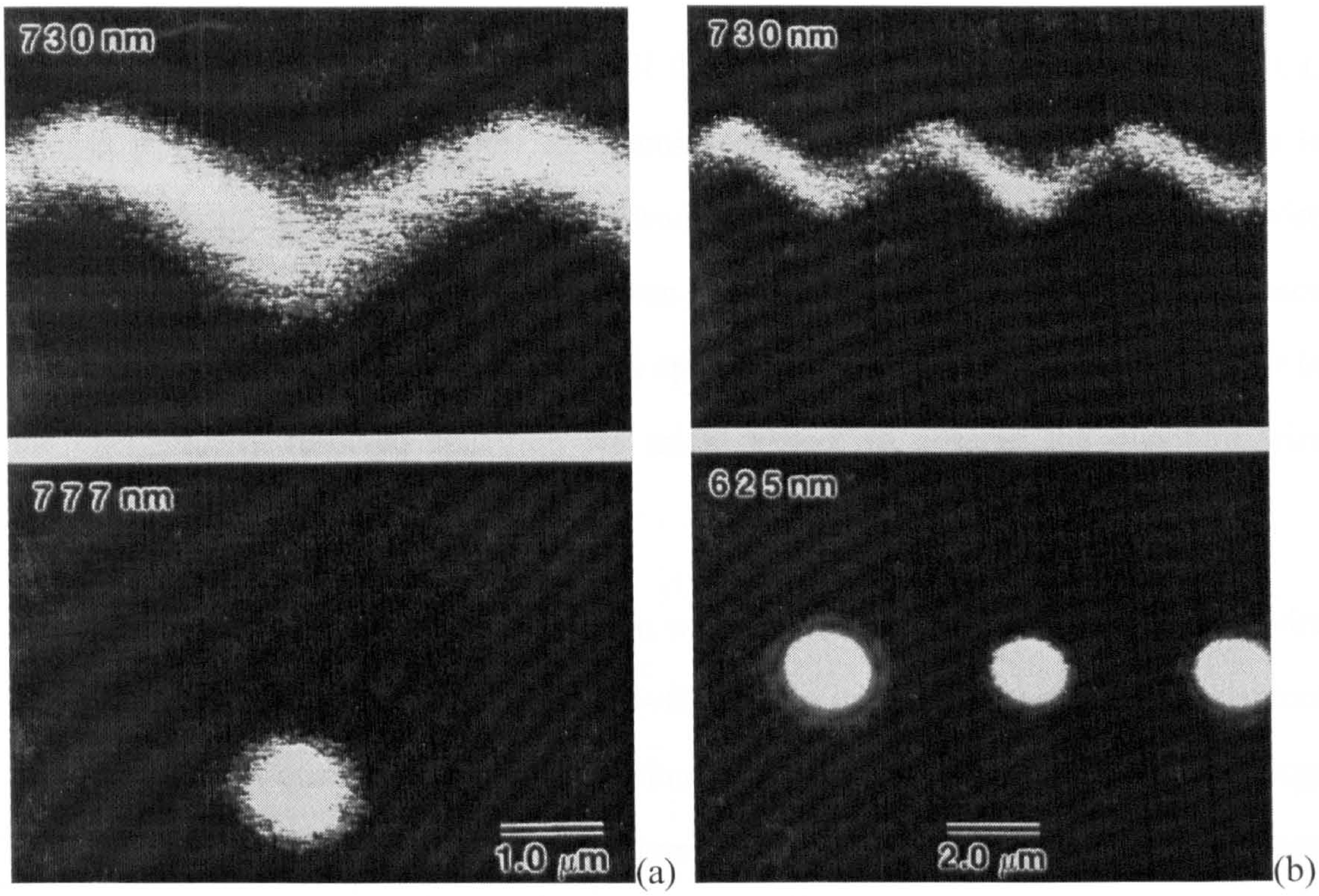

Figure 4.6 Monochromatic CL images of the quantum well, quantum wire and vertical quantum well regions of the spectrum. (a) Quantum well emission at 730nm and quantum wire emission at 777nm. (b) Quantum well emission at 730nm and vertical quantum well emission at 625nm (lower magnification image).

Luminescence at 777nm arises from the base of the groove, for this measurement the spectrometer position was set to a wavelength slightly shorter than that of the peak at 788nm, as observed in the spectrum. This peak sits on the high energy tail of the bulk GaAs luminescence at 820nm. As a consequence, an image recorded at this wavelength is obscured by the luminescence from the substrate and the GaAs cap which is observed over the entire area of the sample. Hence no useful spatially resolved information is obtained. By moving the detection energy away from the maximum of the feature of interest, the effect of the nearby GaAs luminescence was minimised whilst still sampling the luminescence from the high energy tail of the 788nm peak. The isolated spot at the bottom of the groove, observed in the CL image for this wavelength, occurs where luminescence from the quantum wire is expected to emanate from. It is therefore reasonable to conclude that this luminescence is due to the quantum wire in the structure. However, when a monochromatic CL image is recorded for the 625nm luminescence, a spot at the bottom of all the grooves is also seen. From these CL images it would therefore appear that luminescence at two different wavelengths is emanating from the region where we would expect to observe the quantum wire luminescence. Only one of these peaks can be realistically attributed to luminescence from the quantum wire and to explain this apparent paradox we must consider where in the energetically resolved spectrum we might expect to observe the quantum wire luminescence.

The TEM data for a nominal 15Å quantum wire sample (see below) shows that the wire is much thicker in the growth direction (≈60Å) than the adjoining side wall quantum wells (≈15Å). A quantum well of this thickness will hence exhibit a much lower energy emission than the thinner, side wall quantum wells due to the reduced carrier quantum confinement. Although in the quantum wire there is also confinement in a second dimension, which will shift the energy levels to higher energy, this effect is small because the lateral confinement due to the tapering of the crescent shape of the wire is comparatively weak.[10] The emission energy is therefore not expected to be altered very much by this additional confinement. Hence luminescence from the wire should be at a lower energy than that of the quantum well, suggesting that the lower energy emission at 788nm represents the quantum wire emission.

The origin of the higher energy emission at 625nm is most likely to be from the Ga rich AlGaAs stripe which runs down the centre of the groove and is observed in the TEM of the present and related samples.[11] This would give emission at a lower energy than the surrounding AlGaAs barrier material, consistent with the observed emission energies of these features. This reduced Al region forms a so-called vertical quantum well and evidence for its presence in the structures is presented below. The fact that both the quantum wire and the vertical quantum well emission appear to originate from the same spatial position is due to the limited spatial resolution of the present CL technique. This results from the effective size of the exciting e-beam (~0.5μm) which is due to the spatial diffusion of the excited carriers before they recombine.[12]

4.3.2 CL Imaging of an Optimised 15Å Quantum Wire Sample (QT761B)

Sample QT761B represents the optimised quantum wire structure used as a reference for all subsequent experiments. The sample was grown at 680°C on a 4μm pitch grating, the thickness of the various layers in this standard sample are shown for reference in the diagram of Figure 4.7. A reduction in the thickness of the GaAs quantum well layer to 15Å shifted the quantum wire emission to higher energy, away from the bulk GaAs luminescence. In addition, the narrower side wall quantum well luminescence also shifted, but to a much larger degree, leaving the quantum wire emission as a very well resolved peak, suitable for optical characterisation by photoluminescence as described in Chapter 5.

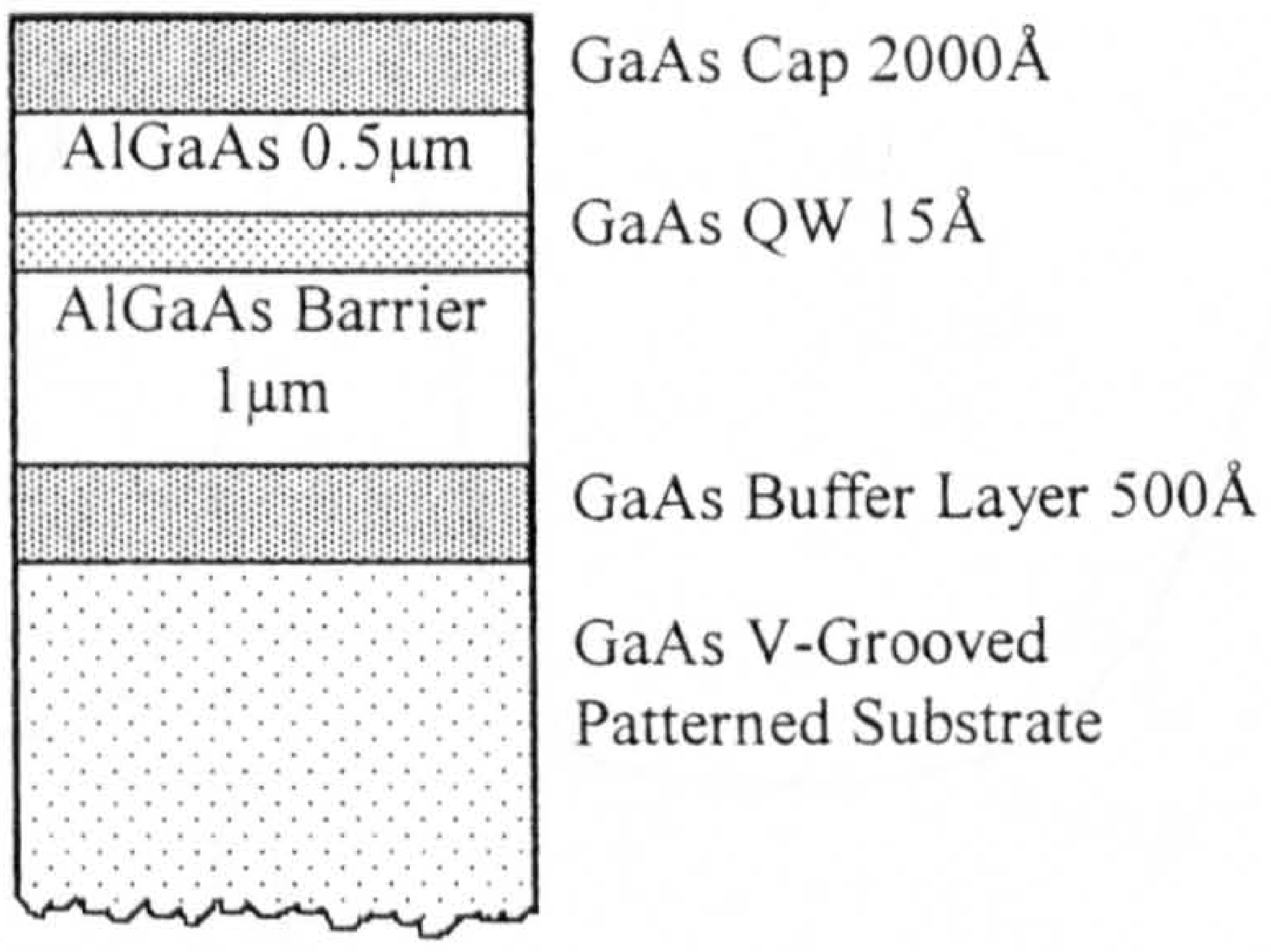

Figure 4.7 Schematic diagram of the optimised quantum wire structure used as a basis for all the subsequent experiments, QT761B.

CL analysis of this sample clearly shows the origin of all the different features of interest in a V-groove quantum wire structure. CL spectra for this sample are shown in Figure 4.8. In addition to the normal plan view spectrum, a cross-sectional edge view CL spectrum is also shown. In this measurement the electron beam has been positioned so that it scans a very small, localised region at the base of the groove. The idea behind this is to preferentially excite the wire, and hence to minimise the number of carriers captured by the quantum wells, thereby enhancing the luminescence intensity of the wire relative to that of the wells. The relative intensities of the features in the edge view spectra do change as a result of this selective excitation and there is also a significant shift of the peak positions to lower energy. It is likely, in these measurements where the excitation density is very high, that there is some localised heating of the sample. This would cause the bandgaps of the semiconductors to decrease, giving rise to the corresponding decrease in the emission energies of the quantum wells and quantum wires, as observed in the CL spectra. The peak at ~750nm in the plan view spectrum becomes the most prominent feature in the edge excited spectra, making it the most likely candidate for the wire emission. This assignment is confirmed by monochromatic CL imaging of a cross section of the sample.

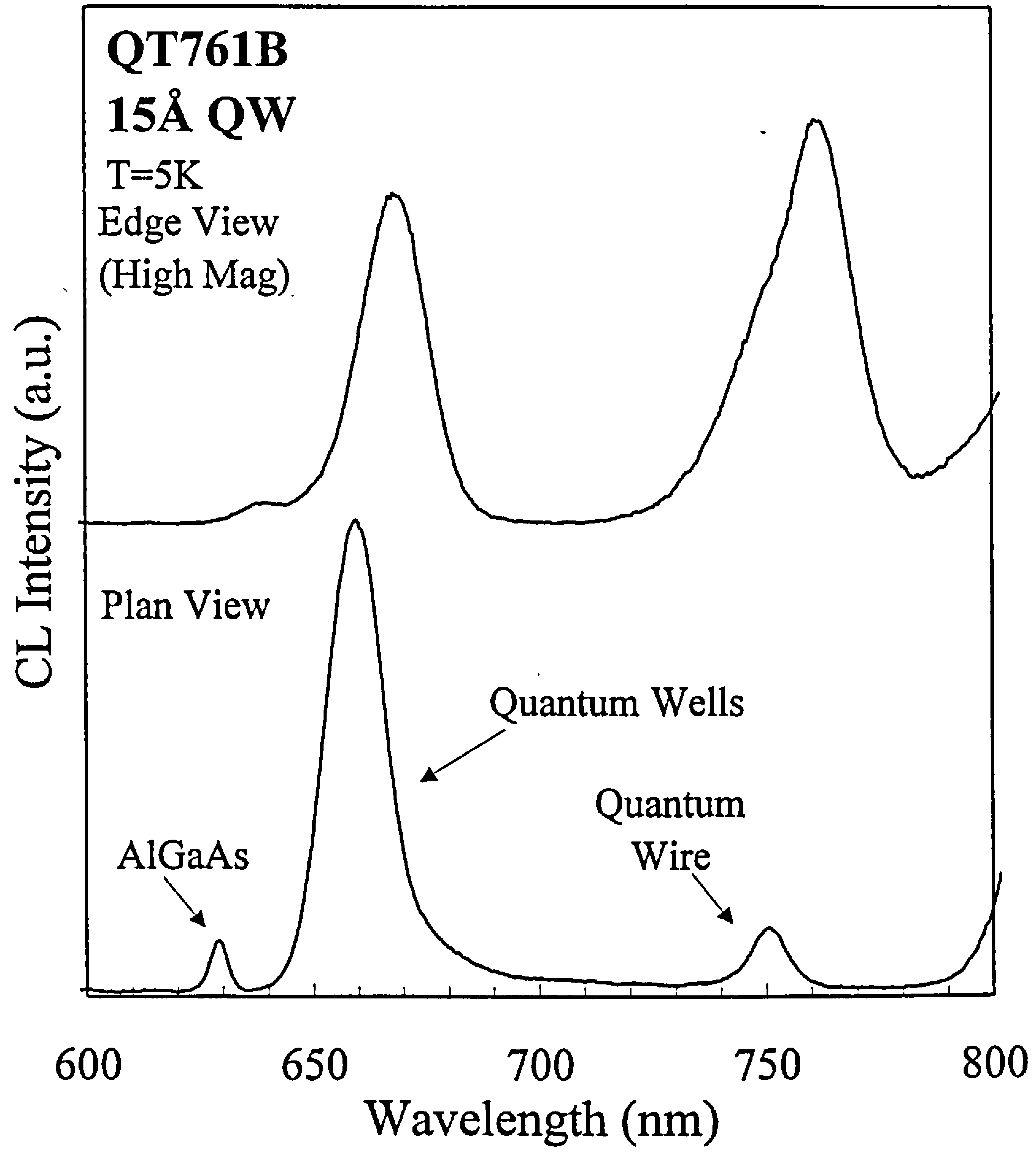

Figure 4.8 CL spectra of QT761B, plan view and high magnification edge view. The intensity of the quantum wire feature is significantly enhanced for the latter geometry with the selective, high magnification excitation.

Monochromatic CL images recorded at various luminescence wavelengths are shown in Figure 4.9. The relative positions of the quantum well and quantum wire features are similar to those observed for the 30Å sample. However, for the present sample the luminescence from the quantum wire, at 750nm, is much more clearly resolved, being spectrally isolated from the bulk GaAs and the quantum well luminescence. This enables the CL detection wavelength to be set on the peak of the wire luminescence, as observed in the plan view spectrum. Detection at 658nm reveals luminescence originating from the side wall quantum wells. Luminescence at 708nm, on the low energy tail of the 658nm quantum well peak arises from the tops of the grooves; in the present structure there is a narrow strip of (001) surface exposed here during the growth. The growth rate on the (001) surface is expected to be greater than that on the (111)A side walls.[3] The thicker top quantum well should therefore exhibit a lower energy emission than the thinner side wall quantum wells, as confirmed by the CL imaging. The 629nm luminescence arises from the base of the groove; as explained above its origin is a region of Ga rich AlGaAs which occurs at the centre of the groove during growth of the AlGaAs barriers. This feature has slightly shifted down in energy, whilst all the GaAs related features have moved to much higher energies, compared with the 30Å sample QT688. The growth of a thinner GaAs layer has therefore not significantly affected this feature, implying that it is related purely to the AlGaAs barrier material. The nominal AlGaAs composition remained constant for the two growth runs and the slight difference in energy observed for the vertical quantum well emission may be a result of slight differences in the as-grown Al composition or different Ga migration rates to the bottom of the groove.

From the present CL measurements we can be confident that our assignments of the origins of the various luminescence peaks in the spectrum are correct. Cathodoluminescence has therefore proved to be an invaluable tool for interpreting and understanding the rather complicated luminescence spectra of the quantum wire structures. In addition, it has provided a good indication of whether changes in growth conditions have been effective and has enabled the optimisation of the growth to give an isolated quantum wire emission suitable for extensive optical investigations by photoluminescence and electroluminescence. These experiments are described in Chapter 5.

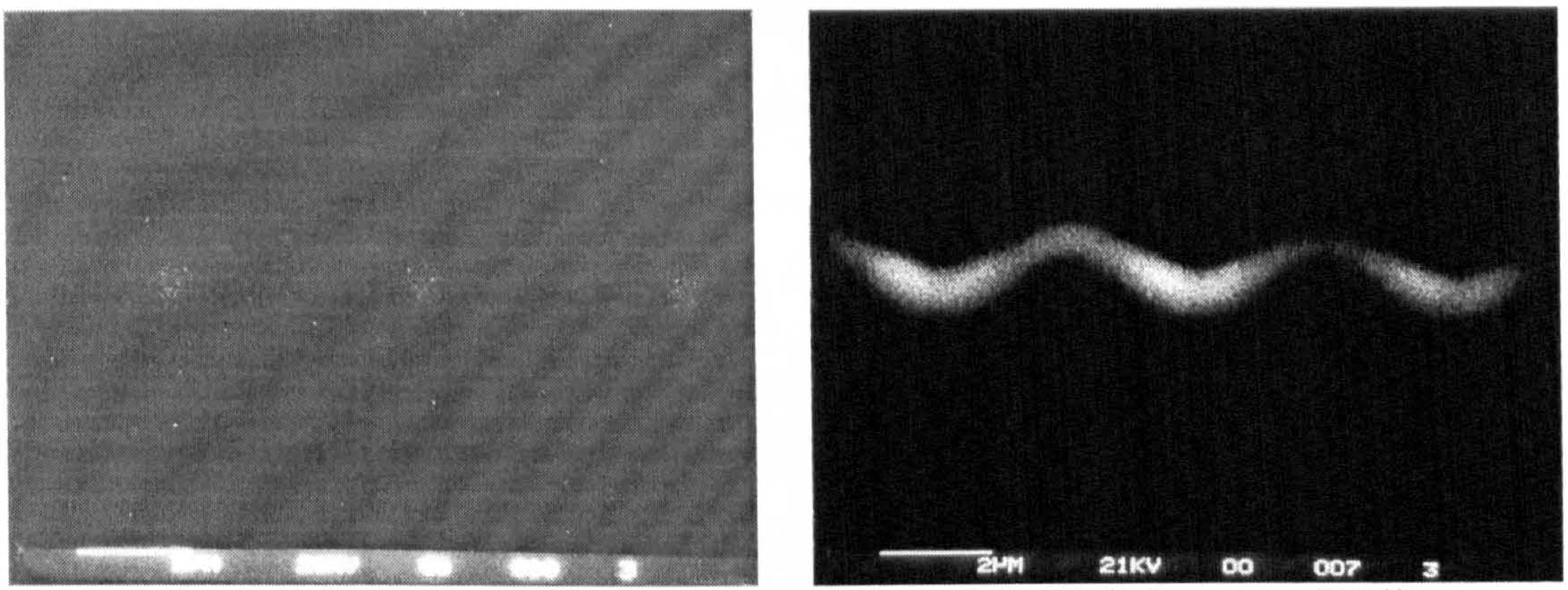

(629nm Vertical Quantum Well) (658nm Side Wall Quantum Well)

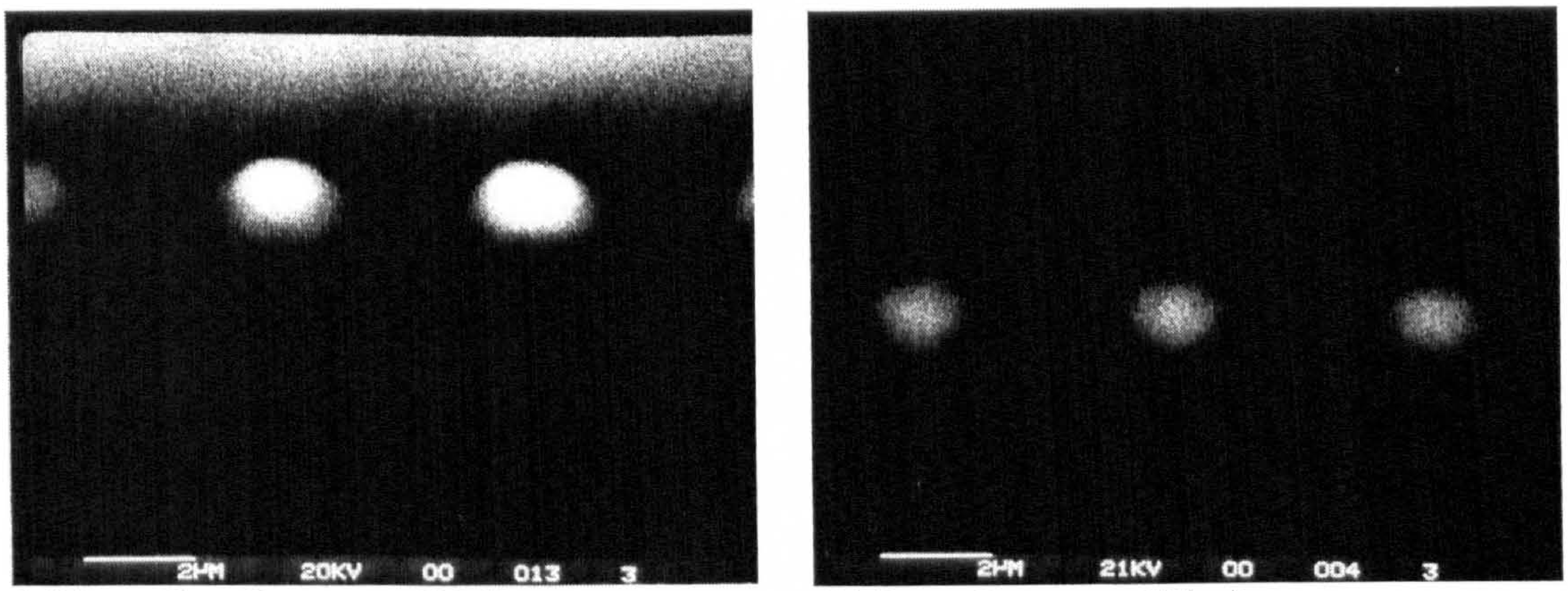

(708nm Top Quantum Well) (750nm Quantum Wire)

Figure 4.9 Monochromatic CL images of quantum wire structure QT761B, recorded for wavelengths of 629nm, 658nm, 708nm and 750nm.

4.3.3 CL Imaging of a Sample Grown on a Substrate having a Mis-orientation of 3°→{110}

The SEM images of a sample with the small substrate mis-orientation of 3°→{110} are described above (Section 4.2.1). Although it was clear from these images that the growth along the side wall had not proceeded uniformly, it was not clear how this would affect the optical and structural properties of the quantum wells. Possible effects of this non-uniformity were investigated using monochromatic CL imaging. The sample under investigation had a 50Å GaAs quantum well (compared to the 15Å reference sample thickness) grown at 720°C. This sample was grown early on in the optimisation procedure and hence does not contain a quantum wire which can be spectrally resolved from the either the bulk GaAs or the quantum wells. It is likely that the thickness of the quantum well grown was too thick so that the emission energy of the quantum wire (if it has formed) is completely obscured by the quantum well luminescence which now occurs at much lower energies. The interest in this sample lies with the possible variation of the emission wavelength for luminescence emanating from the side wall quantum well. Figure 4.10 shows monochromatic CL images recorded at several wavelengths on the main luminescence peak observed in the CL spectra. These images show that there is a distinct spatial variation in the emission energy along the length of the side wall, with the trend being for lower energy (longer wavelength) emission to appear towards the base of the groove. This behaviour is indicative of a lateral tapering of the side wall quantum well down the side of the groove, with the thickness decreasing towards the top of the groove where higher energy emission is observed.

The use of CL in this case has hence served to confirm the occurrence of non uniform side wall growth, resulting in a quantum well of varying thickness. From the point-of-view of optical spectroscopy this effect is undesirable. Disregarding the fact that the quantum wire was not observed in this sample, an ideal sample should contain uniform side wall quantum wells which exhibit a narrow luminescence peak and hence ensuring that the optical spectra are not dominated by complicated non-quantum wire features. The optimised structure grown on an exact (001) substrate, as typified by sample

QT761B, exhibits these properties, with a relatively narrow quantum well luminescence which is spectrally separated from an isolated quantum wire emission.

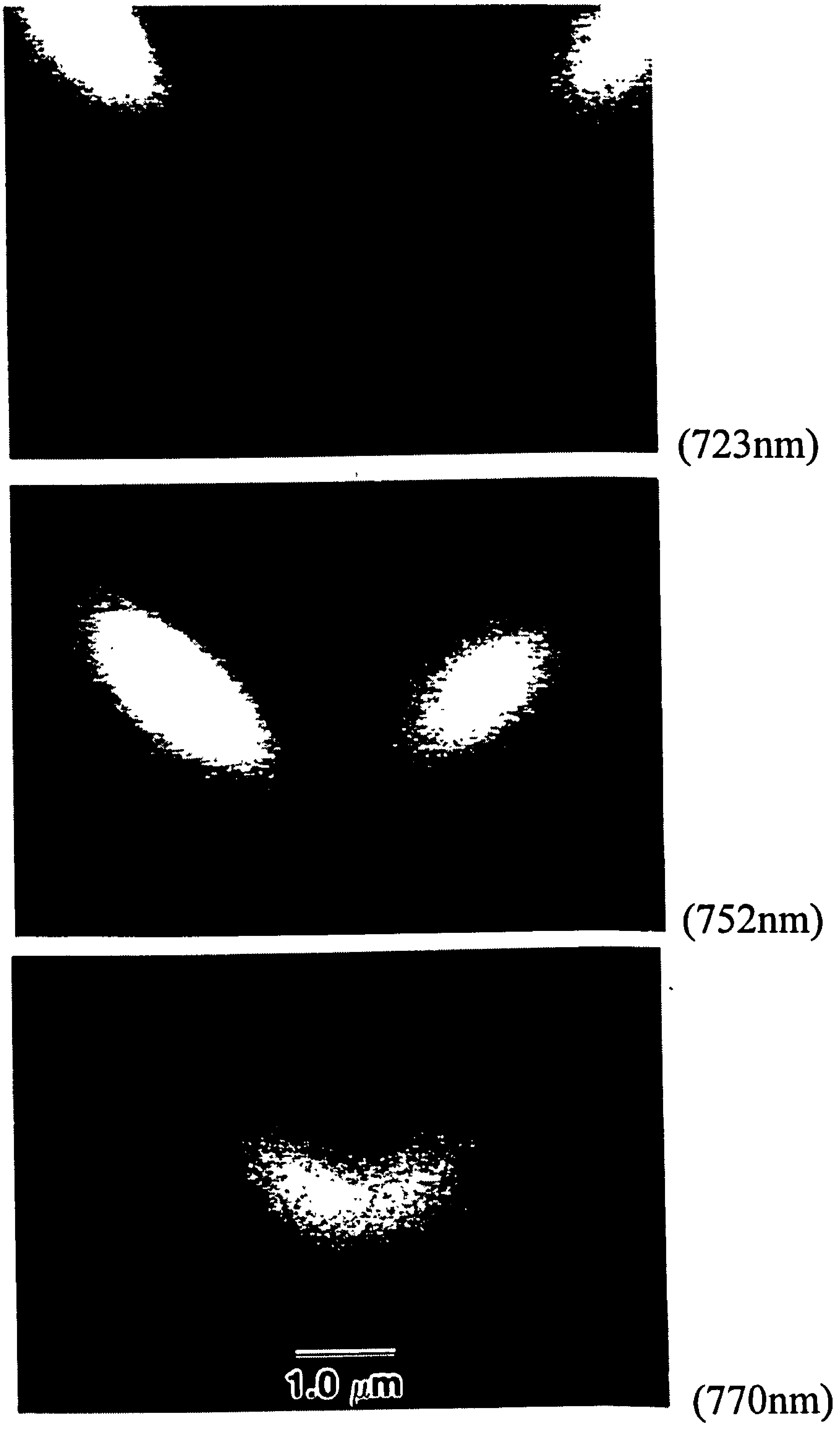

Figure 4.10 Monochromatic CL images of sample QT602B grown on a 3° mis-orientated substrate. Evidence of growth non-uniformities along the side walls is visible.

4.4 Transmission Electron Microscopy (T.E.M.) Studies

An accurate assessment of the quality and shape of V-groove quantum wires can be achieved with high resolution structural and optical imaging of the samples. The CL analysis described in the previous sections indicates that samples with a 15Å deposition of GaAs contained quantum wires exhibiting a significantly different emission energy to those of the side wall or top quantum wells. TEM images of these structures show a significant accumulation of GaAs at the bottom of the groove. This confirms that the growth has proceeded as expected, with the growth rate of GaAs on the (001) surface at the base of the groove being greater than that on the (111)A side walls, and vice versa for AlGaAs growth. The latter effect produces the required sharpening of the V at the base of the groove, allowing a sufficiently small GaAs quantum wire to form. The TEM micrograph of Figure 4.11 shows a cross-sectional image of sample QT761B. This is the established standard sample, as demonstrated by CL and μPL (see following chapter) analysis which show spectrally resolved quantum wire luminescence, with a 15Å GaAs layer grown on a 4μm pitch grating at 680°C. The lateral width of the quantum wire in this TEM image is seen to be ≈600Å and the wire has a maximum thickness at the base of the groove of ~60Å. The latter value is considerably larger than the 15Å thickness for growth on a (001) planar surface, indicating that preferential GaAs growth has occurred at the base of the groove.

A TEM image of sample QT761A, which contains a 5 period quantum wire stack, is shown in Figure 4.12. Reproducible growth of the quantum wires in the stack is clearly demonstrated, with all five wires having a similar shape and dimensions. The curvature at the base of each quantum wire, (the factor that essentially defines the overall quantum wire shape),[11] is very similar implying that a self limiting shape, defined by the Al fraction, has been reached during the 500Å growth of AlGaAs between each wire.[13] An additional interesting feature of this image is the dark stripe running down the centre of the groove. This has been attributed to a Ga rich stripe of AlGaAs, caused by a preferential deposition of Ga at the base of the groove, as the AlGaAs layer is being grown. This results from the different Ga incorporation rates on the (111)A side wall surface and the (001) surface present at the base of the groove. This feature is referred to as the vertical quantum well.[2] Evidence of its existence has been provided by the CL analysis described above, which showed emission from the base of the groove occurring at two distinct energies. More detailed optical investigations of the luminescence originating from this feature is described in the following chapter.

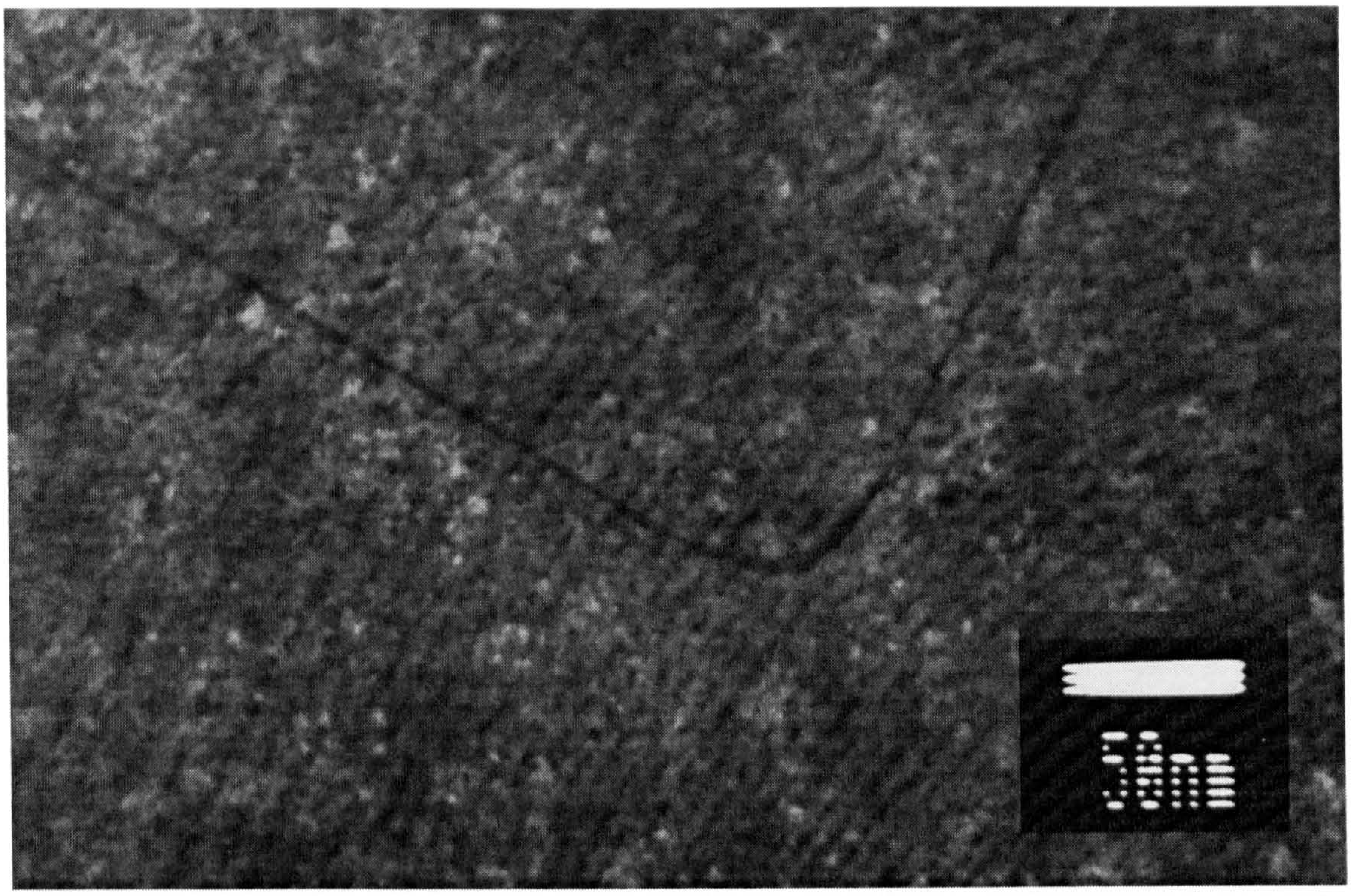

Figure 4.11 Cross-sectional TEM image of a single standard 15Å quantum wire structure (sample QT761B).

Growth of a higher density array of quantum wires on a smaller pitch grating is shown in Figure 4.13. The groove separation in this sample is 2μm. The original surface defined by the etch is visible at the base of the structure. With the initial grooves being very rounded in nature. However, the growth of AlGaAs on this surface has led to the formation of very well defined (111)A side wall facets and (001) tops, allowing a thin quantum wire to form at the base of the groove. This image shows that even though the original template for growth was very curved, with no well defined V shape, stable facets were still able to form by self organised growth. This result has important implications for the fabrication of even higher density arrays of quantum wires. The ability to prepare substrates with a well defined groove shape is not as critical as may at ability to prepare substrates with a well defined groove shape is not as critical as may at first be imagined, because the V-groove shape will self form during the growth. When the groove separation is small (feature sizes <1 μm for GaAs) the selective wet chemical etching used to prepare the V-groove shape becomes hard to control, due to the rapid undercutting of the photoresist mask.[14] However, if a rough pattern is sufficient to provide a template allowing the wires to form, this will make the pre-growth processing stage much less critical. Also visible in the TEM image of Figure 4.13 is the dark vertical quantum well stripe which extends down the entire length of the AlGaAs material. This demonstrates that selective growth on different facets occurs very early on during growth of the barrier material, suggesting that the V shape is formed at quite an early stage.

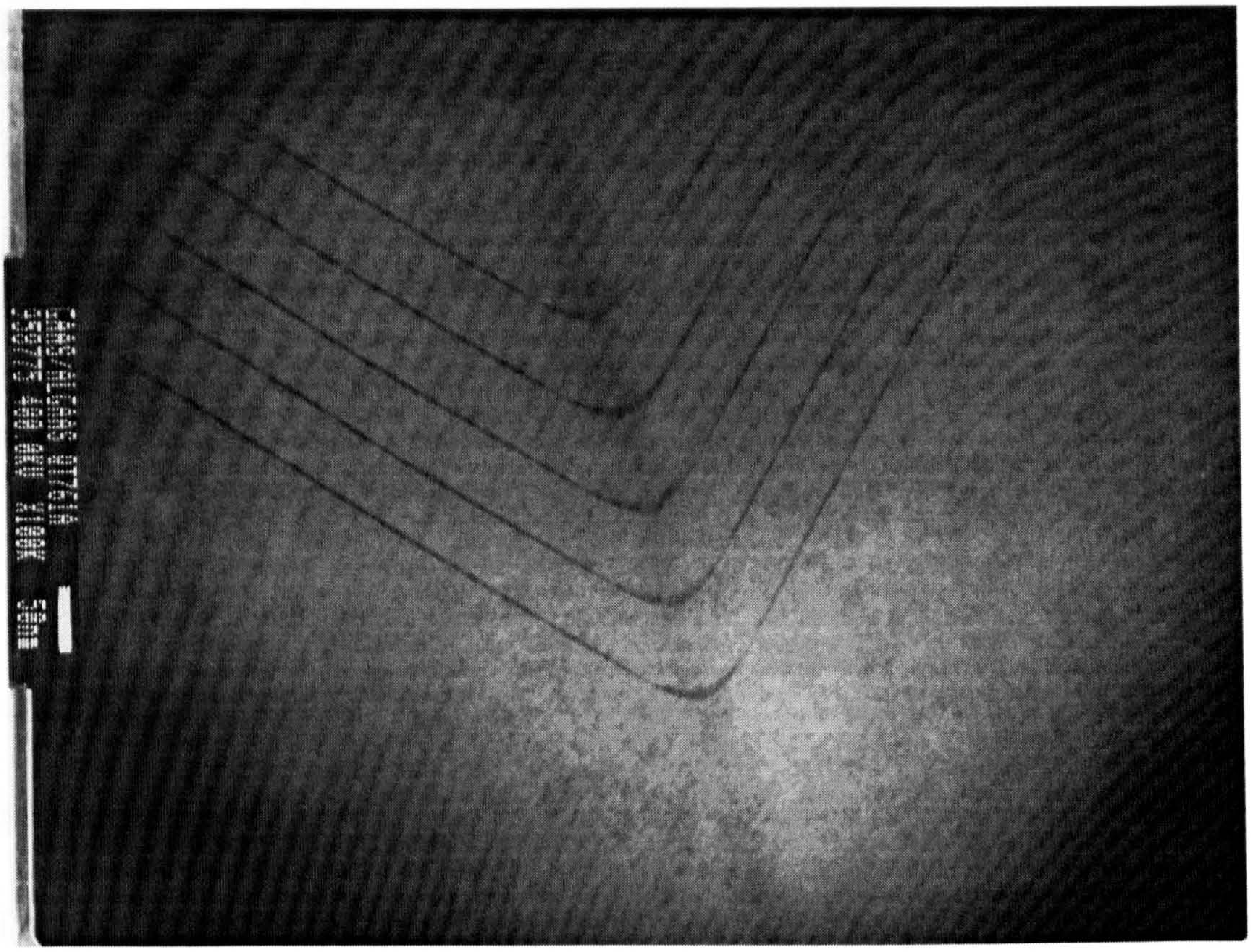

Figure 4.12 Cross-sectional TEM image of a 5×15Å quantum wire stack (Sample QT761A).

As well as proving the existence of a Ga rich vertical quantum well and crescent shaped deposits of GaAs that comprise the quantum wires, TEM provides images that enabled an accurate determination of the quantum wire shape. Obtaining the exact shape and

)

size is necessary to enable theoretical modelling of the energy levels of confined carriers within the quantum wires.[15] A determination of the wave-functions, corresponding to the energy levels in the wires, are used in the following chapter to explain the behaviour of confined quantum wire energy levels when these samples are subjected to a high magnetic field orientated along different spatial directions.

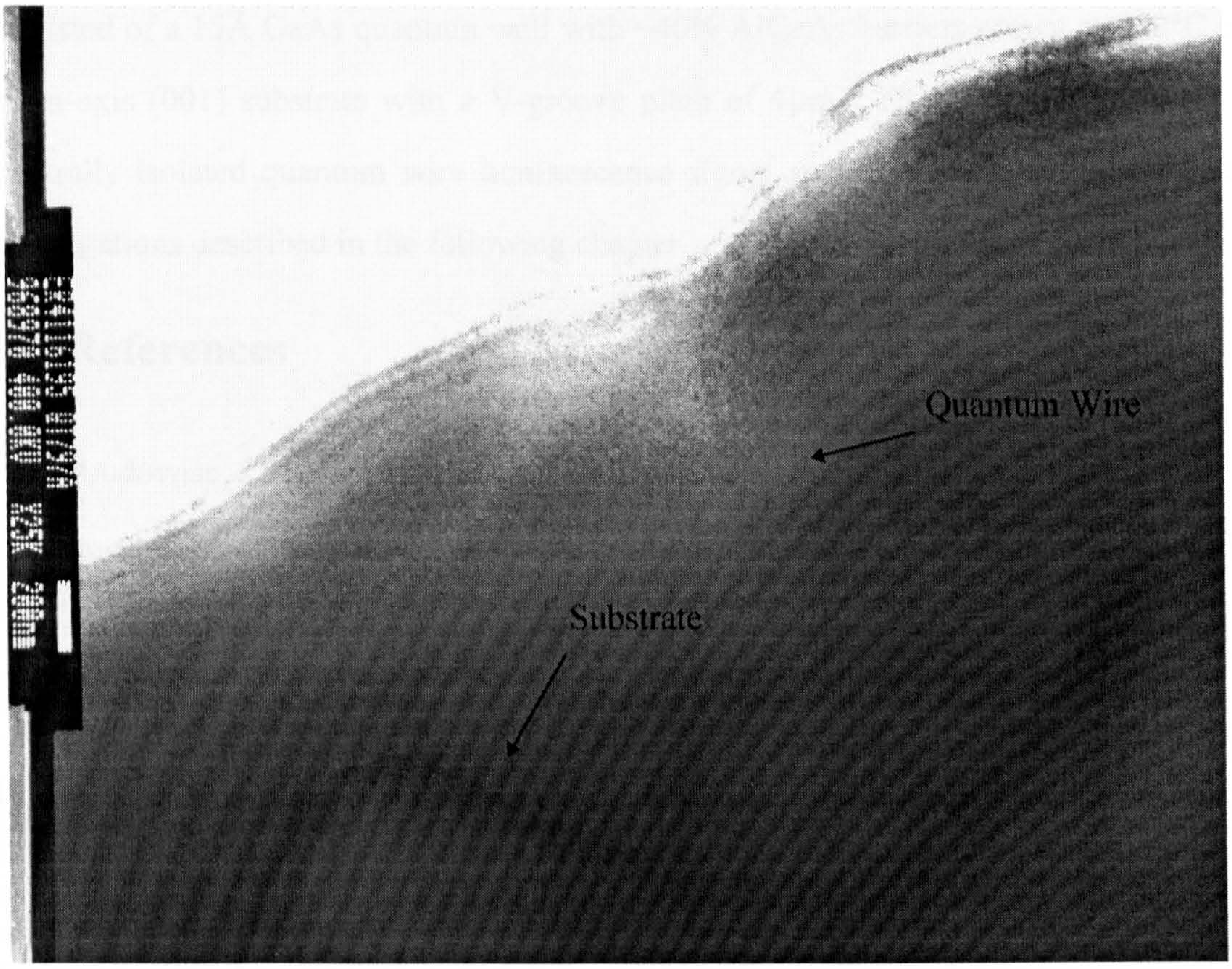

Figure 4.13 Cross-sectional TEM image of a 2μm pitch sample, QT797A. The lower spatial resolution of this image shows the re-sharpening effect which occurs during the AlGaAs growth.

4.5 Conclusions

The MOVPE growth optimisation procedure used to obtain quantum wires suitable for optical studies has been described in this chapter. Initially SEM imaging provided a relatively straight forward method for assessing the growth uniformity of the epitaxial layers and the overall quality of the original etch. High resolution TEM analysis confirmed the existence of crescent shaped quantum wires at the base of the grooves. Structural information regarding the exact shape of the quantum wire that had formed used to investigate the origin of all the features found in the luminescence spectra i.e. the various quantum wells and the quantum wire. During the optimisation of the structure CL was used to monitor growth uniformity, particularly on the side walls where evidence for a lateral tapering of the quantum well was found for samples grown on mis-oriented substrates. Using CL an optimised structure was determined. This consisted of a 15Å GaAs quantum well with ~40% AlGaAs barriers grown at 680°C on an on-axis (001) substrate with a V-groove pitch of 4μm. This sample resulted in a spectrally isolated quantum wire luminescence signal suitable for the detailed optical investigations described in the following chapter.

4.6 References

[1] M.J. Ludowise, J. Appl. Phys. **58**, (8), R31, (1985).

[2] A. Gustafsson, F. Reinhardt, G. Biasiol, and E. Kapon, Appl. Phys. Lett. **67**, (25), 3673, (1995).

[3] S.D. Herse, E. Barbier and R. Blondeau, J. Crys. Growth, **77**, 310, (1986).

[4] C.S. Son, S.I. Kim, Y. Kim, Y.K. Park, E.K. Kim, S.K. Min, I.H.J. Choi, Appl. Phys. **82**, (3), 1205, (1997).

[5] E. Kapon, Optoelectronics, **8**, (4), 429, (1993).

[6] W. Pan, H. Yaquchi, K. Onabe, R. Ito, and Y. Shiraki, Appl. Phys. Lett. **67**, (7), 959, (1995).

[7] D. Bimberg, J. Christen, Inst. Phys. Conf. Ser. **134**, 11, 629, (1993).

[8] J. Christen, E. Kapon, E. Colas, D.M. Hwang, L.M. Schiavone, M. Grundmann and D. Bimberg, Sur. Sci **267**, 257, (1992) .

[9] E. Kapon, K. Kash, E.M. Clausen Jr., D.M. Hwang, and E. Colas, Appl. Phys. Lett. **60**, (4), 477, (1992).

[10] E. Kapon, D.M. Hwang, R. Bhat, Phys. Rev. Letts. **63**, (4), 430, (1989).

[11] E. Kapon, G. Biasiol, D.M. Hwang and E. Colas, Microelectronics Journal, **26**, 881, (1995).

[12] D.B.Holt and F.M.Saba, 'The CL mode of the SEM: A Powerful Microcharacterisation Technique', Scanning Electron Microscopy, p.1023, (1985).

[13] S. Simhony, E. Kapon, E. Colas, D.M. Hwang, N.G. Stoffel and P. Worland, Appl. Phys. Lett. **59**, (18), 2225, (1991).

[14] G. Hill, private communication.

[15] A. Forshaw. PhD Thesis, University of Sheffield (1996).

Chapter 5

Optical Studies of V-groove GaAs-AlGaAs Quantum Wires

5.1 Introduction

The growth experiments described in chapter 4 and detailed structural and optical analysis using Scanning Electron Microscopy, Transmission Electron Microscopy and Cathodoluminescence resulted in the ability to produce quantum wires of excellent structural and optical quality. Sample QT761B represented the optimised growth and all subsequent samples were grown using nominally identical growth conditions. The experiments described in the present chapter reflect detailed optical measurements performed on samples and devices based on this optimised structure.

The present Chapter is organised in the following manner. μPL measurements, with a spatial resolution ~1-2μm, are used to study the optical spectra of single quantum wires, hence removing some of the effects of wire width fluctuations from the optical spectra. In addition, the high laser power densities available with this technique allow subband filling effects to be observed. A brief study of AlGaAs-AlGaAs quantum wires is described and it is demonstrated that such structures are able to produce visible emission. PL measurements from samples which have been etched for different lengths of time provide further confirmation of the origin of the numerous features in the optical spectra. A five period quantum wire sample grown within the intrinsic region of a *p-i-n* structure allows a comparison between the optical and electrical injection of carriers. An enhancement of the quantum wire emission intensity is observed for the latter process. EL spectra recorded as a function of drive current show subband filling and saturation effects for the 1D quantum wire states, in contrast to the 2D quantum well states. Magneto-optical measurements are used to probe the spatial anisotropy of the quantum wire subband wavefunctions; this anisotropy is shown to increase with increasing subband index. In addition, a possible transition from excitonic to free-carrier behaviour is observed for high subband carrier occupancies. Excitation of a single quantum wire, via the cleaved edge of a sample using the μPL equipment, reveals effects attributed to excitonic localisation by potential minima, resulting from wire width fluctuations. Finally, preliminary measurements of a quantum wire laser structure are presented.

5.2 μPL Measurements of V-groove Quantum Wires

The use of the micro photoluminescence (μPL) equipment described in chapter 3 enables the study of individual quantum wires. This reduces, to some extent, problems associated with wire width inhomogeneities. The size of the laser spot produced by the microscope objective is typically around 2μm or less in diameter, depending on the wavelength of the laser light used in the experiments. Unless otherwise stated the 4880Å line of an Ar^+ laser was used as the excitation source. Photoluminescence from the sample was collected by the microscope objective and focused, with suitable lenses, onto the slits of a triple grating spectrometer. This contains an initial double grating filter stage, which gives very good stray light rejection capabilities, followed by the third grating which disperses the light onto a multi-channel, liquid nitrogen cooled silicon CCD detector. The spectral range of each scan is determined by the dispersion of the final grating and the width of the CCD chip (typically ~700Å, corresponding to an energy range of ~130meV at 8000Å, was scanned with each measurement). Because the full emission spectrum from the quantum wire samples covers a larger spectral range (1500meV - 2100meV), an entire spectrum is made up of several (typically 4 or 5) smaller scans.

5.2.1 μPL Measurements of Standard Quantum Wire Samples

In a similar manner to the cathodoluminescence measurements described in the previous Chapter, samples could be studied with the excitation source perpendicular to the layer in 'plan view' or parallel to the wire, by exciting a cleaved cross-section of the sample, in an 'edge view' measurement. Accurate positioning of the laser on the sample was achieved by imaging the surface with the microscope objective and eyepiece and then moving the cryostat and sample relative to the laser position. As the laser spot size (~2μm) was smaller than the V-groove features (which were typically 4μm in size) it was possible to preferentially excite the quantum wire, and hence reduce the relative intensities of the top and side wall quantum well emissions, by positioning the laser at the bottom of a groove. Even greater quantum wire excitation selectivity was achieved by viewing the cleaved edge and exciting slightly below the bottom of the V. In this geometry carriers are photoexcited directly into the wire or diffuse from the nearby AlGaAs. However diffusion into the quantum wells is reduced due to their greater spatial separation from the laser spot.

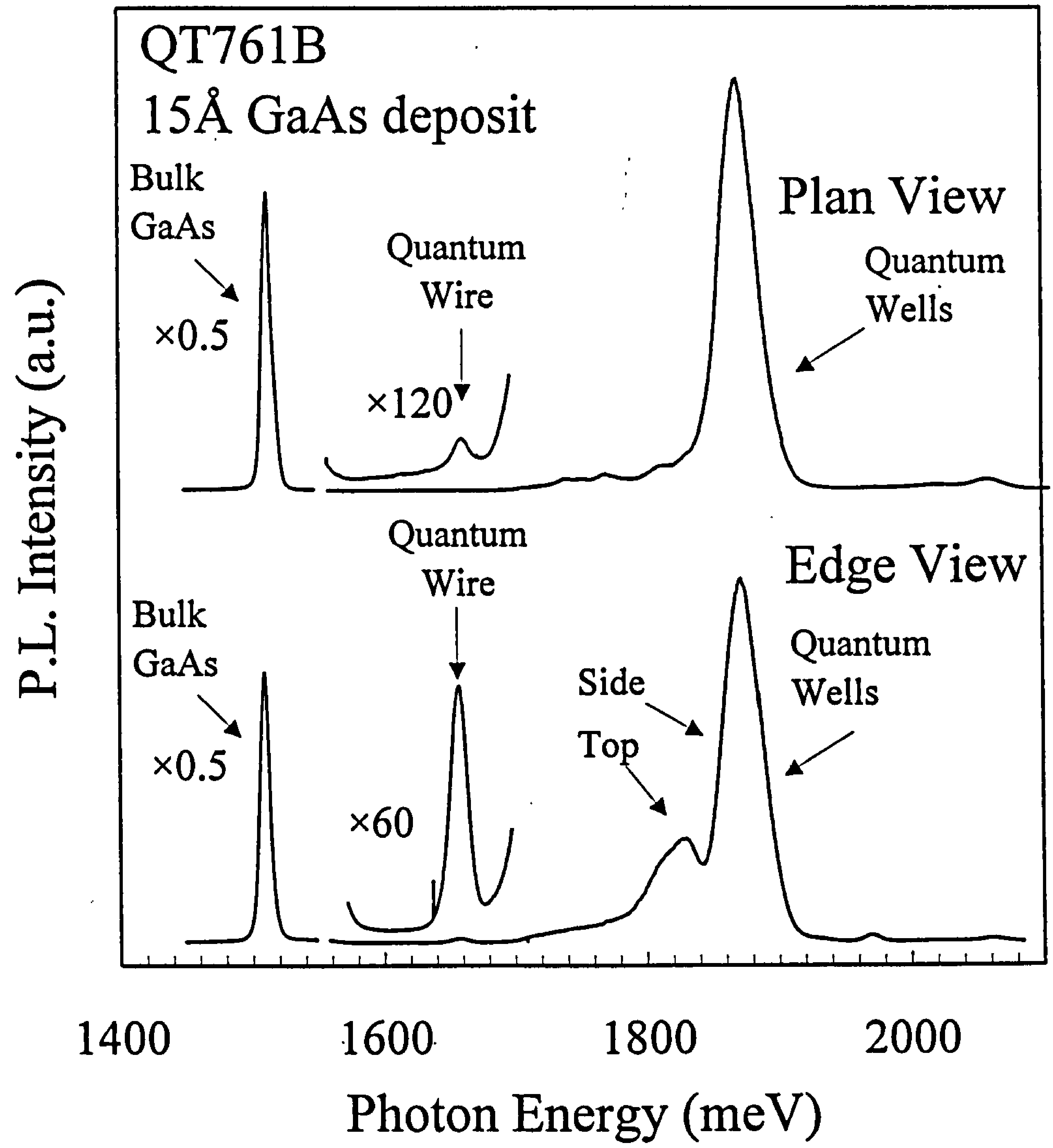

Figure 5.1 μPL spectra at T=4.2K of a standard 15Å sample (QT761B), edge and plan view excitation geometries.

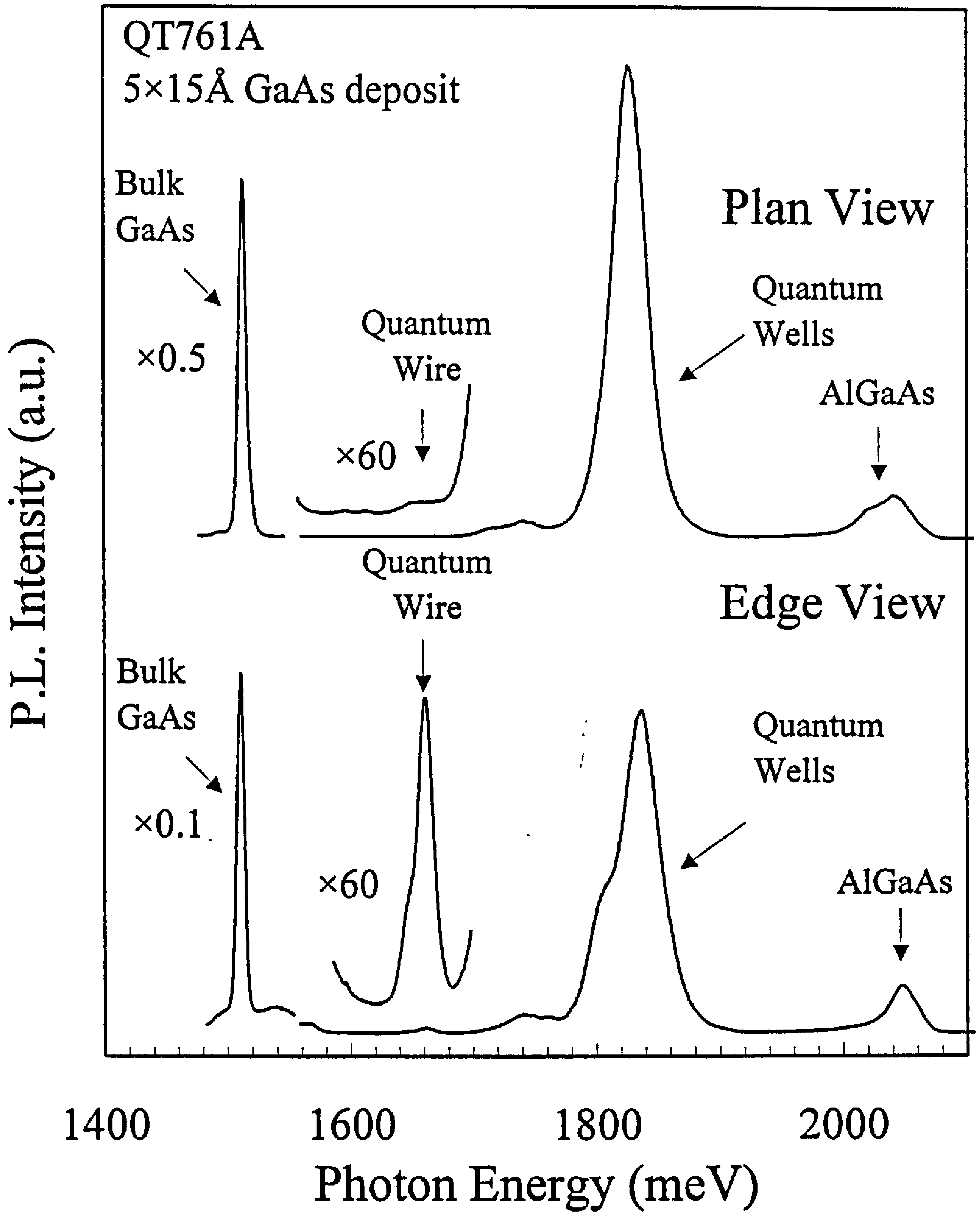

Figure 5.2 μPL spectra at T=4.2K of a 5×15Å wire sample (QT761A), edge and plan view excitation geometries.

Figure 5.1 shows μPL spectra taken with plan and edge view excitation of sample QT761B, which represents the standard, optimised single quantum wire sample described in Chapter 4. CL analysis presented in the previous chapter has been used to identify the origin of the luminescence from all the features marked in the spectra. The strength of the quantum wire luminescence is greatly enhanced for excitation of a cleaved edge compared with plan view excitation. The quantum well features (especially emission from the lower energy top quantum well) also appear relatively weaker for edge view excitation due to the spatial separation of the excitation from these regions of the structure. This result shows that there are significant advantages in using the edge excitation geometry over plan view, when studying the quantum wires. The FWHM linewidth of the quantum wire in the present sample is ≈16meV, with an emission energy of 1658meV. This is well separated from the broad quantum well emission observed at 1810meV.

Figure 5.2 shows the μPL spectra for sample QT761A, which has an array of five wires stacked in the vertical direction, each separated by 500Å barriers. TEM images (see previous chapter) show that re-sharpening at the base of the grooves occurs when the AlGaAs barrier material between the wires is deposited, thus allowing the identical formation of the next quantum wire in the stack. Although this sample was grown at the slightly higher temperature of 720°C, the emission energy remains at ≈1660meV, with a similar FWHM linewidth to the single wire sample. This latter result indicates good wire-wire size and shape uniformity. A weak shoulder appears on the low energy side of the quantum wire emission peak; this may represent emission from one or more of the wires having a slightly different emission energy. This difference could arise if the first wire grown had a different shape compared with the subsequent wires. This is possible if the curvature at the base of the groove does not completely recover during the 500Å of AlGaAs barrier growth,[1] leading to subsequent wires having a different template on which to form. The TEM images in Chapter 4 (Figure 4.13) show the shape of all five wires in the stack and there is no noticeable difference in the shape of any of the wires. Hence if there is any difference in quantum wire shape causing the two features in the PL spectra it must be very small given the high resolution of the TEM images. Another factor possibly affecting the ground state emission energies of the quantum wires, but very difficult to quantify, is the effect of changes in the barrier potential surrounding the quantum wire, caused by a variation in the composition of the aluminium fraction in the AlGaAs. In particular, TEM images show a dark stripe, the vertical quantum well, which comprises a Ga rich AlGaAs region of barrier material running down the centre of the groove (see Figure 4.15). Changes in the composition of this region or of the general AlGaAs region surrounding the wire would result in variations of the quantum wire emission energy. However this effect is difficult to quantify, particularly as it is not possible to determine the aluminium composition of the vertical well or barrier, and how they vary spatially, from the TEM images. The TEM images only show the relative compositions of the barrier material (darker for higher gallium concentrations).

5.2.2 Power Dependent μPL for High Laser Excitation Powers

Using the μPL equipment, a small, well focused laser spot could be obtained, enabling very high laser power densities to be produced on the sample. Experiments were performed on the quantum wire samples to study the effects of high incident laser power on the PL emission. Recorded spectra of the quantum wire emission for various incident laser power densities are shown in Figure 5.3. For the highest laser powers additional emission at higher energy is observed. This emission results from the recombination of carriers in excited quantum wire subbands and indicates that the ground state subbands are full, preventing relaxation from excited states. Emission due to at least two excited subband transitions is observed. From the spectra, subband transition separations of ~30meV are obtained. This reflects the sum of the electron and hole subband separations (assuming $\Delta n=0$ transitions) although due to the smaller electron effective mass, the former provides the dominant contribution. Similar subband filling effects are observed for high current EL measurements which are described later, along with a more detailed discussion of this observation of excited state transitions.

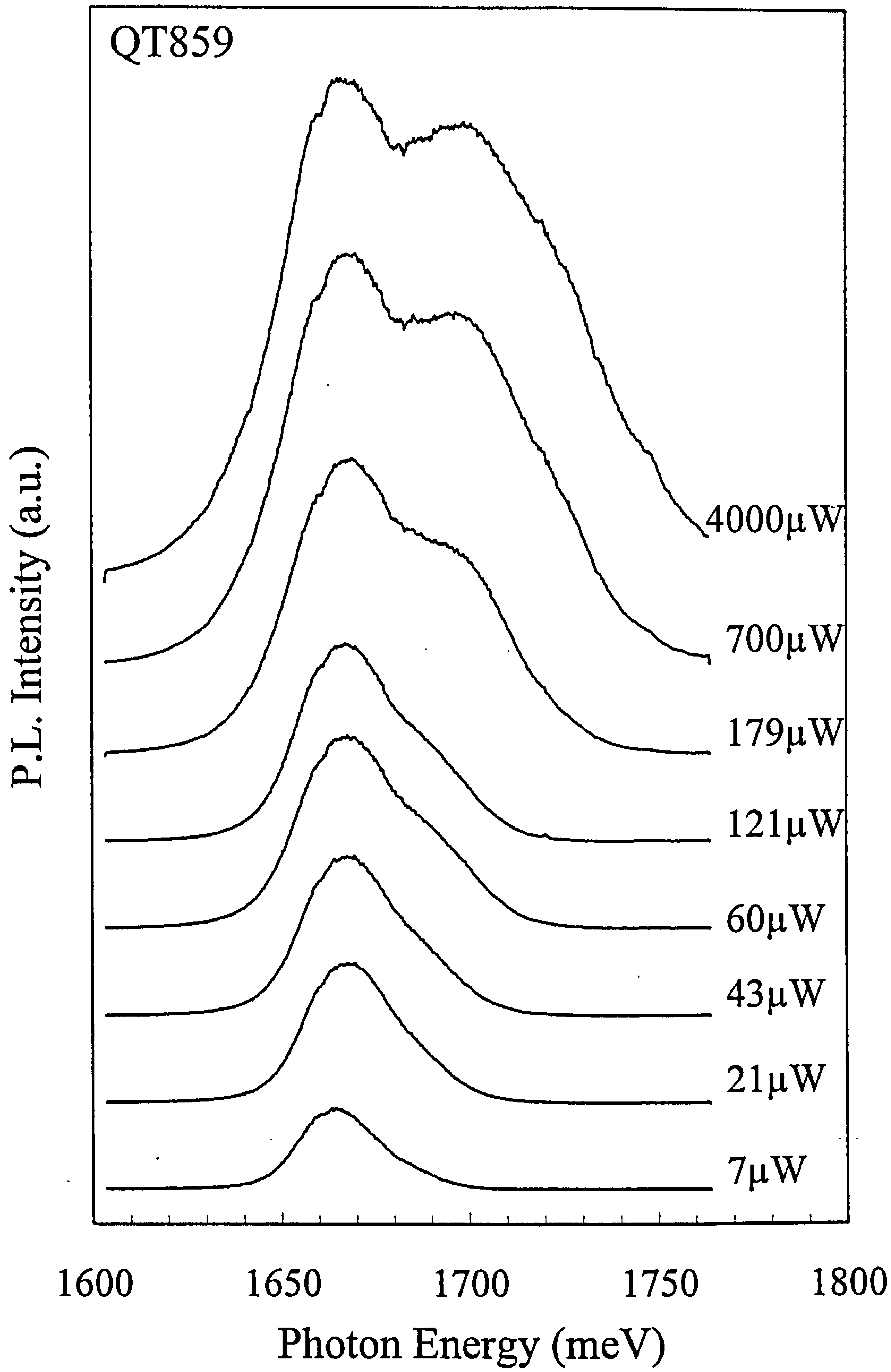

Figure 5.3 μPL spectra at T=4.2K recorded for high incident laser power densities. Higher energy quantum wire sub-band transitions are clearly observed for highest incident laser powers. (100μW≡3×10^3Wcm^{-2}).

5.2.3 Power Dependant μPL for Low Incident Laser Power Excitation

In addition to high power densities, the μPL equipment can be used to excite a small region of the sample with a very low power density. The high PL collection efficiency of the optics, in conjunction with multi-channel CCD detection, makes μPL measurements with very low laser powers feasible. Figure 5.4 shows a series of edge-excited spectra of a quantum wire, recorded for very low laser excitation power densities. Assuming a laser spot size of ~2μm, an absolute laser power of 1nW corresponds to a power density of $\sim 3\times 10^{-2}$Wcm^{-2}. The spectra show that the inhomogeneously broadened ground state luminescence splits into a series of much sharper 2-3meV peaks, which become better resolved as the laser power is reduced. At the lowest power a single, narrow peak is observed on the high energy side of the initial distribution. This behaviour is attributed to exciton localisation by potential minima, resulting from wire width fluctuations that occur along the length of the wire. Similar effects have been observed in quantum wells due to spatial variations of the well width.[2] This result provides evidence that non-uniform growth has occurred, giving rise to mono-layer step variations on the surface of the wire which act as local traps for carriers. For low excitation powers only a smaller number of these potential minima are populated, allowing them to be spectrally resolved. Under higher excitation powers the carrier density is increased, populating a larger number of minima and resulting in the broad emission which represents the average potential seen by the carriers. The fact that it is one of the higher energy minima that appears to remain populated for the lowest carrier density indicates that a thermal distribution of carriers between the potential minima does not exist. This is consistent with the depth of the minima (~6meV from the separation of the sharp lines) and the thermal energy at the measurement temperature (≈1.8meV@ 20K) which is insufficient to allow carrier migration between the minima. The spectra of Figure 5.4 were recorded for a single modulation doped wire. Hence, the potential minima could result from either wire width fluctuations or potential fluctuations due to remote ionised donors. However, very similar effects have been observed in an undoped structure, suggesting that the former is the dominant mechanism. The measurement temperature for the spectra of Figure 5.4 was 20K.

Similar effects, although not as pronounced, are observed with the sample at a lower temperature of 4K. The reason for this difference is not clear.

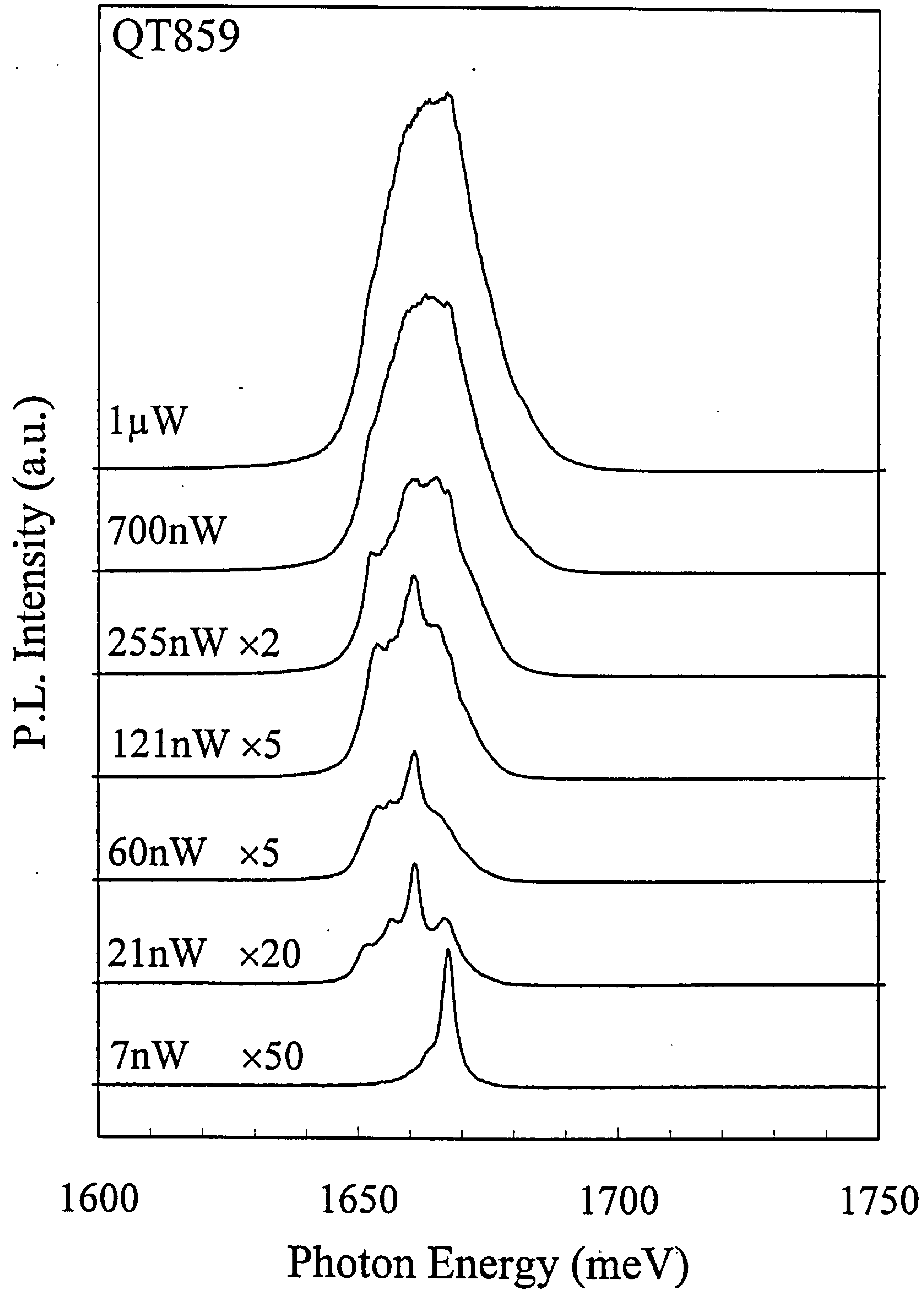

Figure 5.4 Low power μPL spectra at T=20K showing the appearance of sharp spectral features attributed to wire width fluctuation effects. (100nW≡3Wcm^{-2}).

5.2.4 AlGaAs-AlGaAs Quantum Wires

The growth of pure GaAs quantum wires results in an emission energy at approximately 1660meV, or a wavelength of 747nm in the near infra-red. Obtaining higher energy emission, corresponding to the visible region of the spectrum, has the potential for producing visible lasers or LED devices. Increasing the confinement of the wire by growing a thinner GaAs layer would have this effect. However the controlled MOVPE growth of layers <15Å is difficult to achieve. The growth time for a <15Å layer (~1s) is of a similar magnitude to the gas switching time, making the repeatability of the wires difficult to control. This is particularly problematic for the growth of multiple stacked wires. In addition, very narrow wires will become increasingly sensitive to the effects of wire width fluctuations discussed in the previous section. Hence deposition of ≈15Å of GaAs probably represents the practical limit for these wires. An alternative option for shorter wavelength emission is the growth of aluminium containing quantum wires which also has the effect of increasing the band gap of the material, shifting the emission energy of the luminescence into the red without the need to grow thinner layers. Measurements on such structures are described in the present section.

Quantum wires containing a small fraction (7→21%) of aluminium were grown to investigate the possibility of producing quantum wires exhibiting higher energy emission in the visible region of the spectrum. One of the factors controlling the formation of quantum wires by the V-groove technique is the extent to which the growth rate at the bottom of the groove is greater than the growth on the side wall, a large differential growth rate is required to produce a well defined quantum wire. This is normally satisfied when the growth rate on the side walls is very low, hence increasing the flux of atoms that arrive at the base of the groove; this is the case with GaAs. Aluminium arriving on the (111)A side walls is easily pinned and incorporated into the surface. This has the effect of reducing the flux of material to the bottom of the groove which in turn reduces the self-organised curvature at the base of the groove. This behaviour is exploited to give the sharp base needed for wire growth. Hence it is not obvious that with increasing Al composition, AlGaAs quantum wires will continue to form.

For the present investigation nominal 15Å quantum wires were grown with aluminium compositions of 7, 15 and 21%. µPL spectra of these samples with, for comparison, the spectra of the standard 15Å GaAs sample are shown in Figure 5.5. The position of the quantum wire emission is marked in these spectra. The emission energies of the quantum wire and quantum wells shift, as expected, to higher energy as the aluminium fraction is increased from 0% through 7% to 15%. When the Al composition of the wire is 21% there is no evidence of a quantum wire in the µPL spectra. However the bulk AlGaAs emission for this sample is very similar to that of the 15% sample suggesting that the growth has not proceeded as intended. CL imaging of the 7% sample was used to confirm the existence of quantum wire luminescence from the base of the groove for the energy indicated in the spectra. TEM micrographs show that a crescent shaped quantum wire has formed in this sample. However the contrast of the image is very poor and it is not reproduced here. The shape of the 7% wire is however different compared with the pure GaAs sample, being thinner (~30Å) at the base. The reason for this is that less material has diffused to the bottom of the groove because the growth rate on the sidewalls has increased as Al is pinned to the (111)A surface. No TEM images for the 15% and 21% samples were recorded. The µPL spectra show no evidence for wire formation in the 21% sample. However as discussed above there are reasons to suspect that the growth has not proceeded as expected. Hence it is not possible to conclude if the formation of a wire occurs for AlGaAs compositions above 15%. Finally it should be noted that the composition of the AlGaAs wires may not be spatially uniform due to the preferential growth of GaAs at the bottom of the groove. A similar mechanism to that leading to the formation of the Ga rich vertical quantum well may operate, producing a Ga rich, Al deficient region at the centre of the wire. Such a compositional variation will make the theoretical modelling of the quantum wire energy levels very difficult.

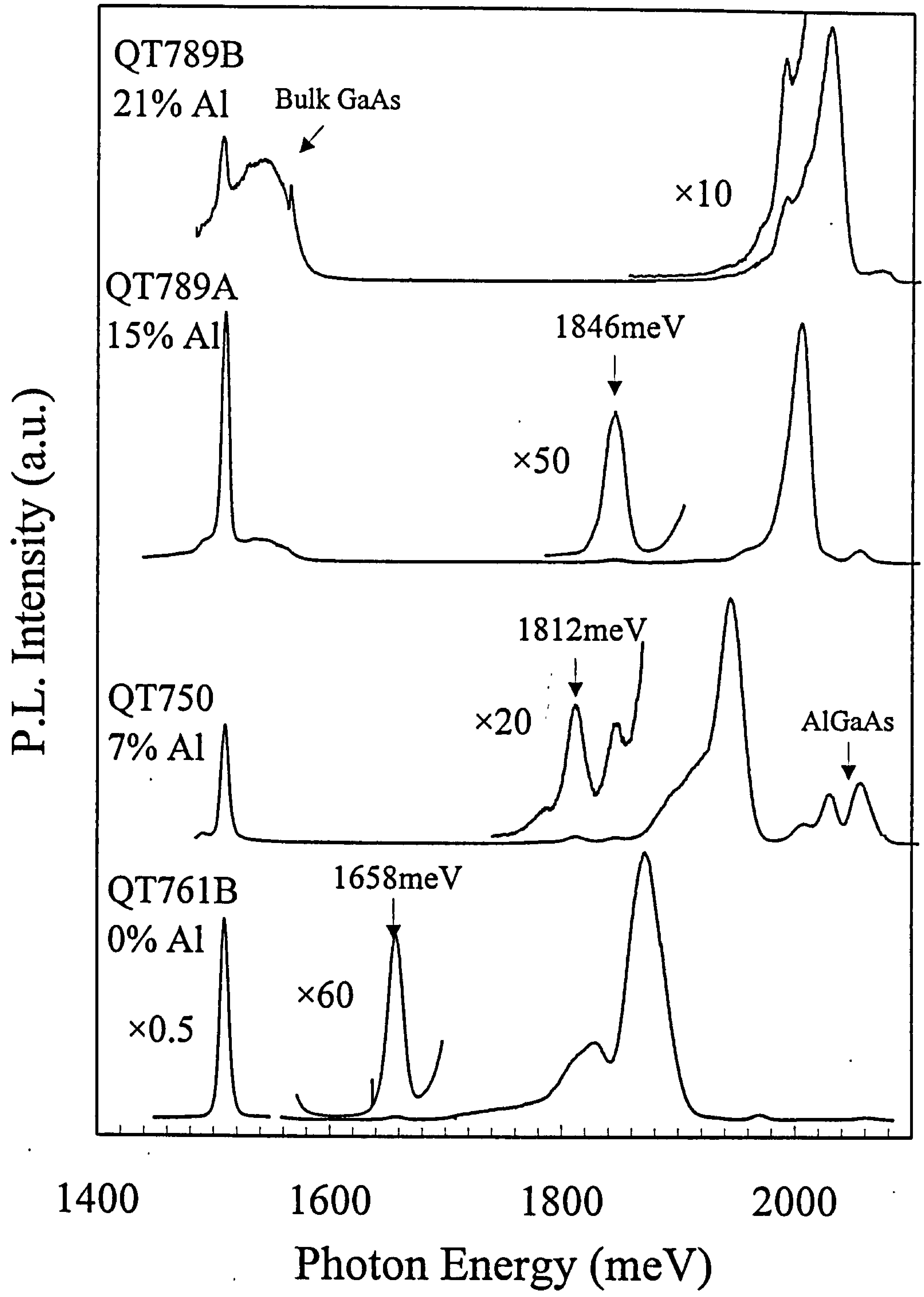

Figure 5.5 PL spectra at T=4.2K of the AlGaAs quantum wire samples QT761B, QT750, QT789A, QT789B. The energy of any quantum wire emission is marked. These samples have nominal Al wire compositions of 0, 7, 15, 21% respectively. The spectral region containing the quantum wire is also shown on an enlarged scale as indicated by the factors shown. Quantum well luminescence appears between 1800-2000meV.

5.3 Etching Experiments

Selective excitation using the micro-photoluminescence technique and with edge excitation enabled a stronger PL signal from the wire to be obtained. Even so, compared with the quantum well signal, the quantum wire emission is still very weak. For devices which use the quantum wires as the active region, minimising the intensity of the quantum well signal is desirable. In the present experiments an effort was made to minimise the quantum well luminescence by removing a substantial part of the side walls by wet chemical etching techniques. An isotropic etch will remove all crystallographic planes at an equal rate which is not desirable as the quantum wire is the same distance from the surface as all the quantum well features. However, when photoresist is spun onto the sample, instead of equally covering the entire surface, it is deposited only at the base of the grooves. When the sample is subsequently placed in the etching solution, initially only the tops and sides of the grooves are attacked by the etchant. Only when these have been completely removed will the etchant start to undercut the plug of resist and etch away the material around the base of the groove including the wire. For the present measurements a strip of the sample was etched, with a graded etch being achieved by simply dipping the strip in the etching solution and withdrawing it slowly so the bottom of the strip remained in solution for a longer period of time, hence being subjected to a greater degree of etching than towards the top of the strip.

The SEM images in Figure 5.6 show the extent to which the sample has been etched for different positions along the length of the strip. At the bottom of the strip, where the etching has occurred for the longest time, the etch has undercut the resist and totally removed the base of the groove, leaving behind no quantum well or quantum wire material. SEM images from further up the strip show that it is possible to selectively remove the top and side wall quantum wells, leaving an isolated quantum wire. Hence the effect of the quantum wells could be minimised, enabling the luminescence from the wire to be studied in isolation without the influence of the large quantum well related emission.

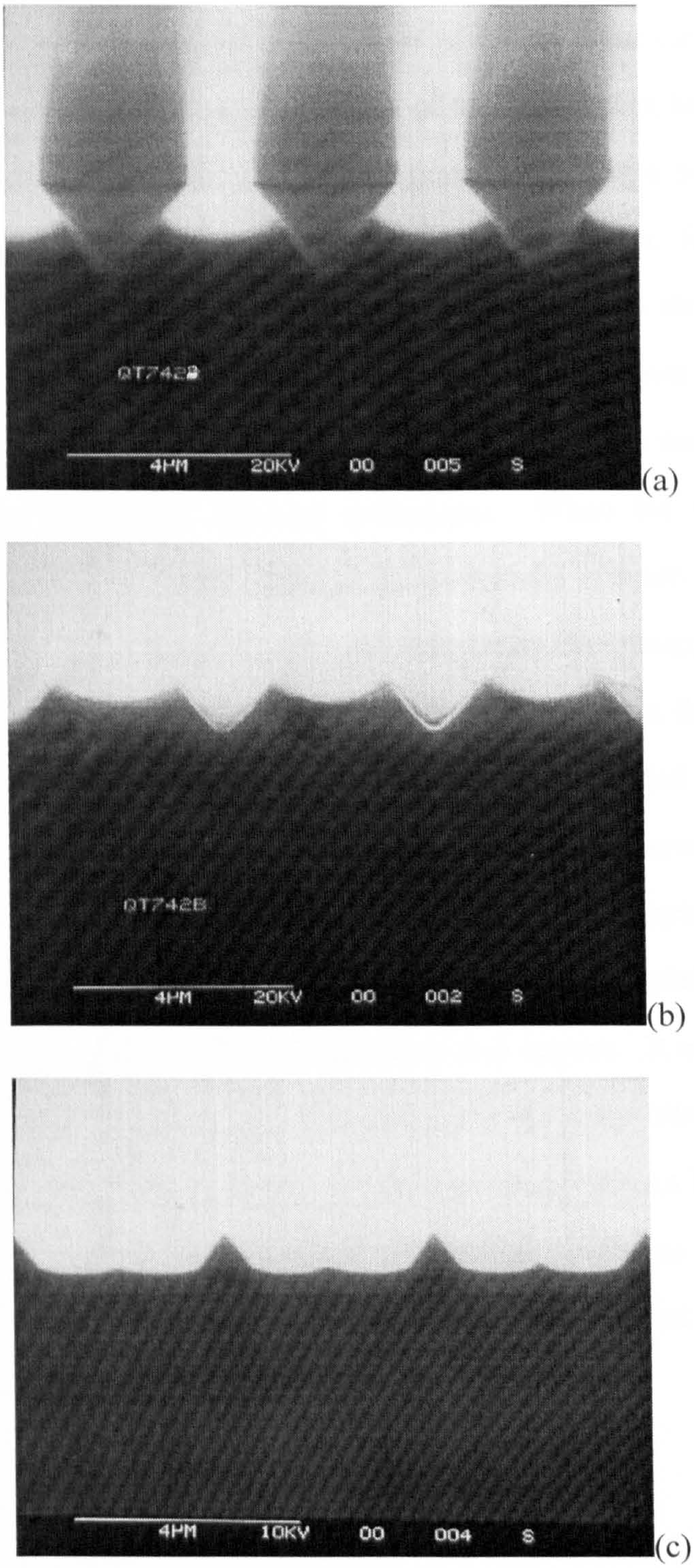

Figure 5.6 SEM images showing the extent of the etching process for different positions along the strip of a 4μm sample. (a) shows the plug of resist at the bottom of each groove, (b) shows that only the bottom of the side wall remains after etch, (c) shows the complete removal of the side wall.

Figure 5.7 shows µPL spectra recorded for three positions along the length of the strip. Near the top of the strip only a small amount of the sample has been removed so the spectrum is similar to that of an unprocessed piece. PL from a position between the etching extremes exhibits a spectrum with the absence of the feature attributed to luminescence from the top quantum well. This shows that the etch has removed this part of the structure. The intensity of the wire emission remains constant, while the intensity of the side wall luminescence is reduced. The intensity and shape of the GaAs and AlGaAs features remain relatively unchanged. When the etch has progressed deeper into the structure, the µPL spectrum shows that the intensity of the luminescence from the side wall quantum well has almost completely disappeared, suggesting that it has nearly all been removed by the etch, but luminescence from the quantum wire still remains. The intensity of the wire emission has slightly increased in the absence of the quantum wells, it is possible that this increased quantum wire luminescence intensity is due to the fact that photo-created carriers can no longer be captured by the quantum wells. The form of the luminescence from the AlGaAs related features changes considerably when compared with the shallower etch spectra. It is known from CL and TEM analysis that there is a lateral variation in the Al composition across the groove. The observed change in luminescence line shape when AlGaAs from the top and side wall of the structure is removed provides further evidence confirming that the composition of the AlGaAs at the bottom of the groove is indeed different compared to that further up the grooves.

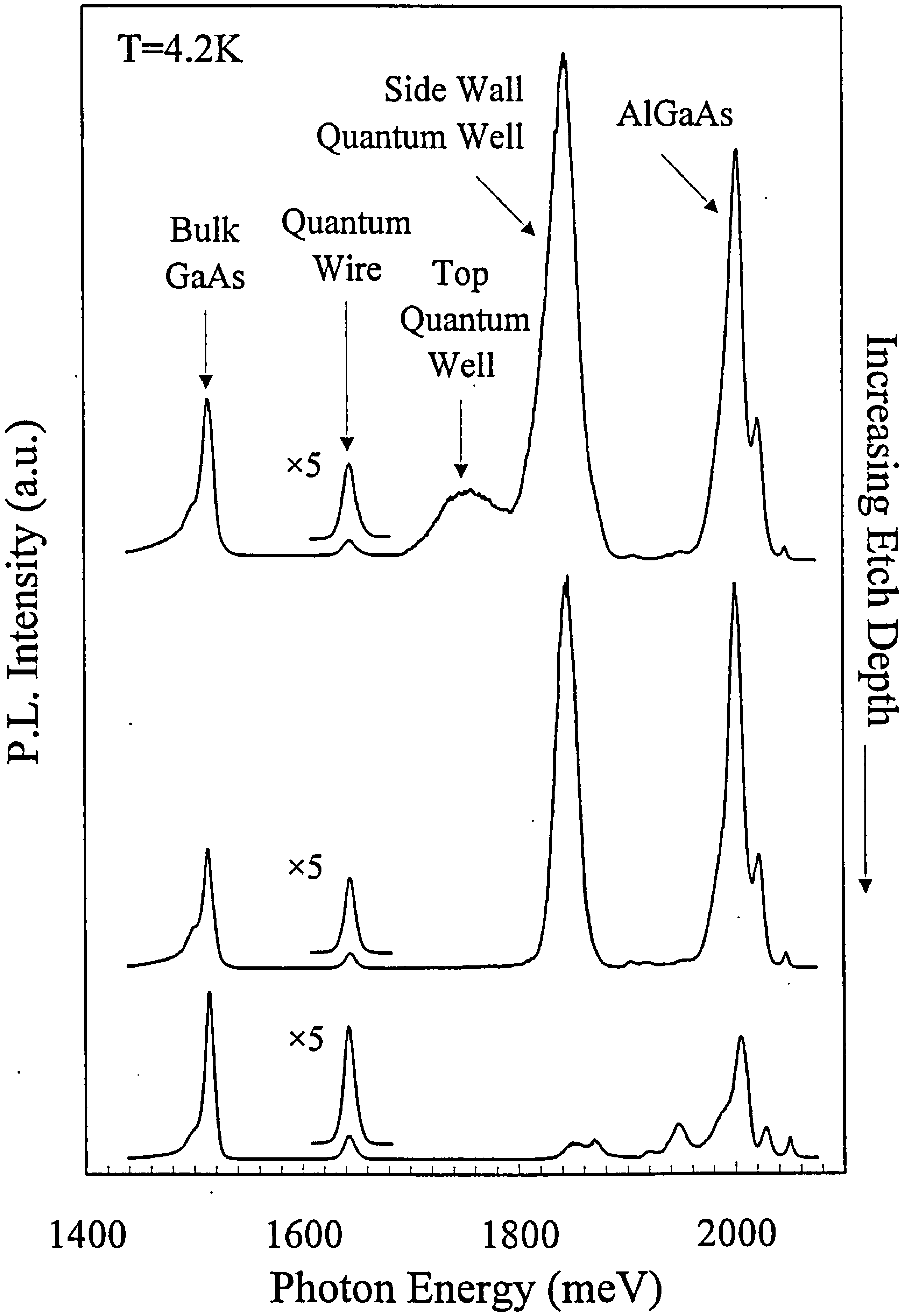

Figure 5.7 μPL spectra recorded at various positions along the etched strip.

The present measurements have shown that it is possible, in a controllable manner, to remove all or most of the quantum wells within the V-groove structure, with no detrimental effect to the quantum wire signal (in fact there is a slight improvement in the intensity of the luminescence). If the etching rate is calibrated and controlled, large areas of sample could be processed in this way. For quantum wire devices this is advantageous as any relative enhancement of the signal from the wire over that from the quantum wells is beneficial. From the point of view of understanding the optical spectra of these samples, these measurements serve to reinforce the information obtained by CL experiments on larger 4μm pitch samples. CL analysis of the present sample, with a groove pitch of 2μm, proved inconclusive as the 1μm resolution of the technique is only slightly smaller than the size of the features under investigation. It was hence difficult to clearly distinguish the emission from the side wall from that from the base of the groove. An unambiguous identification of all the features in the optical spectra was therefore not possible. The present etching experiments confirm the origin of all the features in the optical spectra, and a comparison with samples grown on a 4μm pitch grating show that the similarities observed are due to the growth proceeding in a similar manner, with a quantum wire and a Ga rich AlGaAs vertical quantum well forming in both cases.

5.4 Optical Studies of Quantum Wires Grown in *p-i-n* Structures

All the investigations of the optical properties of V-groove quantum wires described so far have been performed using a laser or an electron beam as the excitation source. These create free carriers that diffuse within the structure and recombine radiatively after capture by the quantum wells or the quantum wire. Opto-electronic devices are based on the *p-n* junction, which allows the electrical generation of light. For example, a quantum well is placed in an undoped (intrinsic) region between *p*- and *n*-type doped barrier layers, forming a *p-i-n* device. Under forward bias (with the *p* region connected to the cathode) holes are injected from the *p*-type region into the intrinsic region, while electrons are injected in the opposite direction. The quantum well captures these free carriers which recombine radiatively to produce photons. This is the basis of the LED and semiconductor laser. With a quantum well *p-i-n* device, the energy of emitted photons can be controlled, to a certain degree, by the size and composition of the quantum well. The electronic structure of the quantum wells can therefore be studied by observing the luminescence emitted for current injection across the junction.

For the present measurements the quantum wires are grown within the intrinsic region of a *p-i-n* structure. This allows the study of the electrical injection of carriers into the quantum wire and quantum wells and, in addition, allows a comparison to be made between the optical and electrical injection of carriers. For these experiments the basic 5×15Å quantum wire structure is unchanged but the barriers on either side of the quantum well are doped *p-* or *n*-type, as shown in the schematic diagram in Figure 5.8. μPL measurements, Figure 5.9, show that the photoluminescence properties are directly comparable with those observed in previous basic samples. Doping in the barriers has consequently not affected the growth mechanism and quantum wires have formed normally in the structure.

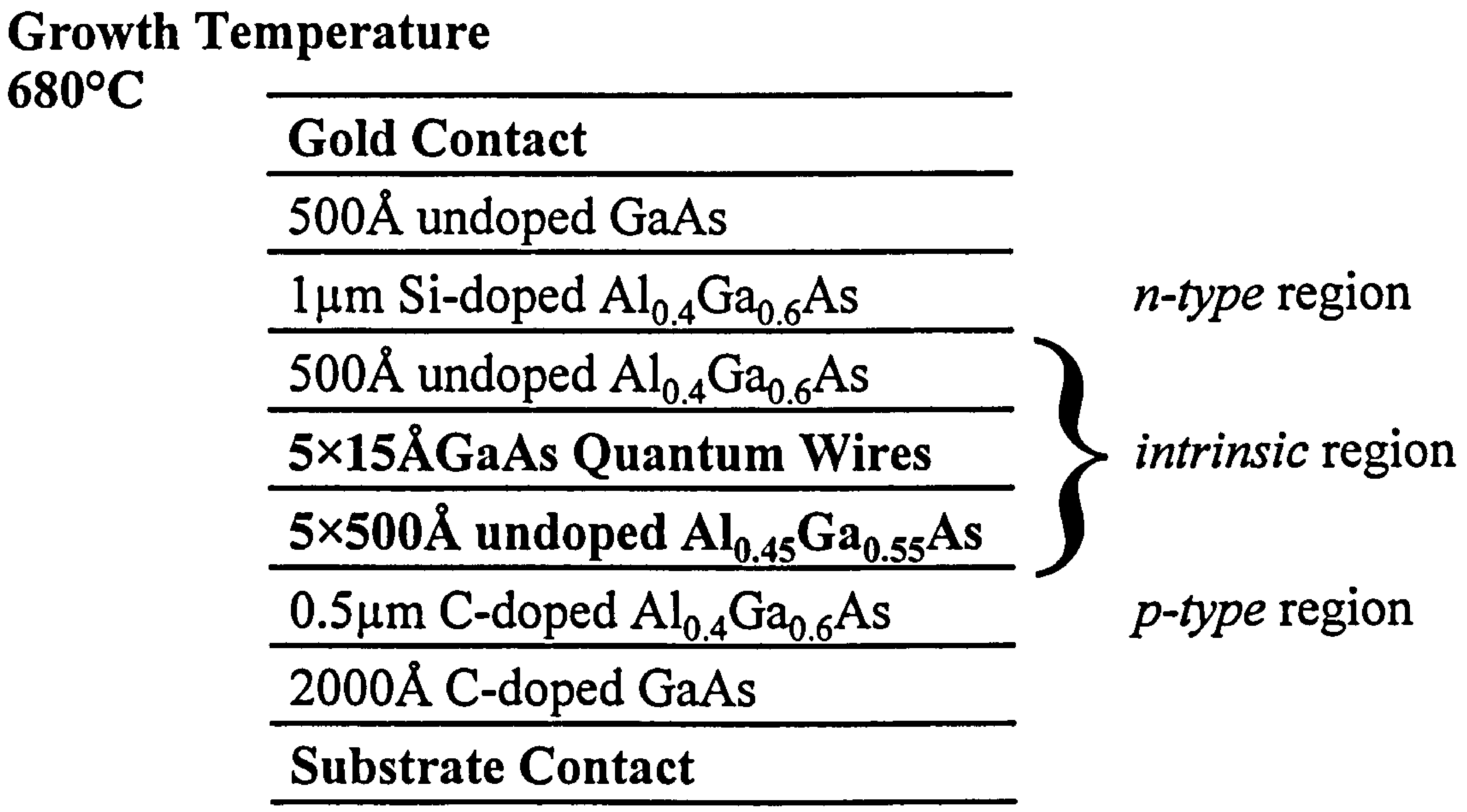

Figure 5.8 Schematic diagram of the *p-i-n* structure.

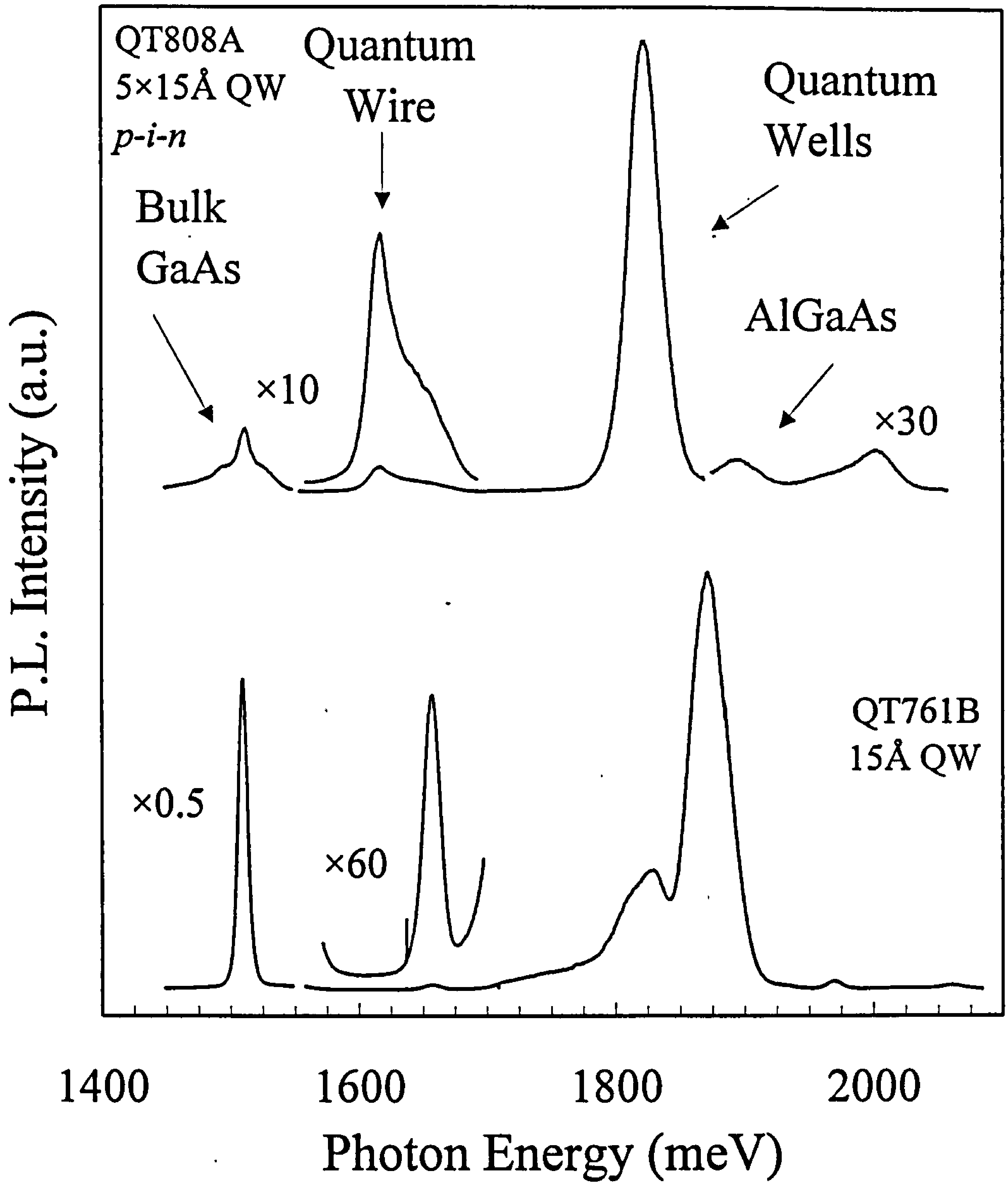

Figure 5.9 μPL spectra at T=4.2K of the *p-i-n* device (compare with QT761B)

5.4.1 Electroluminescence (EL) Measurements

To study the electroluminescence properties of the sample, devices with electrical contacts were fabricated from the grown wafer. For the present experiments 80μm diameter mesas were fabricated with gold, annular contacts placed on the top surface for optical access, allowing the emitted EL to be observed. A bias could be applied across the device using the top gold contact and an ohmic contact connected to the substrate.

5.4.1.1 Experimental Details

The devices used in the present experiments were mounted on a sample stick equipped with external electrical connections, placed in a He continuous flow cryostat and cooled to 4.2K. Electroluminescence (EL), emitted from the device when under forward bias, was detected using a single grating spectrometer and photo-multiplier tube. For small biases and low currents the device could be driven continuously. For high continuous currents, significant device heating occurred leading to thermal run away. Therefore a pulsed voltage source was used for the high current measurements to avoid excessive heating and destruction of the device. The modulated output signal from the photo-multiplier was measured using a lock-in amplifier, detecting at the frequency of the voltage pulses. The current through the device was calculated by measuring the voltage (using an oscilloscope) across a known resistor placed in the circuit. The bias across the sample was controlled using a voltage source which varies the bias across the whole circuit until the bias measured across the sample matches the value set for the experiment (a standard 4 terminal measurement).[3] I-V measurements, Figure 5.10, show that the devices exhibit good diode characteristics with turn on voltages at around 2.6V and reverse bias breakdown voltages of -14.2V.

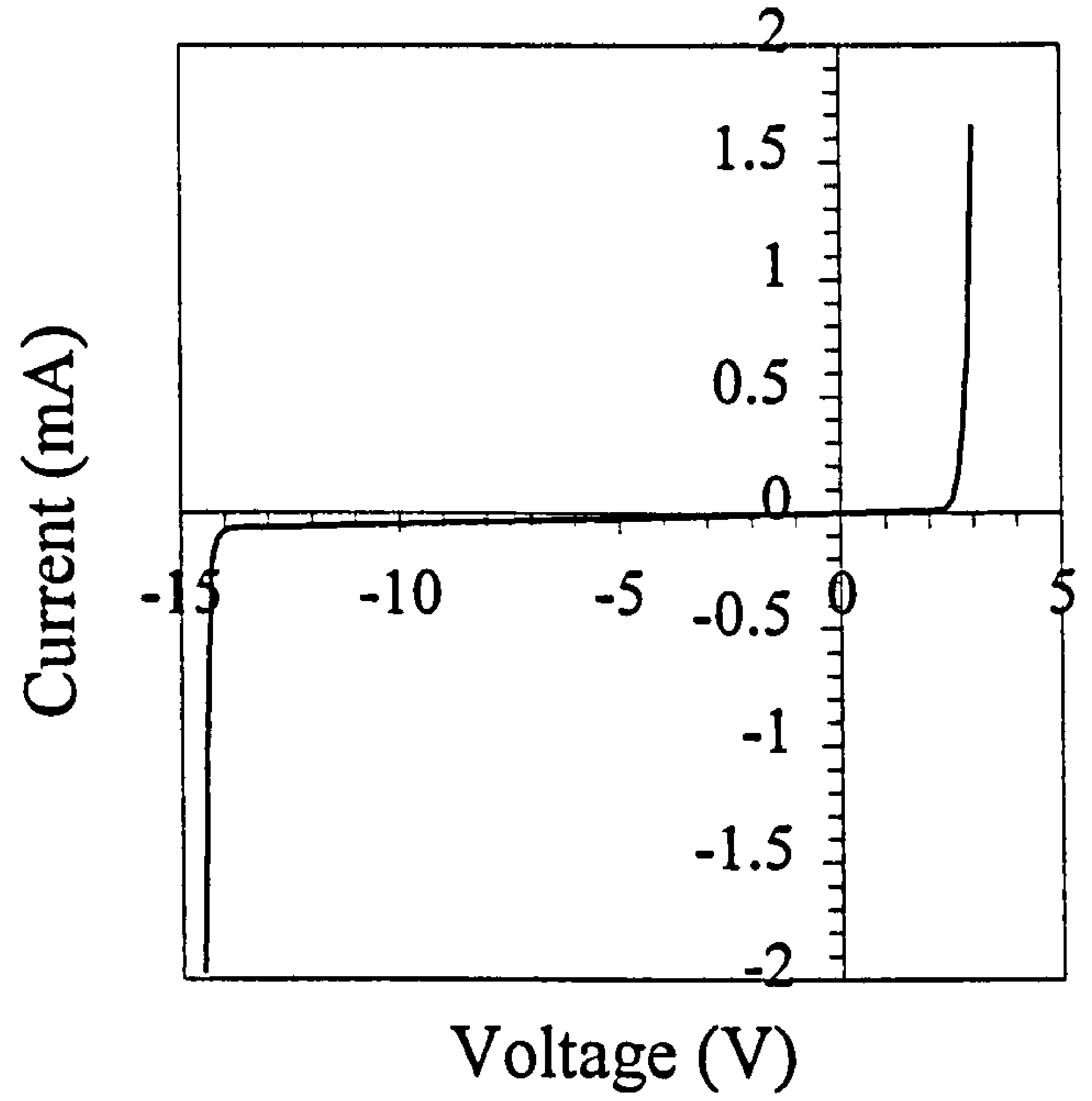

Figure 5.10 Typical I-V characteristics of the *p-i-n* device with the sample at 4.2K.

The application of a forward bias across the device causes carriers from the doped regions to be injected into the intrinsic region where they are captured by the quantum wells and quantum wire before recombining radiatively. In a similar manner to photoluminescence, the energy of the emitted photons are dependent upon the confining potential seen by the carriers in the structure. Figure 5.11 shows EL spectra obtained for various values of forward bias. The PL spectrum shown for comparison was recorded under similar experimental conditions using a ~100μm, 633nm, HeNe laser spot, hence exciting an area of the same order as the size of the mesa. The main difference observed between these two types of spectra is the appearance in EL of a feature attributed to the quantum wire emission. In PL the intensity of the quantum wire is always relatively very weak, even when μPL is used with the laser focused preferentially at the base of the groove (see for example Figure 5.1). In strong contrast, the EL spectra for low currents show that the quantum wire emission is as intense as any of the quantum well features. The EL associated with the quantum wells also exhibits far more structure than is observed with PL. For example, luminescence from the top quantum wells and from the AlGaAs related features are also clearly visible in the EL spectra. As the bias is increased, for higher currents the relative intensity of the quantum wire feature decreases compared with the quantum well features. This is especially the case for the side wall quantum well emission which at high currents becomes the most dominant feature along with the bulk GaAs luminescence.

The high current EL spectra in Figure 5.11 show a saturation of the ground state quantum wire emission and the appearance of higher energy features which are attributed to luminescence from excited quantum wire subbands. Figure 5.12 shows a detailed series of EL spectra for various forward bias currents, recorded in the spectral region corresponding to the quantum wire emission. For low currents only the ground state luminescence is observed at 1.620eV. As the current is increased the intensity from this ground state emission initially increases and additional luminescence corresponding to the first excited state transition appears with an energy of 1.644eV, implying a total subband separation of 24meV from the ground state transition. The spectrum for the highest current of 38mA shows up to three excited state transitions. The observation of further excited state transitions is not possible as the broad luminescence from the top quantum well, the low energy side of which also occurs at this energy, begins to dominate the spectrum.

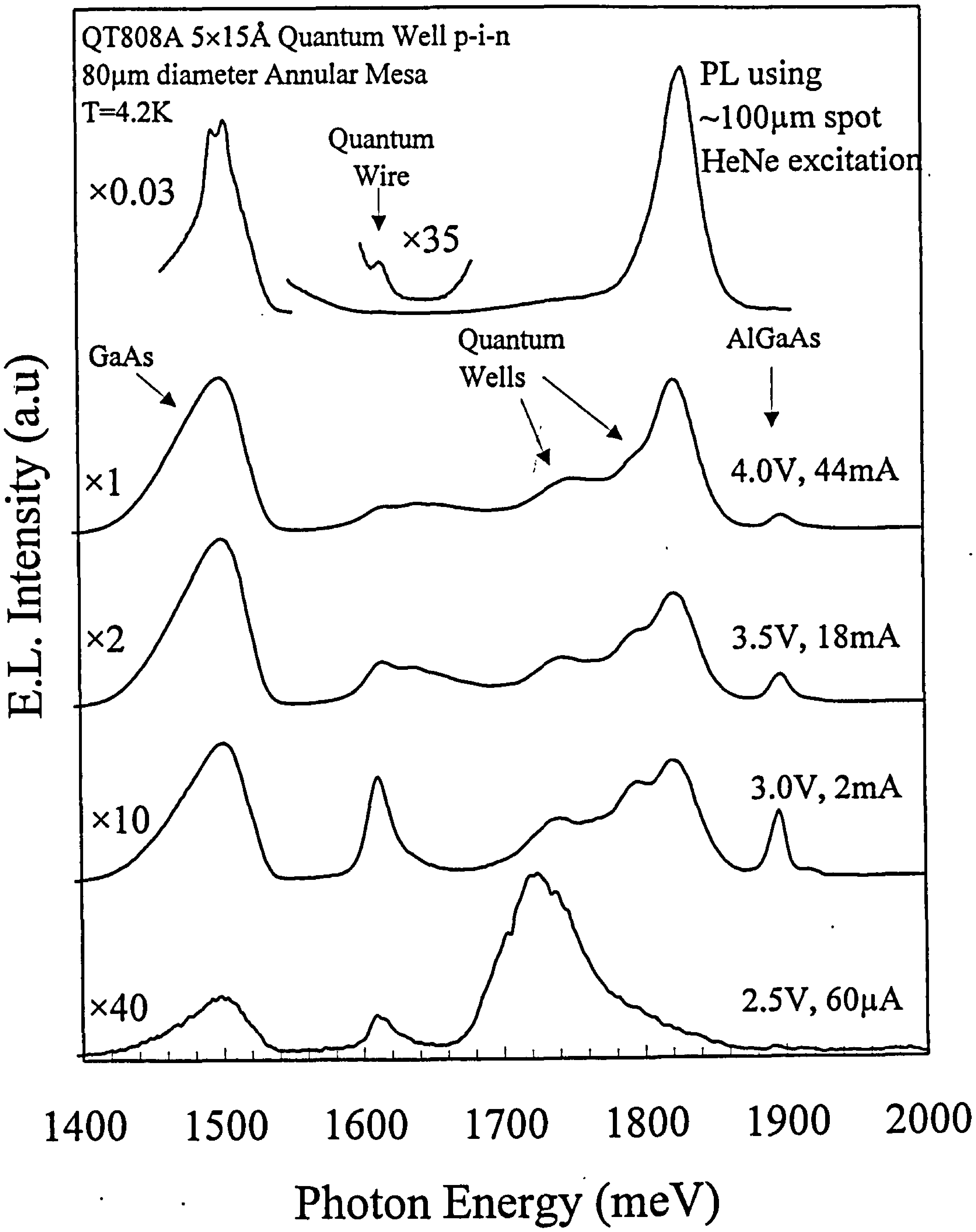

Figure 5.11 EL spectra comparing relative quantum wire intensities with those of the quantum wells for a number of forward bias currents. A PL spectrum taken with HeNe excitation is shown for comparison, (the absolute intensity is not comparable for this measurement).

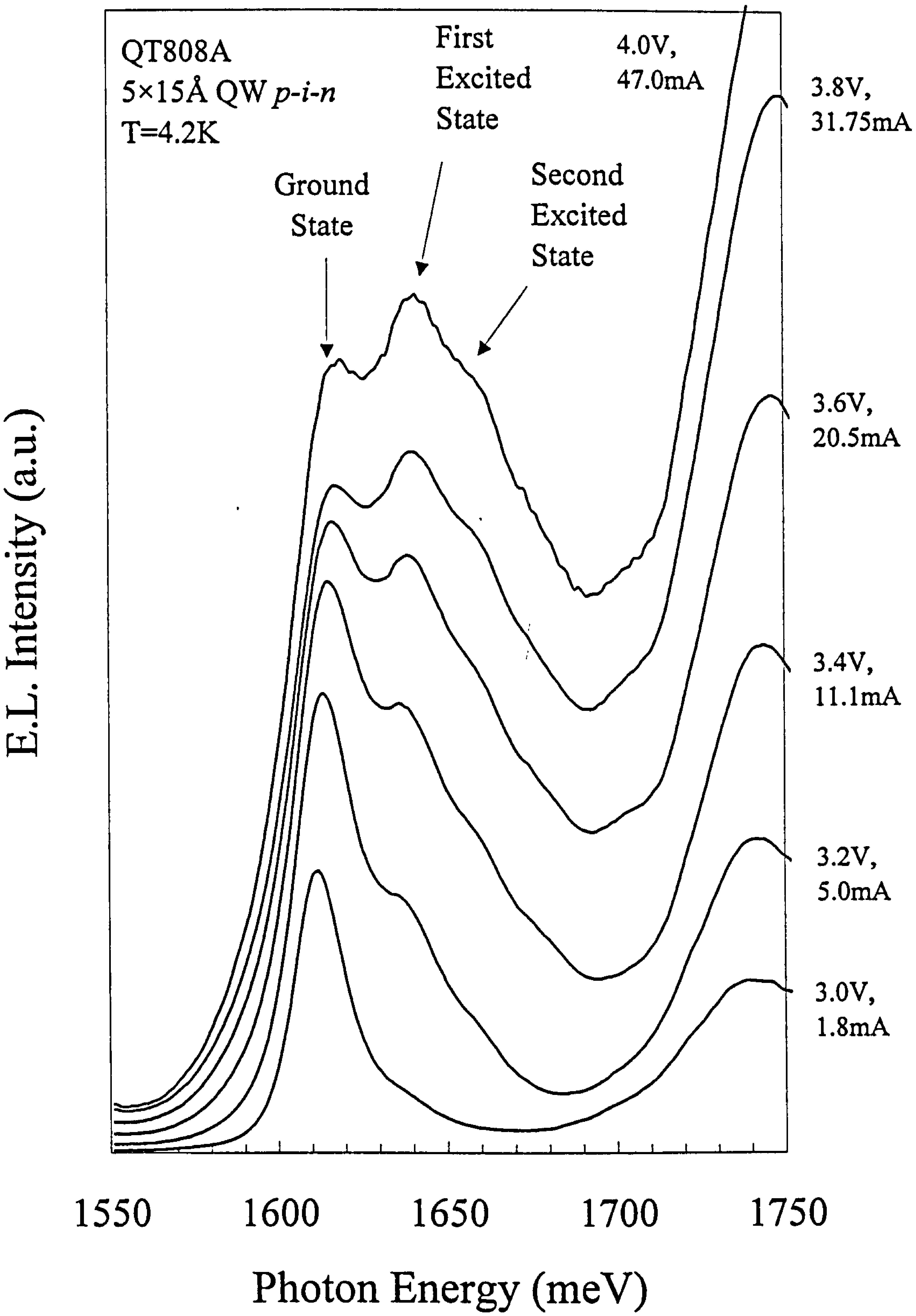

Figure 5.12 EL spectra recorded for a number of forward bias currents. The spectra show the saturation of the ground state emission and evidence for excited state transitions.

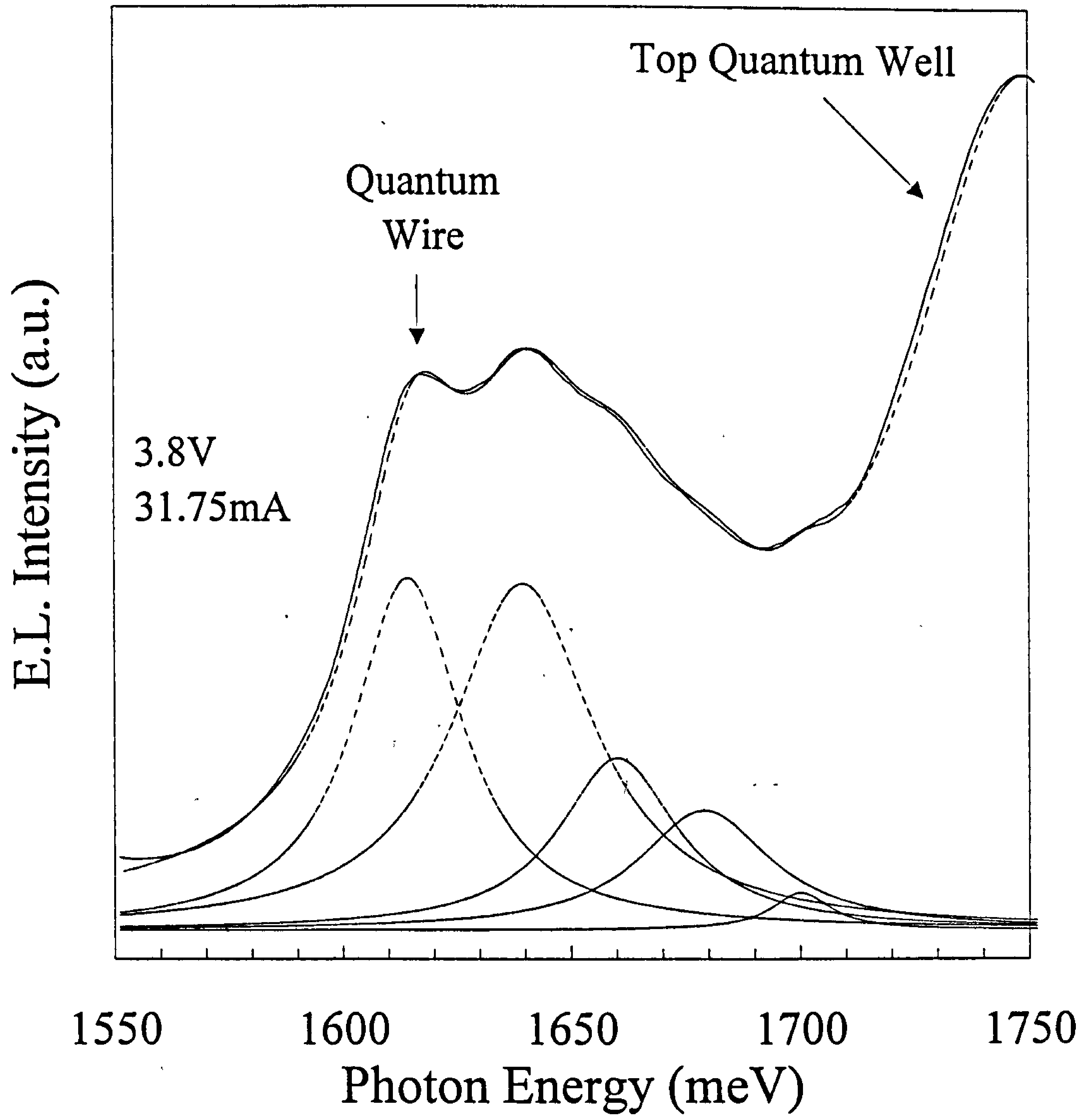

Figure 5.13 Curve fitted data for the subband transitions that appear in a high current (31.75mA) spectra. The dashed lines show the fitted Lorentzian line shapes for each quantum wire subband observed. The curve fitted contribution to the luminescence from the top quantum well is also included in the summation of all the quantum wire peaks to fit the spectra obtained.

Figure 5.13 shows an EL spectrum recorded for a forward bias current of 32mA. By assuming that the luminescence from each quantum wire subband has a Lorentzian lineshape, a numerical fit to the experimental data, showing the relative contribution of the various transitions to the overall spectral lineshape, has been performed. This is shown by the dashed lines in Figure 5.13. An identical analysis of the spectra obtained for different currents in these experiments allows the dependence on current of the various optical transitions, particularly the quantum wire ones, to be determined. The integrated EL intensities of the quantum wire transitions are plotted against applied current in Figure 5.14, using line-width and peak intensity data obtained from curve fitted spectra as shown in Figure 5.13. Also shown in Figure 5.14 is the intensity variation of the top quantum well EL emission.

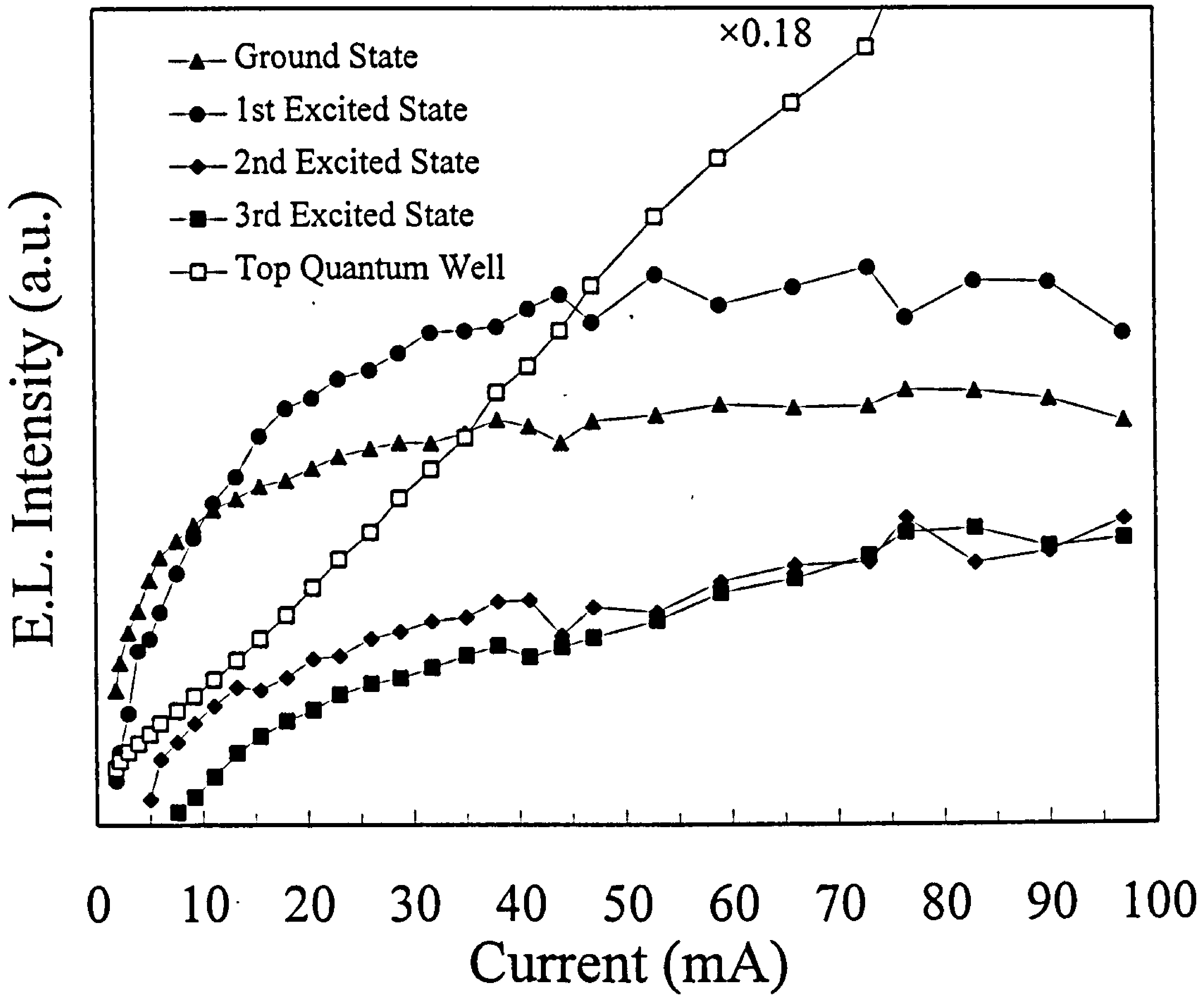

Figure 5.14 The integrated intensities of the quantum wire transitions, as observed in EL, plotted against forward bias current. Also plotted is the integrated intensity of the top quantum well EL.

5.4.1.2 Discussion of the EL results

The enhancement of the quantum wire emission intensity in EL compared with PL is very encouraging from the point of view of device design and operation. Any increase of the quantum wire emission intensity in comparison to that of the quantum wells is beneficial if the aim is to make use of the 1D properties of the quantum wires. The PL spectrum shown in Figure 5.11 was recorded using HeNe laser excitation with a ~100μm spot size (comparable with the size of the mesa, 80μm). With this size spot there is no preferential excitation of the wires, as is the case with μPL measurements. The spectrum shows that the quantum wire emission is very weak in comparison to the other emission lines ($<10^{-2}$ of the intensity of the quantum well emission). This result is not surprising given that the area occupied by wire is only ~1% of the total surface area of the structure. Even using μPL with a 1μm spot size and selectively exciting at the base of a groove, the quantum wire emission is still relatively weak (~5% of the intensity of the quantum well emission).

One complication with the present sample is the presence of a built-in electric field, due to the *p-n* junction, in the as-grown wafer used for the PL measurements. It is conceivable that this field could preferentially sweep out carriers captured by the quantum wire, thereby quenching the wire luminescence. For EL the field across the wire is much smaller because of the forward bias voltage applied across the device. Although very weak wire emission is also observed in the PL of structures without a *p-n* junction (see for example Figure 5.1) this possibility of the built-in electric field quenching the wire PL was investigated by measuring the PL from a mesa under forward bias conditions, just below the point at which EL is initially observed. Under these near flat band conditions the wire PL remains extremely weak (<1% of the side wall quantum well intensity). Hence it is possible to conclude that for all the geometries (top excitation with both a broad area (~100μm) laser spot or μPL and edge geometry selective wire excitation with μPL) and bias conditions investigated, the wire PL intensity is very weak relative to the other emission features (≤1% of the side wall quantum well intensity). In contrast, in EL all the different emission features are of a comparable intensity.

For low currents the quantum wire emission intensity is similar to that of the quantum well features. There is also an increase in the intensity of the emission from the top quantum well in EL, a feature normally unresolved in PL experiments (in μPL this is partly due to the excitation being spatially separated from the top of the V-grooves). The reason for this enhancement of the quantum wire emission in EL is not understood, although there are a number of possible causes. The structure is quite complicated and it is possible that the enhancement is due to the fact that a disproportionate amount of current passing through the device is channelled through the base of the groove where the quantum wire is located. A low resistance pathway within the structure would cause proportionally more current to pass along it; if this lay at the centre of the groove then this could possibly explain why the quantum wire luminescence is enhanced for electrical carrier injection. It is known from TEM analysis that a Ga rich AlGaAs region exists at the centre of the groove, the so-called vertical quantum well (see Chapter 4). This region could provide the required pathway with carriers becoming trapped by the lower bandgap AlGaAs and channelled directly into the wires.[4] The lower Al composition of this vertical quantum well would also produce a lower resistance than that of the surrounding AlGaAs, due to the reduced alloy fluctuation induced carrier scattering.[5] The fact that the emission from the vertical quantum well is also enhanced in EL compared to PL (see below) provides further evidence for the possible importance of this region of the structure for carrier transport. Another possible mechanism for a non-uniform current density distribution could be an uneven distribution of donors or acceptors in the doped regions of the device. This would cause a lateral variation in the doping density and a similar variation in the injected carrier density. This could arise if the rate at which dopant atoms are incorporated is different on the (111)A sidewalls compared with the base of the groove or the (100) surface between the grooves.[6] However, in the absence of any detailed studies of this possible effect it is difficult to make a quantitative statement of the likely behaviour. Whatever the precise mechanism for the enhanced wire emission in EL compared to PL we stress again that this property is potentially very advantageous for opto-electronic device applications. These results also indicate that the relative intensities of the emission from different active regions, as is observed in PL, will not necessarily reflect those present in devices operating with electrical injection.

With increasing current the EL spectra show that the intensity of the ground state quantum wire emission saturates and that additional features are observed to higher energy. These features are attributed to transitions between excited electron and hole quantum wire subbands and are observed because carriers are unable to relax to the ground state subbands as these are fully occupied. The integrated intensities of the quantum wire transitions are plotted in Figure 5.14, the data having been obtained from the curve fitting procedure described above. The behaviour of the 1D quantum wire subband transitions is in strong contrast to the emission from the two dimensional quantum well, which increases continuously with increasing current and exhibits no saturation effects. We hence observe a distinctly different behaviour between emission from a 1D and 2D region of the structure. Although the intensities of all the excited subband transitions appear to show an initial rapid increase, followed by saturation to a constant value, the curve fitting procedure is complicated by the strong underlying luminescence from the top quantum well. Hence the behaviour plotted for the two highest energy subband transitions is only approximate and it is not possible to be totally confident that they show the saturation effect exhibited by the ground state and first excited subband transitions..

Even for the highest currents the different quantum wire subband emissions remain well resolved. This is a consequence of the 1D nature of the subbands. The DOS for a 1D system has an $E^{-1/2}$ dependence for each subband (see Chapter 1), this means that the energy levels in each subband have an effective narrow energy distribution leading to sharp, easily resolvable luminescence peaks even when the subbands are highly occupied. In a two dimensional quantum well system the DOS is constant for each subband and this results in significant line broadening for high carrier densities. Similar band filling effects have been observed in CL spectra measured as a function of excitation beam current.[4]

Calculations of the quantum wire subband energies have been performed by A. Forshaw using a finite difference technique and the Luttinger-Hamiltonian to describe the valence band states.[7] Cross-sectional TEM micrographs were used to determine the wire shape. Excitonic effects were neglected given that the subbands are highly occupied, and band offsets of ΔE_c:ΔE_v=70:30 were assumed.[8] Subband separations of ~25meV were predicted for the electron subbands and much smaller ~4meV subband spacings for the mixed light-heavy hole subbands. However, these values were found to be very sensitive to the precise wire image used with, for example, electron subband spacings of ~20-30meV possible. The measured subband separations in these experiments indicate total subband separations of 24meV for the ground-state-first-excited-state, and 22 and 19meV for subsequent transitions. It is therefore reasonable to conclude from the calculations that different electron subbands are involved in each of the observed transitions but it is not obvious whether different hole subbands are also involved. It is expected that $\Delta n=0$ electron$\rightarrow$hole transitions are more likely as calculations show that the wavefunction overlap is greater for electron and hole subbands having the same index.

Although the electron subband spacing is considerably greater than that of the holes, the density of states of the latter is higher (an in-plane hole mass $\sim 0.1m_0$ is assumed).[9] Calculations therefore indicate that for equal numbers of electrons and holes in the wire, approximately equal numbers of electron and hole subbands will be occupied. For example, the fourth electron subband is predicted to be occupied at a carrier density $\approx 5\text{x}10^6\text{cm}^{-1}$; at this density the fifth hole subband is already partly occupied. With these considerations it seems reasonable to attribute the observed quantum wire subband transitions to those between subbands of the same index ($\Delta n=0$). This attribution is consistent with all the wire transitions saturating to a similar intensity, thus implying a similar electron-hole wavefunction overlap.

5.4.2 Magneto EL Measurements of V-groove Quantum Wires

The application of a magnetic field to a semiconductor or a semiconductor structure provides a large but controllable perturbation of the electronic band structure. Magneto-optical measurements therefore provide powerful experimental techniques for studying electronic band structures and related carrier processes. For example, magneto-optical techniques have been used to determine the band structure of both bulk materials,[10,11] and quantum wells,[12,13] allowing effective masses, g-factors and carrier non-parabolicities to be deduced. In addition they have been used to determine density of states in the quantum hall regime[14] and also to study many carrier effects in quantum wells.[15,16] In the present work magneto-EL measurements are used to probe the spatial extent and anisotropy of the quantum wire subbands, to study a possible excitonic-free carrier transition and to demonstrate the 2D nature of the feature in the optical spectra previously attributed to the vertical quantum well. Related studies of quantum wire subband anisotropies have been previously reported by a number of groups.[17-20]

When a magnetic field is applied to semiconductor structures the optical properties are changed because of the effect of the field on the underlying electronic states.

The Hamiltonian describing a free particle is given by the following equation:

$$\left(\frac{p^2}{2m}+V(r)\right)\psi = E\psi \tag{5.1}$$

Under the influence of a magnetic field the momentum operator becomes **p→p+eA**, modifying the Hamiltonian to give:

$$\left(\frac{p^2}{2m}+\frac{e}{m}p.A+\frac{e^2A^2}{2m}+V(r)\right)\psi = E\psi \tag{5.2}$$

For the present system the term quadratic in **A** results in the dominant perturbation.[21-23] This produces a diamagnetic shift of the state given by $\frac{e^2A^2}{2m}$.

Given that the magnetic vector potential is defined as **B=∇×A**, for a magnetic field **B** applied along the z-direction we can write: $\mathbf{A}=(0,-\mathbf{B}x,0)$. The perturbation term now becomes $\frac{e^2B^2x^2}{2m}$ where x is a direction normal to the magnetic field direction.

If ψ is the wavefunction of the relevant state then first order perturbation theory gives:

$$\Delta E = \int \Psi^* \frac{e^2B^2x^2}{2m}\Psi dx = \frac{e^2B^2}{2m}\int \Psi^* x^2 \Psi dx = \frac{e^2B^2\langle x^2\rangle}{2m} \tag{5.3}$$

$\langle x^2\rangle$ is the expectation value of x^2 and gives an indication of the wavefunction extent in the x direction. Experimentally the diamagnetic shift can be measured and, if the effective mass is known, this can be used to deduce a value for $\langle x^2\rangle$. In practice there is a contribution to the diamagnetic shift of the transition from both the electron and hole states. It is generally assumed that $\langle x^2\rangle$ is approximately equal for both states and the above formula can then be used with m replaced by the electron and hole reduced effective mass.

The effect of an applied magnetic field on the optical spectra will generally depend on its direction; reflecting any spatial anisotropy of the underlying electronic states. For example, in a quantum well the diamagnetic shift of the emission energy is large when the magnetic field is perpendicular to the plane of the quantum well as the carriers are free to move in the plane of the well which is the direction normal to the field. In this case the diamagnetic shift is generally controlled by the spatial extent of the exciton wavefunction.[24] In contrast, when the field is applied parallel to the plane of the well the spatial extent of the wavefunction along the growth direction is small due to the confining potential. Consequently the diamagnetic shift for this orientation of the field is small and is dependent upon the well width.[25,26] Hence by applying the field along the three orthogonal spatial directions it is possible to determine the spatial anisotropy of the electronic wavefunctions.

5.4.2.1 Experimental Details

To study the effects of a magnetic field on the luminescence of V-groove quantum wire samples, the *p-i-n* structure QT808A was used under high forward bias (currents of ~30mA), providing strong emission from a number of quantum wire subbands. As described previously, these samples have quantum wells on different crystal planes ((001) and (111)A) and the magnetic field is expected to affect these wells in different ways dependant on the orientation of the field. The main interest in these measurements lies primarily with the influence of the magnetic field on the ground state and higher subband luminescence from the quantum wire. Hence spectra were recorded with the magnetic field oriented along the three orthogonal spatial directions as shown in Figure 5.15. This allows the spatial anisotropy of the wire subband wavefunctions to be directly probed. In terms of the quantum wells, when the field is parallel to the wires it is also in the plane of all the quantum wells in the structure. The effect on the quantum well luminescence for this geometry is expected to be small as the wells are all very thin, ~15Å.[26] However, with the field along the two directions perpendicular to the wire the effect on the different quantum wells is complicated by the fact that they do not lie in the same plane. For example, the side wall quantum wells experience a field that has a perpendicular and parallel component to the plane of the quantum well and this is different depending on which side wall is being considered. In contrast the top quantum wells only 'see' a perpendicular or parallel magnetic field depending on the geometry. The behaviour of the quantum well emission is therefore expected to be a complicated function of the field direction and has hence not been studied in any detail in the present work.

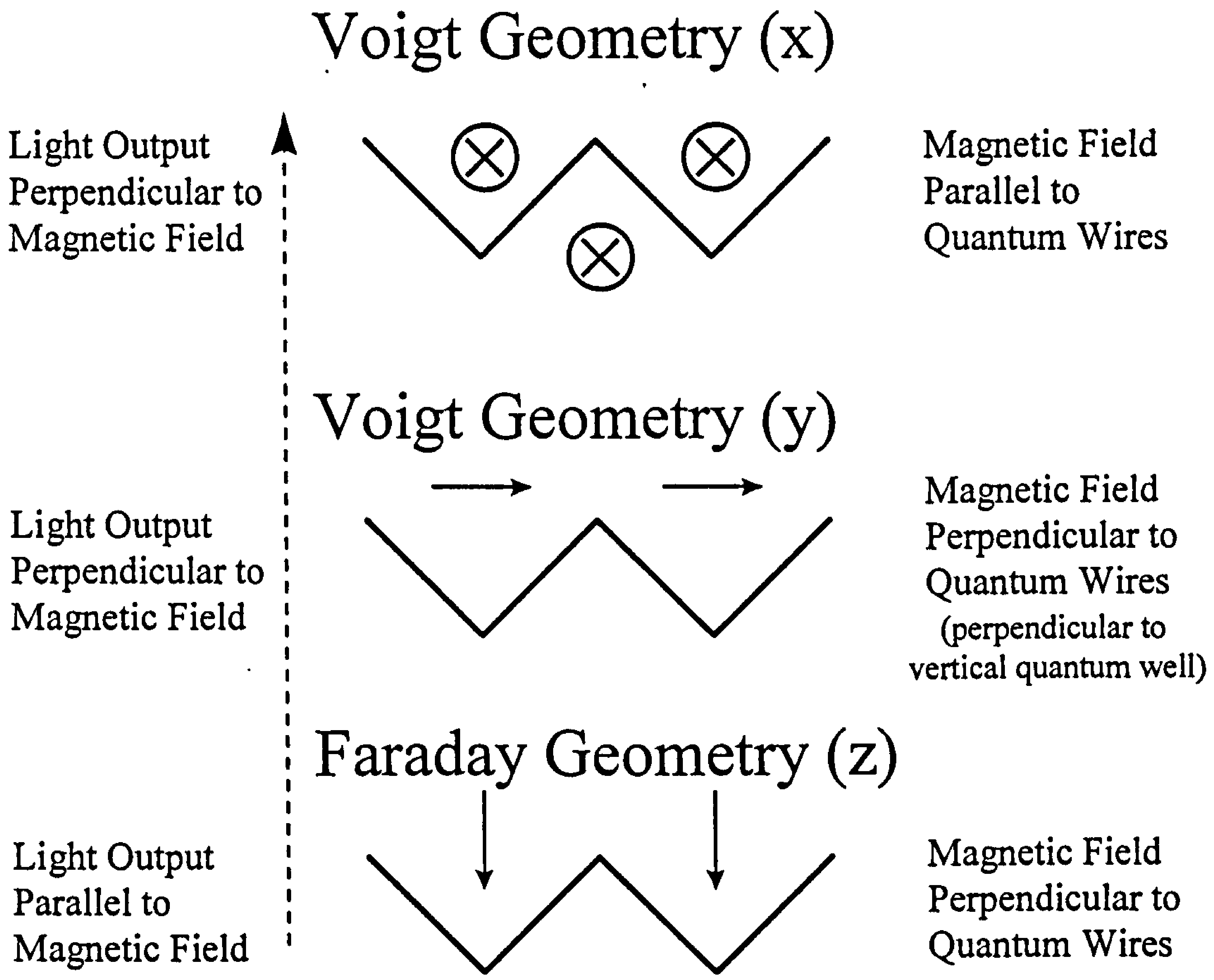

Figure 5.15 Schematic diagrams showing the three orthogonal magnetic field orientations with respect to the V-groove geometry and the detected light output.

The experimental set-up for the magnetic field measurements is described in Chapter 3. A liquid helium cooled 14T super-conducting magnet was used for these measurements. To obtain luminescence from the sample for the three different magnetic field orientations, two sample sticks were used: one for the Faraday and the other for the two

Voigt geometries (as shown in Figure 5.15). As in previous electroluminescence experiments the luminescence was emitted through the top of the mesa, perpendicular to the plane of the wafer. The Faraday geometry is when the magnetic field is parallel to the emitted light, the z-direction shown in Figure 5.15. In this case EL is focused by a small lens mounted on the sample stick onto an optical fibre which then directs the light onto the entrance slits of the triple spectrometer for detection. The Voigt geometry is when the magnetic field is perpendicular to the detected EL, directions x and y in the schematic diagram of Figure 5.15. The sample stick and light collection optics are therefore different for these experiments. For the Voigt geometry sample stick it is possible to rotate the sample through 90° whilst still in the magnet, enabling measurements for both Voigt geometries to be recorded. The resultant EL in this case is reflected off a mirror and out through the window at the bottom of the magnet. It is then collimated and directed towards the spectrometer by a series of lenses and mirrors.

Figure 5.16 shows 0 and 14T magnetic field EL spectra of the quantum wire for the two Voigt geometries. There is no apparent shift in the energies of the ground or excited subband transitions for either of these geometries. Figure 5.17 shows the Faraday geometry results. In this case there is a significant energy shift of the ground state and the two excited subband transitions that are visible for this current. The energies of the quantum wire transitions, plotted as a function of magnetic field, are shown in Figure 5.18 for the three geometries. This data was obtained using the curve fitting analysis described earlier (see Section 5.4.1.2).

The application of a magnetic field has no measurable effect on the GaAs quantum well transitions. However the luminescence from the Ga rich vertical AlGaAs quantum well seen in CL and TEM, is shifted to higher energy when a magnetic field is applied normal to the plane containing this quantum well (one of the two Voigt geometries, the y-direction). Figure 5.19 shows EL spectra recorded at zero and 14T for the vertical quantum well emission for the three orthogonal geometries.

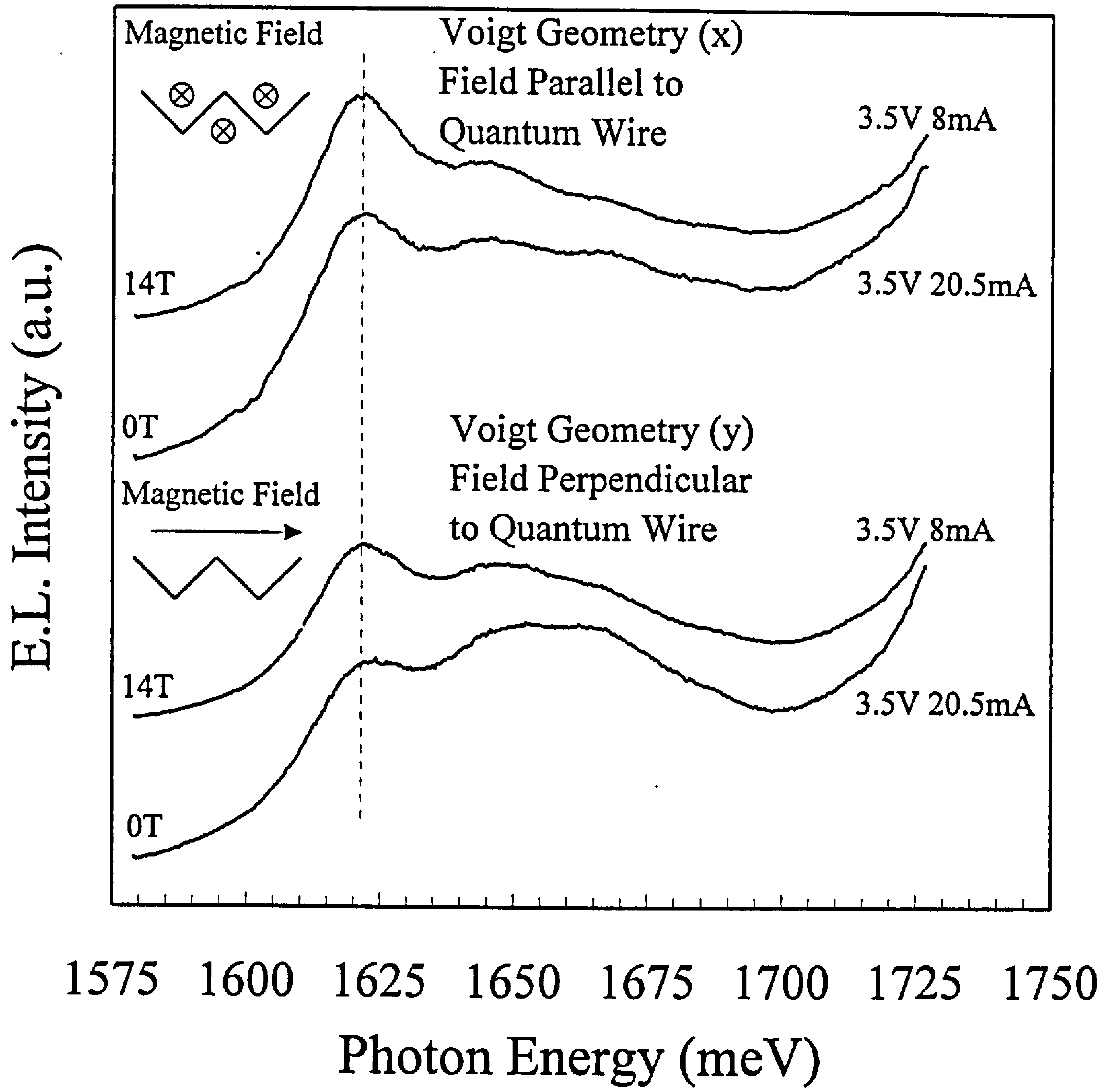

Figure 5.16 0T and 14T quantum wire EL spectra at T=4.2K for the two Voigt magnetic field geometries.

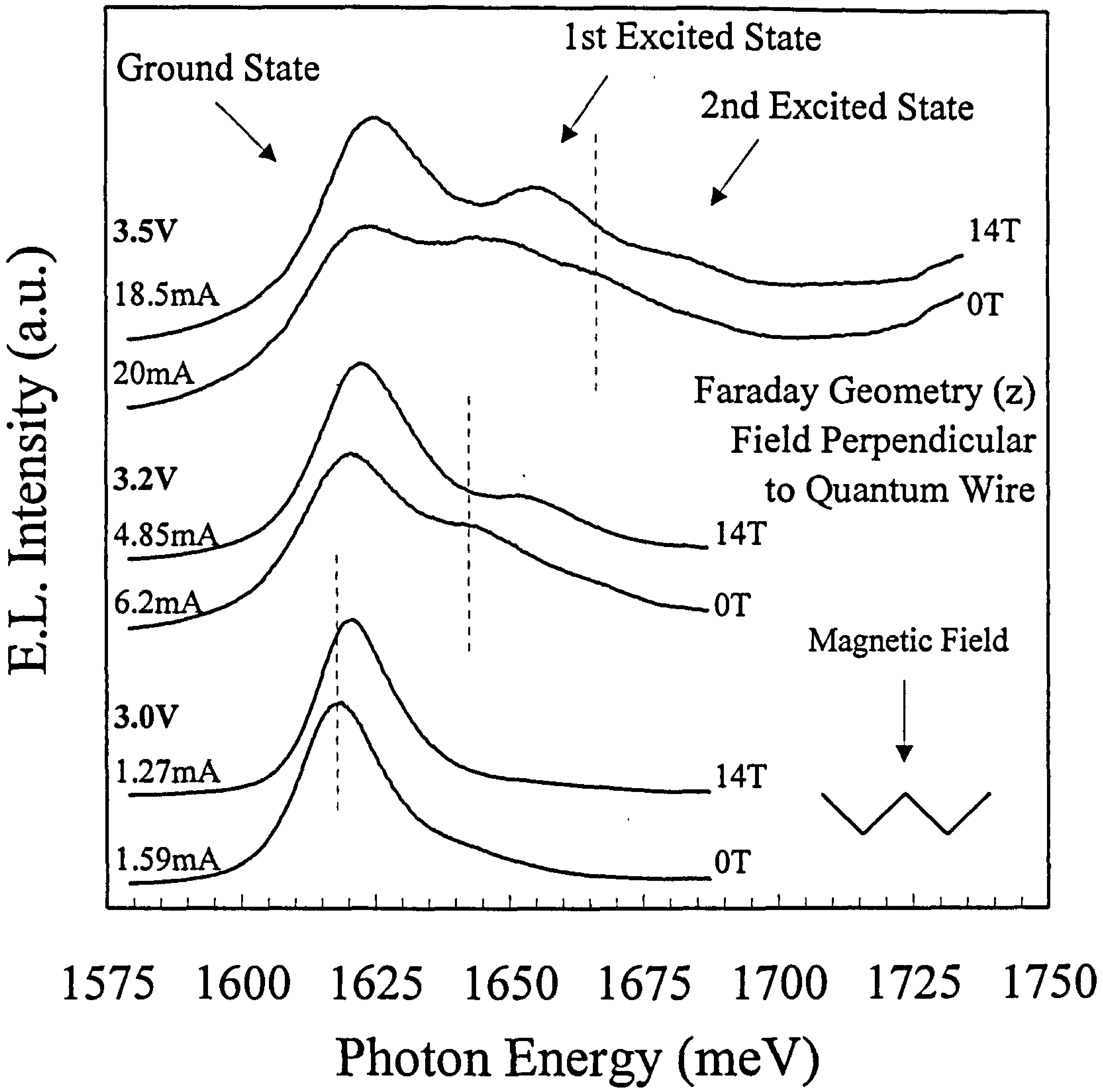

Figure 5.17 Low, medium and high current measurements at T=4.2K for the Faraday geometry at 0T and 14T.

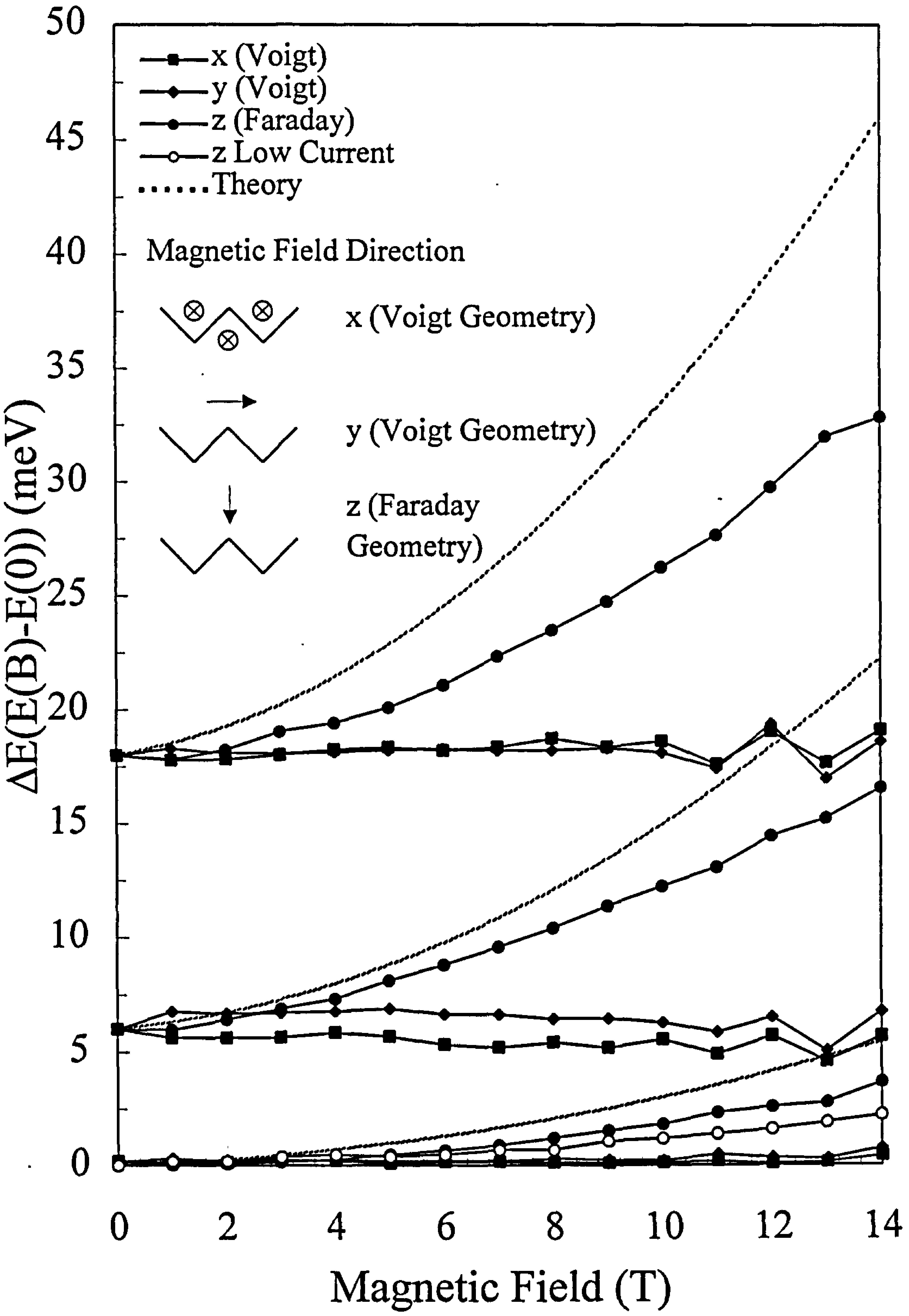

Figure 5.18 Peak positions of the quantum wire sub-band transitions plotted as a function of magnetic field. The three transitions are offset by arbitrary energies.

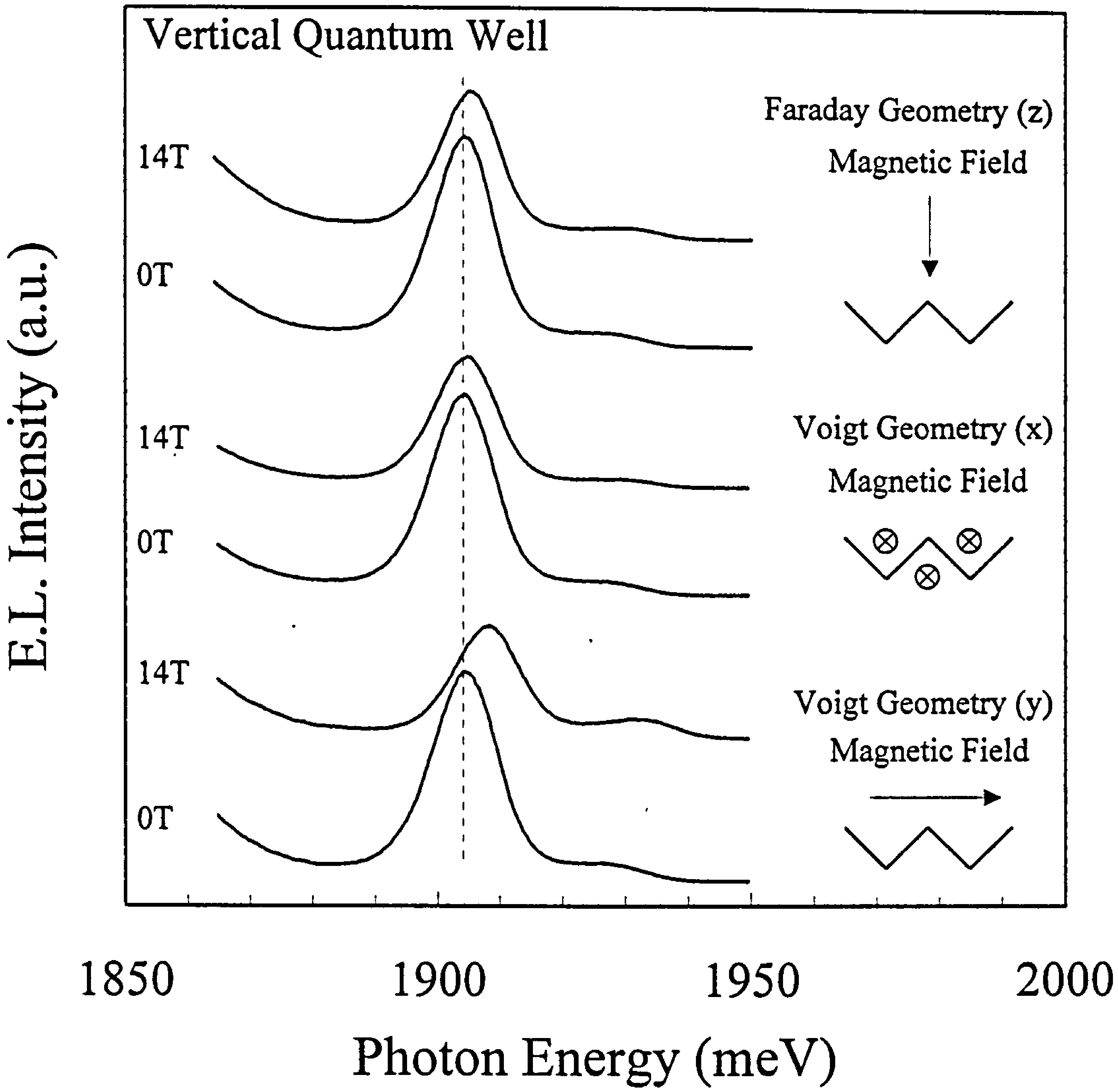

Figure 5.19 Three magnetic field geometries for the vertical quantum well.

5.4.2.2 Discussion of the magneto-EL results

The diamagnetic shifts observed for the quantum wire subband transitions provide information on the confinement that exists in the V-groove structures and the spatial anisotropy of this confinement. A measurable shift of the quantum wire transition energies is only observed when the magnetic field is applied in the z-direction; this behaviour is directly related to the anisotropy in the shape of the wire. TEM images show the quantum wire to be crescent shaped, with a maximum spatial extent along the growth direction (≈75Å) considerably smaller than the in-plane extent (≈600Å). When a magnetic field is applied in the x or y directions it is the small crescent thickness at the base of the groove which governs the magnitude of the diamagnetic shift. In contrast the large lateral extent of the quantum wire in the y-direction determines the diamagnetic shift when a magnetic field is applied in the z-direction. As shown above, the size of the diamagnetic shift is proportional to $\langle x^2 \rangle$ so a larger shift rate is expected when the field is along z than when it is along x or y. This behaviour is observed experimentally and confirms the existence of a strong spatial anisotropy of the subband wavefunctions and hence the shape of the wire.

For the magnetic field applied along the z-direction the diamagnetic shift rate increases with increasing transition energy and hence increasing subband index (see Figure 5.18). Values for the diamagnetic shifts of the first three transitions of 0.018, 0.053 and 0.082 meV/T^2 are determined from the experimental data. To explain this increasing shift rate observed for the excited state transitions a calculated probability contour plot of the wavefunction of the three lowest electronic subbands is shown in Figure 5.20. These wavefunctions were obtained by A. Forshaw using the same model used to calculate the energy levels described earlier.[8] The probability plots show that the spatial extent of the wavefunction in the plane of the structure increases for higher subbands as the wavefunction extends further into the wings of the crescent shaped quantum wire. This increasing in-plane extent of the wavefunctions produces an increase in $\langle x^2 \rangle$ and results in the increasing diamagnetic shift of the higher energy transitions for fields applied along the z-direction. In contrast, the spatial extent of the wavefunction along the growth direction is determined by the thickness of the wire at the centre of the groove and this remains approximately constant for all subbands. Hence, the subband wavefunctions become increasingly anisotropic with increasing index and this is reflected in the magnetic field behaviour of the associated optical transitions.

Also shown in Figure 5.18 are the calculated shifts of the transitions for the field applied along the z-direction. This data was obtained by adding the magnetic potential to the electron confinement potential and numerically solving the resultant Hamiltonian.[27] The resultant behaviour is approximately quadratic in field and shows a reasonable agreement with the experimental data, particularly for the lower energy transitions. The differences between the calculated and measured magnetic field behaviour may be due to uncertainties in the exact shape of the wire, as the calculations were found to be very sensitive to the confining potential obtained from the TEM micrographs. In addition, any carrier localisation will also contribute to a difference between the measured and calculated magnetic field behaviour of the subband transitions.[28]

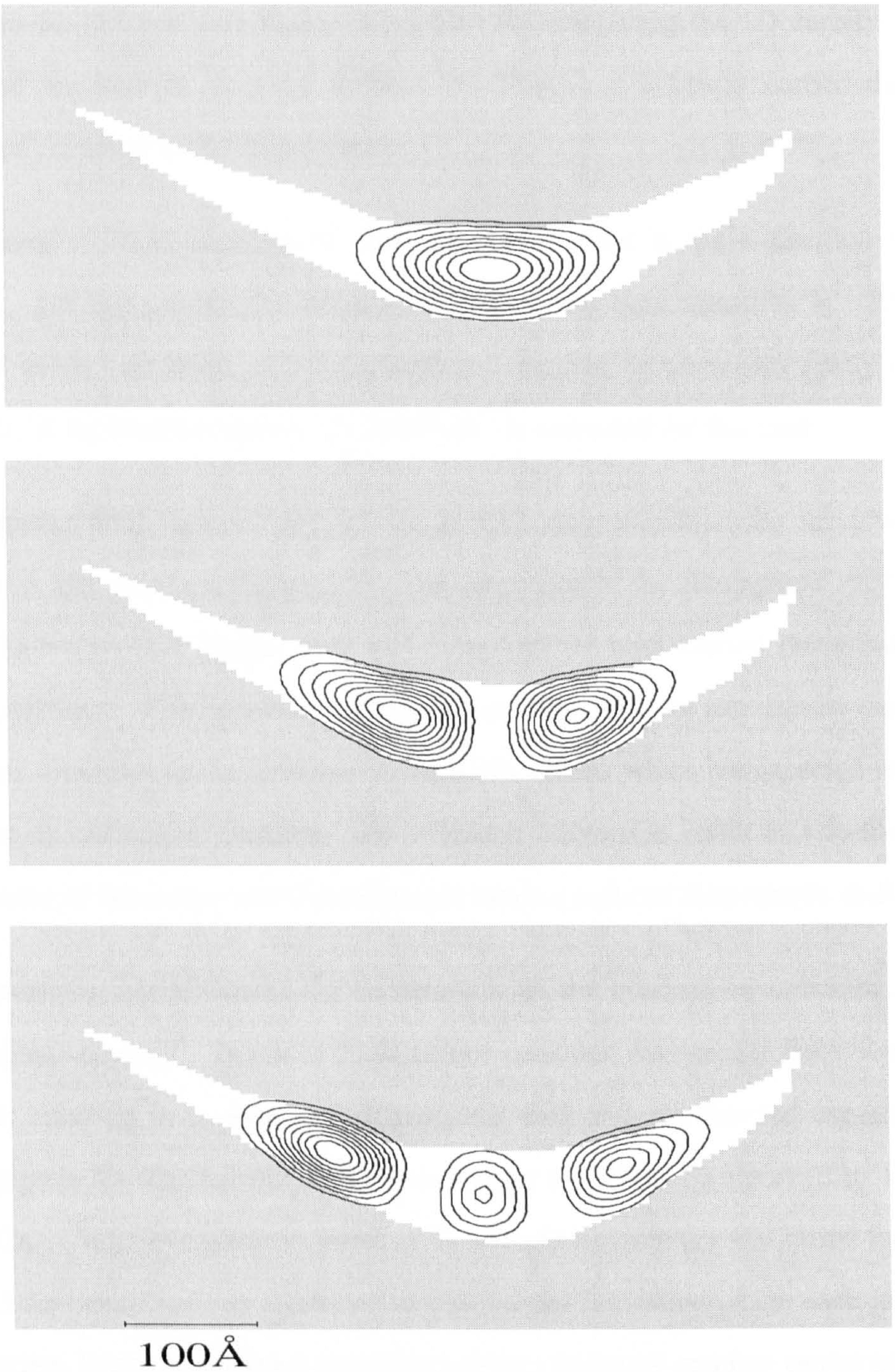

Figure 5.20 Probability contour plots (steps of 10%) for the first three quantum wire electronic subbands. The cross-sectional shape of the quantum wire is obtained from TEM micrographs.

The magnetic field data presented above was obtained for an EL current of 30mA. For this current (see Figure 5.13) the intensities of the three lowest energy subband transitions are close to their saturated values, suggesting that for these experimental conditions the subbands are highly occupied. By integrating the 1D density of states and using an electron subband spacing of 20meV, a subband carrier density of ~$1x10^6cm^{-1}$ is estimated for this current.

Low current (1.5mA) magneto-EL data with the B-field in the z-direction was also obtained. For this current the intensity of the ground state transition is ~20% of its saturated value, consistent with the transition occurring between only partly occupied subbands. A subband occupancy of ~$2x10^5cm^{-1}$ is estimated for this case.

The magnetic field induced shift of the ground state transition for the low current condition is also shown in Figure 5.18. The magnitude of the diamagnetic shift is found to be a factor of ~1.7 smaller than that measured for high current (saturated ground state) conditions. This reduction in the diamagnetic shift for low carrier densities is tentatively attributed to the influence of excitonic effects which are expected to become important at low carrier densities. An excitonic interaction result in a further spatial confinement of the carrier wavefunctions and hence a reduced diamagnetic shift.[29]

With increasing carrier density the carriers quench the excitons by screening or phase space filling effects.[30] Hence at high carrier densities free carrier behaviour should dominate resulting in an increased diamagnetic shift rate as observed experimentally. The change in the diamagnetic shift rate is similar to that (~×2) observed by Rinaldi *et al.*[29] in GaAs V-groove quantum wires as the sample temperature was raised form 4.2 to 180K. This behaviour was attributed to the thermal ionisation of the excitons at high temperatures, hence producing a transition between excitonic and free carrier behaviour.

In the present structure the possible transition between excitonic and free carrier behaviour occurs as the carrier density increases from ~$2x10^5cm^{-1}$ to ~$1x10^6cm^{-1}$; in good agreement with the calculated Mott density for V-groove quantum wires[31] of ~$8x10^5cm^{-1}$. There has been some debate in recent years as to whether an exciton-free-carrier transition occurs in quantum wires because of the reduced carrier screening that is present in a 1D system. Although the calculations of Rossi and Molinari[31] predict such a transition, the time resolved measurements of Ambigapathy et al[32] showed no discontinuity in the luminescence decay time as the carrier density varied over two orders of magnitude. This result was explained by the persistence of excitonic effects up to a carrier density of at least ~3×10^{6}cm^{-1}, well above the calculated Mott density.[31] Unlike a 2D system where the excitonic enhancement at the band edge can be readily observed optically,[30] in a 1D system it is difficult to distinguish the excitonic enhancement from the enhancement which results from the $E^{-1/2}$ form of the density of states. It is therefore considerably more difficult in a 1D system to study a possible exciton-free-carrier transition. If correct, the present results provide important information concerning this subject; indicating that an exciton-free carrier transition is indeed possible in a 1D system.

The attribution of the above magnetic field behaviour to an exciton-free-carrier transition is only tentative because other physical processes could result in a similar behaviour. For example, localised excitons, which become delocalised at high carrier densities, would also result in an increased diamagnetic shift rate with increasing carrier density. The ground state transition energy does increase by ≈5.5meV over the current range 1.5→30mA, consistent with a transition involving excitons which become delocalised. However the voltage across the device, and hence the electric field, also vary significantly (by 0.8V and ~2×10^{4}Vcm^{-1} respectively) and this shift of the transition energy may therefore be due to a quantum confined Stark effect (QCSE).[33] More measurements are clearly required before the observed behaviour can be conclusively attributed to a definite physical process but these preliminary measurements serve to indicate the potential power of the present magneto-optical techniques.

Magnetic field measurements of the emission attributed to the vertical quantum well were shown in Figure 5.19. The measured transition shift between 0 and 14T, when the plane of the well was perpendicular to the magnetic field, was 3.7meV, compared with

0.8meV and 0.5meV for the in-plane Faraday and Voigt geometries respectively. This result provides conclusive evidence that the emission results from an area of the structure which behaves as a vertical quantum well. The small shift in the emission energy for these two $B_{\parallel}$ directions (field in the plane of the vertical well) indicates that carrier motion normal to the field direction is restricted by the well confinement potential and that the extra potential provided by the magnetic field only has a small effect on the confined energy levels. For $B_{\perp}$ there is a larger diamagnetic shift of the transition because the carriers are unconfined in the plane of the quantum well. In this case the diamagnetic shift probably reflects the excitonic behaviour of carriers in the AlGaAs vertical quantum well.[24]

5.5 Quantum Wire Laser Diode Sample

As well as studying the physics of one dimensional systems, one of the main aims of the research carried out into quantum wires is to demonstrate lasing from quantum wires in the active region of the device and hence to exploit the theoretically predicted improvements in device performance. The measurements described in this section are the results of experiments performed on a quantum wire sample similar to the *p-i-n* structure QT808. This sample, however, has in addition a simple optical waveguide formed by growing high Al fraction AlGaAs (lower refractive index) above and below the barrier layers surrounding the wire, as used in a standard double heterostructure laser configuration.[34] The structure is shown in the schematic diagram of Figure 5.21. Stripe laser devices with cleaved facets were prepared with cavity lengths of ~400μm and stripe widths of varying size, typically 10μm. EL and μPL measurements were performed as described earlier in this chapter. In this investigation no attempt has been made to eliminate or at least minimise the luminescence from the quantum wells by, for example, proton bombardment.[35] The main aim of these experiments was to determine the feasibility of making a laser cavity from a V-groove patterned substrate and to determine if lasing from the 1D quantum wires occurred in preference to the various quantum wells, given the enhancement in the quantum wire emission observed for the EL measurements.

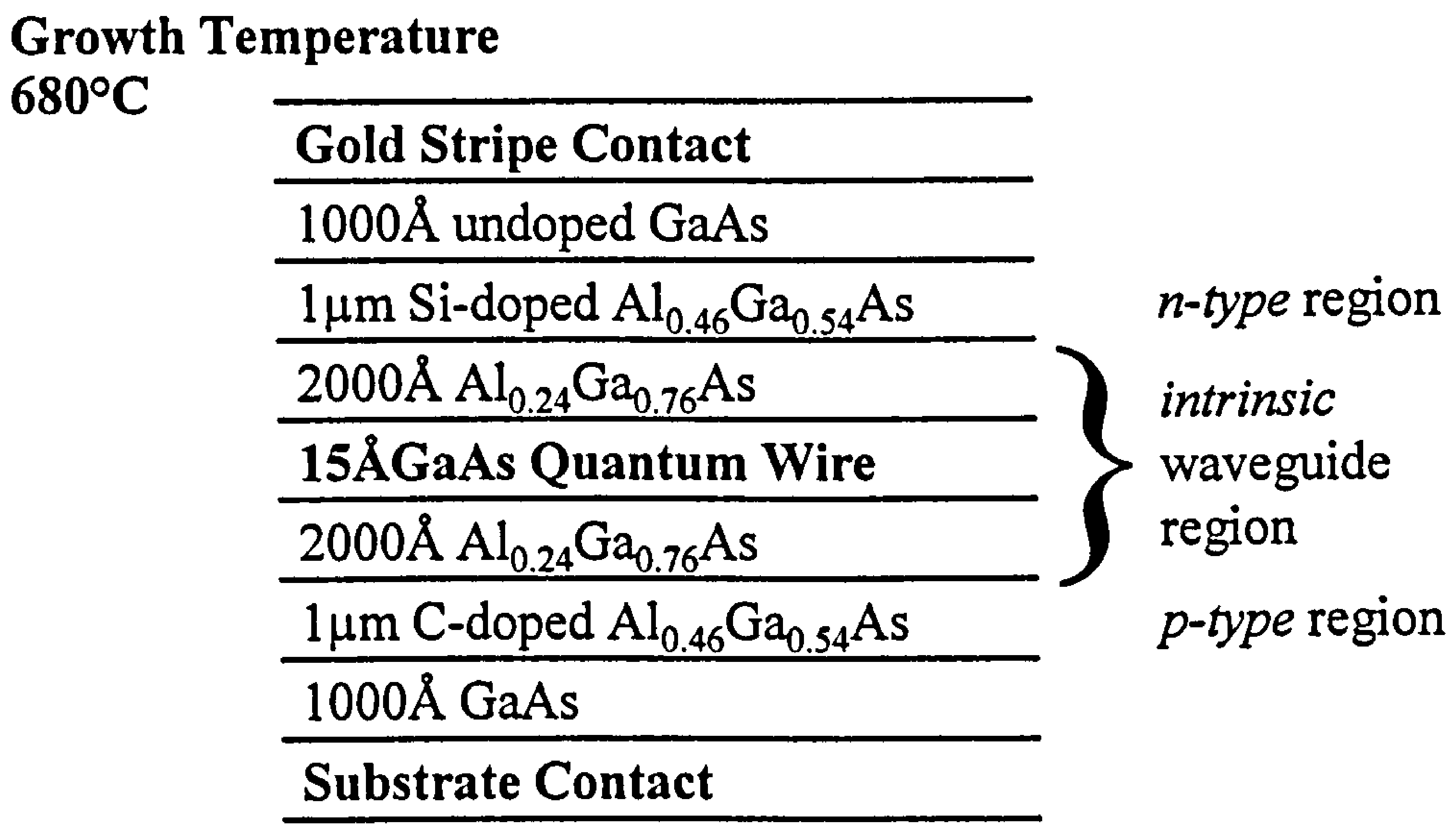

Figure 5.21 Schematic diagram of the quantum wire laser structure.

5.5.1.1 Experimental details

A μPL spectrum of the unprocessed wafer is shown in Figure 5.22 and shows that a quantum wire has formed, having an emission energy of 1596meV. This emission energy is slightly lower than observed in other samples where typical values of ~1660meV are obtained. This lower energy may be due to the Al concentration in the barriers surrounding the wires (20%) being lower than in the standard 40% sample. This may result in the base of the groove being less sharp giving a quantum wire with a different shape and less lateral confinement. To study the electroluminescence and lasing properties of the device, electrical connections were made as described earlier for the standard EL experiments. The current was pulsed to avoid heating effects and cooled to 5K in a cryostat. EL spectra for various currents are shown in Figure 5.23. Sharp lines typical of lasing action are observed in two distinct regions of the spectrum. A high resolution spectrum, recorded for a current above the lasing threshold, showing these lasing lines is reproduced in Figure 5.24.

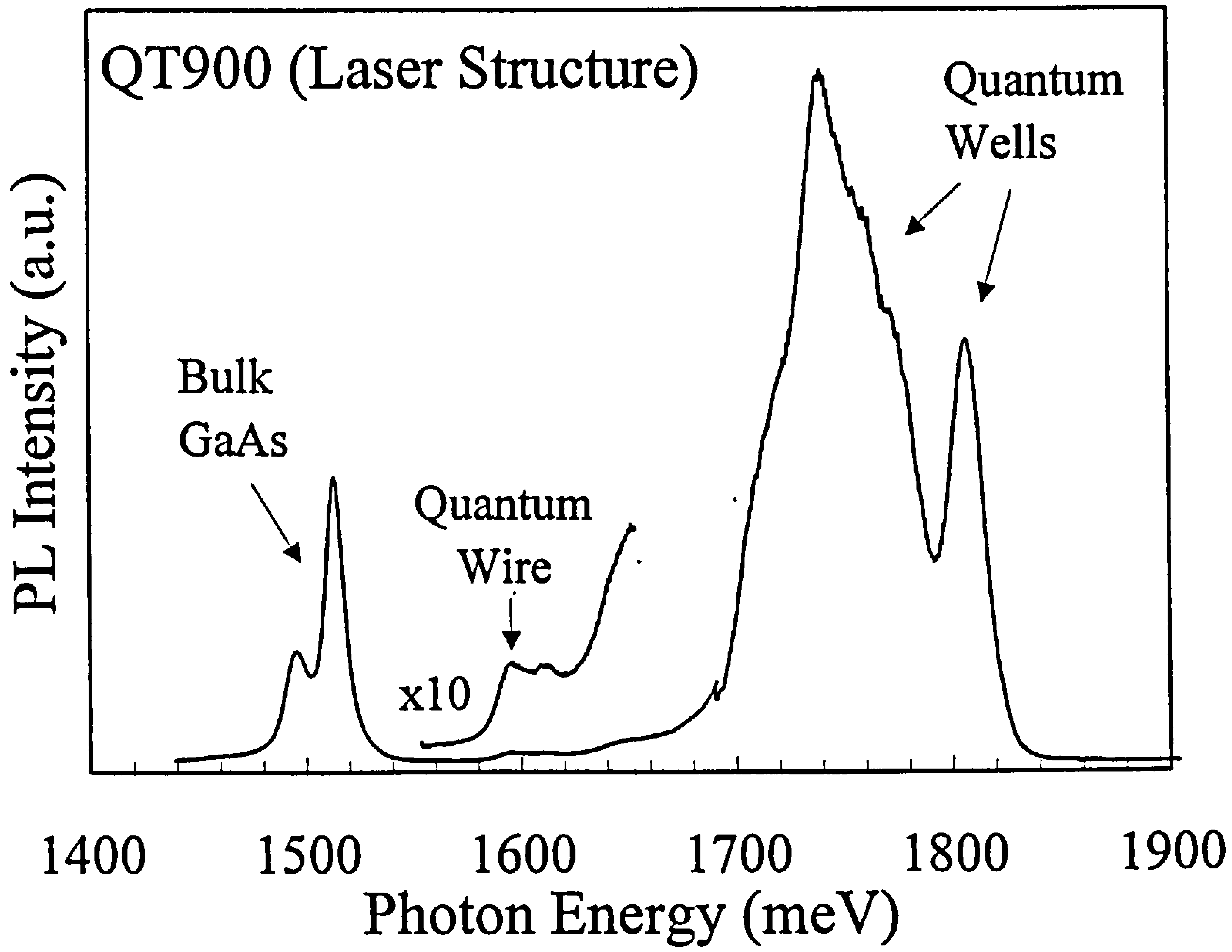

Figure 5.22 μPL spectrum at T=4.2K of the laser diode sample (QT900). A quantum wire feature is observed with an emission energy of 1596meV.

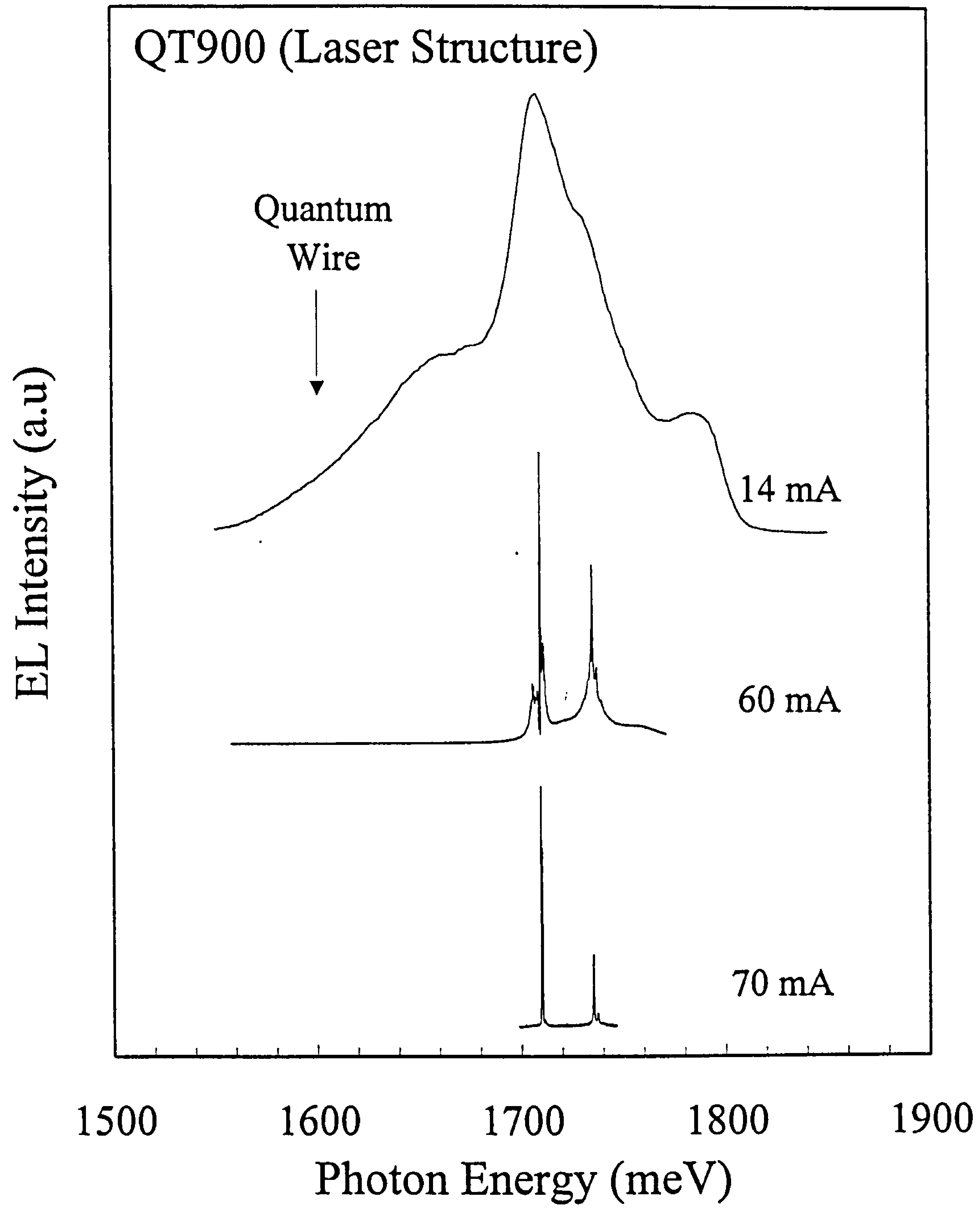

Figure 5.23 EL spectra of the laser structure for various forward bias currents. The position of the quantum wire feature observed with μPL is indicated, in EL it does not appear as a distinct emission line. The high current spectra show lasing occurring from the quantum well region of the spectra.

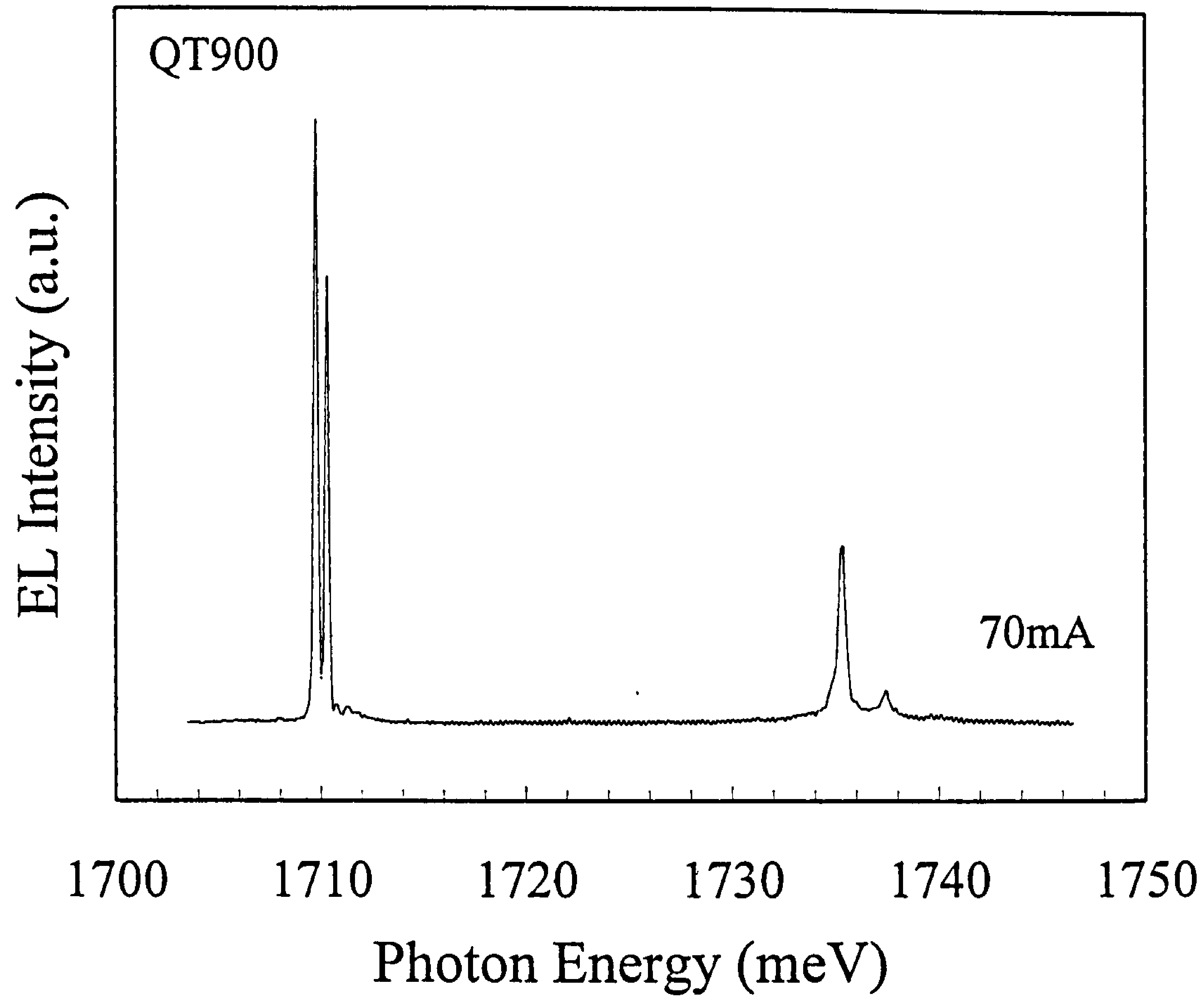

Figure 5.24 A high resolution EL spectra of the lasing emission.

5.5.1.2 Discussion of the experimental results.

Whilst it is clear from the present measurements that lasing has not been observed from the quantum wires, because the sharp lasing lines do not correspond to the emission energy expected for the quantum wire, it has been demonstrated that it is possible to process devices with cavities having mirrors of a sufficiently high quality to enable lasing to occur. A comparison of the low current spectra of the laser device with that of the mesas studied in standard EL measurements of non-laser structures can be made (see Figure 5.11 and Section 5.4.1 above). For the laser device there is no distinct quantum wire luminescence, even for low biases as was observed in the non-laser *p-i-n* device. One possibility in the present structure is that the ability of the vertical quantum well to capture carriers and channel them into the quantum wire may be diminished as a result of the lower Al fraction AlGaAs that surrounds the active region of the device. This would result in a more uniform current flow across the device, hence minimising the quantum wire emission enhancement effect observed in QT808A. However, the vertical quantum well emission still appears to be relatively strong in the EL spectra from this device.

The lasing onset occurs for currents as low as 39mA. The low current EL and μPL spectra show two dominant peaks in the quantum well region of the spectrum. As the current is increased these peaks become narrower and evolve into a series of very sharp laser lines corresponding to different Fabry-Perot longitudinal cavity modes. For the highest currents there are two modes visible on the larger of the two EL peaks and one mode on the smaller peak. Evidence for a tapering of the thickness of the side wall quantum wells in similar samples was obtained from mono-chromatic CL imaging (see Section 4.3.3). It therefore seems reasonable to assume that the observed lasing lines arise from two spatially separate regions of the side wall i.e. from near the top and base of the grooves. The quantum well formed between the grooves (the top quantum well) contributes only weakly to the EL observed for low bias and there are no laser lines in the corresponding region of the spectrum. This is also true for the quantum wire. The dominant intensity of the side wall quantum well emission indicates that this region represents the preferential trapping and recombination site for injected carriers. This is therefore the region where the population inversion and lasing action first occurs. Once lasing commences this region will represent an even more efficient recombination channel and this appears to prevent a population inversion subsequently occurring in the other active regions (the quantum wire and top quantum well).

In order to achieve lasing from the quantum wires of the present sample, isolation of the side wall quantum wells has to be achieved. This can be achieved by physically destroying the side wall by etching techniques similar to those described in section 5.3 or by electrical isolation to prevent current flowing through the side wall or top quantum wells, hence forcing the current to pass through the base of the groove where the quantum wire is situated. However, given the relatively small size of the wire a method for selectively contacting the wire is not obvious. It has also been proposed that ion implantation applied twice at angles to the substrate normal could be used to selectively damage the side and top quantum wells, leaving the quantum wire as the dominant active region.[35] In this technique the sidewalls 'shadow' the wire if the ion beam is applied at the correct angle of incidence, hence protecting it from damage. Lasing from the quantum wires in preference to the quantum wells has been reported by Kapon *et al.*[36] However this was achieved by using selective area proton implantation to confine the injected current to the centre of the grooves. These post-growth implantation techniques are relatively complex and are probably not suitable for the mass production of laser devices. It would therefore appear that advances in the structural design or growth are required if the V-groove technique is to become suitable for the commercial fabrication of laser devices.

5.6 Conclusions

A detailed optical and magneto-optical study of optimised V-groove quantum wire structures has been performed using the experimental techniques of μPL and EL. Spectrally isolated quantum wire emission has been observed in these samples allowing a comprehensive investigation of their optical properties. High incident laser power μPL experiments have shown that higher energy excited subbands exist within the wires. The subband filling effects observed in the optical spectra is evidence that the density of states for the quantum wire is one dimensional in nature. Excitation under very low power densities shows the appearance of narrow linewidth features in the μPL spectra, which are not observed for higher power densities. This behaviour provides evidence for possible wire width fluctuations along the length of the wire. These fluctuations appear to act as potential minima, trapping carriers along the length of the wire.

The feasibility of fabricating AlGaAs quantum wires with Al compositions (up to at least 15%) has been demonstrated. Spectrally isolated quantum wire emission is observed, with the emission energy of these wires varying from ~1660-1845meV (~747-672nm) as the Al composition increases from 0 to 15%. However, it is not clear whether 15% represents the high energy limit set by the growth mechanism in this material system.

Using selective etching techniques, a large proportion of the quantum well material present in the structure was removed. A quantum wire sample grown on a 2μm pitch grating was processed in this manner, with a graded etch removing varying amounts of side wall material. The spatial origin of all the features observed in the luminescence spectra was confirmed by μPL analysis of this sample in the absence of satisfactory CL. The presence of a quantum wire grown on a 2μm pitch grating was demonstrated with this analysis.

Quantum wire samples grown within the intrinsic region of a *p-i-n* structure were the subject of an extensive investigation. It was shown that with the electrical injection (EL) of carriers a greatly enhanced luminescence signal from the quantum wire was observed compared to that seen in optical carrier injection (PL) experiments. The reason for this enhancement is not clear. However, it is thought that the vertical quantum well, present in the structure, plays an important role, possibly by acting to efficiently channel carriers into the wire. The exact mechanism behind the enhanced luminescence intensity observed for electrical carrier injection is certainly another important area for future investigation. As a greater understanding of this mechanism may lead to devices with an improved performance. For high forward bias currents, higher subband transitions were clearly observed with subband separations of ~19-24meV. In addition there was also evidence for subband filling effects as the ground-state and first-excited-state transition intensities appeared to saturate at high currents.

The effect on the EL spectra observed from the quantum wires and vertical quantum wells due to the application of a magnetic field was investigated. The observed diamagnetic shift of the quantum wire transition for the magnetic field oriented along different spatial directions showed that there was a spatial anisotropy of the quantum wire wavefunctions. Higher diamagnetic shifts observed for excited state transitions indicated that the spatial extent of their wavefunctions was larger, in agreement with theoretical calculations by A. Forshaw.[8] A larger diamagnetic shift of the ground-state emission energy observed for high current density experiments, has, tentatively, been attributed to evidence for a transition from excitonic to free-carrier behaviour in a 1D system.

A preliminary study of a laser device was conducted, although lasing was only observed from the side wall quantum wells of the structure. This study has demonstrated that the capability exists to fabricate laser cavities in this complicated structure. Further work needs to be carried out in this area to optimise the structure so as to enable lasing to occur from the quantum wire as opposed to the quantum well. Very low threshold current lasers have been fabricated by Kapon *et al.*[36] using the technique of proton implantation to electrically isolate the quantum wells, allowing current to only pass through the quantum wire.

From the point of view of studying the physics of one dimensional systems there remains much further work that can be carried out on V-groove quantum wires, now that a reliable fabrication procedure exists. For instance the 1D subband structure of quantum wires could be probed using a technique such as PLE. The subband spacing present in the samples discussed in this work are still too small to allow efficient room temperature operation of devices, efforts need to be made to increase the lateral confinement potential that results from the tapering of the quantum wire. This could be achieved by growing the quantum wire on a V-groove pattern with sharper grooves, obtained by increasing the growth selectivity of AlGaAs growth on the (111)A facet, or increasing the growth rate of GaAs on the (001) surface present at the bottom of the groove. Indeed, some increase in the subband spacing (up to ~45meV) has been achieved by Kapon *et al.*,[4] there are also indications that growth by low pressure MOVPE will result in even greater subband spacings. The technique of trench growth (described in section 2.3.4) also offers this possibility as the lateral dimension can be reduced to ~200Å,[37] this seems to be the most promising approach to the problem.

5.7 References

[1] E. Kapon, G. Biasiol, D.M. Hwang and E. Colas, Microelectronics Journal, **26**, 881, (1995).

[2] K. Brunner, G. Abstrieter, G. Böhm, G. Tränkle and G. Weimann, Appl. Phys. Lett. 64, (24), 3320, (1994).

[3] Keithley Model 230, programmable Voltage Source, instruction manual, (Jan 1988).

[4] A. Gustafsson, F. Reinhardt, G. Biasiol, and E. Kapon, Appl. Phys. Lett. **67**, (25), 3673, (1995).

[5] A.K. Saxena and K.S. Gurumurthy, J. Phys. Chem. Solids, **43**, 801, (1982).

[6] C.S. Son, S.I. Kim, Y. Kim, Y.K. Park, E.K. Kim, S.K. Min, I.H.J. Choi, J. Appl. Phys. **82**, (3), 1205, (1997).

[7] J.M. Luttinger, Phys. Rev. **102**, (), 1030, (1956).

[8] A. Forshaw, PhD Thesis, University of Sheffield (1996).

[9] S.K. Lyo, E.D. Jones and J.F. Klem, Phys. Rev. Letts. **61**, 2265, (1988).

[10] E. Burstein, G.S. Picus, R.F. Wallis and F. Blatt Phys. Rev. **113**, (1), 15, (1959).

[11] T. Ruf, R.T. Phillips, A. Cantarero, G. Ambrazevicius, M. Cardona, J. Schmitz and U. Rössler, Phys. Rev. B. **39**, (18), 13378, (1989).

[12] D.C. Rogers, R.J. Nicholas, J.C. Portal and M. Razeghi, Semicond. Sci. Technol. **1**, 350, (1986).

[13] D.C. Rogers, J. Singleton, R.J. Nicholas, C.T. Foxon and K. Woodbridge, Phys. Rev. B. **34**, 4002, (1986).

[14] M.S. Skolnick, K.J. Nash, S.J. Bass, P.E. Simmonds and M.J. Kane, Sol. Stat. Comms. **67**, (6), 637, (1988).

[15] M.S. Skolnick, J. Morrison, K.J. Nash, D.J. Mowbray, P.R. Tapster, S.J. Bass and A.D. Pitt, Phys. Rev. Lett. **58**, (20), 2130, (1987).

[16] M.S. Skolnick, D.J. Mowbray, D.M. Whittaker and R.S. Smith, Phys. Rev. B. **47**, 6823, (1993).

[17] H. Weman, M. Potemski, M.E. Lazzouni, M.S. Miller, J.L. Merz, Phys. Rev. B. **53**, (11), 6959, (1996).

[18] Y. Nagamune, Y. Arakawa, S. Tsukamoto, M. Nishioka, S. Sasaki and N. Miura, Phys. Rev. Lett. **69**, (20), 2963, (1992).

[19] M.V. Marquezini, M.J.S.P. Brasil, M.A. Cotta, J.A. Brum and A.A. Bernussi, Phys. Rev. B. **53**, (24), R16156, (1996).

[20] R. Rinaldi, R. Cingolani, M. Lepore, M. Ferrara, I.M. Catalano, F. Rossi, L. Rota, E. Molinari, P. Lugli, U. Marti, D. Martin, F. Morier-Gemoud, P. Ruterana and F.K. Reinhart, Phys. Rev. Lett. **73**, (21), 2899, (1994).

[21] G. Goldoni and A. Fasolino, Phys. Rev. B. **52**, (19), 14118, (1995).

[22] R. Rinaldi, P.V. Giugno, R. Cingolani, F. Rossi, E. Molinari, U. Marti and F.K. Reinhart, Phys. Rev. B. **53**, (20), 13710, (1996).

[23] M. Bayer, P. Ils, M. Michel, A. Forchel, T.L. Reinecke and P.A. Knipp, Phys. Rev. B. **53**, (8), 4668, (1996).

[24] D.C. Rogers, J. Singleton, R.J. Nicholas, C.T. Foxon and K. Woodbridge Phys. Rev. B. **34**, 4002, (1986).

[25] H. Sakaki, Y. Arakawa, M. Nishioka, J. Yoshino, H. Okamoto and N. Miura, Appl. Phys. Lett. **46**, (1), 83, (1985).

[26] N.J. Pulsford, J. Singleton, R.J. Nicholas and C.T.B Foxon, J. De Physique, **C5**, 231, (1987).

[27] Calculations performed by David Whittaker.

[28] K.J. Nash, M.S. Skolnick, P.A. Claxten and J.S. Roberts, Phys. Rev. B **39**, (15), 10943, (1989).

[29] R. Rinaldi, P.V. Giugno, R. Cingolani, F. Rossi, E. Molinari, U. Marti and K. Reinhart, Phys. Rev. B. **53**, (20), 13710, (1996).

[30] C. Delalande, G. Bastard, J. Orgonasi, J.A. Brum, H.W. Liu, M. Voos, G. Weimann and W. Schlapp, Phys. Rev. Lett. **59**, (23), 2690, (1987).

[31] F. Rossi and E. Molinari, Phys. Rev. Lett. **76**, (19), 3642, (1996).

[32] R. Ambigapathy, I. Bar-Joseph, D.Y. Oberli, S. Haacke, M.J. Brasil, F. Reinhardt, E. Kapon and B. Deveaud, Phys. Rev. Lett. **78**, (18), 3579, (1997).

[33] M.J. Kelly *in 'Low Dimensional Semiconductors Materials, Physics, Technology, Devices'*, Clarendon Press, Oxford, (1995).

[34] N. Holonyak. Jr., R. M. Kolbas, R.D. Dupuis and P.D. Dapkus, IEEE J. Quan. Elec. **QE-16**, 170, (1980).

[35] E. Kapon, D.M. Hwang and R. Bhat, Phys. Rev. B **63**, (4), 430, (1989).

[36] E. Kapon Optoelectronics. **8**, (4), 429, (1993).

[37] T. Sogawa, S. Ando, H. Kanbe, Appl. Phys. Lett., **64**, (4), 472, (1994).

Chapter 6

Structural and Optical Characterisation of InAs-GaAs Self-Organised Quantum Dots

6.1 Introduction

The mechanism behind the self-organised growth of quantum dots has been described in detail in Chapter 2. The structural and optical measurements described in the present chapter were performed on nominally InAs quantum dots grown on (001) GaAs by solid source molecular beam epitaxy (MBE). MBE provides the ability to perform in-situ monitoring of the growth. In particular, reflection high energy electron diffraction (RHEED) measurements allow the 2D to 3D growth transition to be readily observed. MBE is hence the favoured technique for the growth of self-organised quantum dots.

The results described in the present chapter consist of the initial characterisation measurements performed on a series of quantum dot structures, fabricated using a range of growth parameters. The aim was to quickly establish a set of growth conditions, based on the literature available at the time, that would lead to the formation of self organised dots suitable for optical and structural characterisation. A summary of the growth conditions and initial PL results of the samples grown as part of this investigation is given, for reference, in Table 6.1. The initial growth experiments were based on the parameters reported by Moison *et al.*[1] They involve the growth of a few monolayers of InAs on an (001) GaAs substrate, using a very low growth rate of 0.124ML/s and a high arsenic flux. The InAs deposition is carried out as a sequence of ¼ML cycles, with growth interrupts of 4s between cycles to allow atoms on the surface to reach an equilibrium state, corresponding to the lowest surface free energy. The InAs layer is then capped with ~1000Å of GaAs which provides confinement for the quantum dots.

Sample	Thickness (ML)	Growth Rate (ML/s)	Temp (°C)	Peak Position	Linewidth
M879	2.5	0.124	520	1150meV / (10740Å)	-
M927	1.75	0.0645	512	1459meV / (8513Å)	14meV
M928	2.1	0.0645	512	1473meV / (8420Å)	11meV
M929	2.4	0.0645	508	1133meV / (10940Å)	43meV
M965	2.25	0.0645	475	1261meV / (9830Å)	150meV
M981	2.4	0.08	515	1142mV / (10857Å)	65meV
M982	2.4	0.08	450	No measurable PL	-
M983	2.4	0.3	450	No measurable PL	-
M984	2.4	0.3	515	1181meV / (10500Å)	65meV
M1094	2.4	0.0542	518	1104meV / (11225Å)	35meV
M1095	2.4	0.106	518	1269meV / (9767Å)	94meV
M1096	2.4	0.106	518	1119meV / (11073Å)	41meV
M1097	2.4	0.301	518	1150meV / (10775Å)	87meV
M1098	2.4	0.301	518	1168meV / (10610Å)	58meV
M1099	2.4	0.848	518	1171meV / (10589Å)	80meV
M1182	2.4	0.248	513	1245meV / (9954Å)	83meV
M1183	2.4	0.248	513	1222meV / (10147Å)	74meV
M1227	2.4	0.082	523	1209meV / (10255Å)	107meV
M1263	2.4	0.107	512	1192meV / (10400Å)	104meV

Table 6.1 Summary of the MBE growth conditions used for the Quantum Dot samples grown as part of these initial investigations. The corresponding PL peak positions and linewidths obtained from 4.2K PL experiments are also shown.

Photoluminescence (PL) was used initially as a probe to establish whether a 2D quantum well or an ensemble of 0D quantum dots had formed, particularly after the growth had exceeded the critical thickness required for self organised islanding to occur. This transition was monitored during growth using RHEED. TEM analysis of the samples was then used to determine the origin of any non-quantum well luminescence. PL was subsequently used to investigate the effect of changes in growth conditions, for example substrate temperature, growth rate etc. on the optical spectra of the quantum dots. Of particular interest were the emission energy and linewidth, the latter indicating the degree of dot size and shape inhomogeneity. The effects of temperature and excitation density on the quantum dot emission spectra were also investigated. Finally, a PL study of a small number of dots (<100) was conducted using the μPL equipment described previously. These results, in which extremely sharp emission lines from individual dots are observed, demonstrates the expected zero dimensional density of electronic states of the quantum dots.

6.2 RHEED Monitoring During MBE Growth

To monitor the surface quality and structure of the samples during MBE growth, the in-situ technique of reflection high energy electron diffraction (RHEED) is used.[2] The basic experimental arrangement consists of an electron gun and a fluorescent screen. The electron gun is mounted so electrons can be fired at low incident angles (< 3°) towards the substrate surface. The diffracted electrons form a pattern on the fluorescent screen and this pattern can be interpreted to provide real-time information about the surface morphology and symmetry of the layers being grown. During the Stranski-Krastanov growth of highly strained layers, for example InAs on GaAs, the growth mode changes abruptly from 2D layer-by-layer growth to a 3D islanding growth mode. This occurs, under suitable growth conditions, when the elastic strain energy in the growing layer becomes so great that 3D growth, even though it involves a higher surface energy, becomes the lowest total energy state. For suitable growth conditions this is energetically more favourable than the formation of mis-fit dislocations. This

2D→3D change in growth mode can be observed using RHEED as the layer is being grown.

Figure 6.1a shows the streaky (2×4) reconstruction RHEED pattern associated with normal 2D layer-by-layer growth. This pattern is observed for the growth of unstrained material and, in the present case, for the deposition of at least the first monolayer of strained InAs (our observations show that it persists up to ~1.8MLs of InAs). When 3D islanding occurs the growth surface is now no longer flat with the occasional monolayer step and the diffraction pattern suddenly changes to a spotty pattern as shown in Figure 6.1b. This change in the RHEED pattern indicates the onset of 3D island formation. When the GaAs capping layer is grown above the dots, the RHEED quickly reverts back to the streaky pattern of Figure 6.1a as the layer planarises and the growth mode tends to a 2D layer-by-layer one. The RHEED measurements hence provide a rapid determination of when the critical thickness for quantum dot formation is reached. In the present studies this is found to occur after the deposition of 1.8 MLs of InAs. This value is in good agreement with previously reported values for the critical thickness for InAs dot formation of 1.5ML[3] and 1.7ML.[4]

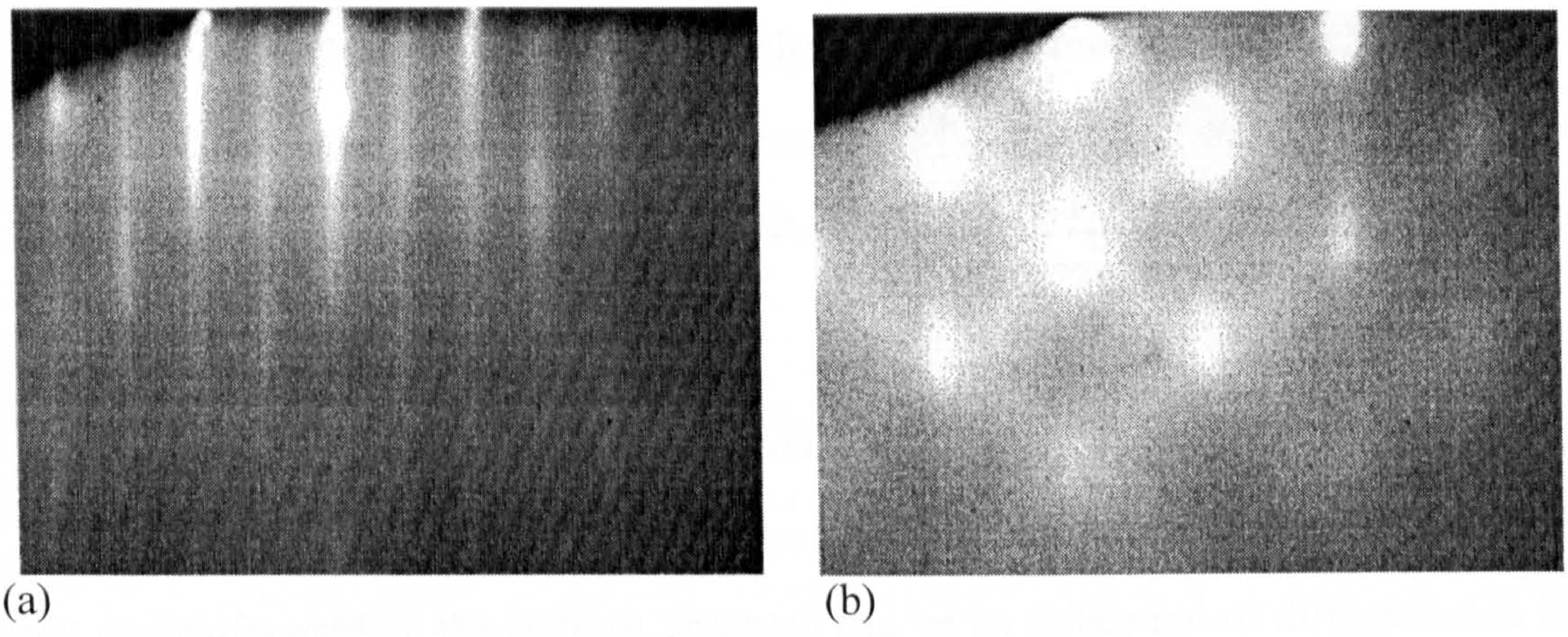
(a) (b)

Figure 6.1 a) RHEED pattern showing 2D growth, b) RHEED pattern showing 3D islanding growth. Both images were captured during the growth of a quantum dot layer.

6.3 TEM Structural Studies

Cross-sectional and plan view transmission electron microscope (TEM) images were obtained to provide structural analysis of the grown layers. These confirmed the existence of coherent, dislocation free InAs quantum dots contained within a GaAs matrix. The optical properties of semiconductor structures are significantly affected by the presence of dislocations within the structure, as they can act as non-radiative recombination sites for free carriers, inhibiting or eliminating the luminescence from the active region of the sample. Dislocations can occur during the growth of strained layers beyond a certain critical thickness because their formation results in the efficient relief of the elastic strain energy.[5] The growth of self-organised quantum dots relies on the strain being relieved by the Stranski-Krastanov growth process, as opposed to dislocation formation. This is achieved by choosing growth conditions that favour islanding over dislocation formation. Minimising the amount of material deposited also reduces the likelihood of dislocation formation. If the islands become too big, then dislocation formation becomes more likely. In addition, large islands may start to impinge on each other resulting in very large island formation and a greatly increased probability of dislocation formation. A balance therefore needs to be reached such that the islands are large enough to have a reasonable homogeneous size distribution, and hence relatively narrow emission linewidth, but not so large that dislocations form or the dots merge together.

A cross-sectional TEM image of sample M929 is shown in Figure 6.2. The position of the InAs layer appears as a stripe across the image. Interpretation of this TEM image is not straightforward as the contrast observed can be an indication of differences in the lattice constant of the materials (strain effect) or in the atomic weight of the underlying atoms (chemical effect). It is known that InAs dots grown on GaAs are highly strained due to the large lattice mismatch of $\approx 7\%$. In practice this strain is a complex function of position both within and outside of the dots. Calculations for pyramidal dots[6] indicate high strain levels at the base of the dots with the strain decreasing as the apex of the pyramid is approached, due to plastic, dislocation free, deformation of the InAs.

Because the InAs at the apex of the pyramid no longer has the GaAs lattice constant, the initial GaAs grown on top of the dots is strained. In addition, the TEM measurements discussed below indicate that the GaAs immediately below the dots is also strained. The strain field associated with the dot hence penetrates into the surrounding GaAs. This complex strain field therefore makes an accurate determination of the dot size and shape from the present TEM measurements difficult. The strain field associated with the dots appears as the dark patches above and below the plane of the wetting layer in the cross-sectional TEM micrograph of Figure 6.2. The InAs dots actually lie between these patches, appearing lighter than the surrounding strained GaAs. The dots appear have an anisotropic shape with their in-plane spatial extent considerably larger than their extent along the growth axis. However, determining their exact shape from these images is not straight forward because of the effects of strain discussed above. An approximate determination of their size gives an in-plane length of ≈12nm and height ≈2nm.

There has been considerable debate in the literature regarding the shape of self-organised quantum dots. An accurate determination is important as theoretical modelling of the confined energy levels depends critically on knowing their exact size and shape. A number of groups have claimed that self-organised InAs quantum dots are of the form of truncated spheres or cone shaped, in both cases the dots posses cylindrical symmetry.[7,8] However, the detailed TEM studies of the St. Petersberg-Berlin group strongly suggest a pyramidal shape.[9] The precise shape of self-organised InAs quantum dots is hence still unresolved. It is worth noting that the measurements suggesting truncated cone or spherical shapes are generally Atomic Force Microscope (AFM) or Scanning Tunnelling Microscope (STM) measurements of uncapped dots[7,8] and it is possible that the subsequent growth of a GaAs capping layer for TEM or optical studies may result in a change of the dot shape. It is also possible that subtle differences in growth conditions result in the formation of two sets of distinctly different shaped dots studied by the different groups of workers.

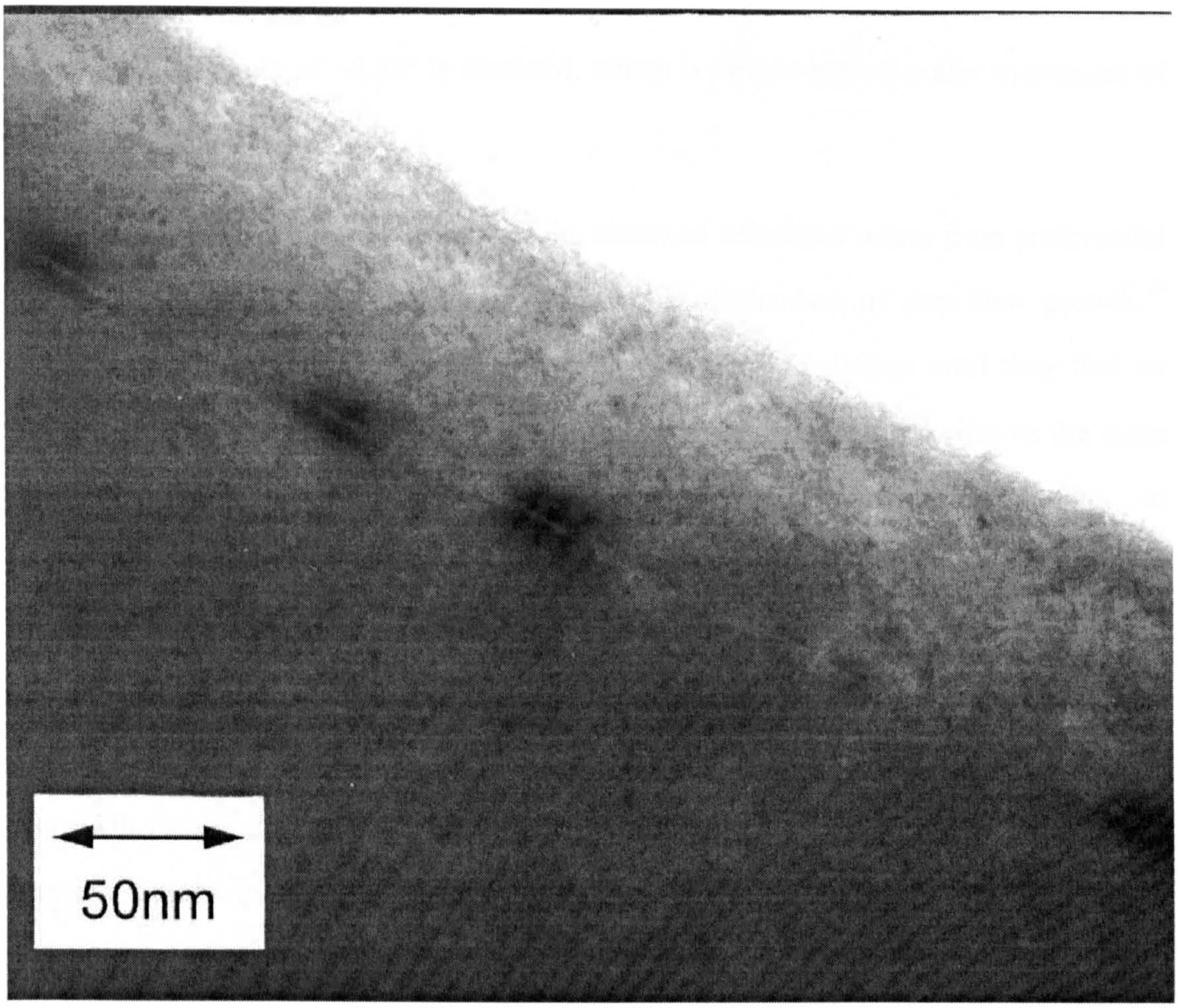

Figure 6.2 Cross-Sectional TEM micrograph of sample M1097 showing the approximate shape of the dots and the presence of a strain field surrounding the dots.

A plan view TEM image of the quantum dots formed in sample M981 is shown in Figure 6.3. Because this image is recorded for a sample for which the dots are capped by 1000Å of GaAs, the observed structure reflects the strain field within the sample, not the actual dot structure. From this image the dot density is estimated to be $\sim 3\times10^{10}\text{cm}^{-2}$.

The apparent arrangement of the dots in roughly parallel rows is a very interesting feature of the image. It is thought that this alignment arises because of the preferential nucleation of adatoms on the naturally occurring monolayer step edges, found on the surface of any wafer, due to the slight substrate mis-orientation away from exactly (001). If the separation, d, between the rows of dots is taken as the step edge separation, then the mis-orientation angle, θ, is given by $\tan(\theta)=a_0/d$, where a_o is the GaAs monolayer thickness (2.8Å). From the average measured row separation of 450Å, a mis-orientation angle of ~0.35° is obtained, which is within typical wafer tolerances of ≈0.5°.

The principle behind the conclusion that the observed behaviour arises from preferential dot nucleation at the step-edges comes from the mechanism of step-flow growth.[10] Atoms arriving from the source impinge on the surface and diffuse until they find an energetically favourable lattice site. Step-edges represent preferential sites as the atom has its motion inhibited in one direction making further diffusion less likely. In contrast, atoms on the plateaux between the steps are more likely to become displaced by the thermal energy of the system. Entire 2D layers can be grown by this method of step-flow growth although in practice it is quite difficult to control as some atoms do stick to the plateaux, promoting further nucleation and the formation of an additional set of growth fronts. The quantum dots in the present sample are grown at 515°C. This is very close to the In desorption temperature of ~520°C,[11] making growth on the plateaux more unlikely because of the increased thermal energy of the Indium adatoms. Step-flow growth is therefore the preferred 2D growth mechanism under these conditions and this favours island nucleation occurring at step-edges where the strain field is first sufficiently large enough to promote 3D growth.

This apparent self-organisation at step-edges is potentially useful as, if it can be controlled, the dot density could potentially be determined by accurately polishing the wafer to a specific offcut angle, defining the step density. In addition, the presence of specific nucleation sites may lead to the formation of a more homogeneous distribution of dot size and shapes. An investigation of this process is not within the scope of the present work but warrants future examination. A better understanding of this growth mechanism will be beneficial if a greater control of the growth, and hence dot size and shape uniformity can be achieved.

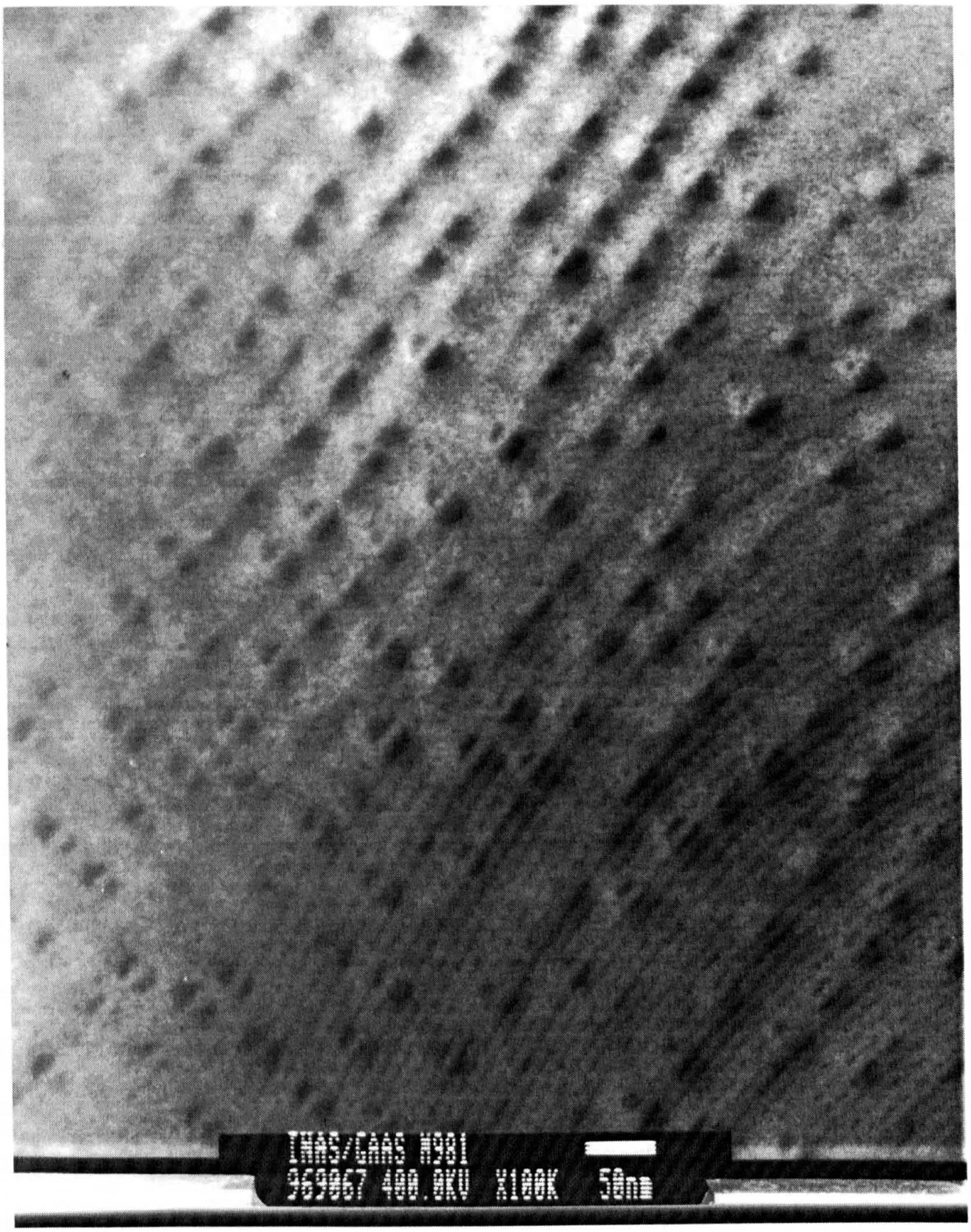

Figure 6.3 Plan View TEM micrograph of sample M981 showing an apparent alignment of quantum dots on step-edges.

6.4 Photoluminescence Study of the 2D→3D Growth Transition

Samples M927, M928 and M929 were grown as a controlled series to investigate the growth mode transition from 2D layer-by-layer to 3D clustering and self-organisation, resulting from the Stranski-Krastanov growth mechanism. The thicknesses used for these samples were known from observations during the growth of sample M879 to span the thickness required to change the RHEED pattern from streaky to spotty, i.e. the 2D to 3D growth transition (see Section 6.2). M879 showed a change in the RHEED pattern after the deposition of 2.0MLs of InAs, so InAs layer thicknesses of 1.75, 2.1 and 2.4MLs were deposited for the three samples M927, M928 and M929 respectively. No change in the RHEED pattern was observed during the growth of the 1.75ML sample, for the 2.1 and 2.4ML samples a change was observed at 1.9 and 1.85MLs respectively. All samples were nominally grown under the same conditions; a growth temperature of ~512°C and a 0.0645ML/s growth rate.

Figure 6.4 shows PL spectra of the three samples. There is a striking difference between the linewidth and peak position of M929, the sample with the greatest InAs thickness, compared with the other two samples. The former sample has an emission energy of ~1130meV and a linewidth of 43meV, in contrast to the higher emission energies of ~1460meV and narrower linewidths of <15meV for the samples with smaller InAs thicknesses. This difference is due to the presence of quantum dots in M929 and a quantum well, the so called wetting layer (WL), with a thickness of either 1 or 2 monolayers in the other two samples. M928 showed a RHEED transition after 1.9ML of InAs had been deposited, suggesting that the 2D→3D growth transition had occurred and that islands were forming on the surface. However, after the sample was capped with GaAs, PL measurements showed a narrow (11meV FWHM linewidth), high energy emission, suggesting that the carriers are actually confined in a very narrow quantum well. This indicates that the InAs surface has planarised during the growth of the cap, suggesting that the In atoms contained in the islands are still very mobile on the surface and that the islands have to reach a critical size before they become stable. It is possible that the flux of gallium on the surface may cause the In atoms to migrate from the islands and alloy with the Ga to form a ternary InGaAs quantum well of reduced strain and hence below the critical thickness. This process is possible if it represents the lowest energy state.

An interesting feature of the spectra shown in Figure 6.4, which is not fully understood, is the relative emission energies of the two 2D wetting layer samples. The thinnest layer, M927, 1.75ML, has a peak position (1459meV) at a lower energy than M928 (1473meV), for which 2.1ML of InAs is deposited. This is unexpected as a thicker quantum well should produce a lower energy transition. In the present case we are dealing with very thin layers which can only be 1 or 2 monolayers thick. Simple finite potential well calculations, neglecting exciton binding energies which are expected to be small in such thin layers,[12] give a transition energy for a 1ML InAs quantum well of ~1458meV[13] compared to ~1328meV for a 2ML thick quantum well. Hence there appears to be a reasonable agreement between the calculated 1ML emission energy and the measured PL energy. However, this agreement is likely to be fortuitous as the calculations neglect the effects of strain which, for a lattice mismatch of 7%, are likely to be large. In addition, the envelope function model, which is used to calculate the transition energy, is only valid for well widths such that the spatial variation of the resultant wavefunction is small on the scale of the rapidly oscillating Bloch functions.[14] This requirement is not satisfied for well widths of only 1 or 2ML. However we note that the emission energy of ≈1458meV is very close to that observed from 1ML InAs layers studied by Dosanjh *et al.*[15] Hence it is possible to be reasonably confident that the luminescence observed in both samples arises from the recombination of excitons confined within a single monolayer of InAs. The reason for the surprising reversal of the PL energies of samples M927 and M928 is unclear. Because of carrier localisation by well width fluctuations, the energy of the recombining excitons may significantly underestimate the true size of the band gap. Only an absorption related technique (for example PLE, as discussed in the following chapter) provides an accurate measure of the band gap and it is possible that the present discrepancy may simply be a result of the

PL measurement technique. An alternative possibility is that the layers are not pure InAs but contain an unknown amount of Ga. A higher Ga content for M928 compared to M927 would explain the observed PL transition energies.

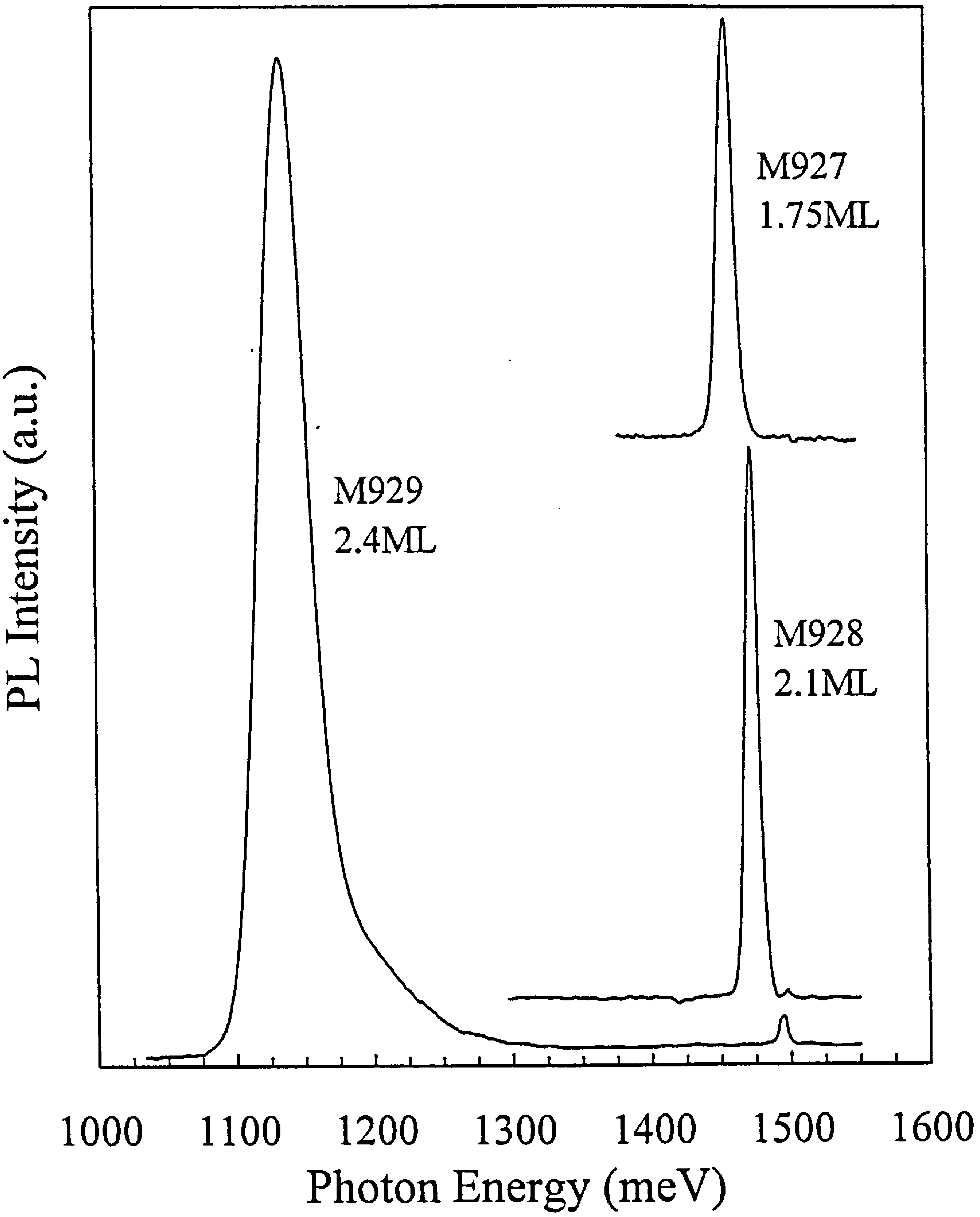

Figure 6.4 PL spectrum of samples M927, M928 and M929 each having different InAs deposits as indicated. The spectra were all taken with a HeNe laser (λ_{ex}=6330Å) at a temperature of 4.2K.

6.5 Effects of Growth Temperature and Growth Rate

To investigate the effects of a change in growth temperature and growth rate, samples M965 and M981-M984 were grown. M965 was grown at a reduced growth temperature of 475°C and an InAs thickness of 2.25ML. This is between the thicknesses of M928 and M929, the PL of which are dominated by quantum well and dot emission respectively. The PL spectrum of sample M965 shows a very broad (150meV FWHM) peak at a higher energy of 1261meV compared to 1133meV for M929 (see Figure 6.5). TEM micrographs of this sample (see Figure 6.6) show it to be full of mis-fit dislocations with only a few features which possibly represent quantum dots. The origin of the PL from this sample is not clear. PL studies of strained InAs on GaAs conducted by Brandt *et al*[16] also exhibit a broad PL peak at ~1256meV (close to emission energy observed in M965 of 1261meV) for several samples having InAs thicknesses varying between 3 and 6 MLs. Brandt *et al*[16] attribute this luminescence to a defect related transition, either a Ga vacancy in GaAs or the 60° dislocations that they observe in their samples. Radiative recombination from dislocations is not normally expected, although reference is made to radiative recombination from dislocations that has been observed in strained SiGe heterostructures.[17]

Samples M982 and M983, which were grown at the lower temperature of 450°C, show no measurable PL whereas M981 and M984, both grown at 515°C, exhibit PL spectra similar to that of M929 (Figure 6.5). Confirmation of the presence of quantum dots in M981 has been shown in the plan view TEM micrograph reproduced in Figure 6.3. It can be concluded from these results that it is not possible to produce quantum dots at the lower growth temperatures (~450°C) using the present MBE system. As a result, all subsequent growth was performed at temperatures around 515°C, close to the In desorption temperature.[11]

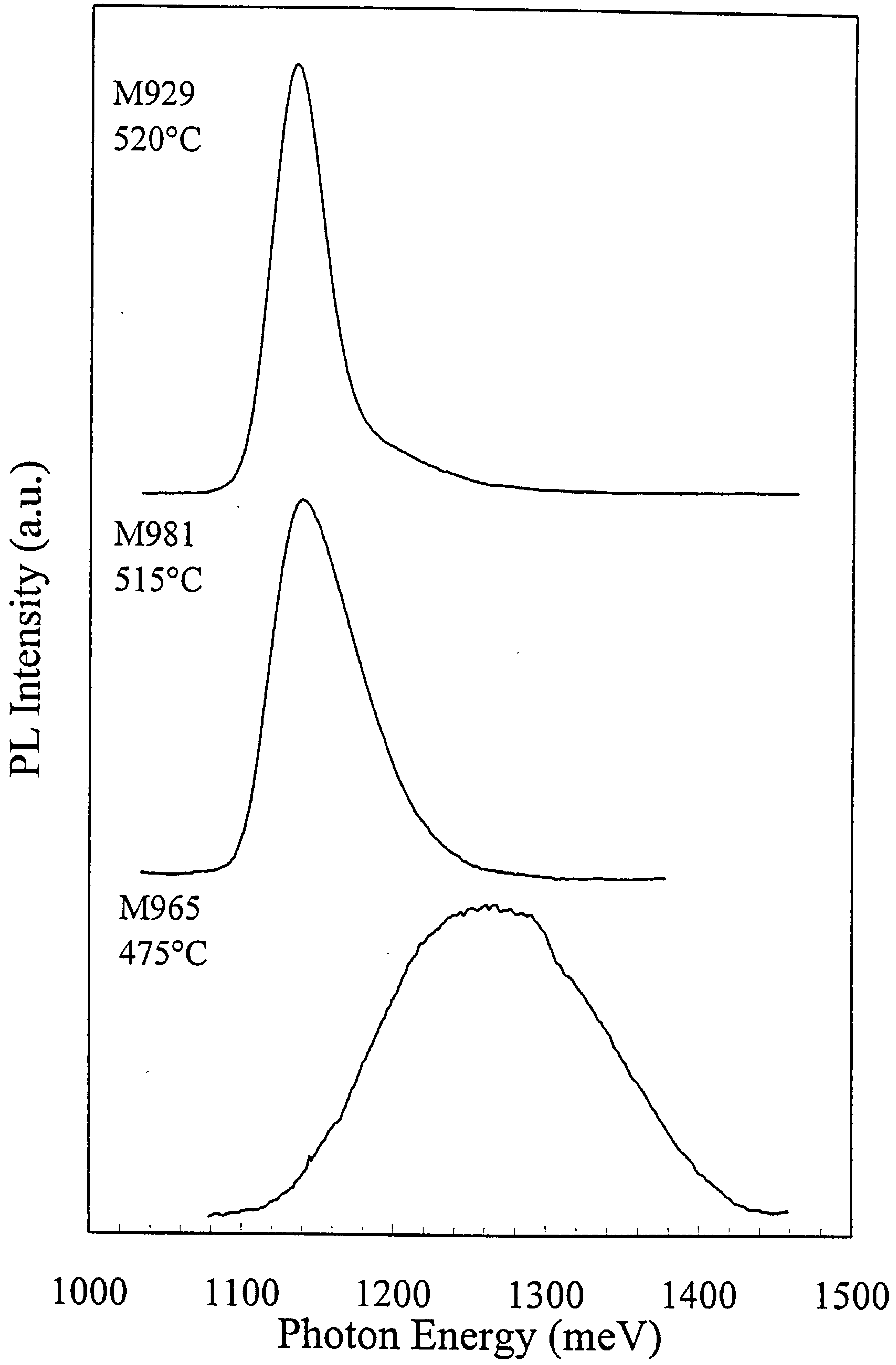

Figure 6.5 PL spectra of samples M965, M929 and M981 each grown at the temperature indicated. The spectra were all taken with a HeNe laser (λ_{ex}=6330Å) at a temperature of 4.2K.

Figure 6.6 Plan-View TEM micrograph of sample M965 grown at 475°C showing mis-fit dislocations across the surface.

6.6 Photoluminescence Studies of Quantum Dot Size and Shape Uniformity

We can visualise the broad quantum dot luminescence as arising from a distribution of delta function-like emission lines of an ensemble of single dots, each of slightly different shape and size, and hence different confined energy levels. The linewidth of the PL is therefore a good indication of the size and shape uniformity of the dots, samples with the narrowest linewidths having dots with the greatest uniformity. For device applications dot size and shape uniformity is a very important requirement. This is particularly so for laser devices where, ideally, all the dots need to be identical; emitting at the same energy and hence maximising the gain and light output, whilst minimising the current required to drive the device.

The effect of growth rate on the PL linewidth was investigated. Although no exact correlation was found, the samples grown with the lowest growth rates appear to show the narrowest linewidths. This is in contrast to the results of Gérard[4] where faster growth rates resulted in significantly smaller PL linewidths. Figure 6.7 shows the low temperature PL linewidths of all the measured samples plotted against growth rate. Figure 6.8 shows the PL peak position as a function of growth rate for the same set of samples, all grown at temperatures around 515°C. Again there is no strong correlation of the emission energy with the growth rate. However, there does appear to be a relationship between linewidth and peak position, as shown in Figure 6.9. This figure shows that samples with a lower emission energy (longer wavelength emission) tend to have a narrower linewidth. This observation is in line with that expected for the effects of dot size and shape fluctuations. The energy levels of smaller dots, with higher energy emission, should be more sensitive to small changes in size than larger dots which have a lower energy emission. In the same way, the emission energy of a narrow quantum well is shifted more by a mono-layer thickness fluctuation than occurs for a thicker quantum well.[14]

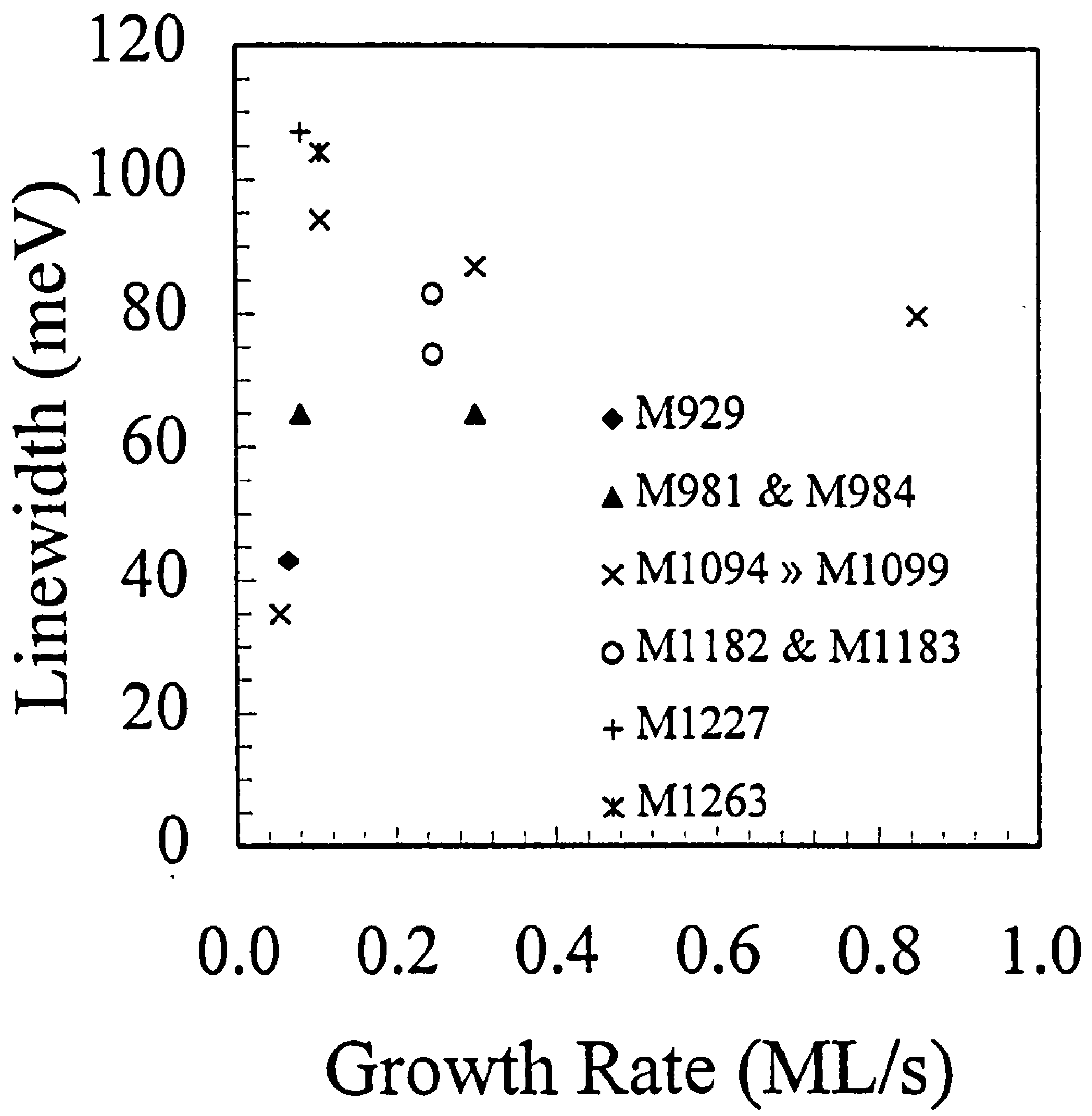

Figure 6.7 PL linewidth vs Growth rate for a series of samples, all grown at temperatures ~515°C.

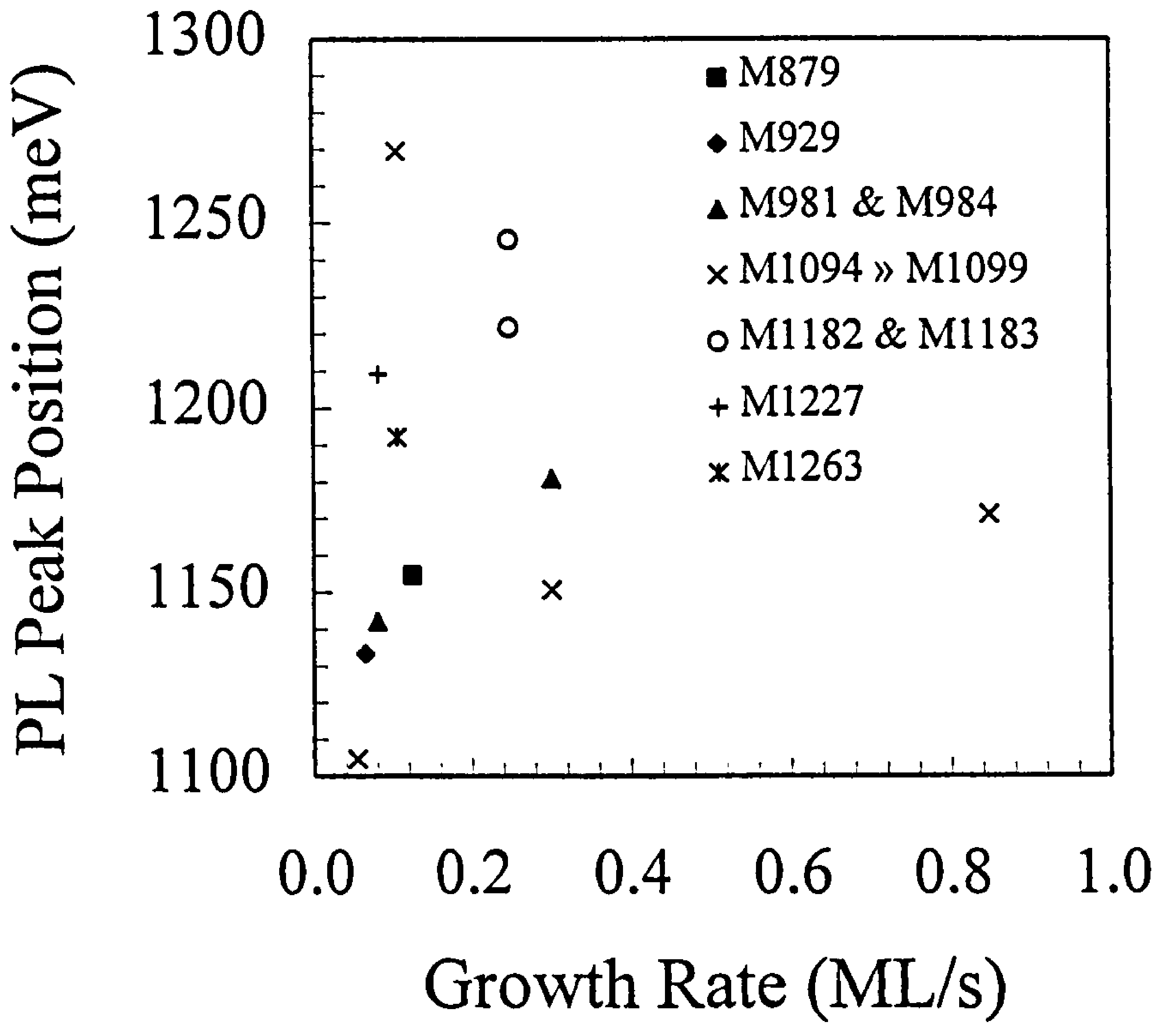

Figure 6.8 PL peak position vs Growth Rate for a series of samples grown at ~515°C.

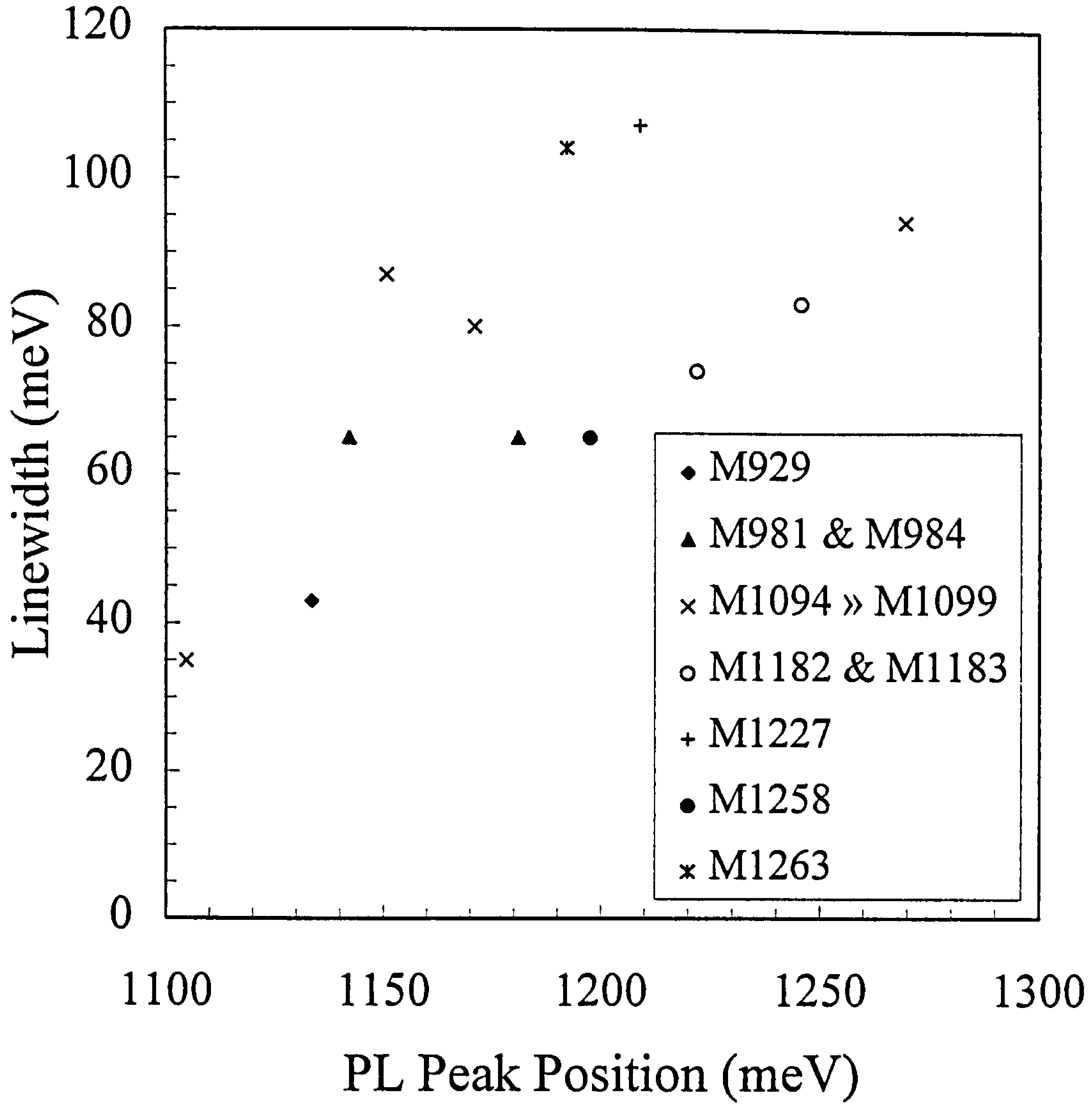

Figure 6.9 PL linewidth vs peak position for a series of samples grown at ~515°C.

Photoluminescence spectra from several samples, grown under nominally identical conditions, are shown in Figure 6.10. A significant variation in the position and linewidth of the PL peak is observed, indicating that the structure of the dots is sensitive to small day-to-day changes in the growth conditions. Hence a detailed study of the relationship between growth conditions and optical spectra appears to be difficult. In the remainder of this chapter, therefore, results will be presented on samples M929 and M981 which, from TEM structural studies, are known to contain well formed quantum dots.

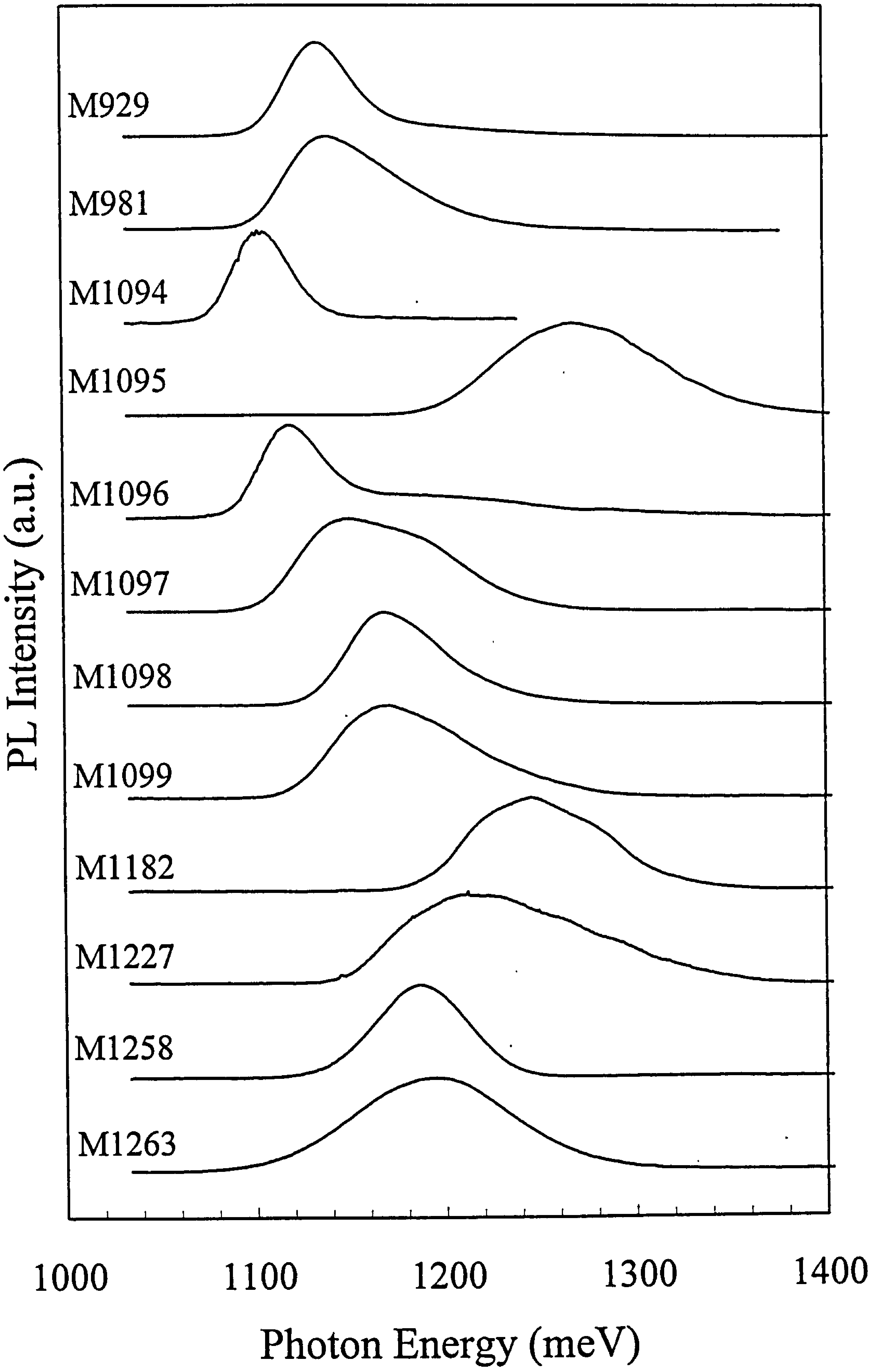

Figure 6.10 Typical PL spectra at T=4.2K for a series of nominally identical quantum dot samples, showing a significant variation of the linewidth and peak position.

6.7 Temperature Dependence of the PL

A crucial aspect for the operation of quantum dot based electro-optical devices is the trapping and/or emission of carriers by/or from the dots. For example, a laser device requires fast carrier trapping and any subsequent carrier re-emission will lead to degraded performance. Information on carrier emission from dots is provided by temperature dependent PL measurements and such measurements are described in this section.

Photoluminescence spectrum were recorded using both a HeNe and an infra-red diode laser to give excitation wavelengths of 6330Å and 7850Å respectively. Both wavelengths correspond to excitation into the GaAs which surrounds the dots. The photo-created carriers diffuse into the dots and PL from their subsequent recombination is observed. Sample M929 was placed in a continuous flow He cryostat where the temperature could be varied between 4.2K and room temperature. Figure 6.11 and Figure 6.12 show PL spectra for various temperatures, excited with the HeNe and infra-red lasers. Both sets of spectra show a broad PL peak, attributed to luminescence from the ground state of the quantum dots. At high temperatures the PL becomes weaker although it remains visible with the HeNe laser up to around 250K. In addition there is evidence of a high energy tail to the distribution at low temperature which becomes weaker as the temperature is raised. It is believed that this weak higher energy PL represents the ground state emission from a low number of very small dots. Results obtained with the infra-red laser also show luminescence from the wetting layer and the GaAs barriers, neither of which is observed with shorter wavelength, HeNe excitation. This difference may be a result of the difference in the penetration depth for the two lasers used. The greater penetration depth of the infra-red laser (~1μm)[20] may produce some carriers sufficiently far from the dot layer (0.1μm from the surface) which are unable to diffuse to the dots before recombining in the GaAs. This is less likely with the shorter penetration depth (~0.3μm)[20] of the HeNe laser. However, this mechanism can not explain the enhancement of the wetting layer signal obtained with the infra-red laser and it appears possible that some form of resonant enhancement may be occurring.

Figure 6.13 shows how the intensity of the luminescence varies as a function of temperature. The PL intensity increases slightly up to around 100K then decreases rapidly at higher temperatures. The reason for this initial increase is unclear but may result from an enhanced probability of carrier diffusion, due to an increasing thermal energy, from the GaAs to the dots. The rapid decrease in the PL intensity above 100K represents the thermal loss of carriers from the dots. More detailed temperature dependent measurements[18] conducted on M929 indicate an activation energy of ≈40meV, as extracted from a ln(I)*vs* 1/T plot. Due to a lack of knowledge of the form of the dot energy levels it is not clear if this energy represents the thermal loss of electrons or holes to the GaAs or wetting layer, or alternatively the loss of carriers to non-radiative centres in the GaAs. No increase in the wetting layer or GaAs luminescence is observed above 100K, suggesting the involvement of non-radiative mechanisms.

The linewidth of the PL peak measured as a function of temperature is also an interesting feature of these spectra. Surprisingly, a slight decrease is observed with increasing temperature (42meV→38meV). In bulk materials or quantum wells the PL linewidth increases with temperature due to the increasing thermal distribution of the carriers and the continuous nature of the electronic density of states (DOS). In a quantum dot the discrete nature of the DOS should give a temperature independent PL linewidth as long as there is negligible carrier excitation to higher energy states. Hence this decrease in PL linewidth with increasing temperature is difficult to understand. A similar behaviour has been reported by Xu *et al.*[19] and was explained by the preferential loss of carriers from the smallest dots of the probed distribution. Such a mechanism should produce a change in the emission lineshape with increasing temperature as the higher energy (small dot) side of the distribution is lost. This type of behaviour is observed in the spectra of Figure 6.11 and Figure 6.12 where the high energy shoulder of the distribution becomes less intense with increasing temperature suggesting that this is a possible explanation for the decreasing linewidth observed with increasing temperature.

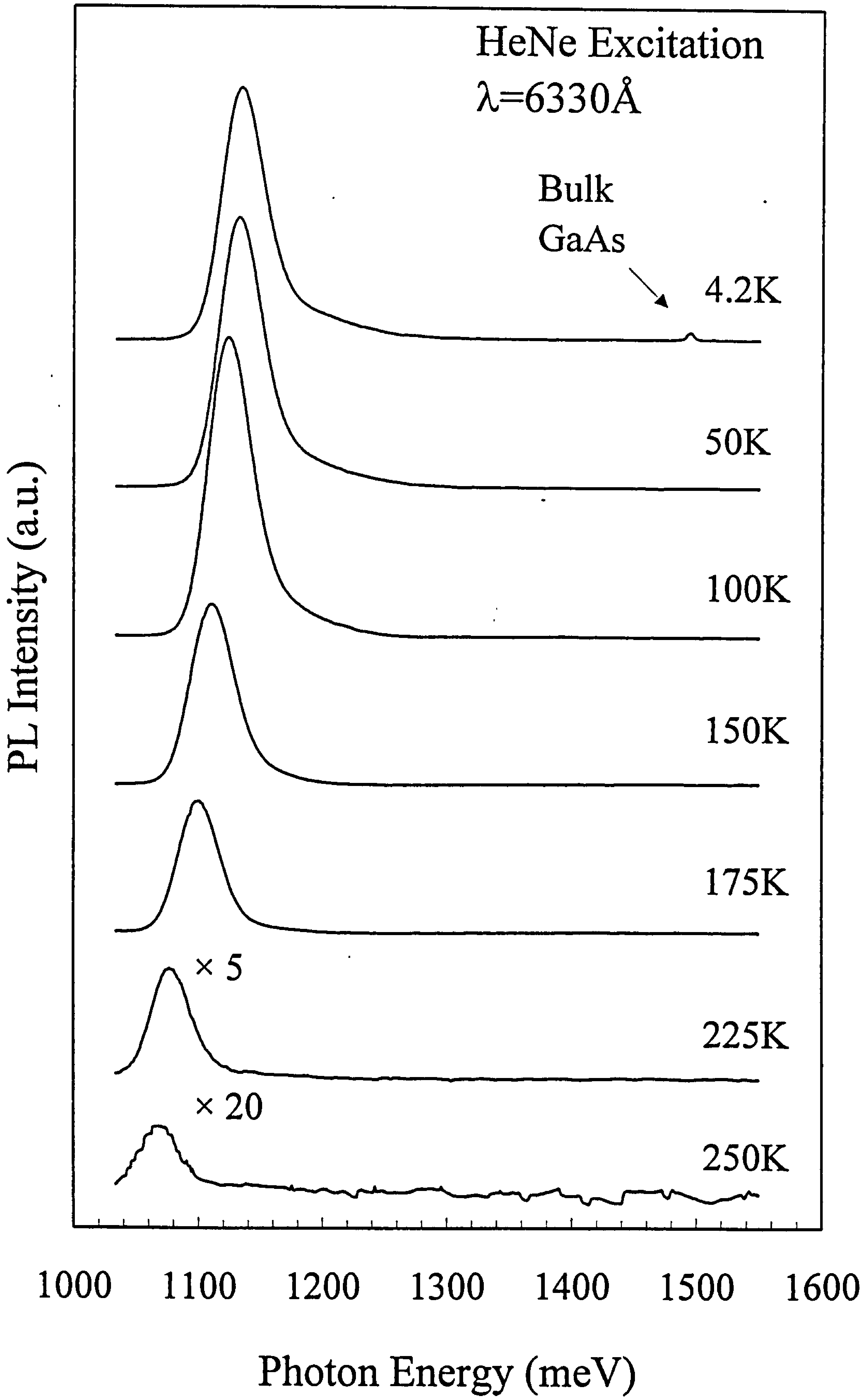

Figure 6.11 Temperature dependent PL spectra of sample M929 excited with the HeNe Laser (λ_{ex}=6328Å).

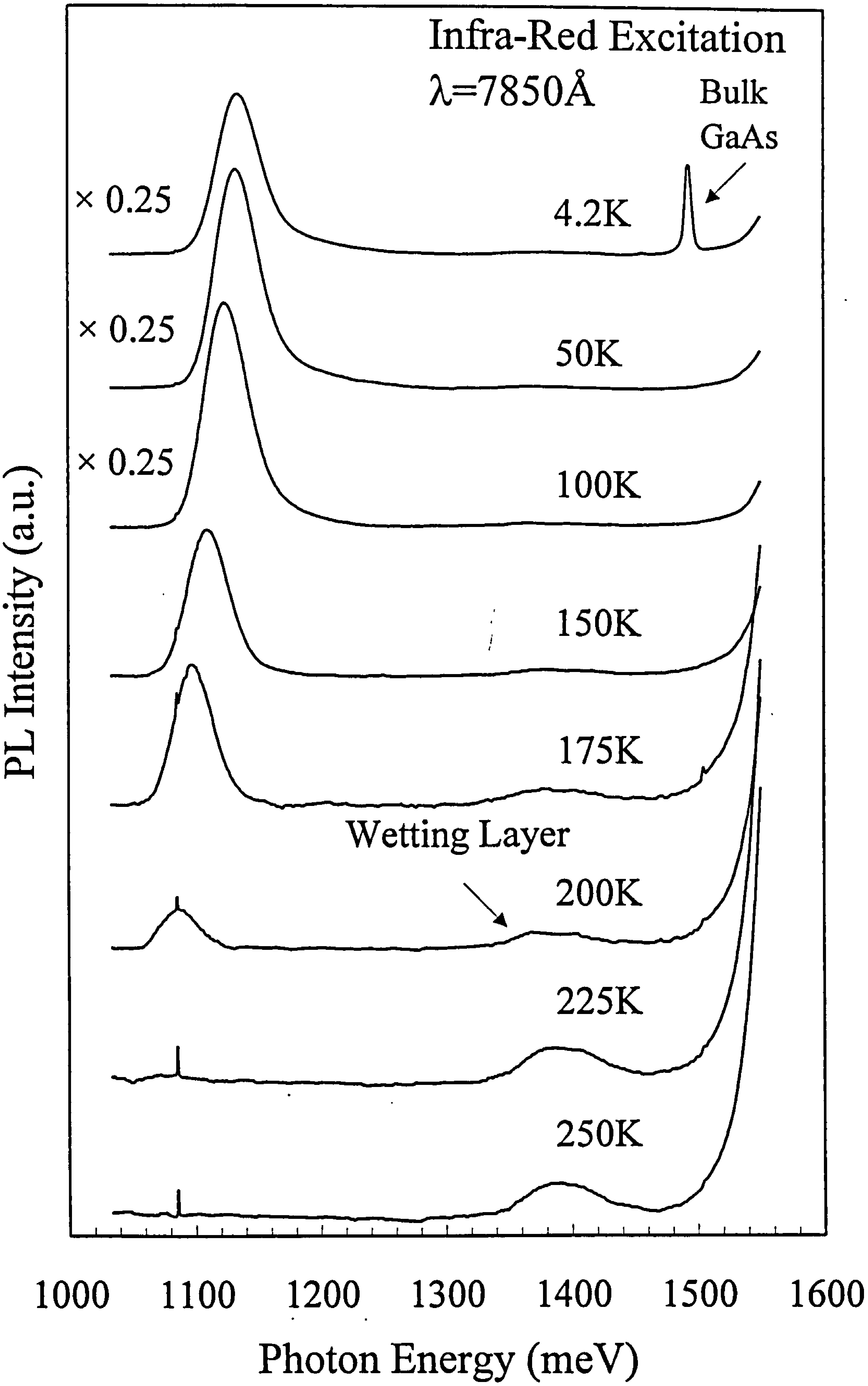

Figure 6.12 Temperature dependent PL spectra of sample M929 excited with the Infra-red diode laser (λ_{ex}=7850Å).

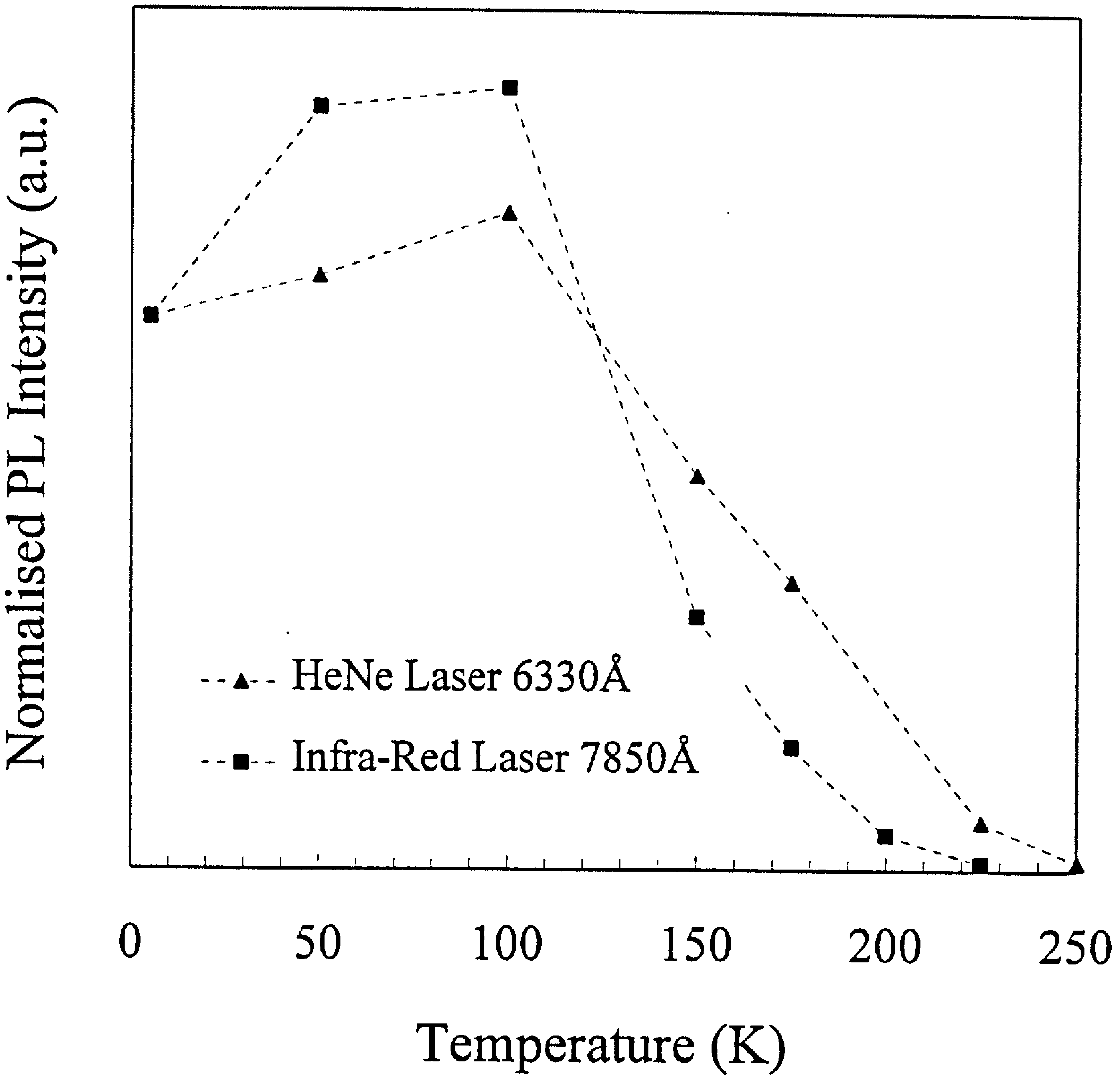

Figure 6.13 PL peak intensity as a function of temperature for both λ_{ex}=6330Å and λ_{ex}=7850Å excitation. The peak intensities are normalised at the intensity obtained for the 4.2K temperature measurement.

6.8 High Laser Power Density μPL Measurements

High incident laser power densities can be achieved using the μPL equipment due to the small, ~2μm, laser spot size obtainable. PL measurements performed using this equipment and various incident power densities are shown in Figure 6.14. Excitation is with the 4400Å line of a HeCd laser. The very short penetration depth of this light (~0.05μm)[20] ensures almost total absorption in the GaAs capping layer (thickness 0.1μm). Because of the high probability of the subsequent capture of the photo-excited carriers by the dots it is possible to achieve very high dot carrier densities. For low power excitation, 45Wcm^{-2}, the ground state luminescence is observed, identical to that seen with low power density HeNe excitation in the standard cryostat. Assuming a carrier relaxation time of 1ns[21] and a dot density of 3×10^{10}cm^{-2}, the dot occupancy for these conditions is ≈2 assuming all the carriers diffuse into the dots and that there is no significant non-radiative recombination. This figure also assumes that there is no significant lateral carrier diffusion away from the illuminated area, an assumption which may not be valid (see below). This result implies that for power densities above 45Wcm^{-2} the ground state which, including spin, can contain two carriers[22] should saturate, hence allowing the population of excited states. Indeed, as the power density is increased, a second peak appears to higher energy, indicating that carrier recombination is occurring from excited dot states. For the highest laser power densities obtainable with the system, 4500Wcm^{-2}, a third peak is observed indicating the population and recombination from a second excited state. The two excited state transitions are separated from the ground state transition by 74meV and 139meV. Similar results for high power density excitation have been observed Grundmann *et al.*[23] and Schmidt *et al.*[24]

These large transition separations imply large dot energy level separations. Large energy level separations are a requirement for device applications as they result in negligible thermal populations in excited states and hence maintain a true 0D behaviour. Energy level spacings ≥3kT are generally required, implying a value ~75meV for room temperature device operation. The present samples would appear to satisfy this condition.

The present results provide no information on the nature of the excited state transitions, i.e. whether they involve excited electron states, excited hole states or a combination of the two. The current theoretical calculations from different groups give conflicting results. Calculations by Marzin[8] indicate two confined electron levels for cone shaped dots. In addition calculations and measurements of self-organised stressor dots,[25] which have cylindrical symmetry, indicate that only transitions between electron and hole levels of the same index ($\Delta n=0$) are allowed. In contrast Grundmann *et al*[6] suggest that for pyramidal shaped dots of a size consistent with the present dots, that there is only one confined electron level, but several confined hole levels. Similar results are predicted by the calculations of Cusack *et al.*[26] If the later more detailed calculations are correct, all the present experimentally observed transitions involve a common, ground electron state. In this case the lack of cylindrical symmetry allows $\Delta n\neq0$ transitions to occur. Obviously the nature of the electronic states and the optical transitions depends critically upon the exact shape of the dots, which is still a subject of great debate and may well be different in samples obtained from nominally identical but different sources. No theoretical modelling has been performed on the present dots although their optical properties are similar to the assumed pyramidal shaped dots of the Berlin-St. Petersberg group[23] and modelled by Grundmann *et al.*[6] We note however that evidence for <u>either</u> a single confined electron or hole level has been observed in recent temperature dependent, high laser power density PL and magneto-PLE measurements conducted on sample M929.[18]

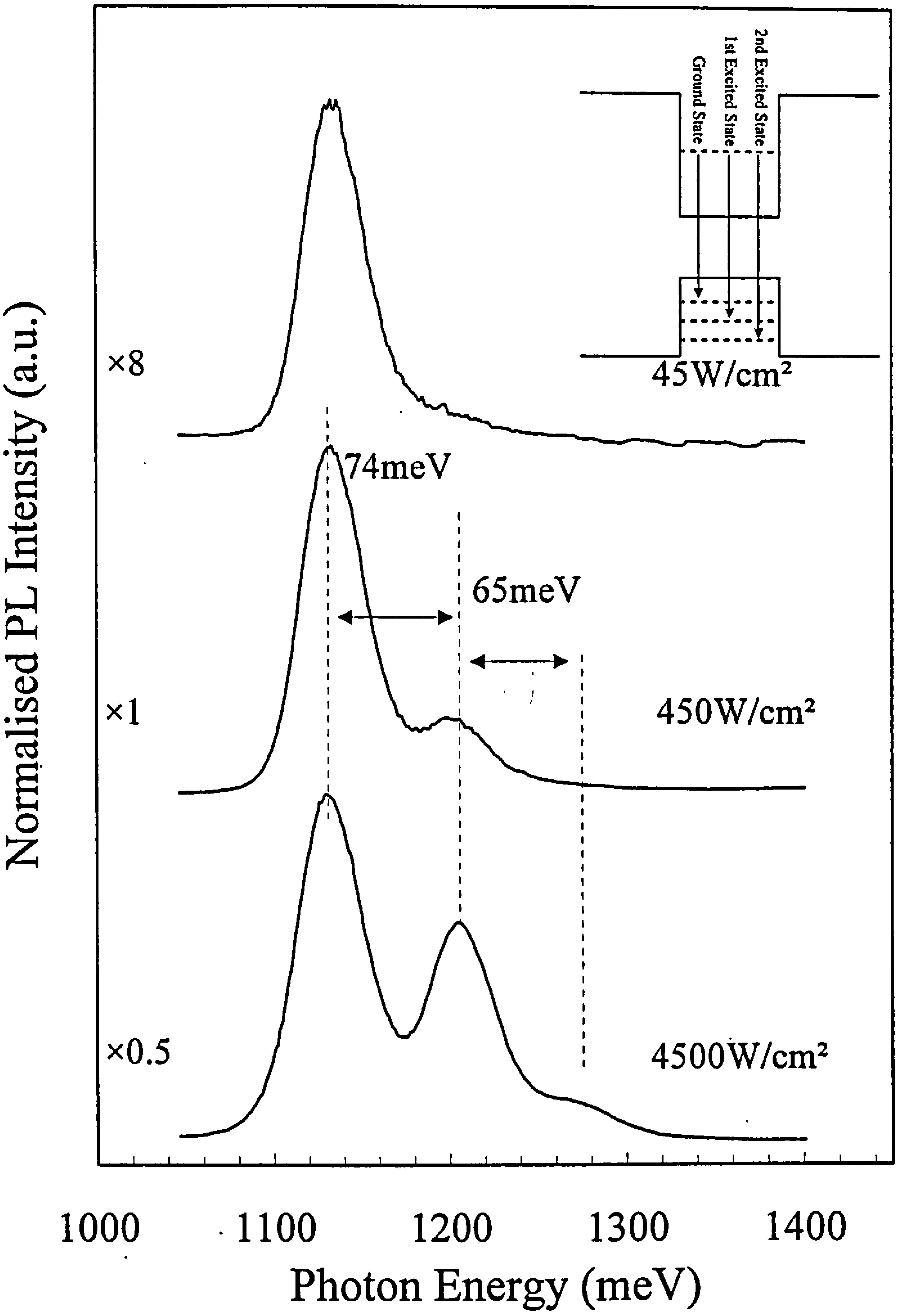

Figure 6.14 High laser power density excitation PL spectra at T=4.2K obtained using the μPL equipment, (spot size ~1μm, λ_{ex}=4400Å). For the highest laser power density two excited states are observed. The average excited state separations are shown. The PL spectra are normalised, the appropriate scaling factors are indicated. The inset figure shows the proposed energy level transitions proposed by Grundmann *et al*[6] with a single confined electron level and three confined hole levels.

6.9 μPL of Etched Mesa Samples - Single Dot Studies

All the PL experiments described so far have involved the study of a large ensemble of dots, even using the μPL equipment with a ≈1-2μm diameter laser spot results in the excitation of »10^2 dots because of significant carrier diffusion away from the illuminated region. Excitation with the μPL system gives rise to the inhomogeneously broadened PL spectra shown in Figure 6.10. Thus the study of individual quantum dots is not possible with the basic μPL system because of the high dot density and the significant lateral carrier diffusion which appears to occur.

To prove that the luminescence arises from an ensemble of many independent dots, the sample area probed needs to be reduced so that it contains of the order of a few hundred dots. This can be achieved by etching a small sub-micron mesa containing ~100 dots. For these experiments mesas with sizes ~0.8μm were patterned onto a small piece of sample M929. Using the μPL equipment, a high intensity Ar^+ laser (4880Å line) was used to excite the mesa, the resultant weak PL being detected using a multichannel charge coupled device (CCD) detector and a high resolution triple grating spectrometer. Unfortunately the sensitivity of the CCD falls off rapidly in the energy range of interest (<1400meV) as the detected photon energies approach the band gap of the Si CCD pixels. Figure 6.15 shows a comparison of the response of the CCD compared to that of the Ge detector when the laser power density is sufficiently high to observe the excited state transitions on an unpatterned region of the sample. Below ≈1300meV the signal intensity recorded with the CCD falls off to such an extent that the 2nd excited state transition appears to be far more intense than the ground state transition. This data shows that a measurable signal can only be obtained for the present sample from the spectral region containing the excited state luminescence (E≥1180meV). The use of the CCD instead of the more uniform response of the Ge photodiode is not ideal but multi-channel detection is required to observe the weak, single dot emission with the necessary high spectral resolution. Use of the Ge detector, a single channel device, requires the spectrometer to scan in very small steps over the spectral region of interest.

This means that very long scan times are needed which requires a very stable laser spot position, making the experiment very difficult.

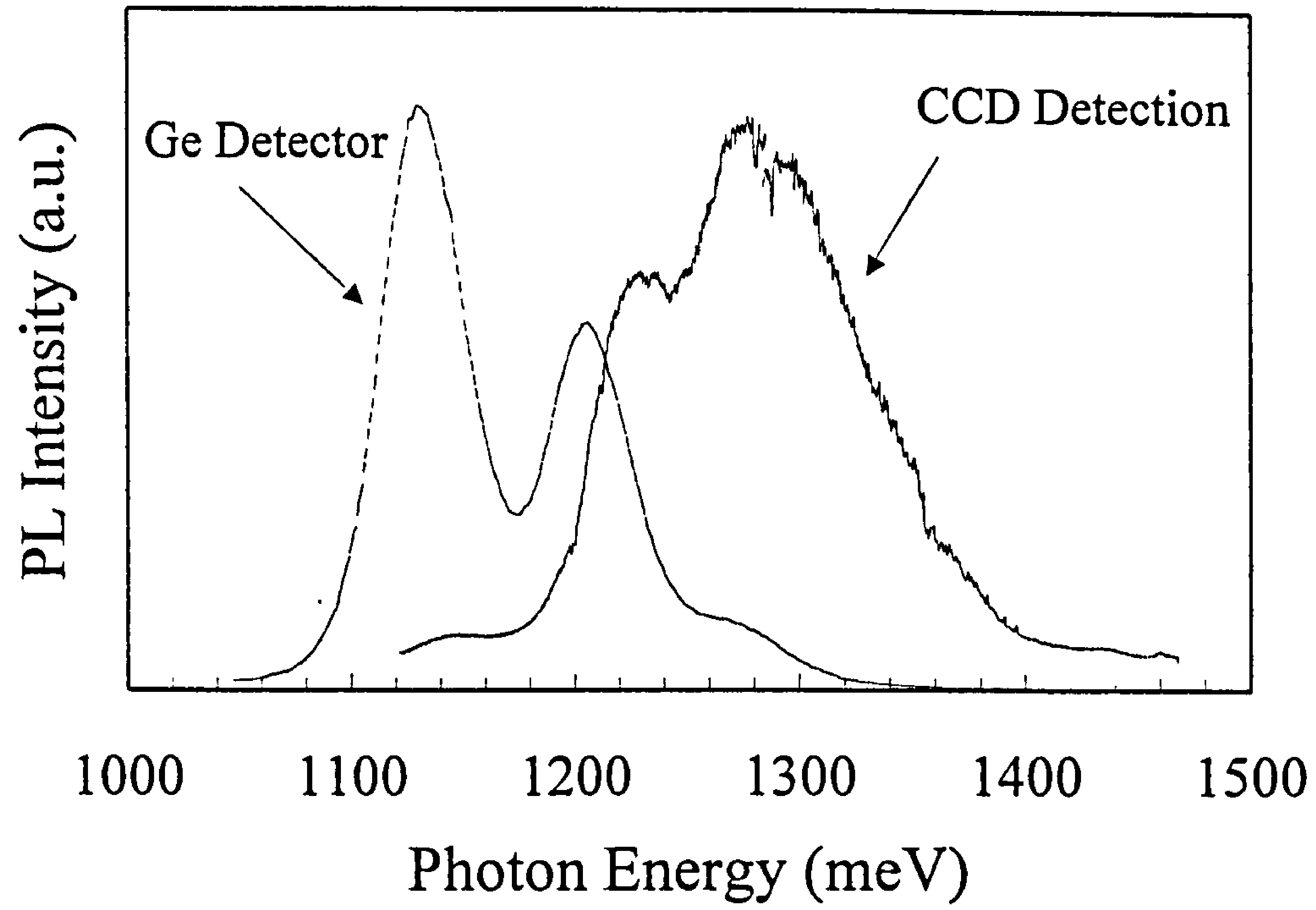

Figure 6.15 The relative spectral responses of the Si CCD and Ge detector. The PL spectra are obtained from sample M929. Note that the intensity of the ground state transition in the spectrum obtained with the CCD is very weak in contrast to the relative intensities observed with the Ge detector.

Quantum dots are predicted to have atomic-like energy levels so it is expected that a series of very sharp luminescence lines will be observed when a small number of dots is probed.[27,28] Figure 6.16 shows a PL spectrum emitted from a small sub-micron mesa using the lower resolution 300 lines/mm grating in the final stage of the spectrometer. The very narrow PL peaks observed from this small number of dots is confirmation that the broad luminescence is indeed composed of emission from an ensemble of independent dots. Also shown for comparison on the figure is the high power PL spectra of an unpatterned region recorded with a Ge detector. This shows that the sharp, single dot PL peaks arise predominantly from excited state transitions. Most of the ground state transitions are not measurable with this setup due to the very low sensitivity of the CCD at those energies. A very high resolution spectra taken using the 1200 line/mm grating and spectrometer slits of 50μm is shown in Figure 6.17. The

FWHM linewidths of the narrowest peaks are less than 0.1meV, very close to the absolute resolution limit of the spectrometer, as defined by the CCD pixel size (~30μeV). By using the Heisenburg uncertainty relationship ΔEΔt~ħ, the linewidth of the peak can be used to determine the minimum lifetime of the carriers in the corresponding electronic states. For peaks having a linewidth of 0.1meV a lower limit on the lifetime is set at ~7ps. The actual lifetime of the carriers is expected to be higher than this due to the fact that the true linewidth of the peaks is likely to be narrower than 0.1meV. Hence this value of ~7ps is in good agreement with the value of ≈30ps determined for the lifetime of the excited state in InAs self-organised quantum dots.[29] In the figure an 0.1meV linewidth Gaussian peak is shown for comparison with one of the measured spectral peaks.

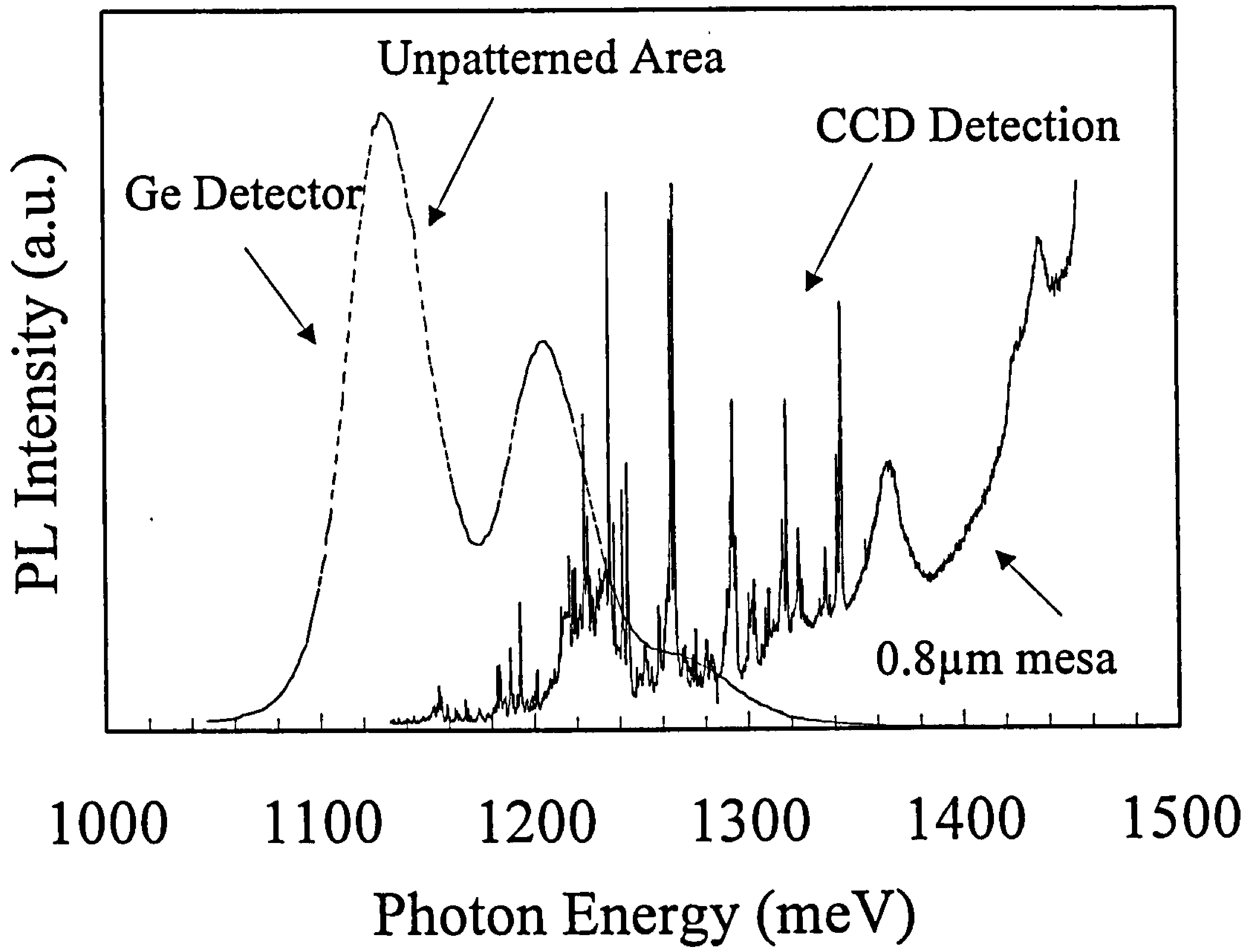

Figure 6.16 PL spectrum at T=4.2K of a 0.8μm mesa containing ~100 dots. The spectrum shows a series of sharp lines attributed to luminescence from individual quantum dots. A high power μPL spectrum of an unpatterned area is also shown which indicates the position of the ground state and excited state transitions.

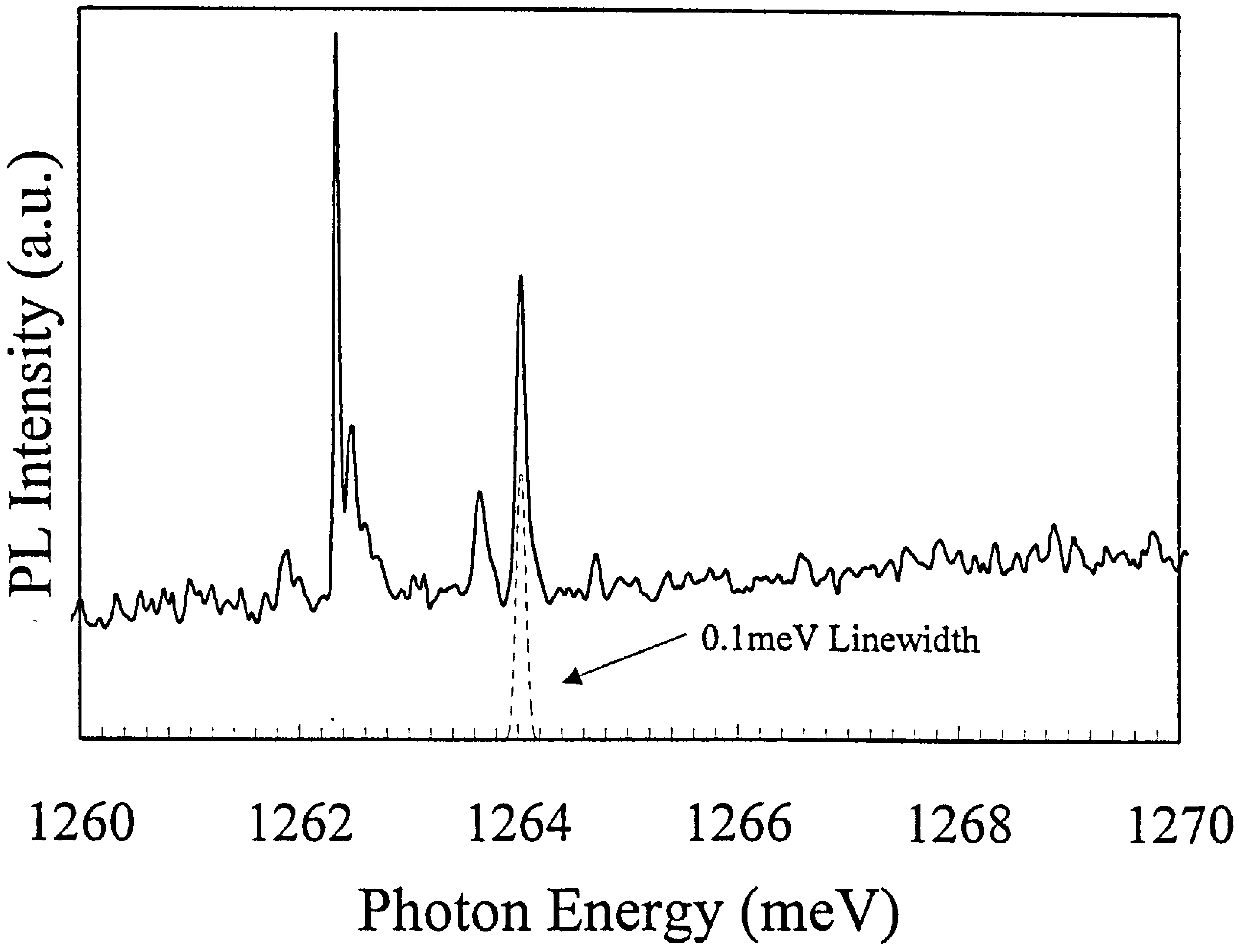

Figure 6.17 High resolution μPL spectrum taken using the 1200 l/mm grating. Note the very narrow linewidths of the features in the spectrum. A Gaussian peak with a linewidth of 0.1meV is also shown to allow a comparison with one of the narrow lines in the spectrum.

Figure 6.18 shows the temperature dependence of a small region of excited state transitions. An increase in temperature reduces the intensity of the luminescence but the narrow linewidth of the peaks is maintained up to 50K, where kT has a value of ~4meV which is over an order of magnitude greater than the linewidth of the peaks. A similar behaviour is observed by Grundmann *et al.*[27] The absence of thermal broadening effects in the spectra provides clear evidence for a system that has a zero dimensional density of states, with δ-function like energy levels (i.e. no dispersion). In such a system there are no nearby energy states which may become populated above T=0, resulting in a broadening of the emission peak. This is in contrast to systems of dimensionality one or greater where the continuous distribution of electronic states results in an increasing emission linewidth with increasing temperature.[14] The next available energy level in the present dots is a higher excited state, over 50meV higher in energy. Significant thermal excitation of carriers into this state therefore does not occur over the present temperature range. The shift in the position of the peaks in Figure 6.18 is attributed to the change in band gap of the material as the temperature is increased.

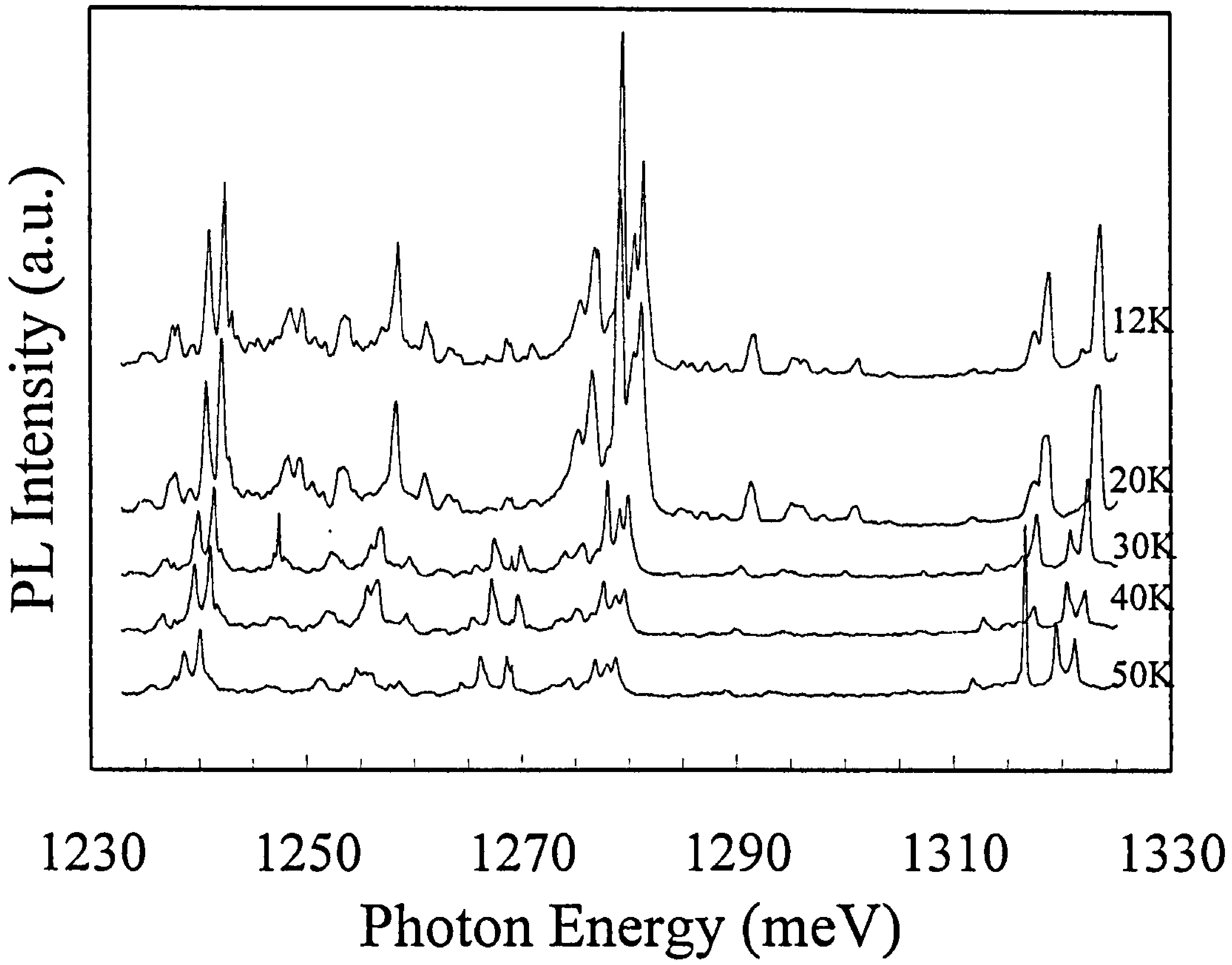

Figure 6.18 Temperature dependence study of a region of the spectrum containing single quantum dot emission.

6.10 Conclusions

The experimental results presented in this chapter have shown that the MBE growth of a thin layer of highly strained InAs on GaAs, results in the formation of self-organised quantum dots. Structural analysis by TEM, in both cross-sectional and plan-view geometries, shows the presence of coherent, dislocation-free quantum dots within the structure. There is also some evidence that ordered arrays of quantum dots have formed on the naturally occurring step-edges on the substrate. Photoluminescence analysis of samples containing quantum dots show the presence of a broad ground state emission. This behaviour is consistent with a large number of independent dots emitting photons with slightly different energies, all of which contribute to the overall observed PL lineshape. μPL studies of a small number of dots, defined by an etched mesa, reveal that this broad emission breaks up into a series of very narrow linewidth peaks, further supporting this model. These very sharp peaks are attributed to emission from individual quantum dots, each having the δ-function, atomic-like energy levels expected in a 0D system. A temperature dependent study of these sharp emission lines indicates that there is no thermal broadening of the transitions, consistent with there being no dispersion in the discrete energy levels. High laser power density μPL measurements reveal that higher energy, excited states are present in the dots. However, it is not clear what the nature of these excited states is, i.e. whether they arise from excited electron or hole levels or both. The energy level separations are of the order of 3kT at 300K, making self-organised quantum dots in this material system very attractive for opto-electronic devices operating at room temperature.

6.11 References

[1] J.M. Moison, F. Houuzay, F. Barthe, L. Leprince, E. André and O. Vatel, Appl. Phys. Lett. **64**, (2), 196, (1994).

[2] B.A. Joyce and C.T. Foxton, Philips Tech. Rev. **43**, (5/6), 143, (1987).

[3] D. Leonard, K. Pond, and P.M. Petroff, Phys. Rev. B **50**, (16), 11687, (1994).

[4] J.M. Gérard in *'Confined Electrons and Photons: New Physics and Applications'*, Ed. C. Weisbuch and E. Burstein, NATO ASI series, Plenum, (1995).

[5] J. Singh, *'Physics of Semiconductors and their Heterostructures'*. McGraw Hill International (1993).

[6] M. Grundmann, O. Stier, D. Bimberg, Phys. Rev. B **52**, (16), 11969, (1995).

[7] A. Wojs, P. Hawrylak, S. Fafard, and L. Jacak. Phys. Rev. B **54**, (8), 5604, (1996).

[8] J.-Y Marzin, G. Bastard, Solid State Comms. **92**, (5), 437, (1994).

[9] S. Ruvinmov, P. Werner, K. Scheerschmidt, U. Gösele, J. Heydenreich, U. Richter, N.N. Ledentsov, M. Grundmann, D. Bimberg, V.M. Ustinov, A. Yu. Egorov, P.S.Kop'ev, Zh. I. Alferov, Phys. Rev. B 51, (20), 14766, (1995).

[10] J.L. Merz and P.M. Petroff, Mat. Sci. and Eng., **B9**, 275, (1991).

[11] M.J. Ekenstedt, H. Yamaguchi, Y. Horikoshi, Appl. Phys. Lett. **67**, (26), 3948, (1995).

[12] C. Weisbuch and B. Vinter, '*Quantum Semiconductor Structures*', p.25, Academic Press Ltd. (1991).

[13] R. Tessier, '*Energy levels and wavefunctions calculations in GaAs/AlGaAs/InGaAs heterostructures*', (program used for energy level calculations), (1995).

[14] G. Bastard in '*Wave Mechanics Applied to Semiconductor Heterostructures*' les éditions de Physique, (1988).

[15] S.S. Dosanjh, P. Dawson, M.R. Fahy, B.A. Joyce, R.A. Stradling, R. Murray, J. Crys. Growth, **127**, (1-4), 579, (1993).

[16] O. Brandt, M. Ilg and K. Ploog, Microelectronics Journal, **26**, 861, (1995).

[17] U. Schmid, N.E. Christensen and M. Cardona, Phys. Rev. Letts. **65**, (20), 2610, (1990).

[18] L.R. Wilson, D.J. Mowbray, M.S. Skolnick, L. Harris, M. Morifuji, I.A. Larkin, M.J. Steer and M. Hopkinson, *To be published* J. Physica E. (1997).

[19] Z.Y. Xu, Z.D. Lu, X.P. Yang, Z.L. Yuan, B.Z. Zheng, J.Z. Xu, W.K. Ge, Y. Wang, J. Wang and L.L. Chang, Phys. Rev. B **54**, (16), 11528, (1996).

[20] D.E. Aspnes and A.A. Studna Phys. Rev. B., (27), 985, (1983).

[21] G. Wang, S. Fafard, D. Leonard, J.E. Bowers, J.L. Merz and P.M. Peteroff, Appl. Phys. Lett. **64**, (21), 2815, (1994).

[22] A. Wois and P. Hawrylak, Phys. Rev. B **51**, 10880, (1995).

[23] M. Grundmann, N.N. Ledentsov, O. Stier, D. Bimberg, V.M. Ustinov, P.S.Kop'ev, Zh. I. Alferov, Appl. Phys. Lett. **68**, (7), 979,(1996).

[24] K.H. Schmidt, G. Medeiros-Ribeiro, M. Ostreich, P.M. Petroff and G.H. Döhler, Phys. Rev. B **54**, (16), 11364, (1996).

[25] J. Tulkki and A. Heinämäki, Phys. Rev. B **52**, 8239, (1995).

[26] M.A. Cusack, P.R. Briddon and M. Jaros. Phys. Rev. B **54**, (4), R2300, (1996).

[27] M. Grundmann, J. Christen, N.N. Ledentsov, J. Böhrer, D. Bimberg, S. Ruvinmov, P. Werner, U. Richter, U. Gösele, J. Heydenreich, V.M. Ustinov, A. Yu. Egorov, A.E. Zhukov, P.S. Kop'ev and Zh. I. Alferov, Phys. Rev. Letts. **74**, (20), 4043, (1995).

[28] J.-Y. Marzin, J.-M Gérard, A. Izraël, D. Barrier, G. Bastard, Phys. Rev. Letts. **73**, (5), 716, (1994).

[29] R. Heitz, M. Veit, N.N. Ledensov, A. Hoffmann, D. Bimberg, V.M. Ustinov, P.S. Kop'ev and Zh. I. Alferov. Submitted to Phys. Rev. B.

[11] M.J. Ekenstedt, H. Yamaguchi, Y. Horikoshi, Appl. Phys. Lett. **67**, (26), 3948, (1995).

[12] C. Weisbuch and B. Vinter, '*Quantum Semiconductor Structures*', p.25, Academic Press Ltd. (1991).

[13] R. Tessier, '*Energy levels and wavefunctions calculations in GaAs/AlGaAs/InGaAs heterostructures*', (program used for energy level calculations), (1995).

[14] G. Bastard in '*Wave Mechanics Applied to Semiconductor Heterostructures*' les éditions de Physique, (1988).

[15] S.S. Dosanjh, P. Dawson, M.R. Fahy, B.A. Joyce, R.A. Stradling, R. Murray, J. Crys. Growth, **127**, (1-4), 579, (1993).

[16] O. Brandt, M. Ilg and K. Ploog, Microelectronics Journal, **26**, 861, (1995).

[17] U. Schmid, N.E. Christensen and M. Cardona, Phys. Rev. Letts. **65**, (20), 2610, (1990).

[18] L.R. Wilson, D.J. Mowbray, M.S. Skolnick, L. Harris, M. Morifuji, I.A. Larkin, M.J. Steer and M. Hopkinson, *To be published* J. Physica E. (1997).

[19] Z.Y. Xu, Z.D. Lu, X.P. Yang, Z.L. Yuan, B.Z. Zheng, J.Z. Xu, W.K. Ge, Y. Wang, J. Wang and L.L. Chang, Phys. Rev. B **54**, (16), 11528, (1996).

[20] D.E. Aspnes and A.A. Studna Phys. Rev. B., **(27)**, 985, (1983).

[21] G. Wang, S. Fafard, D. Leonard, J.E. Bowers, J.L. Merz and P.M. Peteroff, Appl. Phys. Lett. **64**, (21), 2815, (1994).

[22] A. Wois and P. Hawrylak, Phys. Rev. B **51**, 10880, (1995).

[23] M. Grundmann, N.N. Ledentsov, O. Stier, D. Bimberg, V.M. Ustinov, P.S.Kop'ev, Zh. I. Alferov, Appl. Phys. Lett. **68**, (7), 979,(1996).

[24] K.H. Schmidt, G. Medeiros-Ribeiro, M. Ostreich, P.M. Petroff and G.H. Döhler, Phys. Rev. B **54**, (16), 11364, (1996).

[25] J. Tulkki and A. Heinämäki, Phys. Rev. B **52**, 8239, (1995).

[26] M.A. Cusack, P.R. Briddon and M. Jaros. Phys. Rev. B **54**, (4), R2300, (1996).

[27] M. Grundmann, J. Christen, N.N. Ledentsov, J. Böhrer, D. Bimberg, S. Ruvinmov, P. Werner, U. Richter, U. Gösele, J. Heydenreich, V.M. Ustinov, A. Yu. Egorov, A.E. Zhukov, P.S. Kop'ev and Zh. I. Alferov, Phys. Rev. Letts. **74**, (20), 4043, (1995).

[28] J.-Y. Marzin, J.-M Gérard, A. Izraël, D. Barrier, G. Bastard, Phys. Rev. Letts. **73**, (5), 716, (1994).

Chapter 7

Optical Studies of Self-Organised Quantum Dots

7.1 Introduction

The detailed optical and structural characterisations described in chapter 6 provide conclusive evidence that coherent, self-organised InAs quantum dots have formed in a GaAs matrix. Photoluminescence (PL) studies of a small number of dots demonstrate a zero dimensionality density of states, with δ-function like energy levels. PL measurements performed under high laser excitation power densities show that higher energy excited states exist within the dots. However the nature of these states (i.e. whether they are excited electron, excited hole or both) is unclear.

In the present chapter a more detailed optical spectroscopic study of the quantum dots is described. As discussed in Chapter 1, it has been proposed that the properties of quantum dots could be affected by the so-called 'phonon bottleneck',[1] where the efficient relaxation of carriers by the emission of a cascade of single LO phonons is inhibited by the discrete nature of the energy levels. Such a bottleneck could prove highly deleterious/catastrophic? for the operation of devices containing quantum dots, where rapid relaxation of optically or electrically injected carriers to the luminescing states is generally desirable. However, it has been suggested that other carrier relaxation mechanisms may operate in quantum dots, for example multi-phonon[2], Auger[3] etc. As described in Chapter 3 the experimental technique of photoluminescence excitation (PLE) involves both the absorption of photons and the subsequent relaxation of the photoexcited carriers. It hence appears an ideal technique for the study of energy levels and carrier relaxation mechanisms in quantum dots. In systems with a continuum of energy states (e.g. bulk semiconductors, quantum wells and wires) the form of the PLE spectra is found to be dominated by the absorption part of the process.[4] In the present 0D case, however, the PLE spectra appear to be controlled by the second step, the relaxation of carriers. Hence little direct information on excited states is obtained.

However the PLE and PL spectra do suggest that carrier relaxation is efficient in the dots and provide evidence for two distinct carrier relaxation mechanisms - a non-resonant mechanism from upper excited states and a resonant mechanism, involving the emission of multiple LO phonons, from the first excited state.

7.2 Photoluminescence Excitation Spectroscopy

7.2.1 Experimental Details

The experimental set-up for this investigation was initially the lamp and monochromator arrangement described in Chapter 3. The excitation source used was a 150-W tungsten-halogen lamp which could be tuned continuously over a wide range of wavelengths, through the visible spectrum and into the infra-red, after dispersion by a single stage 0.22m monochromator (600 l/mm grating blazed at 1μm). For these experiments 2mm slits on the monochromator were required to obtain a reasonable signal. This resulted in a fairly broad 80Å spectral linewidth excitation source.

The InAs quantum dot samples under investigation showed luminescence at around 1μm, well within the range of the lamp and monochromator combination. The samples were placed in a continuous flow cryostat and cooled to 4.2K. Light from the monochromator was collimated and focused down to a spot size of ~3mm, (excitation area ~0.1cm^2) on the sample, exciting a large number (~3×10^9) of dots. Photoluminescence from the sample was dispersed using a 0.75m single grating spectrometer and detected using a liquid nitrogen cooled Ge p-i-n photodiode. To maximise the signal the spectral resolution of the detection set-up was set at 60Å, the lowest resolution possible for the 0.75m spectrometer and comparable to the band width of the excitation light used. To minimise the amount of elastically scattered incident light entering the detection spectrometer, the sample was placed with its surface normal approximately parallel to the direction of the incident light. In this geometry the recorded PL is emitted almost perpendicular to the surface normal and hence direct reflections of incident light from the surface are directed away from the spectrometer. This geometry allowed the emitted PL to be detected as close as possible to the excitation energy, and also reduced the effects of stray light reflections occurring within the detection spectrometer from the relatively bright excitation source.

7.2.2 Experimental Results

PL from sample M929, when excited by monochromatic light above the GaAs band gap with either the HeNe or HeCd laser, showed a broad (FWHM=35meV) ground state luminescence at around 10950Å≡1132meV. Under high incident laser power densities, the micro-PL measurements showed evidence for the existence of higher energy excited states within the dots. The aim of the present experiments was to probe these excited states, exciting directly into them by tuning the energy of the excitation source over the region of the excited states and measuring the PL from lower excited states or the ground state of the dots. For the confined excited states of the dots, the energy of this excitation is lower than the bandgaps of the GaAs barriers and the InAs 2D wetting layer, so absorption of the incident photons can only occur into the dots, assuming there is only minimal absorption into deep level traps in the GaAs.[5] The excitation energy was scanned from well above the GaAs bandgap down to the detection energy, which was set to several positions over the range of ground state energies as indicated by low power PL for excitation below the GaAs barrier band gap.

The results of these measurements are shown in Figure 7.1. Also shown on this figure is a PL spectrum for the sample, obtained by exciting close to the GaAs band edge at an energy of 1526meV, a value that is close to the maximum absorption in the PLE. This serves to indicate the positions of the detection energies for the PLE spectra. Also visible in this PL spectrum is a high energy feature at 1487meV, probably GaAs related, which is not normally observed with laser excitation high above the GaAs bandgap. The general absence of features related to the bulk GaAs band gap for high energy excitation PL spectra indicates that there is rapid diffusion and efficient capture by the dots of carriers initially created in the GaAs.[6,7] However, in the PL spectrum shown, for excitation at the GaAs band edge, carriers are created with essentially zero kinetic energy, which inhibits their spatial diffusion. Instead the carriers are localised by defect or impurity states in the GaAs and a GaAs related PL signal is observed.

The sharp rise in intensity at low energies in the PLE spectra of Figure 7.1 shows the point at which reflected light from the excitation source is detected. The onset of the detection of this reflected light is ultimately governed by the spectral bandwidth of the excitation light which can be varied by altering the slit width, and hence the resolution, of the excitation spectrometer. However, reasonably large slit widths are required to obtain sufficient signal strength and the bandwidth of the lamp and monochromator combination is always very broad compared with the linewidth obtained from a laser.

The PLE spectra of Figure 7.1 show a number of features, some of which (generally the higher energy ones) remain at a constant absolute energy as the detection energy is varied and some of which (the lower energy ones) remain at a constant energy from the detection energy. This behaviour is clarified in Figure 7.2 where the PLE spectra of Figure 7.1 are plotted against the difference between the incident photon energy and the detection energy.

The higher energy features in Figure 7.1 and Figure 7.2 are associated with absorption into the wetting layer (1300-1400meV) and the bulk GaAs (1520meV) and, as expected, remain at a constant absolute energy. Carriers created by this absorption diffuse spatially and are captured by the dots, with the subsequent radiative recombination detected in the PLE experiment. The fact that both the GaAs and wetting layer produce strong features in PLE spectra for detection at the quantum dot ground state emission, and the general absence of GaAs and wetting layer features in PL spectra, is consistent with the efficient capture of carriers by the quantum dots. Dot capture times of ~30-100ps have been measured using time resolved photoluminescence techniques[6,7] and these times are short in comparison with typical bulk recombination times of ~1ns. This behaviour is advantageous for device applications and can be contrasted with that observed for the quantum wire structures studied in Chapters 4 and 5 where emission from all the different regions of the samples is generally observed. The splitting of the wetting layer absorption into two components probably reflects the splitting of the normally degenerate light and heavy hole valence bands by the combined effects of strain and quantum confinement.

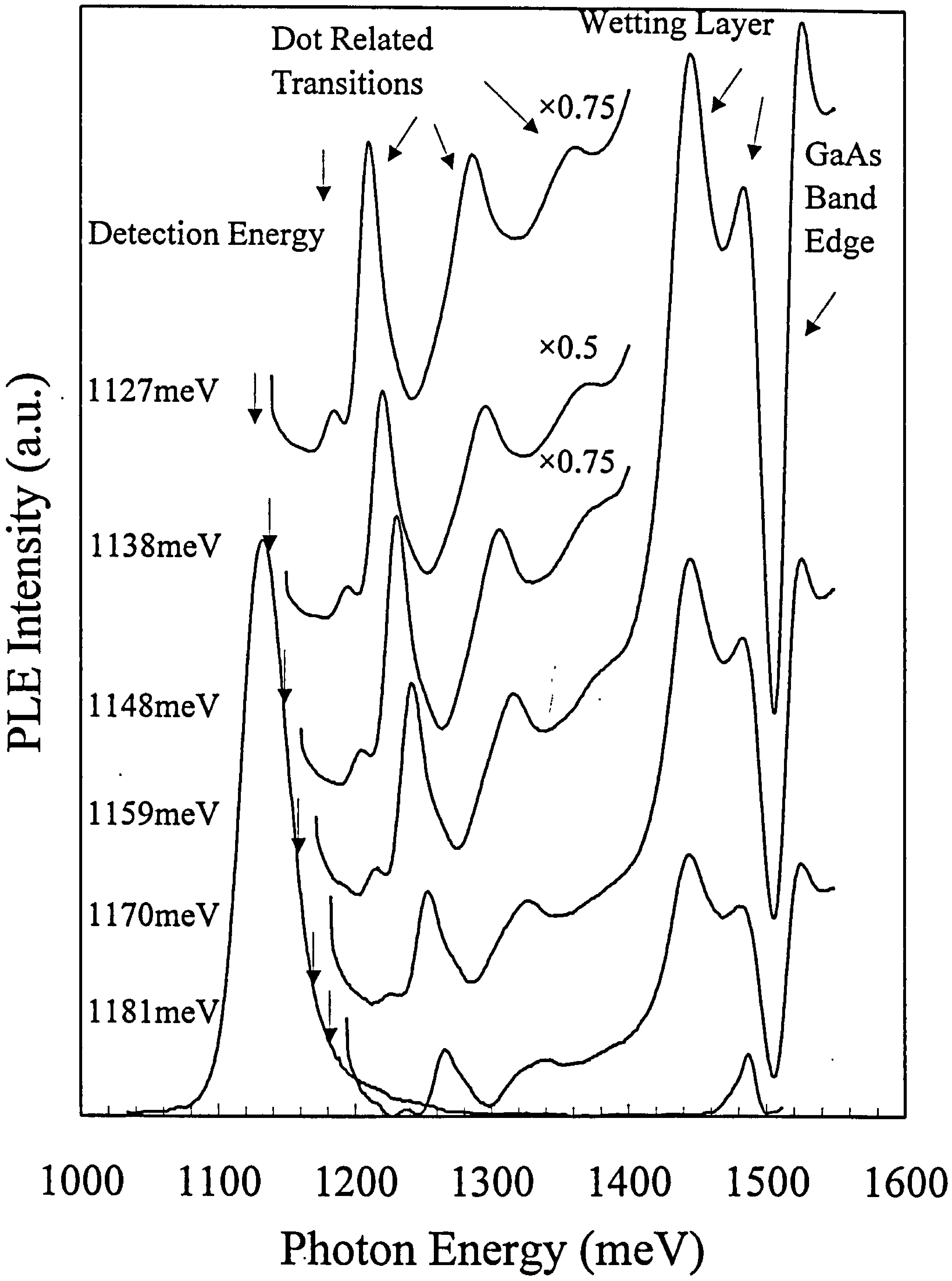

Figure 7.1 PLE spectra at T=4.2K of sample M929 recorded with a lamp and monochromator. The spectra are plotted on an absolute energy scale. The PL spectrum, recorded for excitation close to the GaAs band gap, indicates the position of the detection energies used for the PLE spectra.

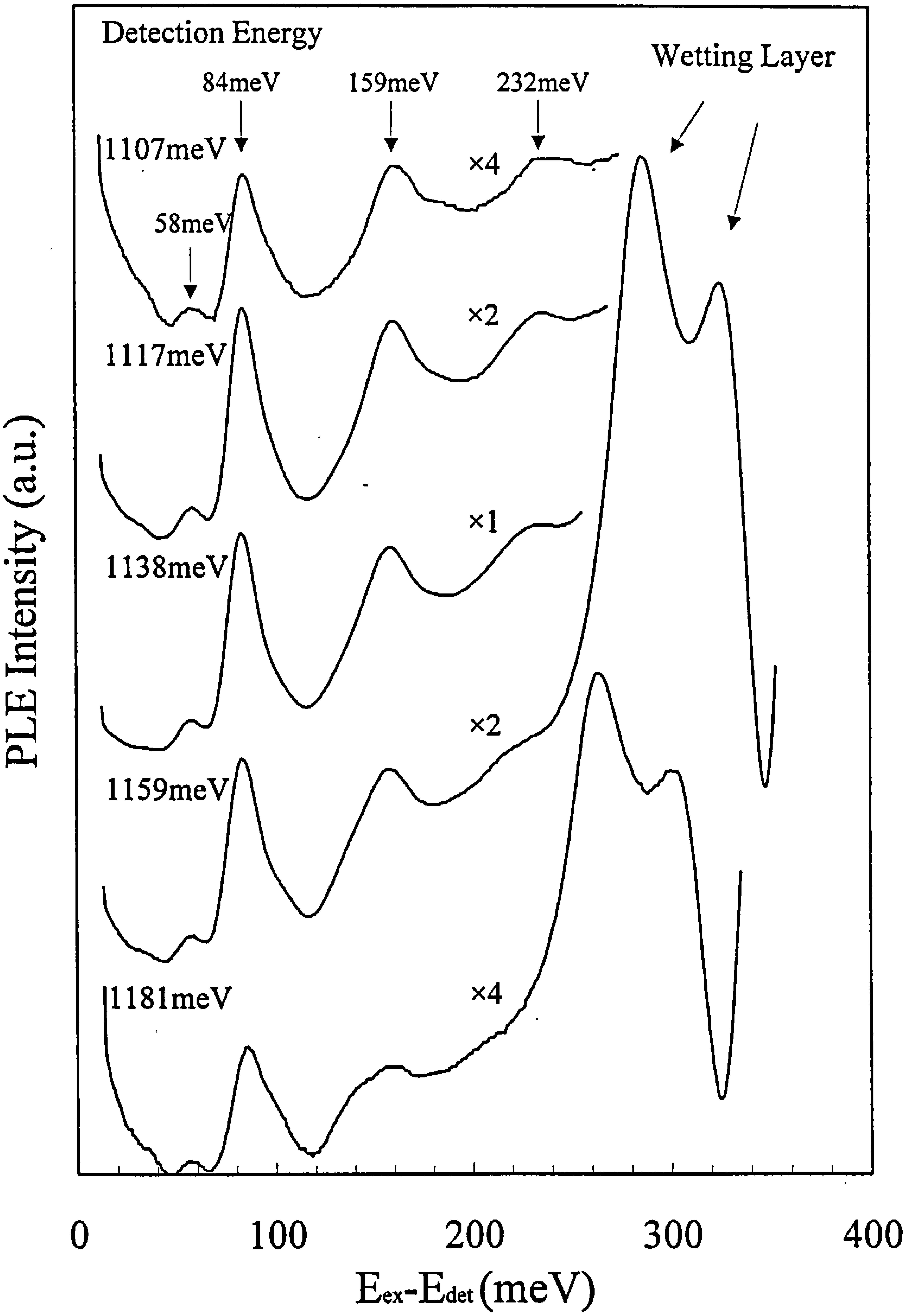

Figure 7.2 PLE spectra at T=4.2K of sample M929 recorded with a lamp and monochromator. The spectra are plotted against the difference between the incident photon energy and the detection energy. There are a number of features in the spectra which appear to remain at a constant energy separation from the detection energy.

The low energy features in the PLE spectra, which are associated with the quantum dots, shift rigidly with detection energy (see Figure 7.2), with peaks occurring at energies of 58, 83, 159 and 232meV from the detection energy. This behaviour suggests that these features do not represent absorption into the excited states of dots as the ground-state-excited-state separations might be expected to change as different size dots are selected by varying the detection energy. Instead this behaviour appears to reflect the second part of the PLE process, the carrier relaxation step, within a subset of the dots probed. This behaviour will be discussed in more detail later.

7.2.3 PLE with the Ti:Sapphire Laser

The PLE measurements were repeated using a tuneable Ar^+ pumped Ti:Sapphire laser as the excitation source instead of the lamp and monochromator. In addition, a double grating spectrometer, with a resolution of 10Å, was used for the detection system. The main advantage of this configuration is that the linewidth of any features in the PLE spectra can be considered to be independent of the excitation linewidth, as the spectral linewidth of the laser is very narrow (<0.5Å). Excitation closer to the detection energy is also possible because of the narrow laser linewidth and greater stray light rejection capability of the double spectrometer. The use of laser excitation results in much higher incident power densities than can be achieved with the lamp and monochromator excitation, although in the present case a cylindrical lens was used to reduce the power density and increase the number of dots probed. An area $\approx 2\times10^{-2}$cm^2 was illuminated which resulted in a typical incident power density of 0.5Wcm^{-2}, corresponding to a dot carrier occupancy of <1. Typically ~10^8 dots were probed with this arrangement. The spectral range of a Ti:Sapphire laser is dependent on the mirror set used. For the present experiments, using the infra-red mirror set allowed excitation in the region of the ground state and lower energy excited states, but the highest energy excitation, 1340eV, fell well short of the wetting layer energy of 1490meV. The output power of the laser was not constant as the wavelength was varied and so a small fraction of the laser light was reflected off into a germanium photodiode and the resultant photovoltage was used to scale the output voltage from the detector by using an electronic ratiometer. This procedure assumes that the intensity of any PLE signal is a linear function of the incident power exciting the sample. PLE spectra were recorded for various detection energies within the ground state luminescence.

Figure 7.3 shows PLE spectra plotted in a similar manner to those of Figure 7.2, with the excitation energy plotted relative to the detection energy. The positions of the detection energies are shown on the inset PL spectrum. The range of excitation energy is limited by the mirror set used in the laser and at high excitation energies the power output from the laser is unstable, giving rise to the noise at high energies visible in the spectra. Direct reflection of the incident laser light into the spectrometer was again minimised by exciting normal to the sample layer and detecting luminescence emitted parallel to the plane of the layer. The spectra show that excitation much closer to the detection energy (7meV) is possible than is achievable with lamp and monochromator excitation (compare with Figure 7.2 where stray light is detected at ≈40meV). The limiting factors now are mainly the stray light rejection capabilities and the resolution of the double grating spectrometer which are controlled by the slit widths.

The PLE spectra show that there is no absorption into the dots when the excitation energy is close (<40meV) to the detection energy. This behaviour is consistent with that expected for a zero dimensional system with discrete atomic-like energy levels. There can only be absorption and emission at these discrete energies, between these energies, unlike the case of higher dimensionality systems which have a continuous distribution of states, no states exist and absorption is not possible. Although absorption is possible into the ground state of the dots, the subsequently re-emitted light will occur at exactly the same energy (zero Stokes' shift) and hence will be obscured by the much stronger elastically scattered laser light. Ground state absorption is hence not observable using the present experimental techniques.

The general form of the PLE spectra shown in Figure 7.3 are identical to those of Figure 7.2 recorded with the lamp and monochromator. Again there are features which appear at a constant energy separation from the detection energy. These are labelled 2LO and

3LO on the figure as they appear to be indicative of a multiple LO phonon relaxation process occurring between energy levels in the dots. This is discussed in more detail below.

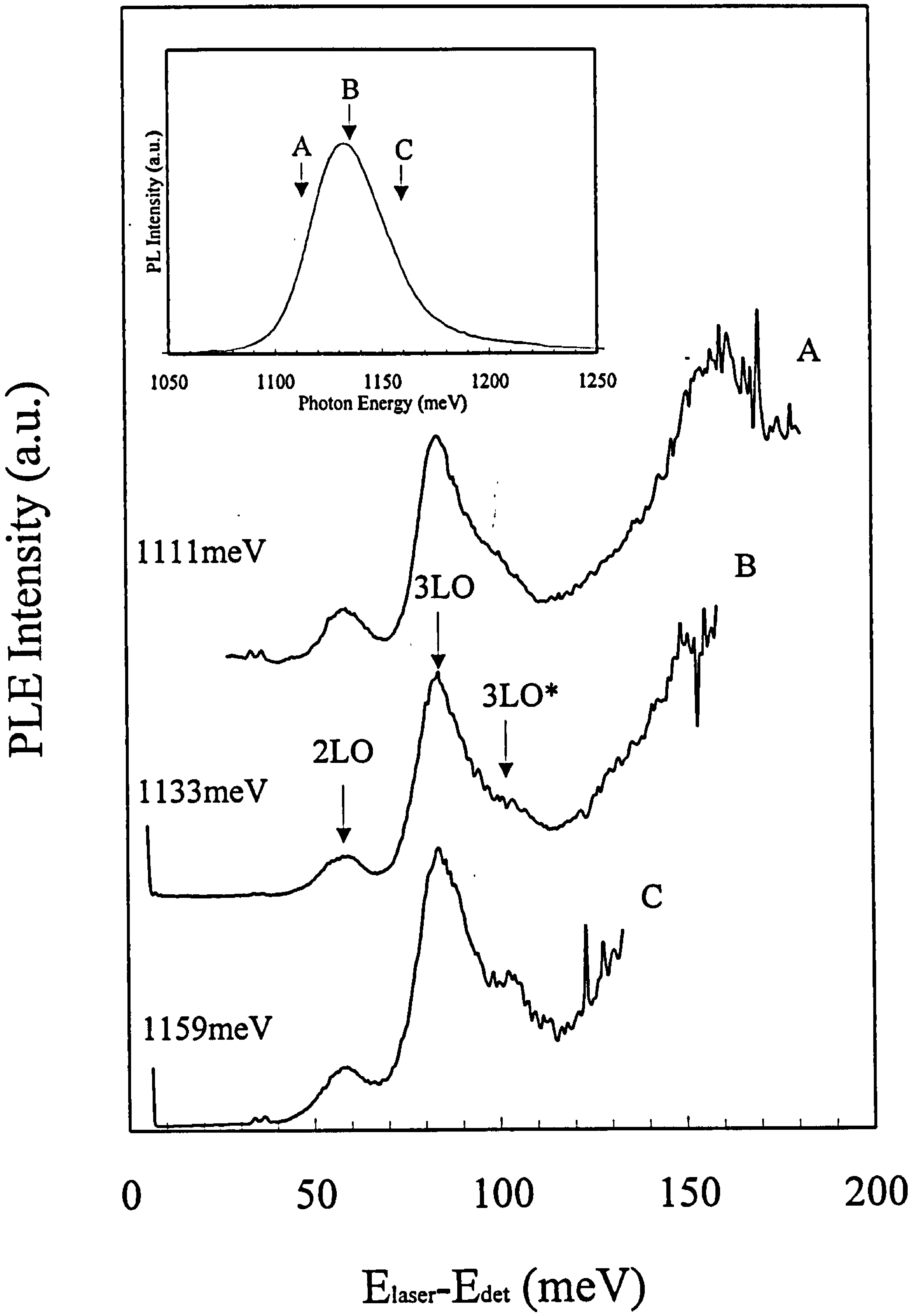

Figure 7.3 PLE spectra at T=4.2K of sample M929 recorded with Ti:Sapphire laser excitation. The spectra are plotted against the difference between the excitation and detection energies. The PL spectrum in the inset shows the position of the detection energies used to record the PLE spectra.

7.3 Selectively Excited Photoluminescence

7.3.1 Experimental Details

The PLE spectra show features that remain at a constant energy separation from the detection energy, regardless of the position of the detection energy on the PL peak. With this in mind, selectively excited photoluminescence is a technique that provides information about carrier relaxation into lower energy excited and ground states when the excitation is tuned to that of the excited states. This measurement is the reverse of the PLE process where the detection energy is fixed at a particular ground state energy while the laser is scanned through the excited states. The present experiment is simply a standard PL measurement but with the excitation energy tuned to lie at different positions within the distribution of excited states. The experimental set-up was the same as that used in the laser PLE measurements, consisting of a Ti:Sapphire laser and a double grating spectrometer. By tuning the laser to the highest possible excitation energy a PL spectrum could be recorded, measuring the detector output whilst scanning the spectrometer from just below the excitation energy to beyond the point at which there is no dot luminescence. A series of PL spectra were recorded for different excitation energies through the distribution of excited states and into the range of ground states, up to the point at which the PL signal disappeared. This occurs when most of the absorption is into the ground state of dots and (as described above) the re-emitted light is undetectable using the present experimental conditions due to the zero Stokes' shift which is expected because of the zero dimensional, atomic-like energy levels that exist within the dots. All the spectra were normalised to the incident laser power to take into account variations in the output power from the laser.

7.3.2 Experimental Results

The results of the selectively excited PL measurements of sample M929 are shown in Figure 7.4 where the PL spectra are plotted on an absolute energy scale. For high energy excitation the PL appears similar to that obtained with the HeNe laser. A typical spectrum recorded for HeNe excitation is also shown in the figure. As will be discussed below, this broad PL reflects the emission from all the dots probed. As the excitation energy is reduced and brought closer to the PL peak, extra structure develops in the PL spectra. These features, similar to the case of PLE, shift with excitation energy. Figure 7.5 shows the PL spectra plotted against the difference between the excitation energy and the emitted photon energy, allowing the constant relative energy behaviour of these new features to be clearly observed.

For high energy excitation the PL spectra are dominated by a broad, strong feature which shifts very slightly with excitation energy. The form of this feature in the selectively excited PL spectra is identical to that obtained for excitation above the GaAs band gap and represents emission from the ground state of all the dots being probed. This broad luminescence in the selectively excited PL is hence referred to as non-resonant ground state, (NRGS) emission. This non-resonant PL shifts slightly when the excitation energy is reduced in the energy range where the resonant features begin to dominate the spectra. The origin of this shift is due to the selective excitation of different size dots and will be discussed in greater detail below.

Unlike PLE, the relative positions of the resonant features in the PL spectra do apparently shift slightly although this shift is small compared to that of the exciting laser energy. This effect is due, in part, to the background luminescence from the non-resonant contribution to the PL which is prominent at excitation energies >1.245eV. The shift is not as pronounced for lower excitation energies when the resonant peaks dominate the spectra. However there is still a slight shift and the mechanism for this behaviour is discussed below.

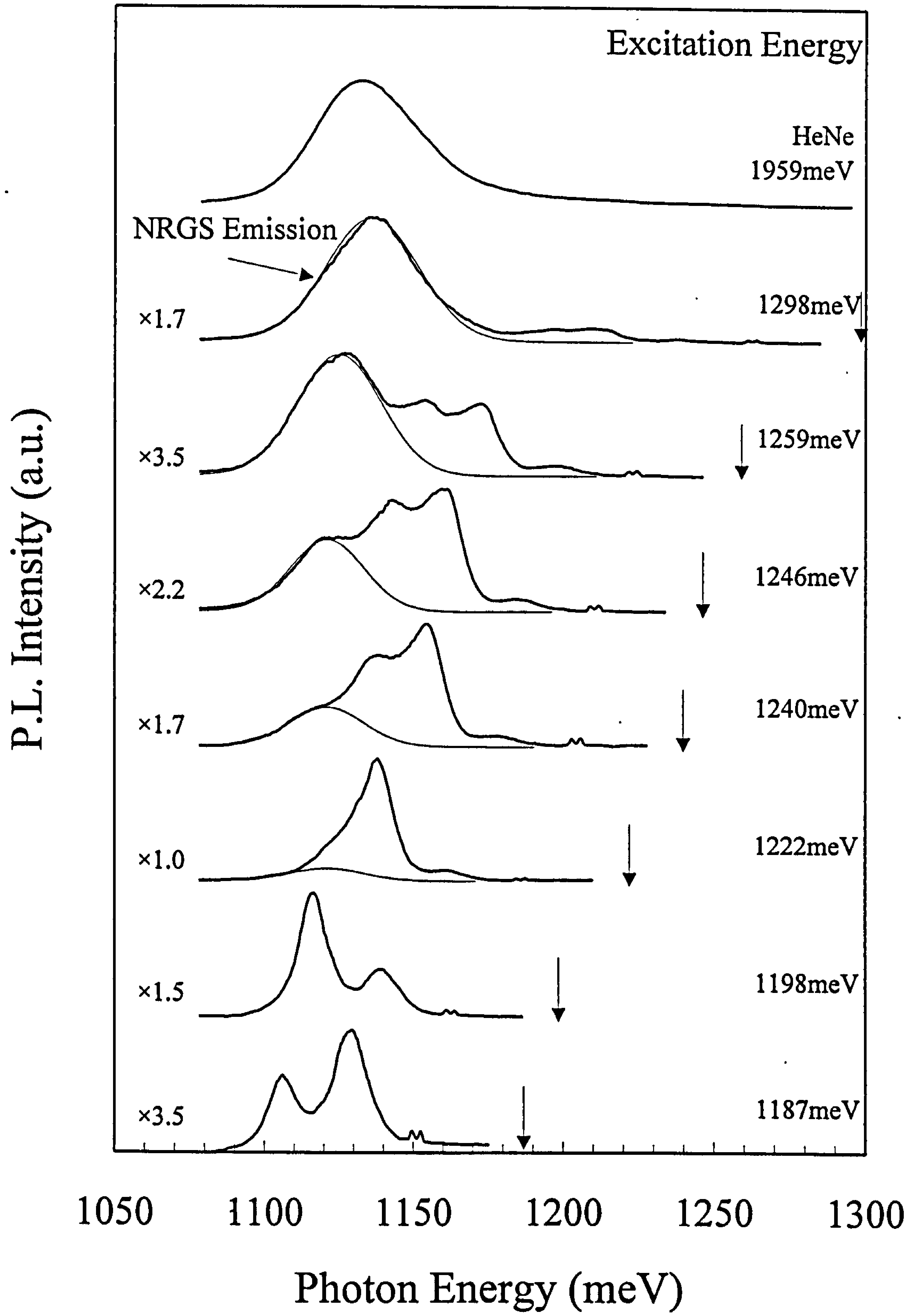

Figure 7.4 Selectively excited PL spectra at T=4.2K of sample M929 obtained with the tuneable Ti:Sapphire laser. The spectra are plotted on an absolute energy scale. A spectra taken with non-selective HeNe excitation is also shown. Peaks are identified in Figure 7.5.

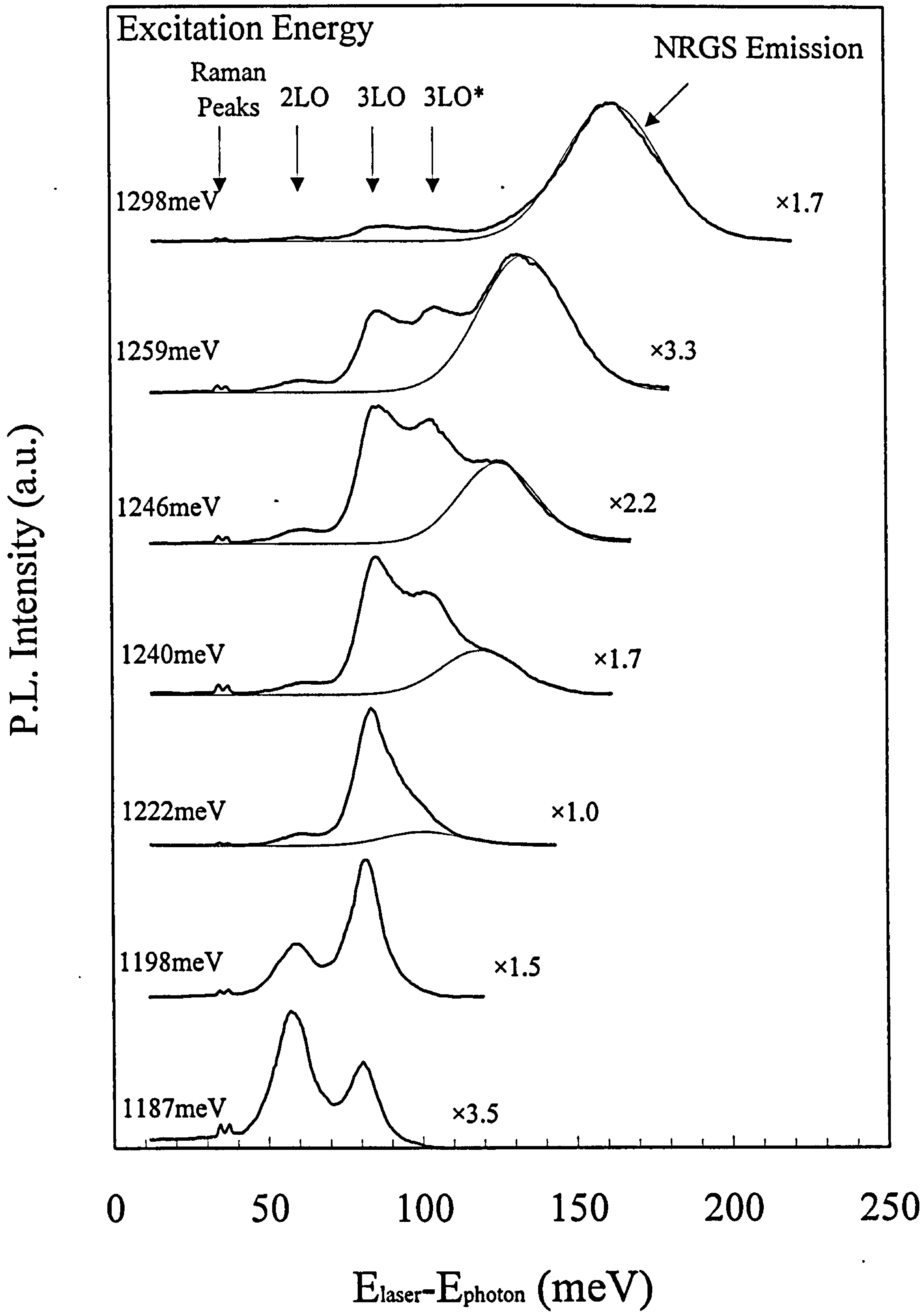

Figure 7.5 Selectively excited PL spectra at T=4.2K of sample M929 obtained with the Ti:Sapphire laser. The spectra are plotted against the difference between the laser excitation energy (which is indicated) and the emitted photon energy. The positions of two resonant features are labelled 2LO and 3LO.

7.4 Discussion of the PLE and Selectively Excited PL Results

The two experimental techniques of PLE and selectively excited PL both show similar results as they are essentially measuring the same effects. However, the slight differences between the two techniques provide information that can be used to partly explain the physical mechanisms behind the observed spectra. Figure 7.6 shows the similarity of the PLE and selectively excited PL spectra, indicating the coincidence of the resonant features that appear in both techniques. The selectively excited PL spectrum is plotted against the difference between the incident laser energy and that of emitted photons ($\Delta E=E_{ex}-E_{photon}$) and is hence reversed compared to those plotted in previous figures. The PLE spectrum is plotted against the difference between the incident photon energy and the detection energy ($\Delta E=E_{photon}-E_{det}$).

The selectively excited PL spectrum is recorded when the position of the laser excitation (E_{ex}=1192meV) is reasonably close to the ground state luminescence (1132meV). For this energy excitation the PL spectrum is dominated by the resonant features labelled 2LO and 3LO. These features are referred to as 'resonant' because of their relatively narrow spectral linewidth (≈10meV) compared to that of the ground state luminescence (≈35meV), which results under non-selectively excited conditions (see below). This implies that the process leading to these features is able to populate only a small fraction of the dot ground states of the total ensemble of dots probed (a resonant process). Similar 2LO and 3LO features are observed in the PLE spectrum. However, because the relative intensities of these features depends upon the excitation energy in PL (see below) they have different relative intensities in the PL and PLE spectra. The PLE spectra also show two additional features at 159 and 232meV from the detection energy. Similar features are not observed in the PL spectra although they could be obscured by the broad, non-resonant PL which is very intense for the excitation energies which would be necessary to observe them.

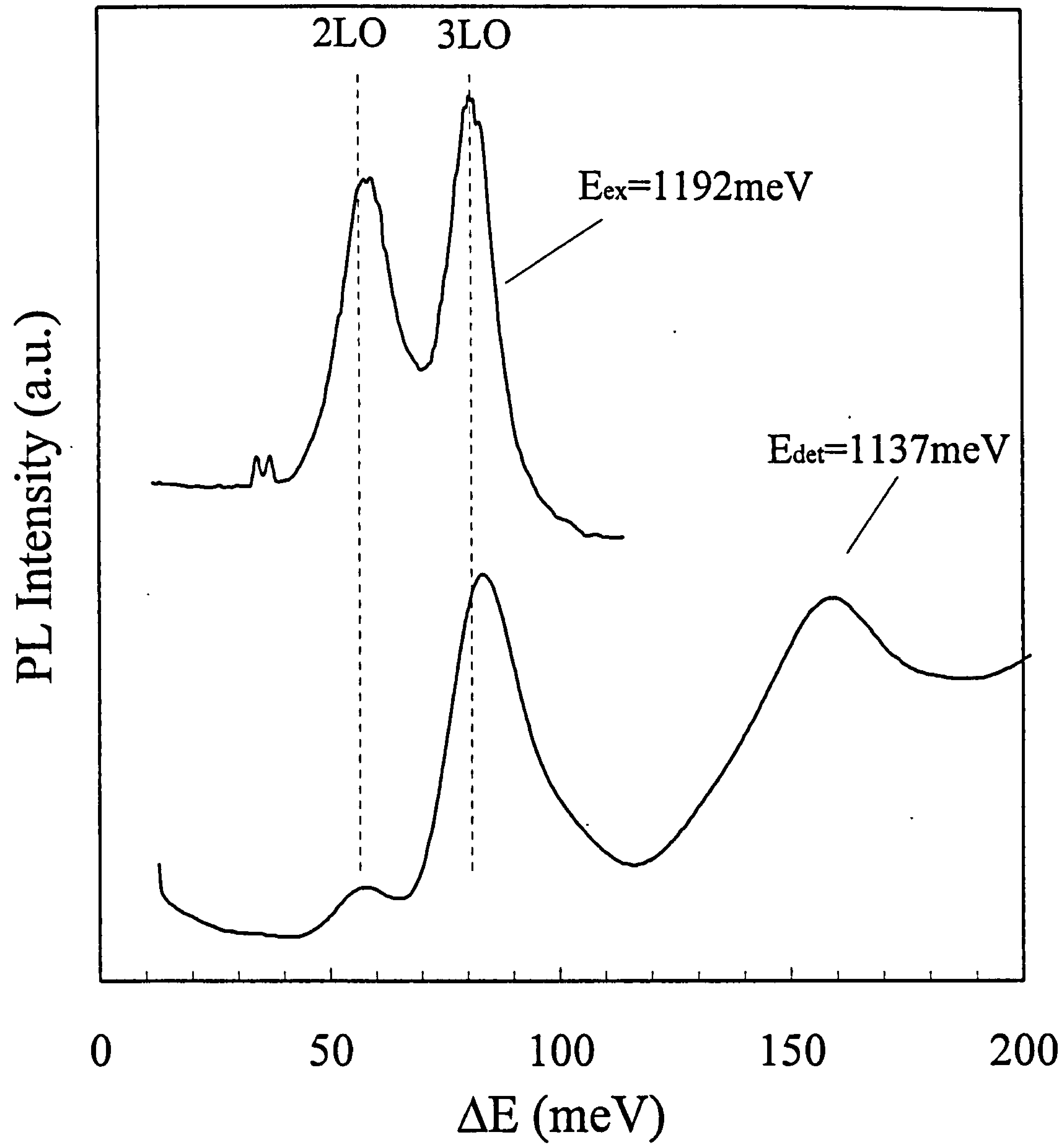

Figure 7.6 PLE (minimate excitation) and selectively excited PL (reversed scale) spectra at T=4.2K of sample M929 showing the coincidence of the resonant features observed using the two techniques. For the PL spectrum $\Delta E=E_{ex}-E_{photon}$ and for the PLE spectrum $\Delta E=E_{photon}-E_{det}$.

To understand the nature of the features in the optical spectra we need to appreciate what is actually occurring in the PLE and selectively excited PL processes. Consider first the selectively excited PL. The experiment results in the injection of carriers into the dots by absorption directly into the excited states. After absorption there are three possible processes that can occur: radiative recombination from the initial excited state, escape of carriers from the dot into deep traps in the GaAs (resulting in no radiative emission) or relaxation to lower energy states followed by radiative recombination.

Only the latter can be detected with the current experimental set-up. Recombination from the initial excited state could occur if relaxation to the ground state is blocked or is slow compared to the radiative recombination rate. However, assuming there is no Stokes' shift between absorption and emission as is expected for a quantum dot, the same energy photon will be emitted as was absorbed and these photons cannot, in this experiment, be distinguished from the more intense incident laser light of the same energy. If carrier relaxation, by some mechanism, is allowed from the initial excited state down to a lower excited state or the ground state, a photon of a different energy to the one absorbed may be emitted, the difference between the absorbed and emitted photon energies simply reflecting the energy difference between these initial and final states. The selectively excited PL measurements are detecting these lower energy re-emitted photons. The detected PL in the spectra hence shows that carrier relaxation from the excited state to the ground state must occur by some mechanism. The PLE process is very similar. Here the emission at a fixed ground state energy is monitored whilst the excitation energy is varied. The observation of a signal implies that absorption is occurring into an excited dot state followed by the relaxation of the carriers to the monitored ground state energy.

The origin of the features observed in the PL and PLE spectra will now be discussed and possible mechanisms which produce them will be suggested. The two peaks closest to the excitation energy in PL and detection energy in PLE (see Figure 7.5 and Figure 7.3) are very sharp, with a linewidth which is not characteristic of the other features seen in the spectra. These features have a constant energy separation from the excitation or detection energy of 33.7 and 36.5 meV and are simply Raman lines that correspond to the zone-centre TO and LO phonon energies of bulk GaAs.[8] They are not associated with the dots, but arise from Raman scattering occurring in the substrate and cladding layers. The intensity of these lines is found to remain approximately constant as the laser excitation energy is varied over the range of the dot electronic levels. This absence of any resonance with the dot electronic states indicates little or no coupling between these states and the GaAs phonons as probed by the Raman scattering.[9]

The main resonant features in the spectra appear at approximately 58, 84 and 102 meV (measured in PLE). Within the experimental accuracy these energies remain constant as the detection energy is varied across the ground state emission peak. If these features represented just absorption into excited dot states then their energy might be expected to vary as different size dots are selected by varying the detection energy. This is shown schematically in Figure 7.7. In fact, comparison with available calculations (see section 7.5 below) indicates that the separation between the ground and first excited state in the dots should vary by 12meV as the detection energy is varied over the range used in Figure 7.3. This variation should be experimentally observable. Hence the constant energy behaviour of the main features observed in the PLE spectra suggests an origin other than just absorption into excited dot states. We now discuss the possibility that these features represent carrier relaxation processes involving the emission of multiple LO phonons.

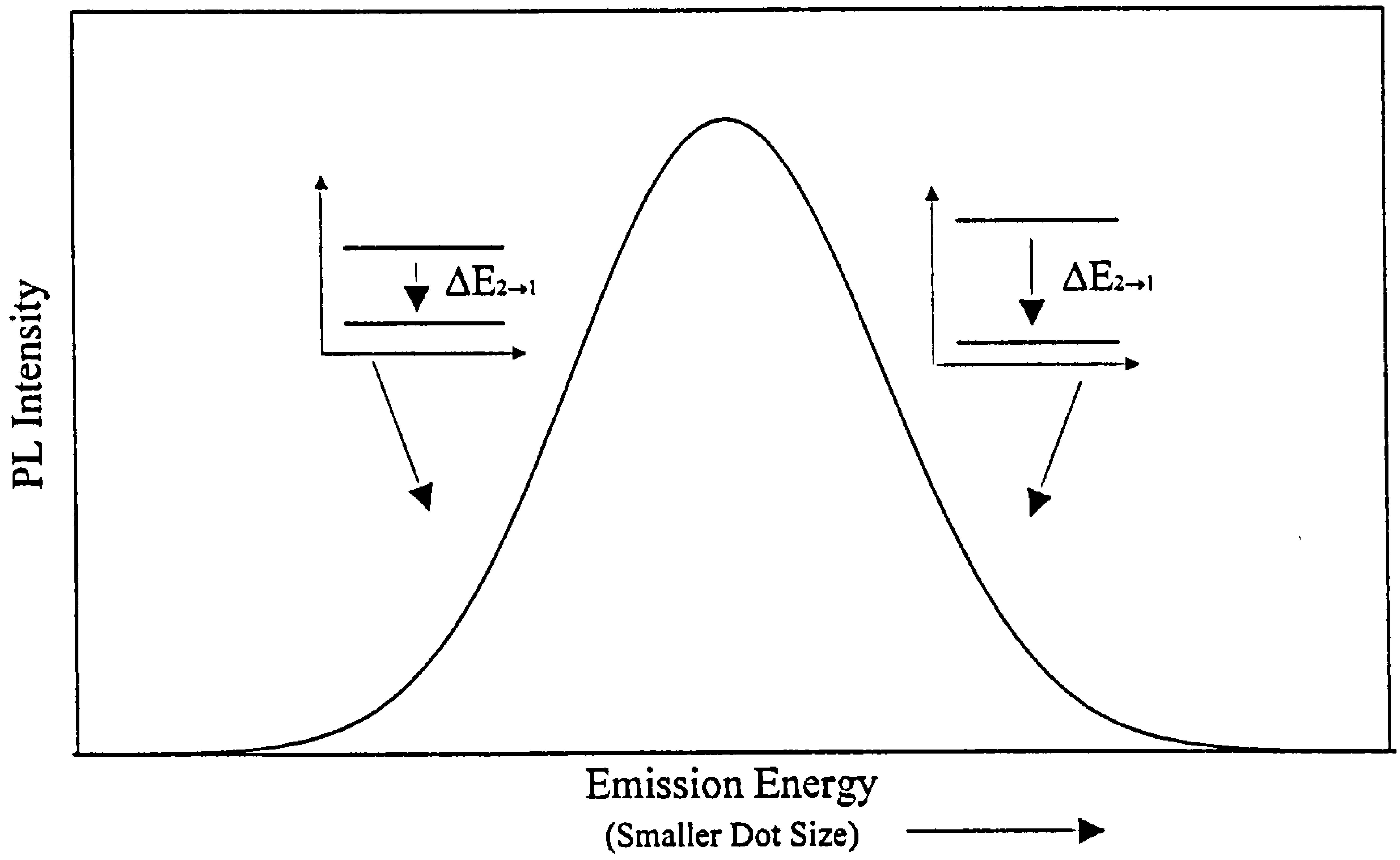

Figure 7.7 Schematic diagram showing the variation of dot energy level separations across an inhomogeneously broadened PL line (a function of the dot size).

The LO phonon energy of bulk, unstrained InAs is 29.9 meV.[10] However, modification of this energy will occur for phonons subjected to the influence of strain and confinement in the complicated dot structure. Calculations show that, for pyramidal shaped dots, the LO phonon energy is increased to 32.1 meV when strain and phonon confinement are taken into account,[10] with the influence of strain having the largest effect on the phonon energy. In the thin two-dimensional wetting layer the influence of phonon confinement competes with strain so smaller phonon energies are expected, a value of 29.6meV for the InAs LO phonon is calculated.[10] These calculations do not take into account the Ga incorporation which may occur in the dots and which will reduce the energy of the InAs LO phonon.[11] In addition, other LO phonons are present in the structure including GaAs (36.4meV)[8] and interface phonons, the energies of which lie between the InAs TO (27.3meV)[8] and GaAs LO phonon energies.[12] Coupling to these phonons by carriers confined within the dots is possible if the electronic wavefunctions have a non-zero value at the edge of the dot or penetrate into the surrounding GaAs. Given these considerations and the likely variables of dot size, shape and composition, it is not unreasonable to expect that a wide range of phonon energies are allowed in this system centred around approximately the unperturbed InAs LO phonon energy of ≈30meV.

As a consequence of their constant relative energies and the approximate coincidence of these energies to those of integer multiples of the LO phonons, the features observed in the PL and PLE spectra have been attributed to carrier relaxation processes involving the emission of multiple LO phonons.[2] In PLE the form of the spectra is hence controlled by the second, carrier relaxation step of the process not just the first absorption step. The multiple LO phonon energies associated with the three peaks observed in PL and PLE are hence labelled 2LO, (2×29) meV for the 58 meV peak, and 3LO, (3×28) or 3LO*,(3×34) meV for the 84 meV and 102 meV peaks respectively. The two and three multiples of ≈28meV suggest coupling to a predominantly InAs phonon either in the dots or wetting layer. The second 3LO phonon (3LO*) at 102(3×34)meV may represent coupling to an interface phonon. The reason for the apparent absence of the second multiple of this higher energy phonon (~68meV) is unclear but it is possibly obscured by the low energy tail of the much more intense

84meV 3LO feature. Unlike the work of Heitz *et al,*[2] fine structure, which was attributed to multiples of different energy phonons, is not observed on the relatively broad peaks observed in the present PL and PLE spectra.

A possible model for the observation of the multiple LO-phonon carrier relaxation features in the optical spectra has been proposed by Heitz *et al.*[2] Unlike quantum wells, where there is only one variable dimension (the well width), it is possible that an ensemble of quantum dots can exhibit independent and non-correlated fluctuations along the three orthogonal spatial directions. Dots having different values for their base dimensions and height may therefore have the same ground state energy but different excited state energies. Hence in a PLE measurement, in which the ground state energy is fixed by the detection energy, there will be a non-zero distribution of excited state energies, the width of this distribution (ΔE) being related to the degree of dot size and shape inhomogeneity. As the excitation energy is scanned, carriers are excited into dots having different excited-state-ground-state separations ($E_{2\rightarrow1}$). If the only efficient carrier relaxation process available involves the emission of multiple LO phonons then carrier relaxation to the ground state will only occur in those dots which satisfy the condition $E_{2\rightarrow1}=n\hbar\omega_{LO}$, where n is an integer. Only in these dots will carriers hence reach the ground state and emit a photon which is detected to give a non-zero PLE signal. Carriers excited into dots for which $E_{2\rightarrow1}\neq n\hbar\omega_{LO}$ are unable to relax rapidly to the ground state and hence do not contribute to the PLE signal. Such carriers must either recombine radiatively from the excited state or are lost to non-radiative centres in the GaAs barriers. The overall effect of this process is that features are observed at constant multiples of the phonon energies from the detection energy in PLE or the excitation energy in PL, as is observed experimentally. This behaviour therefore results from the selection, from the large ensemble of dots probed, of the fraction of dots for which $\Delta E=n\hbar\omega_{LO}$ and hence for which an efficient carrier relaxation mechanism exists.

The diagrams of Figure 7.8 and Figure 7.9 show schematically how this process may occur for both PLE and selectively excited PL. In PLE (Figure 7.8) the main peak represents luminescence from all the possible ground states. Detection is set on the peak of this broad ground state distribution and the small number of dot ground states probed in the measurement is shaded. The smaller peak to higher energy represents the broader distribution of excited states that have this narrow range of ground state energies. In the course of the experiment as the incident laser energy is varied, excitation into all the excited states shown occurs, if there were no restriction on carrier relaxation to the ground state the PLE would (as in quantum wells and quantum wires where efficient carrier relaxation occurs) reflect this entire distribution of excited states. However, as the observed PLE spectra shows, in the majority of quantum dots carrier relaxation cannot occur efficiently. The PLE spectra therefore indicate only those dots where efficient carrier relaxation can occur, in the present case where $E_{2\rightarrow1}=n\hbar\omega_{LO}$. The shaded regions under the excited state peak indicate the fraction of dots that contribute to the observed PLE, these shaded regions lie at multiples of LO phonon energies away from the detection energy. Hence in the present 0D system the PLE is dominated by the carrier relaxation mechanism not, as is usually the case, the absorption process which reflects the electronic DOS. Although it is more usual in higher dimensionality systems for the absorption step of the PLE process to determine the form of the spectra, there are some exceptions. For example, in bulk AlGaInP the large number of non-radiative centres quenches the PL for excitation above the free exciton energy.[13] Similarly, in some superlattices[14] efficient transport of carriers, created with non-zero momentum, occurs to the surface where non-radiative recombination occurs. In both cases the excitonic transitions ‘sit on’ an extremely weak free carrier continuum, in strong contrast to a true absorption spectrum.

Selectively excited PL occurs in much the same way. The schematic diagram of Figure 7.9 shows the total distribution of states that exist in the dots under investigation. The small number of excited states selectively excited by the laser is shown by the shaded area at high energy. The range of ground state energies of dots that have the same excited state energy as the laser is shown. Luminescence from all these dots is manifested by the broad NRGS emission observed in the spectra. The shaded regions under the NRGS emission peak lie at multiple phonon energies from the excitation energy. Luminescence from these dots is enhanced at these energies due to the efficient relaxation mechanism that exists resulting in the resonant peaks in the PL. The resultant PL signal observed experimentally is indicated by the dashed curve.

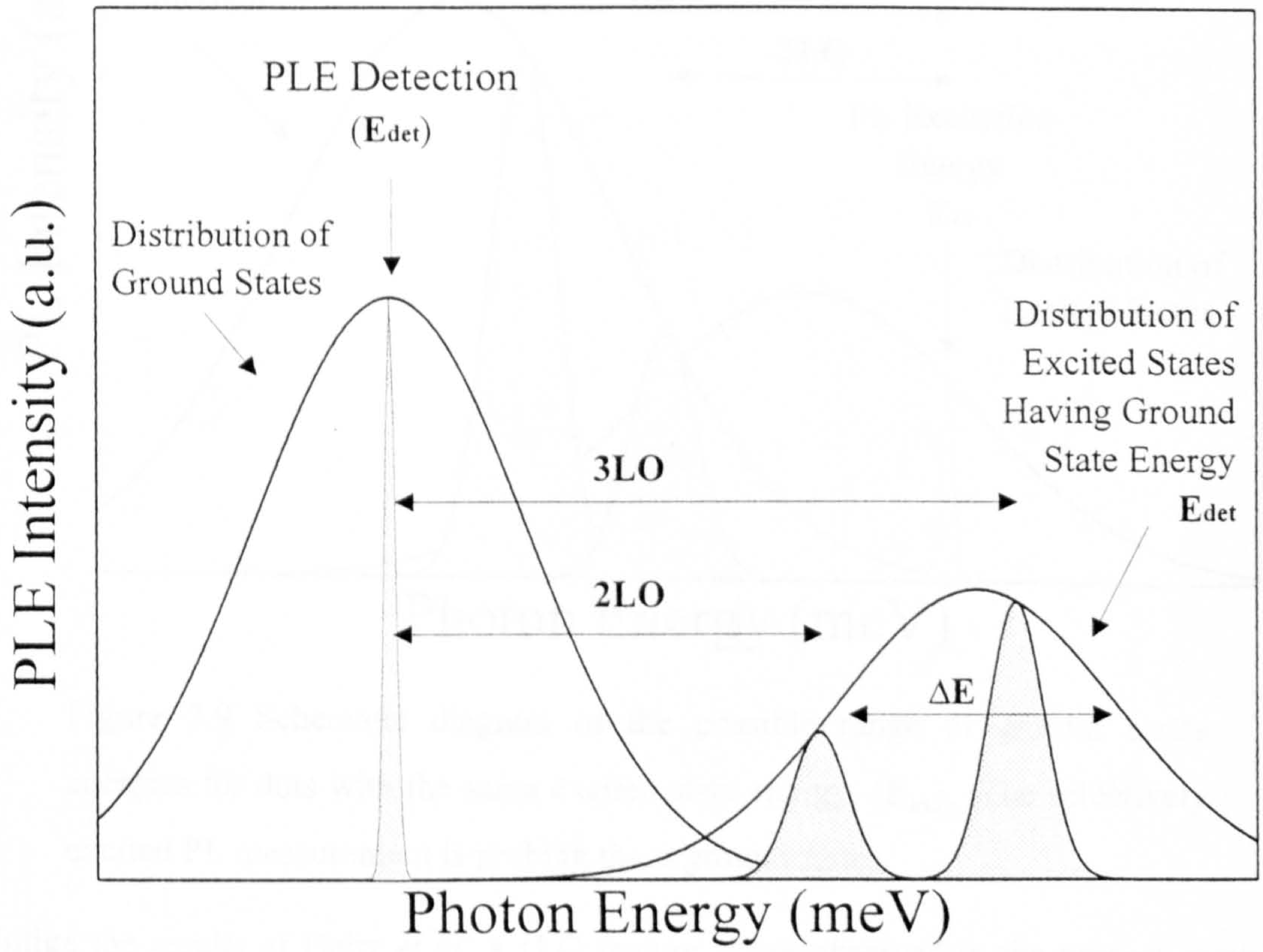

Figure 7.8 Schematic diagram of the distribution of excited states that have a common ground state energy (**E_{det}**). These excited states are being probed in a PLE measurement.

For the proposed phonon model to be valid there must exist (in PLE) a distribution of excited state energies (ΔE) for a given ground state energy, with the number of observed orders of multiple-phonons being proportional to ΔE. Heitz *et al*[2] claim that calculations for their sample (PL FWHM linewidth=45meV) indicate that ΔE is sufficiently large to account for their observation of 1LO, 2LO and 3LO features. However, no details of these calculations are given so it is not possible to apply them to the present sample. For the present sample (FWHM=35meV) the 2LO and 3LO phonon features are observed for detection at all energies within the inhomogeneous distribution of ground state energies, as indicated by the non-resonant ground state PL.

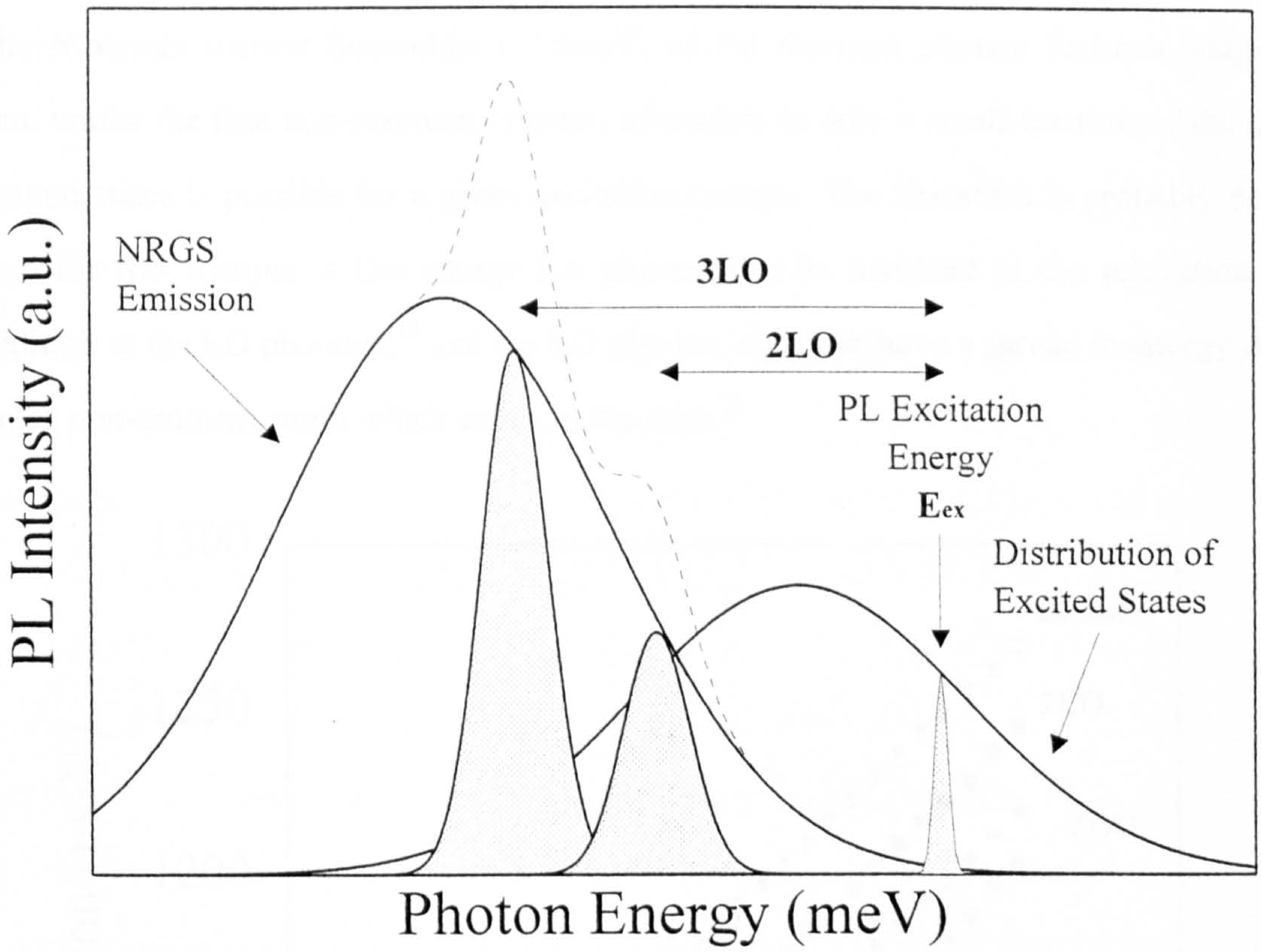

Figure 7.9 Schematic diagram of the possible range of ground states energies for dots with the same excited state energy, ($\mathbf{E_{ex}}$). The selectively excited PL measurement is probing these ground states.

Unlike the results of Heitz *et al*[2] a 1LO feature is not observed in the present sample, suggesting that the ground-state-excited-state separation is never small enough in any of the dots to allow its observation. However, for a sample having a much larger PL linewidth than the present sample (67meV compared to 35meV), and hence presumably having a larger degree of dot size and shape inhomogeneity and hence larger ΔE, a 1LO (and 4LO and 5LO) feature is observed. The results for this sample are presented below (section 7.5). A study of other samples showing differing degrees of dot size and shape inhomogeneity confirms that a rough correlation exists between the number of phonon orders observed and the PL linewidth. Hence there is some experimental evidence that the number of multiple-phonon orders observed does depend upon ΔE, consistent with the proposed model for their origin,[2] although it is difficult to determine if the size of ΔE is sufficient to account for the observed behaviour.

The relatively narrow linewidths (~10meV) of the resonant phonon features suggest that, unlike the first non-resonant process, relaxation to only a small fraction of the dot ground states is possible for a given excitation energy. The linewidth is probably non-zero for two reasons: a low-energy LA phonon can be involved in the relaxation in addition to the LO phonons,[15] and the LO phonon itself can have a spread in energy due to the non-uniform strain which exists in the dots.[10]

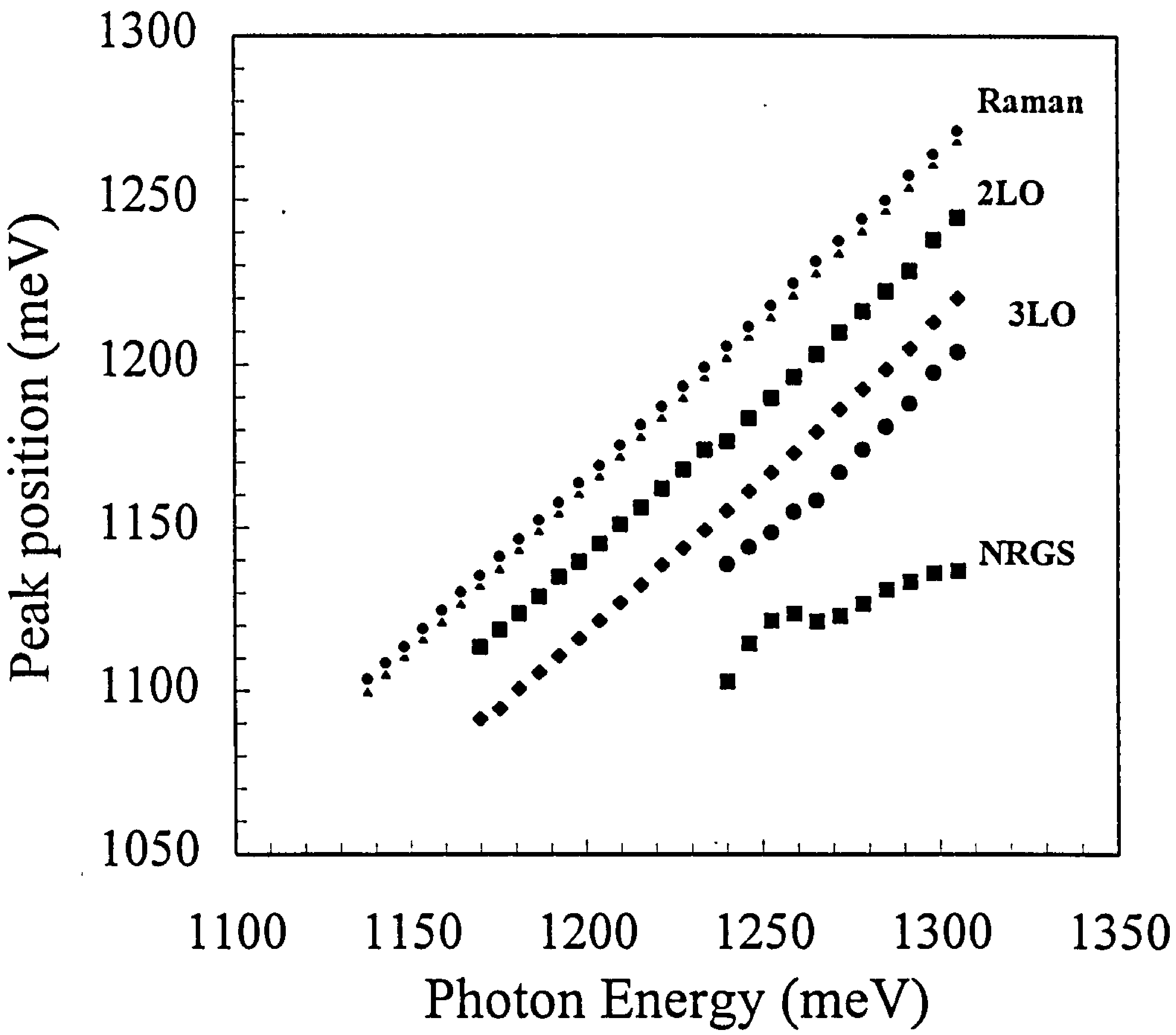

Figure 7.10 Peak position of the selectively excited PL resonant features. The data points are obtained from a curve fitting of the experimentally measured spectra.

Whilst, within the accuracy of the experimental measurements, the features observed in the PLE spectra remain at constant energies relative to the detection energy, the corresponding features in PL show some variation in their relative energies. Figure 7.10 shows the absolute energies of all the features observed in the selectively excited PL plotted as a function of excitation energy. Peak positions were determined from a curve fitting analysis of the spectra. On this plot, a feature having a constant separation from the laser should exhibit a gradient of unity. The Raman lines, because of their isolation from other features and their relatively narrow linewidths, exhibit the most reliable peak positions. These features, which are not related to the dots, are expected to be independent of excitation energy and this is consistent with their approximately unity gradients (1.0003 and 1.0006 for the two lines). The energy separation for the phonon related features is not quite so rigid (gradient of 1.05 for the 2LO and 3LO features). This behaviour manifests itself such that the phonon features in PL have a larger value than that measured in PLE when they fall on the high energy side of the ground state PL and a smaller value when they fall on the low energy side. The PLE measured value is obtained when the phonon features occur at the peak of the ground state PL. This small shift in the apparent energies of the multiple-phonon features is probably due to the effects of probing a non-uniform distribution of ground state energies, resulting from the inhomogeneous distribution of dot size and shapes. This means that curve fitting, which involves fitting totally symmetrical Gaussian curves is not entirely valid, the curves required are probably Gaussian in form but they should be weighted further by the distribution of ground states they represent, which would make them take an asymmetric form. Because of the non-uniform distribution of ground state energies, the apparent maxima of the phonon features are 'pulled' towards the peak of the distribution, giving the observed experimental behaviour. The resultant spectra is the convolution of the phonon features and the distribution of ground state energies. In contrast to PL, in PLE the multiple-phonon energies remain constant. This difference may result from a broader distribution of excited state energies (which determines the PLE process) which produces a smaller apparent shift of the phonon energies. The shift of the phonon energies in PL is inherent in the measurement technique and can only be eliminated by a deconvolution of the probed dot distribution from the overall distribution to give the true PL distribution of the resonant features. However, such a deconvolution requires a detailed knowledge of the relaxation process which results in the phonon features, in particular the energy selectivity of this process. In the absence of this knowledge it is not possible to perform this deconvolution.

The remaining feature of interest in the selectively excited PL spectra of Figure 7.4 is the broad luminescence corresponding to the non-resonant ground state, (NRGS) emission. The NRGS luminescence represents the emission from all the dots in the ensemble being studied as it is identical in form to that obtained when exciting above the wetting layer and GaAs band gap. It represents a non-selective mechanism by which the ground state of all the dots are populated by relaxing carriers. For high energy excitation, just below the wetting layer energy, the NRGS emission is the dominant feature in the spectrum with only weak luminescence related to resonant phonon relaxation visible on the high energy tail. For this excitation energy, carriers in a high proportion of the total number of dots excited relax via this non-resonant mechanism. With decreasing excitation energy the intensity of the NRGS emission becomes weaker and the spectra become dominated by the resonant multiple-LO-phonon relaxation features which allow only a small fraction of dot ground states to be populated. Figure 7.4 shows dashed curves on the higher energy excitation spectra. These represent the contribution to the PL from the NRGS process given after Gaussian functions have been fitted to the spectra.

The absolute position of the NRGS emission also shifts slightly to lower energy as the excitation energy is reduced, indicating a small degree of selectivity as the excitation energy selects the excited states of different dots. The linewidth of the peak also becomes slightly narrower on the high energy side, varying from 36meV to 28meV as E_{ex} is reduced from 1298meV to 1245meV. This behaviour does not imply there has been a change in the emission energy of any particular dot, but that the distribution of dots for which relaxation by NRGS emission occurs changes slightly as the excitation energy is varied.

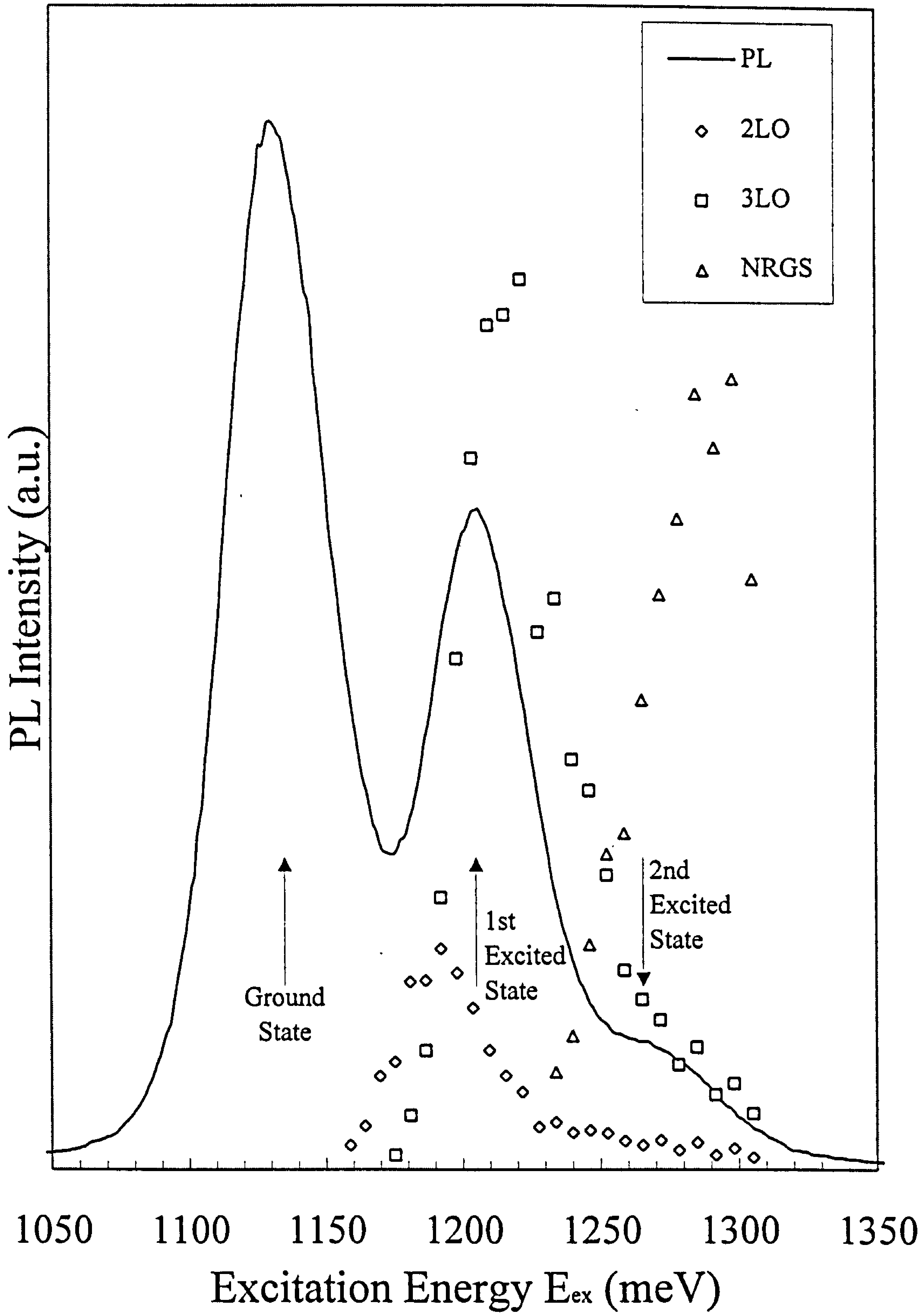

Figure 7.11 Peak intensities of the resonant phonon features and NRGS emission, observed in the selectively excited PL spectra, as a function of the excitation energy. Also shown is a high power μPL spectrum with the positions of the excited state dot transitions indicated.

Figure 7.11 shows the intensities of all the features observed in the selectively excited PL spectra plotted as a function of excitation energy, E_{ex}. Also indicated in this figure are the positions of the ground state emission and the two excited state transitions observed in the high incident laser power PL spectra plotted in the figure. As the excitation energy is reduced below 1280meV the intensity of the NRGS emission decreases. In contrast the intensity of the resonant relaxation phonon features increases as relaxation to the ground state now becomes possible by the emission of either two or three LO phonons. These processes become important when the energy difference between the incident photon and the ground state energy is close to a multiple of the LO phonon energy ($2\hbar\omega_{LO}$ or $3\hbar\omega_{LO}$). The intensity of the NRGS peak becomes negligible when E_{ex} is less than 1230meV, the predominant carrier relaxation mechanism is now via multiple phonon emission. This behaviour indicates that there are two distinct mechanisms for carrier relaxation, the relative strengths of these mechanisms being dependent on the energy of the excitation photons.

The intensities of the resonant phonon features are plotted as a function of their emission energies as determined from the selectively excited PL spectra, in Figure 7.12. Also plotted is a PL spectrum, recorded for non-selective excitation above the GaAs band gap (HeNe E_{ex}=1959meV), showing the distribution of ground states for the ensemble of dots probed. The intensities of the resonant phonon features exactly follows this distribution, showing that the luminescence observed in these selectively excited PL measurements is the radiative ground state recombination and that the strength of the resonant process is dependent upon the density of final available ground states.

In Figure 7.11 the positions of the two excited state transitions, observed in the high incident laser power μPL measurements described earlier, are indicated. The regime where the NRGS emission dominates the spectra mainly occurs within the range of the 2nd excited state transition whilst the resonant relaxation via multiple phonon emission becomes dominant when E_{ex} is in the range of the 1st excited state transition. This result indicates that the dominant carrier relaxation mechanism which occurs, depends on the particular excited state into which the carriers are excited. The NRGS process occurs when the carriers are excited into the 2nd (or higher if they exist) excited state. When carriers are excited into the 1st excited state relaxation by multiple phonon emission is more likely. This behaviour is probably mainly due to the range of energy level spacings between the ground and 1st excited states closely matching a small number of 2LO multiple phonon energies.

The absence of the NRGS emission for excitation into the first excited state is more revealing as it suggests that for states deeper in the dots the mechanism which results in this process is less probable in comparison to the multiple-phonon mechanism. A possible explanation for this behaviour is that the NRGS emission involves inter-dot tunnelling since the probability of this occurring should be greatly increased for higher energy states where the height of the tunnelling barrier is smaller. In this case the relaxation mechanism would consist of the initial non-resonant tunnelling between dots, followed by intra-dot relaxation, possibly by the emission of multiple LO phonons. Approximately similar rates for the inter-dot tunnelling and the intra-dot energy relaxation are required to ensure an overall quasi-non-resonant process. If T_{tun} is the inter-dot tunneling time and T_{relax} the intra-dot relaxation time then $T_{tun} \ll T_{relax}$ would allow all the carriers to migrate to the dot with the lowest energy excited state whereas $T_{tun} \gg T_{relax}$ would result in relaxation within the initial dot. Only for $T_{tun} \sim T_{relax}$ will carriers excited into a given dot eventually populate the ground states of a wide distribution of dots. We note that tunnelling assisted by acoustic phonons has been observed between the ground states of very closely spaced quantum dots[16] although tunnelling rates in the present dots are unknown. There is no conclusive evidence for this proposed mechanism and there are other mechanisms that could equally well explain the observed behaviour. For instance the upper excited state could consist of a number of closely spaced, unresolved states between which acoustic phonon relaxation could initially occur until the energy level spacing to the ground state reaches a multiple of the LO phonon energy. Hence we conclude that until further evidence is forthcoming, the exact mechanism for the NRGS emission will remain unclear.

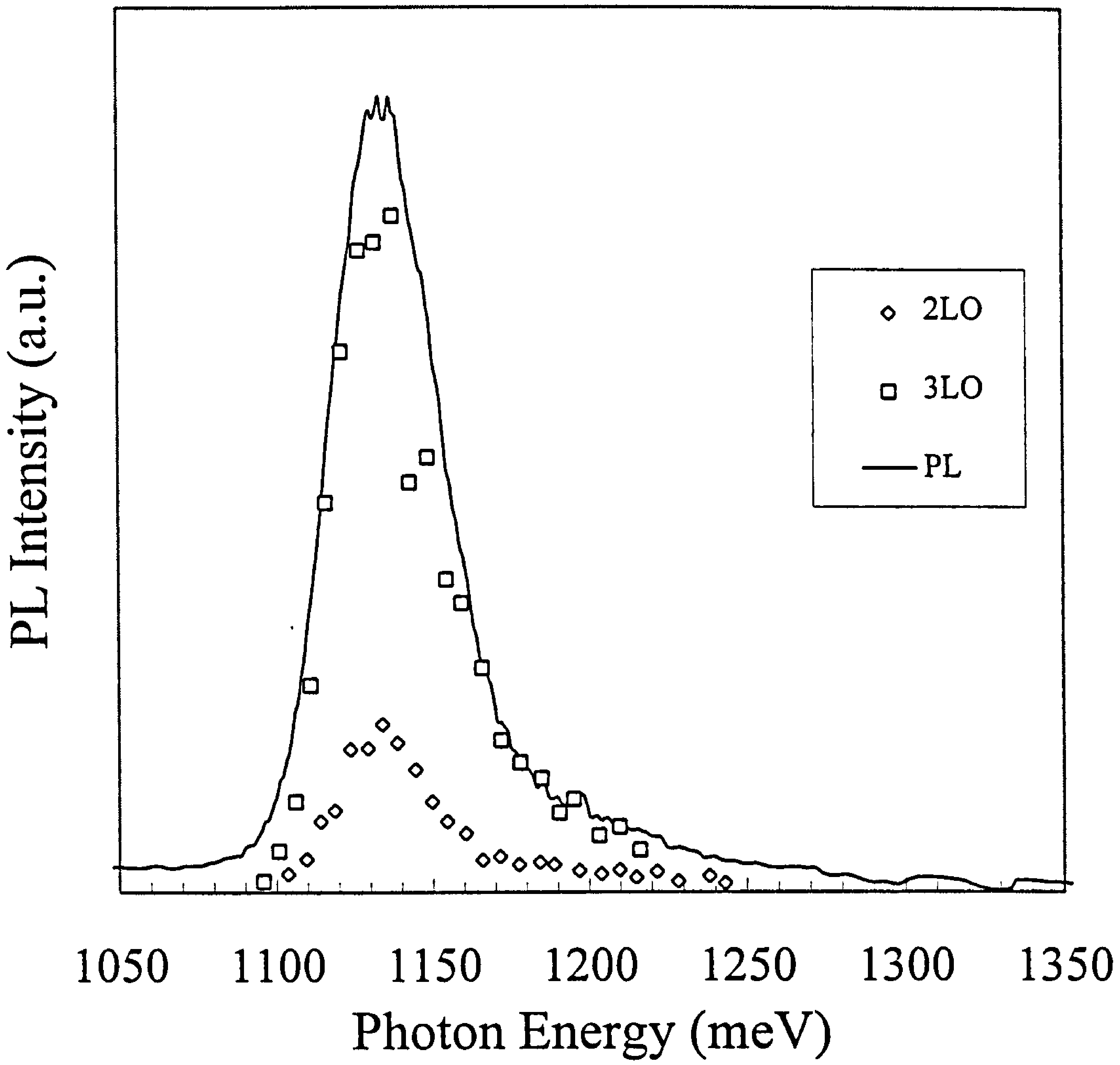

Figure 7.12 Intensities of the resonant phonon features, plotted as a function of their respective emission energies, as observed in the selectively excited PL spectra. The distribution of ground state energies is also shown as determined by a non-resonant PL spectrum excited with a HeNe laser, E_{ex}=1959meV.

The resonant PL in the present experiments represents the ground state luminescence from a subset of dots, all of which have an excited state energy corresponding to the energy of the laser excitation used. PLE is the inverse of this measurement. Here the excited states of dots with a common ground state energy are probed. Hence the PLE measurement probe a different distribution of dots to those excited by PL where the excitation energy is kept constant. In the lamp and monochromator excited PLE spectra (Figure 7.1) there are a number of features that are not observed in the corresponding PL spectra. Although the Raman lines and the 2LO and 3LO features are common to both PL and PLE, the PLE spectra show additional features which remain at a constant energy separation of 160meV and 237meV from the detection energy. Only the lower energy feature would be expected to be seen in the laser excited PL spectra because of the limited tuning range (1130-1290meV) of the mirror set used. However, no corresponding feature is observed and PL spectra taken with the lamp and monochromator show no evidence for a feature at 237meV below the excitation energy. For excitation energies above 1300meV the PL spectra are dominated by the broad NRGS emission and it is possible that this obscures the weaker, resonant features. However, the actual reason for this different behaviour in PL and PLE and the origin of these higher energy features is unclear. Although they appear at multiples of ~ ×5 (32meV) and ×8 (30meV) of the approximate phonon energy this may simply be a coincidence. Higher energy features are also observed in other samples (see below) where there is better agreement between PL and PLE.

7.5 Selectively Excited PL and PLE of Samples with a Broader PL Linewidth

The results described in the previous sections were performed on sample M929, this had the narrowest PL linewidth (≈35meV) of all the samples studied, hence representing the sample with the lowest dot size and shape inhomogeneity, possibly due to a large average dot size (low energy emission). Sample M981, which exhibited a similar linewidth (43meV) and emission energy, behaved in a similar manner with 2LO and 3LO phonon features present in the PL and PLE spectra. Other samples with a broader linewidth and higher energy emission however, exhibited a slightly different but related behaviour. These samples contain a distribution of dots with a smaller average size than those found in M929 and M981. Sample M1097 has an emission energy of 1150meV and a linewidth of 87meV. PLE recorded with a lamp and monochromator for this sample is shown in Figure 7.13, plotted on an absolute energy scale, and in Figure 7.14 plotted on an energy scale relative to the detection energy. Selectively excited PL spectra taken with various excitation energies are shown in Figure 7.15. Figure 7.16 shows the same PL data plotted on an energy scale which is relative to the excitation energy.

A comparison of the results for sample M1097 and those of M929 indicate that relaxation by multiple phonon emission occurs in both samples. However the absolute energies of the resonant features are at a slightly different energy and there are also higher multiple phonon features present in the spectra of sample M1097. For the more homogeneous sample (M929) features occur at 58(2×29) and 84(3×28)meV for the 2LO and 3LO phonon resonances respectively. However in M1097 features occur at 32.3, 67.6(2×33.8), 97(3×32.3), 128(4×32) and 168(5×33.6)meV corresponding to 1LO, 2LO, 3LO, 4LO and 5LO respectively. The reason behind the slight difference in the absolute phonon energy is not understood, but may be due to the coupling to physically different phonons or alternatively coupling to the same phonon, the energy of which depends on the size of the dots probed.

The additional features (1LO, 4LO and 5LO) observed in the spectra of sample M1097 appear to be related to the larger PL linewidth of this sample as other samples which have similar size linewidths also exhibit these features in their PL and PLE spectra. Hence there is some evidence that the observation of the multiple-phonon features requires the presence of a distribution of energy level separations, resulting from dot shape and size inhomogeneities, consistent with the proposed model of Heitz *et al.*[2] The observation of five, approximately equally spaced, features in the spectra is also consistent with a non-electronic origin. A constant transition or energy state separation implies an underlying parabolic confinement potential[17] and such a potential is not consistent with the calculations of Grundmann *et al*[10] and Cusack *et al*[18] where the confinement potential which results from effects of strain and dot shape is shown to be highly non-parabolic.

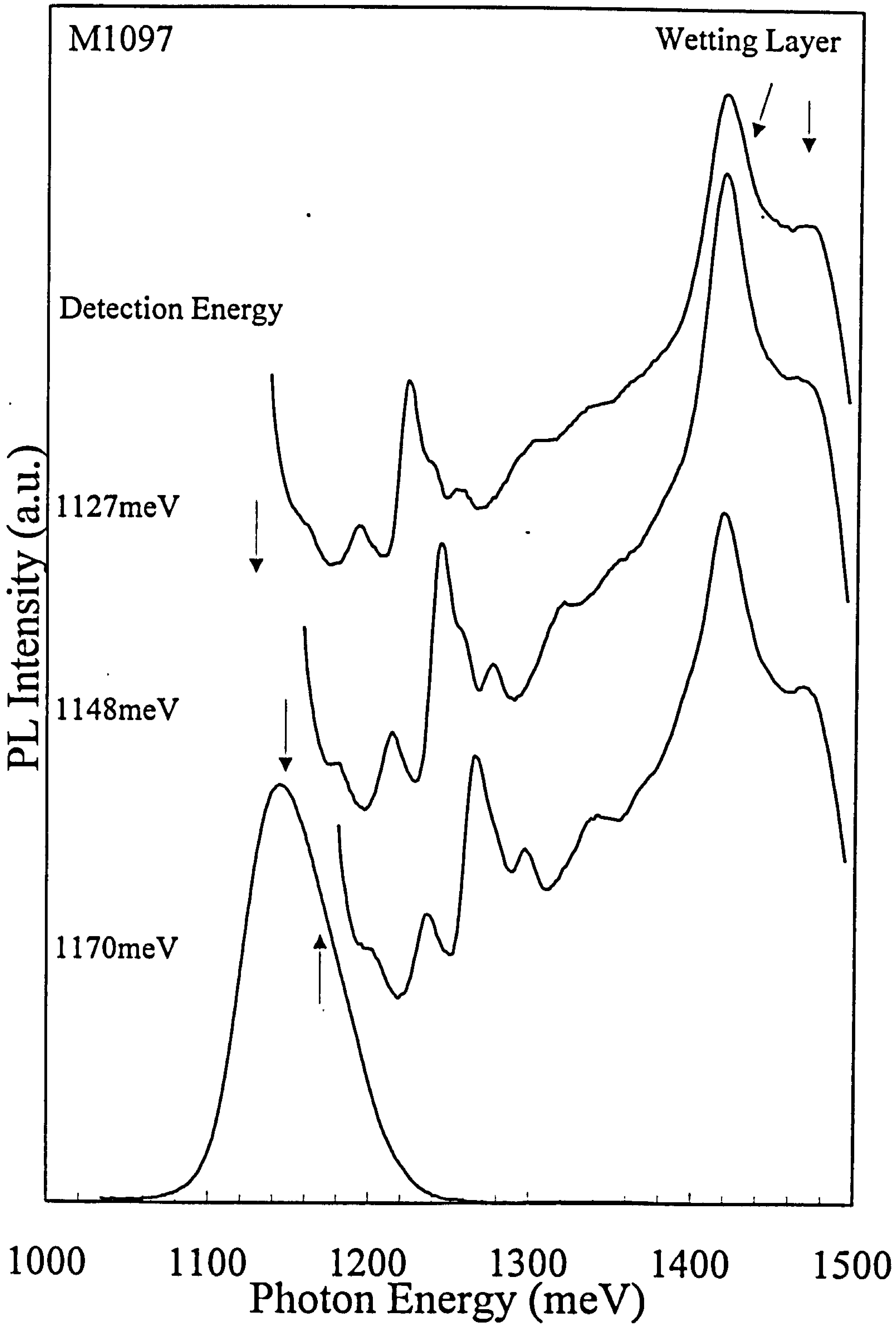

Figure 7.13 PLE spectra at T=4.2K of sample M1097 excited with the lamp and monochromator combination. The spectra are plotted on an absolute energy scale and the positions of the detection energies are shown on a PL spectra obtained using non-selective excitation. The origin of the resonant features is indicated in Figure 7.14.

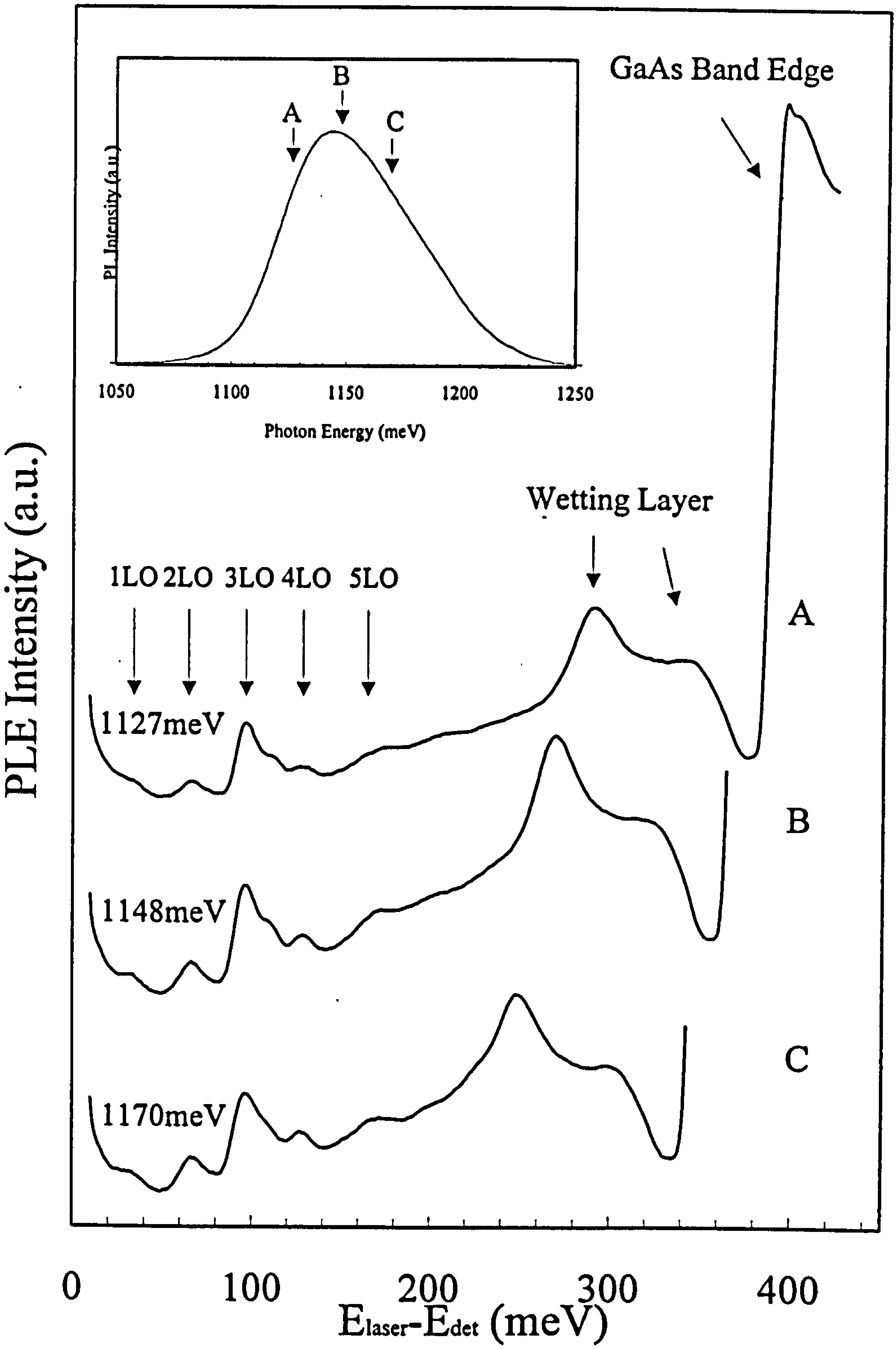

Figure 7.14 PLE spectra at T=4.2K of sample M1097 excited with the lamp and monochromator combination. The spectra are plotted against the difference between the incident photon energy and the detection energy. The inset figure shows the position of the detection energies on a PL spectra.

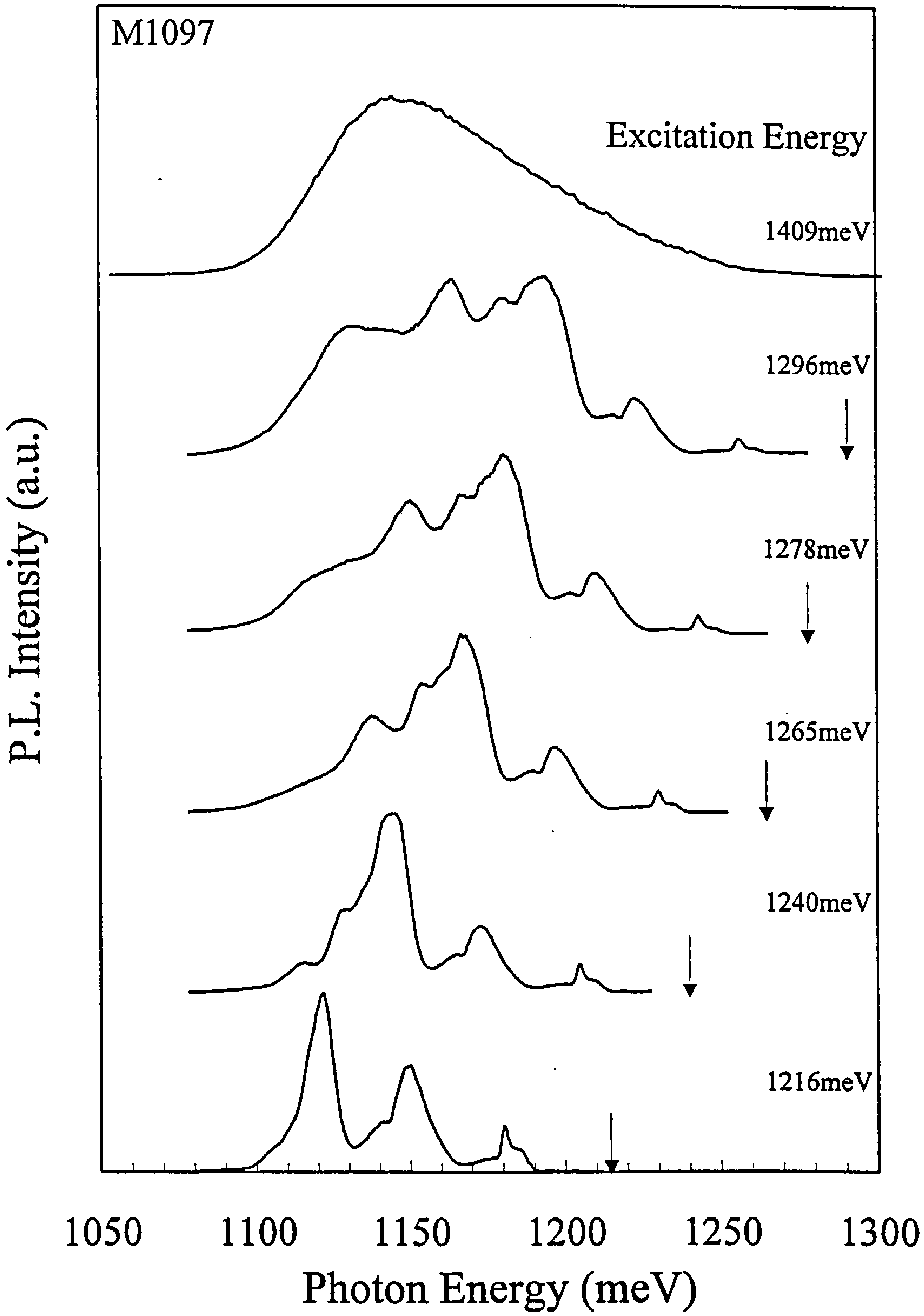

Figure 7.15 Selectively excited PL at T=4.2K obtained using a Ti:Sapphire Laser. The spectra are plotted on an absolute energy scale. The positions of the excitation energies are indicated on the spectra. The peaks are identified in Figure 7.16.

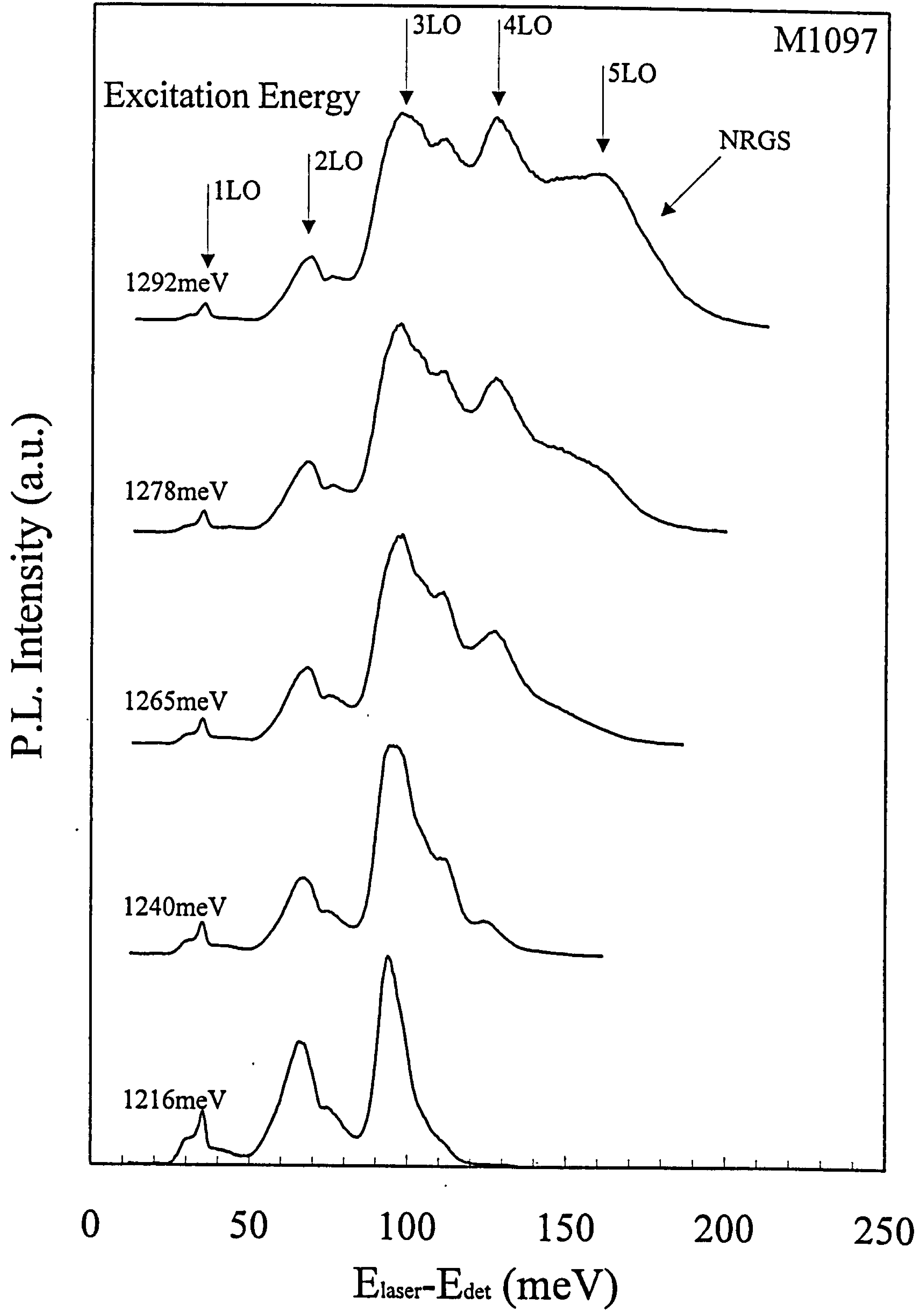

Figure 7.16 Selectively excited PL spectra at T=4.2K recorded with the Ti:Sapphire Laser. The spectra are plotted on a relative energy scale showing the difference between the excitation energy and the emitted photons.

7.6 Current Theoretical Modelling of Self-Organised Quantum Dots

In this section the currently available theoretical models of the electronic structure of InAs self-organised dots will be reviewed. The results will be discussed in an attempt to determine whether the proposed carrier relaxation mechanism (multiple phonon emission) is, in principal, feasible. Modelling of quantum dots in this particular material system is extremely difficult due to the present uncertainties regarding the exact shape, size and compositional content of the dots. In addition, the strain distribution within the dots and the surrounding GaAs is highly complex. The high degree of strain and confinement is expected to strongly modify the carrier effective masses compared to their bulk values. Hence, in contrast to the much studied case of quantum wells, the correct choice of model input parameters is not obvious.

Grundmann *et al*[10] have calculated the energy level structure for square based, pyramidal shaped InAs dots and their results are reproduced in Figure 7.17. The results are plotted as a function of the base length, with the other dimensions scaled accordingly. Hence possible independent fluctuations of the three spatial dimensions (shape fluctuations) are neglected. The results of Figure 7.17 show only one confined electron state but a number of confined hole states, suggesting that the excited state transitions observed in the high power PL spectra represent transitions from the ground electron state to excited hole states. Using the results of Figure 7.17 the measured ground state PL energy of sample M929 corresponds to a base length of 10.5nm and the PL linewidth indicates a base size fluctuation of ±0.5nm. For this degree of size fluctuation the ground-state-first-excited state energy separation is found to vary by ≈12meV. Hence if the features observed in the PLE spectra represented just absorption into the first excited state they should exhibit a variation of this amount as the detection energy is moved across the ground state distribution. Such a variation, which is well within the experimental accuracy, is not observed experimentally indicating that the PLE features can not be attributed to purely excited state absorption. Similar calculations have been performed by Cusack et al.[18] These also show only one confined electron state and indicate that the observed PLE features do not exhibit the necessary variation required for them to be attributed to purely electronic transitions. Calculations have also been reported by Marzin and Bastard for cone shaped dots[19] and Hawrylak and co-workers for GaInAs truncated sphere shaped dots.[20] Neither of these latter calculations are therefore totally relevant to the present dots.

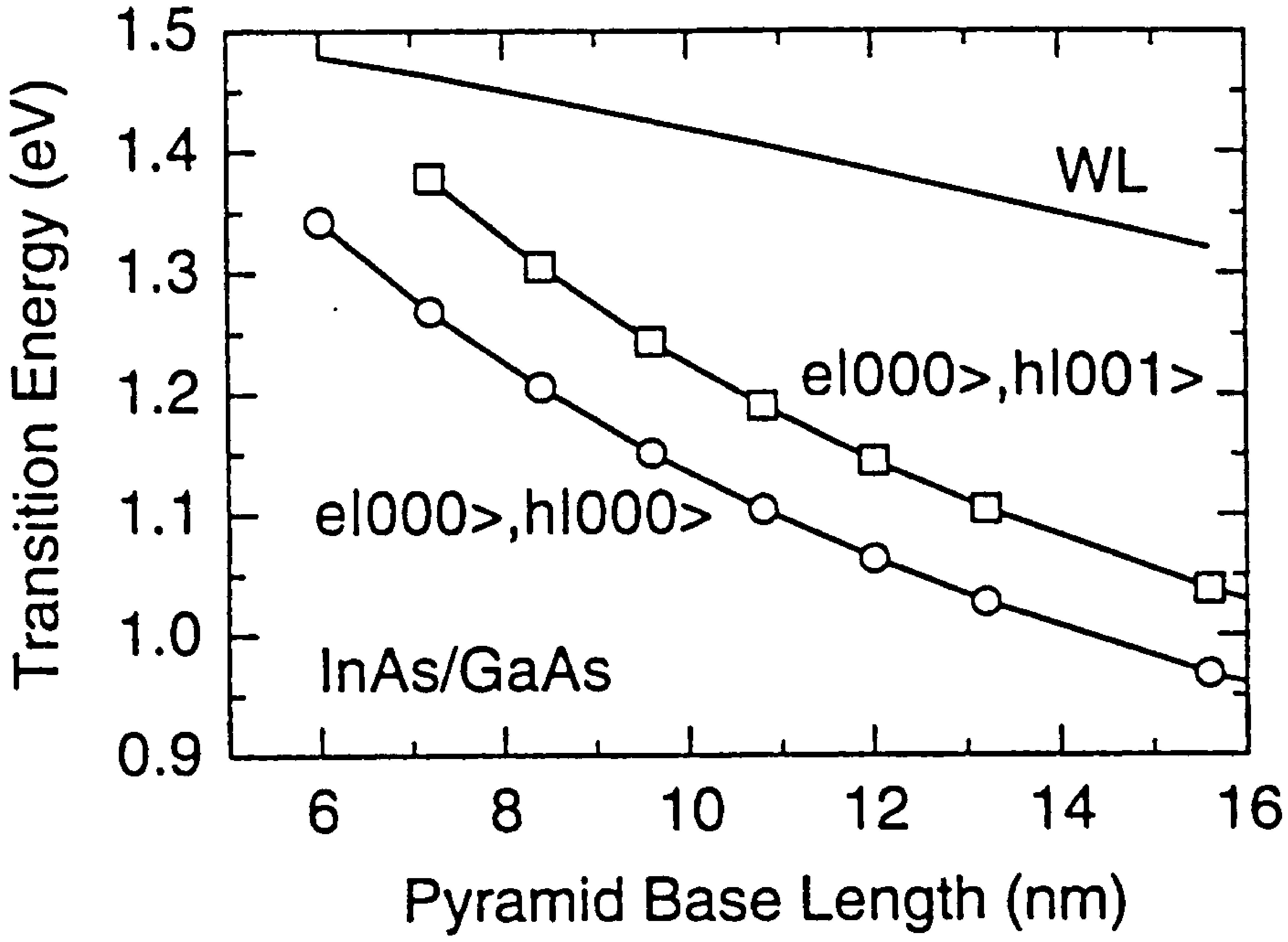

Figure 7.17 Theoretical calculations from Grundmann *et al*[10] showing the variation of dot energy levels as a function of base length.

Grundmann *et al*[10] have also investigated the effects of size and shape variations on the dot energy level separations. These authors have calculated energy levels for two different dot shapes, with {101} or {203} facets,[21] and find a difference in the ground-state-first-excited state separation, for a given ground state energy, of ~10-20meV depending on the ground state energy. Experimentally they deduce an inhomogeneous broadening, of 30meV, resulting from size and shape fluctuations, for the variation of the energy level separation for a fixed ground state transition energy.[2] Variations of this order of magnitude are sufficient to account for the experimental observation of the multiple-phonon features, although, as discussed above, it is difficult to determine this experimentally.

To conclude this section, the available theoretical calculations[2,18-21] of the dot electronic states indicate that the features observed in PLE (and PL) do not reflect simple absorption processes into excited dot states as they do not exhibit the calculated variation with changes in the detection energy. Although the calculations do not 'explain' the observed behaviour they suggest that the size of fluctuations in the energy level separation is consistent with that required by the multiple-phonon carrier relaxation model proposed by Heitz *et al.*[2]

Finally we note that in addition to the work by Heitz *et al*,[2] which is similar to that described in this thesis, other groups have observed evidence for carrier relaxation by the emission of one or more LO phonons in self-organised quantum dots. For example Schmidt *et al*[22] observed features at ×2 and ×4 of the LO phonon energy in the PLE spectra of InAs dots and Fafard *et al*[23] observed enhancement of the selectively PL at various single LO phonon energies below the excitation energy in AlInAs/AlGaAs quantum dots. Hence carrier relaxation by LO phonon emission appears to be a general feature of self-organised quantum dots. Time resolved optical studies of MOVPE grown GaInAs quantum dots by Ohnesorge *et al*[24] have shown that carrier relaxation within the dots is rapid although slower than in comparable quantum wells where the LO phonon intersubband scattering times of ≈600fs have been measured.[25] At low temperatures and low excitation power a relaxation time of ≈70ps is measured for excitation of carriers into excited dot states. The relaxation mechanism in this case is attributed to multiple-phonon emission. With increasing excitation power the carrier relaxation rate decreases by ~40ps, this behaviour is attributed to the switching-on of an Auger process as the dot carrier occupancy is increased above unity. These results show that even when carrier relaxation proceeds by emission of multiple-phonons it is still relatively rapid compared, for example, to recombination processes which occur on a timescale ~1ns.[26]

7.7 Conclusions

A detailed optical study of self-organised InAs quantum dot samples has been performed using the techniques of PLE and selectively excited PL. These results provide important information regarding the carrier relaxation mechanisms that exist in self-organised quantum dots. Evidence for two distinct carrier relaxation mechanisms has been found using the technique of selectively excited PL - a non-resonant mechanism from upper excited states and a resonant process, whereby carriers relax in a subset of the dots by the emission of a multiple number of LO phonons, from the first excited state. The form of the PLE spectra is shown to be dominated by the carrier relaxation part of the process and hence do not reflect the absorption of the dots as is generally the case for this type of measurement performed on systems of high dimensionality. Again carrier relaxation by multiple phonon emission appears to be the favoured carrier energy loss mechanism. The phonon bottleneck has been predicted to inhibit efficient carrier relaxation in 0D structures with discrete energy levels. The observation of efficient ground state luminescence in the selectively excited PL measurements provides strong evidence that any phonon bottleneck has been efficiently bypassed by both carrier relaxation mechanisms. If the potential problem of the phonon bottleneck in quantum dot structures is overcome, then the prospects for optical devices which employ quantum dots in their active region is very promising.

In terms of future experimental work perhaps the most desirable would be a measurement of the true dot absorption. This would allow the quantum dot energy level structure to be determined and correlated with other optical properties. Although high power density PL has allowed the observation of excited states, the true oscillator strengths of the transitions is not obtained and it is possible that the transition energies may be perturbed by many carrier effects.[27] The absorption of a single layer of dots is too low to measure directly. Although the approximate absorption spectra of single quantum wells and wires has been measured by PLE, for the present system, as described above, the form of the PLE spectra is dominated by the carrier relaxation part of the process. Photocurrent and photo-induced absorption measurements have been attempted on the present dots but without success. It is likely that carriers are too strongly confined in the dots to produce a photocurrent signal. Grundmann[28] has reported calorimetric absorption measurements of quantum dots similar to those studied in the present work. However, this is again a two step process (photon absorption followed by the conversion of the absorbed energy in to heat (phonons)) and it is not obvious if it results in the true absorption spectrum of the dots. Hence, at present, no comprehensive and reliable determination of the quantum dot energy level structure exists. This prevents a full understanding of the observed quantum dot properties, for example carrier relaxation mechanisms.

To obtain structures that are suitable for opto-electronic device applications there are other problems which need to be overcome. The main problem is that of dot size and shape uniformity. This can only really be solved through a more detailed understanding of the relevant growth mechanisms, so that a greater degree of growth control can be obtained. However, with any process that relies on a self-organised mechanism, some degree of variation is to be expected. Calculations by Grundmann *et al*[29] show that the addition of a single InAs molecule to an island that contains ~3×10^3 InAs molecules shifts the confinement energy by ~0.06meV. Hence, to obtain very narrow linewidth samples a very high tolerance of the growth control is required. At present this level of control is not possible. However, we conclude by noting that there have been several reports of low threshold, high temperature sensitivity laser structures grown with InAs self-organised dots as their active region.[30] The performance of these devices is already comparable to the best quantum well based devices,[31] suggesting that the present obtainable PL linewidths are already sufficient to allow the predicted advantageous properties of quantum dots to be realised.

7.8 References

[1] H. Benisty, C.M. Sotomayor-Torrès and C. Weisbuch, Phys. Rev. B 44, (19), 10945, (1991).

[2] R. Heitz, M. Grundmann, N.N. Ledentsov, L. Eckey, M. Veit, D. Bimberg, V.M Ustinov, A. Yu. Egorov, A.E. Zhukov, P.S. Kop'eV, and Zh. I. Alferov, Appl. Phys. Lett. **68**, (3), 361, (1996).

[3] U. Bockelmann and T. Egeler, Phys. Rev. B **46**, (23), 15574, (1992).

[4] M.D. Dawson and G. Duggan, Phys. Rev. B **47**, (19), 12598, (1993).

[5] Even if there is appreciable absorption into deep levels such carriers may not be mobile and so may be unable to migrate into the dots.

[6] B. Ohnesorge, M. Albrecht, J. Oshinowo, A. Forchel and Y. Arakawa, Phys. Rev. B **54**, (16), 11532, (1996).

[7] H. Yu, S. Lycett, C. Roberts and R. Murray, Appl. Phys. Lett. **69**, (26), 4087, (1996).

[8] Landolt-Börnstein, New Series, Vol 17a Physics of Group IV Elements and III-V Compounds, Springer-Verlag, Berlin (1982).

[9] A.K. Sood, J. Menéndez, M. Cardona and K. Ploog, Phys. Rev. Letts. **54**, (19), 2111, (1985).

[10] M. Grundmann, O. Stier, D. Bimberg, Phys. Rev. B **52**, (16), 11969, (1995).

[11] M.H. Brodsky and G. Lucovsky, Phys. Rev. B **21**, (14), 990, (1968).

[12] A.K. Sood, J. Menéndez, M. Cardona and K. Ploog. Phys. Rev. Letts. **54**, (), 2115, (1985).

[13] D.J. Mowbray, O.P. Kowalski, M. Hopkinson, M.S. Skolnick and J.P.R. David. Appl. Phys. Lett. **65**, (2), 213, (1994).

[14] D.W. Peggs. PhD Thesis, University of Sheffield (1996).

[15] T. Inoshita and H. Sakaki, Optoelectron. Devices Technol. **8**, 539, (1993).

[16] A. Tackeuchi, Y. Nakata, S. Muto, Y. Nishikawa, N. Yokoyama, and O. Wada, Jpn. J. Appl. Phys. 34, (L1439), (1995).

[17] R.C. Miller, A.C. Gossard, D.A. Klienman and O. Munteanu, Phys. Rev. B **29**, (6), 3740, (1984).

[18] M.A. Cusack, P.R. Briddon and M. Jaros. Phys. Rev. B **54**, (4), R2300, (1996).

[19] J.-Y Marzin, G. Bastard, Solid State Comms. **92**, (5), 437, (1994).

[20] A. Wojs, P. Hawrylak, S. Fafard, and L. Jacak. Phys. Rev. B **54**, (8), 5604, (1996).

[21] M. Grundmann, N.N. Ledentsov, O. Stier, J. Böhrer, D. Bimberg, V.M. Ustinov, P.S. Kop'eV and Zh. I. Alferov, Phys. Rev. B, Rapid comms. **53**, (16), 10509, (1996).

[22] K.H. Schmidt, G. Medeiros-Ribeiro, M. Oestreich, P.M. Peteroff and G.H. Döhler. Phys. Rev. B **54**, (16), 11346, (1996).

[23] S. Fafard, R. Leon, D. Leonard, J.L. Merz, P.M. Petroff. Phys. Rev. B **52**, (8), 5752, (1995).

[24] B. Ohnesorge, M. Albrecht, J. Oshinowo, A. Forchel and Y. Arakawa. Phys. Rev. B **54**, (16), 11532, (1996).

[25] K. Turner, L. Rota, R.A. Turner, J.F. Ryan and C.T. Foxon, Appl. Phys. Lett. **66**, (23), 3188, (1995).

[26] G. Wang, S. Fafard, D. Leonard, J.E. Bowers, J.L. Merz and P.M. Petroff, Appl. Phys. Lett. **64**, (21), 2815, (1994).

[27] S Raymond, P Hawrylak, C Gould, S Fafard, A Sachrajda, M Potemski, A Wojs, S Charbonneau, D Leonard, P M Petroff and J L Merz, Sol. Stat. Commun. **101,** 883 (1997).

[28] M Grundmann, Advances in Solid State Physics, **35**, Vieweg, Braunschweig (1995).

[29] M. Grundmann, J. Christen, N.N. Ledentsov, J. Böhrer, D. Bimberg, S. Ruvinmov, P. Werner, U. Richter, U. Gösele, J. Heydenreich, V.M. Ustinov, A. Yu. Egorov, A.E. Zhukov, P.S.Kop'eV and Zh. I. Alferov, Phys. Rev. Letts. **74**, (20), 4043, (1995).

[30] N. Kirstaedter, N.N. Ledentsov, M. Grundmann, D. Bimberg, V.M. Ustinov, S.S. Ruvimov, M.V. Maximov, P.S. Kop'eV, Zh. I. Alferov, U. Richter, P. Werner, U. Gösele, and J. Heydenreich. Elec. Letts. **30**, (17), 1416, (1994).

[31] M. Dion, Z.R. Wasilewski, F. Chatenoud, V.K. Gupta, A.R. Pratt, R.L. Williams, C.E. Norman, M.R. Fahy and A. Marinopoulou, Can. J. Phys. (suppl.) 74, S1, (1996).